SHEARING STRESSES AND TURBULENCE IN A TIDAL CURRENT.

Thesis submitted in accordance with the requirements of the University of Liverpool for the degree of Doctor in Philosophy by Juan Brown, June, 1985.

ABSTRACT

Simultaneous measurements of the velocity profile and turbulence were made at 4 heights within 2 m of the sea bed in the Eastern Irish Sea. A photographic unit was also deployed to observe sediment motion. The design, construction and performance of the instruments are described and the results from 36 trials, for a variety of bedforms and water depths of 8 to 50 m, are discussed.

The velocity profile was recorded by means of Aanderaa rotors and the velocity fluctuations with e.m. heads. Their measurements, according to flume calibrations, were accurate to ±1%. Angular corrections were necessary to compensate for the loss in response when the turbulence rig was poorly orientated with respect to the mean flow direction. The minimum in situ velocity was 20 cm s^{-1}, at which speed inertial 'pumping' of the rotors by turbulent fluctuations was estimated to produce overreading by ~ 1 cm s^{-1}. At speeds above 30 cm s^{-1} this effect was negligible. The resolution of the e.m. heads was at least 5.0 mm s^{-1}, as determined by the noise level, and d.c. drift less than 1.0 mm s^{-1} over periods of up to 17 hours. Data were recorded on 9 track tape aboard ship for later analysis onshore.

The measurements were made in a bottom boundary layer which could be decribed as accelerating, non-rotational, hydrodynamically rough, neutrally stratified and comprised a layer of constant Reynolds stress.

The stress, as determined from the log-profiles, either uncorrected or corrected for acceleration, was observed to be significantly greater (~ 26%) than that determined by eddy correlation techniques. This could not be attributed to uncertainties introduced by misalignment of the e.m. heads, or inadequate correction for cospectral losses. Doubt was cast on the validity of von Karmann's constant (κ_0) = 0.4, with a more appropriate value apparently being closer to 0.35. κ_0 and $u_*^2/-\overline{u'w'}$ exhibited no dependence on bedform or sediment type, except in one case, where high ratios corresponded to high z_0's.

Evidence of a tidal hysteresis of stress was observed at one station only. Apparent z_0 minima at peak tidal velocities were, for the most part, attributed to the non-removal of accelerating effects when applying the log-law. Initially high values of z_0, when present, were supposed to be due to streamlining of bedforms with increasing velocity. z_0 and C_{100} varied from 0.02 - 0.25 and (2 - 3) x 10^{-3} respectively for mud, unrippled sand and various sand combinations. For gravel and rippled sand values they were 0.10 - 0.20 and (3 - 8) x 10^{-3}.

A comparison of events comprising 90% of the stress with movement of bed material, observed by the photographic unit, failed to reveal a correlation. During periods of sediment motion events in which $u' > 0$ were dominant. For events comprising 90% of the stress, those in which $u' < 0$ and $u' > 0$ occurred in groups of 5 - 20. In addition, a number of coherent events, occuring between 5 - 12 times per minute independently of velocity, were observed between 100.0 and 172.5 cm above the bed.

ACKNOWLEDGMENTS

I would like to express my gratitude to Professor K.F. Bowden for his supervision during the first two years of this study, and advice following his retirement. In addition, I wish to thank Drs. R.I. Tait and M.R. Howe for assuming the role of supervisor during the final period of this study. I am especially grateful to Dr. S.R. Ferguson for providing me with the opportunity to use the equipment he designed, and for his help during his time at the department.

Financial support was provided by the Isle of Man Government, with the ship time and equipment being funded by N.E.R.C., through a grant awarded to Professor K.F. Bowden.

For his assistance during my time at Liverpool, and understanding whilst drawing a number of Figures, I am grateful to Mr. J. Murphy. Also to Mr. R. Tennant for his advice during the design of the equipment and the subsequent construction of the pressure casings and other hardware. Mr. P. Evans provided invaluable assistance during the deployment of the equipment and Mr. F.C. Dewes in drawing the majority of the Figures.

My colleagues, E. Gmitrowitz, H. Rogers and S. Boxall provided much needed advice, critisism and support throughout this study. Finally, I especially wish to thank Penny for her understanding and moral support during this study, without which this thesis may not have been completed.

CONTENTS

LIST OF FIGURES

LIST OF TABLES

CHAPTER 1 - INTRODUCTION

1.1 INTRODUCTION

Turbulent flow in fluids has been the subject of intensive theoretical study and practical laboratory and field experiments. It is intended in this chapter to present a summary of the relevant theory applicable to turbulent boundary layer flow, as observed during an experimental programme in the Eastern Irish Sea, detailed in Chapter 2. This is followed by a summary of previous experimental work investigating such turbulent flow, with particular relevance to the study described in the ensuing chapters.

1.2 BACKGROUND THEORY TO TURBULENT BOUNDARY LAYER FLOW

1.2.1 The Navier - Stokes Equations of Motion.

For a fluid of constant density (ρ), and molecular viscosity (μ), the Navier - Stokes equations of motion can be written in Cartesian tensor notation as:

$$\frac{\partial u_i}{\partial t} + u_j \frac{\partial u_i}{\partial x_j} = -\frac{1}{\rho}\frac{\partial p}{\partial x_i} + \nu \frac{\partial^2 u_i}{\partial x_j^2} + f_i \quad , \qquad 1.1$$

where ν = kinematic viscosity (μ/ρ), and f_i represents body forces.

A flow with a total pressure gradient normal to the streamlines (i.e. shear flow) may become unstable to small disturbances. These disturbances may be intensified by a process known as 'vortex stretching', arising from the interaction of vorticity (= curl $\tilde{u}$) and velocity gradients. As the process continues disturbances are passed to higher harmonics leading to a broadening of the wavenumber spectrum. This broadening continues over smaller and smaller length scales until viscous stresses dissipate the

smallest scale eddies. Upon reaching a fully turbulent state, energy is being transferred to smaller spatial scales across a continuous wave - number spectrum, this being a three dimensional, non-linear phenomenon (Bradshaw, 1975 and 1978).

Once turbulent flow has developed, the instantaneous velocity (u_i), in equation 1.1, can be replaced by $U_i + u_i$ (mean flow + fluctuations) and the equation averaged. Strictly speaking an ensemble average should be used. In practice stationarity in the flow is assumed and a time average employed. Equation 1.1 becomes:

$$\frac{\partial U_i}{\partial t} + U_j \frac{\partial U_i}{\partial x_j} = -\frac{1}{\rho}\frac{\partial \bar{p}}{\partial x_i} + \frac{\partial}{\partial x_j}\left[\nu \frac{\partial U_i}{\partial x_j} - \overline{u_i u_j}\right] + F_i \quad , \qquad 1.2$$

where an overbar represents a time average. The term $\nu\, \partial U_i/\partial x_j$ represents the viscous stresses, whilst $\overline{u_i u_j}$ represents the Reynolds stresses, both arising from the non-linear term of equation 1.1.

1.2.2 Energy Balance.

Perhaps the clearest indication of the 'source' (generation) and 'sink' (dissipation) terms in the equations of motion can be obtained from the kinetic energy (K.E.) balance. The K.E. balance can be expressed in terms of mean K.E. per unit mass ($U_i^2/2 = Q^2/2$) and turbulent K.E. ($\overline{u_i^2}/2 = \overline{q^2}/2$) and given below by equations 1.3 and 1.4 respectively:

$$\frac{D}{Dt}\frac{Q^2}{2} = -\frac{\tau_{ij}}{\rho}\frac{\partial U_i}{\partial x_j} - \frac{\partial}{\partial x_i}\frac{PU_i}{\rho} + \frac{\partial}{\partial x_j}\frac{U_i \tau_{ij}}{\rho} + \nu U_i \frac{\partial^2 U_i}{\partial x_j^2} + U_i F_i \quad , \qquad 1.3$$

$$\frac{D}{Dt}\frac{\overline{q^2}}{2} = -\frac{\partial}{\partial x_i}\overline{u_i\left[\frac{p}{\rho} + \frac{q^2}{2}\right]} + \frac{\tau_{ij}}{\rho}\frac{\partial U_i}{\partial x_j} + \nu \overline{u_i \frac{\partial^2 u_i}{\partial x_j^2}} \quad , \qquad 1.4$$

where $$\frac{D}{Dt} = \frac{\partial}{\partial t} + U_j \frac{\partial}{\partial x_j}$$

$$\overline{\nu u_i \frac{\partial^2 u_i}{\partial x_j^2}} = \nu \left[\frac{\partial^2}{\partial x_j^2} \overline{\frac{q^2}{2}} - \frac{\partial^2}{\partial x_i \partial x_j} \overline{\frac{\tau_{ij}}{\rho}} \right] - \epsilon \quad , \quad 1.5$$

$$\epsilon = \nu \overline{\frac{\partial u_i}{\partial x_j} \left[\frac{\partial u_i}{\partial x_j} + \frac{\partial u_j}{\partial x_i} \right]} \quad , \quad 1.6$$

$\tau_{ij} = -\rho \overline{u_i u_j}$, the Reynolds stress.

The first term on the right hand side of equation 1.3 represents energy lost from the mean motion by the working of the Reynolds stresses against velocity gradients. The second and third terms represent the transport of the mean flow energy by mean pressure gradients and Reynolds stresses. The fourth term represents the effects of viscous forces , with the final term representative of body forces (Townsend, 1956; Tennekes and Lumley, 1974)

Considering equation 1.4, giving the rate of change of turbulent K.E., the first term on the right is the sum of the mean energy transport and pressure fluctuation terms and represents the turbulent energy transport. The second term is the production of turbulent K.E., appearing as the first term in 1.3. The final term represents viscous effects and can be expressed as shown in equation 1.5, showing the viscous transport and dissipation (ϵ). The transport term redistributes energy throughout the fluid, whilst ϵ acts as the sink for all K.E. lost from the moving fluid, other than the small proportion lost directly from the mean flow (Bradshaw, 1975 and 1978; Townsend, 1956).

In Summary, the 'driving' energy originates from the external

body forces. Some of this energy is converted to turbulent K.E. by the interaction of the Reynolds stresses and the velocity gradients. Viscous stresses eventually convert this energy to heat. The remainder of the energy is redistributed throughout the fluid before it too is dissipated.

For this study the body force term, F_i, includes gravitational attraction, tide generating forces and the Coriolis acceleration. The latter term is not significant in comparison to the longitudinal component of tidal stream and is therefore not considered further.

1.2.3 Flow Near a Solid Boundary.

For fluid flow adjacent to a smooth boundary the velocity of the fluid at the boundary must equal the velocity of the boundary. This constraint is enforced by the viscosity of the fluid, resulting in velocity shear above the boundary and a shear stress τ_0 at the boundary. At a height z above the boundary, mean flow in the x direction depends on z, τ_0, ρ and ν. If the changes in τ_0 and the pressure gradient are small over values of x and y large in comparison to z, then flow can reasonably be said to depend on these four parameters only.

The entire boundary layer of thickness δ, as shown in Fig. 1.1, can be said to be comprised of an inner and outer layer. The inner layer comprises the 'viscous sublayer' and 'log - law' region. The viscous sublayer can be subdivided into the 'buffer layer' and the 'linear layer'. The thickness of the various layers can be expressed in terms of the length scale ν/u_* , where $u_* = (\tau_0/\rho)^{1/2}$ is a velocity scale known as the friction velocity. Closest to the wall is the 'linear sublayer' , $z \lesssim 4\nu/u_*$, where viscous forces predominate and the velocity profile is linear. The 'buffer layer',

$4\nu/u_* < z < 40\nu/u_*$, represents a region where viscous and Reynolds shear stresses are comparable. In the 'log - law' region, $40\nu/u_* < z < 0.2\delta$, the velocity profile varies as the logarithm of z, assuming the turbulent Reynolds number $u_*z/\nu > 35$. In this layer, in non-accelerating flow, the total shear stress gradient is small and the region is often referred to as the 'constant stress' layer. Typically it occupies 10 to 20% of the boundary layer. Monin and Yaglom (1971) state that Reynolds stress can vary by up to 20% and still be said to constitute a constant stress layer, as vertical profiles of the mean dynamic variables are only slightly sensitive to variations of τ_o. The 'outer layer', $0.2\delta < z \leq \delta$, can be sub-divided into an inner region of rotational flow and outer of irrotational flow. The division between the two flows is known as the 'viscous superlayer' and is intermittent in nature. The thickness is of the order of the Kolmogorov length $\eta = (\nu^3/\epsilon_0)^{1/2}$, where ϵ_0 = viscous dissipation within the turbulent fluid. The rate at which the interface propagates into the irrotational flow is governed by the large turbulent eddies, not viscosity. This is similar to the small eddies in the viscous sublayer. For a further explanation see Bradshaw (1975, 1978) and Fernholz (1978). The mean velocity outside the boundary layer is termed u_∞.

Up to this point, only flow over a smooth boundary has been considered. If the wall has roughness elements of dimension k_r, for zero pressure gradient flows the following cases can be distinguished (Fernholz, 1978):

1) Hydraulically smooth ($0 \leq k_r \leq 5\nu/u_*$). Roughness elements are submerged in the viscous sublayer and do not affect flow. The velocity distribution is viscosity dependent and takes the form:

$$U(z) = \frac{u_*}{\kappa_0} \ln\left[\frac{z}{9z_0} \right] + B \quad , \qquad 1.7$$

where B is a dimensionless universal constant, found experimentally to be 5.0 - 5.2 and z_0 is given by equation 1.9 below.

2) Transitional ($5\nu/u_* \leq k_r \leq 70\nu/u_*$). The velocity profile is affected by wall roughness, but roughness elements do not protrude above the sublayer. The effect is taken into account by a function $f(k_r u_*/\nu)$ in the log-law equation replacing the constant of integration.

3) Hydraulically rough ($70\nu/u_* < k_r$). Roughness elements protrude through the sublayer and the velocity distribution in the log-law region is independent of viscosity taking the form:

$$U(z) = \frac{u_*}{\kappa_0} \ln\left[\frac{z}{z_0} \right] \quad , \qquad 1.8$$

1.3 BENTHIC BOUNDARY LAYER

For the purposes of the study presented in the following chapters, the benthic boundary layer can be defined as that layer adjacent to the sea bed in which a strong velocity gradient exists resulting in the generation of Reynolds stress. In thickness it extends to the order of 10's of metres above the sea bed. At the boundary, where the processes of erosion, deposition and chemical exchange occur the layer can be said to extend to the order of cm into the sediment.

For constant density flow over a rough, flat, non-rotating surface laboratory studies have shown that a characteristic length scale associated with the roughness elements (z_0) can be given by:

$$z_0 \approx 0.11\nu/u_* \quad , \qquad 1.9$$

for smooth flow and

$$z_0 \approx k_r/30 \quad , \qquad 1.10$$

for rough flow. A transition from smooth to rough flow occurs between the above range of z_0.

If a constant stress layer is present the mean velocity is given by the log-law:

$$\frac{\bar{U}}{u_*} = \frac{1}{\kappa_0} \ln\left[\frac{z - d}{z_0} \right] \quad , \qquad 1.11$$

where d = displacement height.

This combined with the quadratic stress law:

$$\tau_0 = \rho C_D U_D^2 \quad , \qquad 1.12$$

allows a drag coefficient (C_D) to be defined, characteristic of the bed and flow conditions, where U_D = mean velocity. Generally D is taken as z = 100 cm above the sea bed giving:

$$C_{100} = \left[\frac{u_*}{U_{100}} \right]^2 = \left[\frac{1}{\kappa_0} \ln(z/z_0) \right]^{-2} \quad , \qquad 1.13$$

von - Karman's constant (κ_0) is generally taken as the laboratory defined value 0.40 - 0.41, although there is some evidence to suggest that this is affected by suspended sediment, as mentioned in Section 1.4.

Jackson (1981) presented a derivation of equation 1.11, indicating how the displacement height d can be regarded as the elevation at which the mean drag may appear to act on flow well above the roughness elements. Two regions were considered, one where flow is dependent mainly on bed shear stress, characterised by u_*, and only weakly on bed geometry. In the other the flow can be said to be dependent on the free stream velocity U_∞ and the boundary layer thickness δ, but not the bed geometry. By assuming there is a range of height z over which the two regions overlap, equation 1.11 was derived. The derivation illustrates the danger in taking d = 0 cm in the calculation of z_0 for the velocity profile, especially in the

presence of a rippled bed. Generally the sampling height $z \gg d$, but d (often taken as 0.7 x roughness element height) could be of the order of several cm, introducing considerable error into the value of z_0 derived from equation 1.11. This factor should be held in mind when dealing with flows in the marine environment.

For the purposes of the study detailed in the ensuing chapters, the boundary layer was assummed to be formed in a neutrally stratified fluid flowing over a flat surface in a non-rotating system. In such a layer the thickness (δ) increases continuously downstream of a point, but remains steady in time at that point. For the case of a rotating earth the boundary layer thickness is limited to the Ekman depth $L_E \approx 0.4u_*/f$, where f is the Coriolis parameter. The stress at the boundary is balanced by the resultant of the Coriolis force and the pressure gradient and boundary layer flow is confined to a layer of uniform thickness. For a stratified flow the thickness is further limited to the order of the Monin - Obukhov length given by $L_m \approx \rho U_*^3/g\kappa_0\overline{\rho'w'}$, where $\overline{\rho'w'}$ is the buoyancy flux at the boundary due to fluctuations in density ρ' and vertical velocity w'. L_m represents the height of a density interface above the bed, below which the generation of turbulent kinetic energy exceeds the loss of potential energy that would maintain a neutrally stratified layer. A further length scale given by $L_\sigma = U_{\sigma*}/\sigma$ is found for a boundary layer oscillating with an angular frequency σ and having an oscillatory friction velocity amplitude U_{0*} (Bowden, 1978).

The length scale quoted for an oscillatory boundary is for $\sigma \gg f$. For semidiurnal tidal flow σ is of the same order as the inertial frequency f, hence the tidal boundary layer will be of the same order as the Ekman layer thickness. For the Eastern Irish Sea (the area of interest in this study) u_* is typically of the order 2 cm s^{-1} for a

value of $U_{100} \approx 40$ cm s^{-1}, and if $\sigma \approx f \approx 10^{-4}$ s^{-1}, then $L_E \approx 0.8 \times 10^4$ cm $\approx$ 80 m. The water column within 5 m of the sea bed was observed to be neutrally stratified in the area of this study, as is shown in Section 2.3, so L_m need not be considered. With L_E and L_σ both greater than the water depth the whole depth may be said to comprise the boundary layer. As the layer under examination only extends to 2 m above the bed in this study rotating and/or oscillatory flow was not considered applicable.

A comprehensive review of the nature of boundary layers observable in shelf seas was presented by Soulsby (1983). Emphasis was placed on the definition of the current structure throughout the layers and the characteristics of the turbulence. Theory was supported by observations and a number of models used to illustrate the text.

1.4 PREVIOUS EXPERIMENTAL WORK

Perhaps the first attempts of note to measure turbulence in the benthic boundary layer of the sea were made in the 1950's. Lesser (1951) utilised Ekman - type meters, whilst Charnock (1959), and Bowden, Fairbairn and Hughes (1959) employed cupwheels to record velocity profiles at up to 5 heights above the sea bed. The log-law of equation 1.11 was verified, with an apparent value of $\kappa_0 \approx 0.4$ as for laboratory flows. The first direct evaluations of Reynolds stress were also made during this period, using electromagnetic flowmeter heads of diameter 10 cm (Bowden, 1955; Bowden and Fairbairn, 1956; Bowden, 1962). The stress was found to be of the same order as that measured by the log profile method above. Some degree of spatial correlation was recorded between the u values at two heights of 75 cm and 150 cm, and similarly for the v values. The wavenumber ranges of

the u, v ,w spectra and uw co-spectra were also observed. Other early measurements of marine turbulence were reviewed by Bowden (1962).

The above period of study was followed by a comparative lull until several papers were published by Sternberg and Creager (1965) and Sternberg (1966, 1968). A system was developed to record the velocity profile within 1.5 m of the sea bed and to photograph the sediment in the immediate vicinity of the instruments during deployment. Taking 10 minute time averages at six stations near to Vancouver Island the mean C_{100} was found to vary between 2.3 x 10^{-3} and 4.0 x 10^{-3}, despite the principal roughness elements varying by an order of magnitude. A logarithmic profile was found to be present for between 62% and 100% of the time, with a mean of 85%. It was suggested that the hydrodynamic nature of the flows varied between transitional and fully rough, based on the dispersion of C_{100}.

Nece and Smith (1970) used a Preston tube close to the boundary in the Puget Sound and Columbia River in an attempt to record directly the bottom shear stress τ_0. In addition, up to eight ducted impellors were used to determine τ_0 by the log-law. As flow was considered non-stationary over the 30 minute averaging interval, only limited valid comparisons were possible, but it was suggested the two methods were comparable.

A study of the benthic boundary layer in the deep ocean was carried out by Wimbush and Munk (1970) at depths of 2 - 4 km off Southern California. The velocity profile, determined by six heated thermistors placed within 2.5 m of the bed, was found to be logarithmic and the flow hydrodynamically smooth. Weatherly (1972, 1977) placed ten Savonious rotors within 30 m of the sea bed in 750 m of water in the Florida current. The log layer was found to extend up to 8 m above the bed, with flow again being hydrodynamically smooth. A

model of the flow compared favourably with the results in the Florida Current (Weatherly, 1975), but with some doubt of whether Ekman veering occurred inside or outside the the log layer.

A camera and dye-pulser system was deployed by Sternberg (1969, 1970) to record velocity profiles within 65.0 cm of the sea floor, in water of depth up to 4000 m off Southern California. Logarithmic profiles were observed for 22 - 57 % of the time, whilst C_{100} and u_* varied between 10^{-3} - 10^{-2} and 0.02 - 0.9 cm s^{-1} respectively. The hydrodynamic nature of the flow was observed to be predominantly transitional, with a small proportion classified as smooth.

Caldwell and Chriss (1979) employed a heated thermistor to record the velocity profile from 2 cm below to 19 cm above the sediment interface in a depth of 200 m on the Oregon continental shelf. The authors claimed to have verified for the first time the presence of a viscous sublayer, apparent in a linear relationship between velocity and the height over which the greatest shear occured, 0.6 cm above the sediment interface. Above this, flow was observed to be hydrodynamically smooth, with the data fitting a logarithmic profile. Finally, von Karman's constant was estimated as 0.415 ± 0.020.

From data obtained at ten stations to the south west of England, Channon and Hamilton (1971) found the velocity profiles to be logarithmic within 2.0 m of the sea bed. The exception to this was at periods close to slack water. Boundary layer flow was classified as hydrodynamically transitional to rough, with highly variable values of z_0 and C_{100} given in the ranges 1 x 10^{-6} to 7.0 cm and (0.5 - 12.0) x 10^{-3} respectively. Even greater variability was observed in Chesapeake Bay by Ludwick (1975). The velocity profiles, obtained at

eleven points throughout the water column, using a Plessey current meter, were applied to a velocity defect law of parabolic form. The values of C_{100} ranged from 1.0×10^{0} to 1.0×10^{-4}, with two-thirds of the values between 3.5×10^{-3} and 54.0×10^{-3}. The variability of C_{100} was attributed to the mutual adjustment between the moving bed and time varying flow.

By deploying eight Braystoke current meters, spaced logarithmically above the sea bed in the West Solent, Dyer (1971) observed the velocity profiles above gravel dunes. The dunes, of height 0.25 - 2.0 m and wavelength 5.0 - 18.0 m, were found to modify the velocity profiles significantly. The upstream slopes of the dunes exhibited a logarithmic profile throughout the column. The other profiles indicated portions of higher or lower shear at mid depth, whilst the upper and lower portions were logarithmic. It was suggested these two profiles resulted from an adjustment of the boundary layer to a reduction and increase of bottom roughness respectively. Finally, a profile obeying a power law of the form $u/u_D = (z/z_D)^p$, where u_D = velocity at height z_D and p varied between 1/3 and 1/7, was observed in the troughs between the dunes. For the majority, the bottom metre of the profiles could be said to be logarithmic.

McCave (1973) found the velocity profiles to be predominantly logarithmic within 2.0 m of the sea bed, during experiments in the North Sea and English Channel. Suspended sediment was found to modify the profiles, resulting in probable over estimates of u_*. A method by which von Karman's constant could be corrected for this, based on previous laboratory experiments, was suggested. The lag of u_* behind U_{100}, during the initial accelerating phase of the tide, was attributed to possible variations in bedforms.

Vincent and Harvey (1976) and Harvey and Vincent (1977) suspended Plessey current meters from a North Sea gas platform in 35.0 m of water. The velocity profiles were observed to be logarithmic within 3.0 m of the sea bed at peak velocities. It was suggested that z_0 and C_{100} decreased with increasing mean velocity, despite what were thought to be non-changing bedforms. A possible explanation for this was offered in terms of the magnitude of the turbulent eddies at the sea bed. Larger eddies, present at higher velocities, were supposed to be unable to penetrate as far between the roughness elements as the smaller scale eddies present at lower velocities. The roughness elements were in a sense larger at lower velocities. However, a corresponding increase in z_0 and C_{100} for decreasing flow was not observed.

In an extension of previous work in the Columbia River (Nece and Smith, 1970), Smith and McLean (1977) examined the flow over sand waves of differing wavelengths and heights. The shear stress profile was related to the bottom topography and boundary roughness, and compared with a simple model. In addition, the variation of z_0 with suspended sediment concentration was examined, both of which exhibited an increase with bed shear stress τ_0. In a paper by Smith (1977), a number of models to compute bedload and suspended sediment concentrations were examined, taking into account the influence of bedforms. Verification of the models was hampered by insufficient field data.

From measurements in a tidal current, using a pivoted ducted impellor suspended below a bridge over the Choptank River, Gordon and Dohne (1973) were able to measure the uw components of Reynolds stress throughout the 7 m depth. At mean velocities of 50 - 60 cm s^{-1} the stress decreased from approximately 5 dynes cm^{-2} at 1 m above the

sea bed to zero at the surface. An approximately linear relationship between $\tau = -\rho\overline{uw}$ and turbulent intensity q^2 was found to exist with a slope $\tau/\rho q^2 \approx 0.13$. Large increases in turbulent intensity $(\overline{u^2})^{1/2}/U$ were observed in the decelerating flows. Effects of the horizontal pressure gradients on the boundary were also discussed. Subsequent to this paper, Gordon (1974) noted the intermittent nature of the Reynolds stress, finding 60% of the stress to be generated by events occupying 10% of the time. Gordon (1975) interpreted the intermittent events in terms of the bursting phenomenon previously observed in laboratory flows. A comparison of the periods between events in geophysical and laboratory flows was made, based on similar scaling of the period between events in terms of the mean flow parameters.

Gordon (1975a), again from data collected in the Choptank River, observed the Reynolds stress at a fixed height of 2.5 m above the bed throughout a 6 hour tidal cycle. The peak Reynolds stress was found to lag the peak mean velocity at 100 cm by 1 hour. In addition, for periods of comparable mean velocity the turbulent kinetic energy, Reynolds stress and the number of burst-sweep events were 2-5 times greater in decelerating (adverse pressure gradients) than accelerating (favourable pressure gradients) flows. This agreed with laboratory flows where the frequency and intensity of events were greatest in adverse pressure gradients.

A study of the intermittent nature of the Reynolds stress by Gordon and Witting (1977), indicated that the boundary layer turbulence could be separated statistically into two main components. These being large-scale, coherent, momentum transporting events superimposed upon relatively small-scale isotropic turbulence, contributing little to momentum transport. It was indicated that the presence of the large-scale structures limited the precision of the

Reynolds stress estimates in marine flows, where time series are of limited length. The latter structures were found to have dimensions of the order of the boundary layer, appeared to be independant of one another and closely resembled the bursting phenomenon of laboratory flow (see also Gordon, 1975).

In a paper appearing alongside Gordon (1974), Heathershaw (1974) noted the intermittent nature of the Reynolds stress during a comprehensive programme of measurements using electromagnetic heads in the Eastern Irish Sea. Approximately 57% of the stress occured in 7% of the time, with the duration of the events and the period between them given as 5 - 10 and 20 - 100 seconds respectively. Heathershaw (1976, 1979) detailed the results of the above programme, carried out in depths of 10 - 50 m, with boundary layer velocities within 2 m of the bed reaching 50 cm s^{-1}. Turbulence statistics (i.e. $(\overline{u^2})^{1/2}$, $(\overline{w^2})^{1/2}$, $\overline{uw}$, correlation coefficients) were examined between 50 and 200 cm above the sea bed. In addition, the u and w energy spectra and uw co-spectrum were calculated. The spectra indicated the existence of an inertial subrange with a $k^{-5/3}$ dependance, to wavenumbers much lower in the u than the w spectrum. A mean drag coefficient C_{100}, obtained using the quadratic friction law, was given as (1.73 ± 0.18) x 10^{-3}. No significant correlation was found between τ and $1/2\rho q^2$, with only a weak correlation between τ and $1/2\rho\overline{w^2}$. The influence of suspended sediment on the turbulent structure was considered. The energy dissipation rate ϵ, of the order 1 cm^2 s^{-3}, calculated from spectra, was estimated to be 2-10 times greater than the production, calculated assuming a logarithmic velocity profile. Plotted spectra indicated that the turbulence was not fully isotropic. Uncertainties introduced by sensor misalignment and the tilt of the recording rig were discussed. Heathershaw and Simpson (1978), in an analysis of the

sampling error associated with Reynolds stress estimates, attributed the sampling variability in Reynolds stress to the intermittent coherent stress events. An average sampling error of ± 45% was said to be typical in stresses of the order of 10 dynes cm^{-2}. Similar variability was also suggested to be responsible for the large scatter in C_{100} estimates from logarithmic velocity profiles.

A series of measurements made by McPhee and Smith (1976) in the boundary layer below pack ice, driven by the wind at velocities of approximately 24 cm s^{-1}, were probably the first published measurements of mean velocity and turbulent stresses made simultaneously throughout an entire planetary boundary layer. In stationary, neutrally stable flow within 4 m of the under surface of the ice, the Reynolds stress derived from the $\overline{u'w'}$ products, was found to be in reasonable agreement with the value of u_*, derived from the velocity profiles, allowing for the form drag of the lower surface of the ice.

It was demonstrated by Soulsby (1977) that a plot of wavenumber weighted spectra and co-spectra, as a function of wavenumber (k) times measuring height (1), show similarity when scaled by variance, or co-variance for the latter. Comparisons of spectra from the neutrally stratified atmospheric surface and the marine bottom layers showed they coincided. Significant contributions to the variance were made at $kl \approx 0.02 - 1.5$ for u, $kl \approx 0.1 - 20.0$ for w and $kl \approx 0.05 - 15.0$ for uw.

Soulsby (1980) considered six factors (low and high frequency spectral cutoff; stationarity; sampling variability, also discussed by Heathershaw and Simpson (1977); sensor averaging in frequency response and length scales; size of the data set) resulting in conflicting requirements for the choice of record length and

digitising rate, when choosing an averaging interval for data in a tidal bottom boundary. Data collected in Start Bay, using electromagnetic heads, indicated the worst source of error was due to low and high frequency spectral losses in $\overline{u^2}$ and $\overline{w^2}$ respectively, and random errors in $\overline{uw}$. All time series, with record lengths under 12 minutes, were observed to be stationary, with the exception of the mean velocity $\bar{U}$, stationary for record lengths under 8 minutes. Finally, methods for compensating for some of the sources of error were considered.

Ferguson (1979), and Bowden and Ferguson (1980) detailed an experimental programme, using electromagnetic heads, in the Eastern Irish Sea, in shallower water to the south of the area investigated by Heathershaw (1979). An investigation of the Reynolds stress $-\rho\overline{uw}$ and turbulent intensities $\overline{u^2}$ and $\overline{w^2}$ with height above the sea bed, in the range 50 - 200 cm, indicated no variation, excepting a slight increase in $\overline{w^2}$ at 200 cm. Of the above, including $\overline{v^2}$, when normalised by the mean velocity at 100 cm (U_{100}) only the Reynolds stress varied with tidal phase, decreasing on the decelerating phase of the tide. When a constant stress layer was assumed, and the quadratic friction law was applied, an average value of C_{100} for the area was estimated as $(4.35 \pm 0.33) \times 10^{-3}$. Energy density spectra of u, v and w had the same form throughout the tidal cycle, differing only in their general levels. The turbulence appeared to be isotropic for wavenumbers $k \gtrsim 6 \times 10^{-2}$ cm^{-1}, with the spectra diverging at lower wavenumbers, such that the components of the spectra were given as $u \gtrsim v \gtrsim w$. A decrease in the u spectral density was evident with height, whilst that of w increased with height for $k \lesssim 10^{-2}$ cm^{-1} and decreased for higher values of k. Hysteresis effects in turbulent intensities

and Reynolds stress due to accelerating and decelerating flows were found to be small. Surface wave velocities were thought to be negligible at the boundary for mean tidal flows λ 13 cm s^{-1}.

Hamilton, Sommerville and Stanford (1980) examined the sorting of sediments on and around large sand and gravel banks at depths of 40 - 140 m in the Celtic Sea. The mean velocity profile recorded at five positions within 1.8 m of the sea bed was was found to be logarithmic for the majority of the tidal cycle. By comparisons with time lapse super 8 cine photographs, the critical value of u_* for sediment motion was observed to be easily exceeded during maximum spring tides. The influence of surface waves on sediment transport was considered negligible in comparison to that of tidal currents in the area.

Dyer (1980) combined velocity profile measurements, at four points within 2 m of the sea bed in Start Bay, with underwater television observations of the bedforms. This enabled the threshold criteria for sediment motion and the variation of the bedform characteristics with tidal phase to be investigated. An examination of the relationship between z_0 and U_{100} indicated considerable hysteresis. An initial increase of z_0 with U_{100} was followed by a decrease with the onset of sediment motion, continuing beyond peak values of U_{100}. A brief increase of z_0, observed before the cessation of sediment motion, was followed by a rapid decrease during the decelerating phase of the tide. An explanation of this was offered in terms of the varying form of the sand ripples, with z_0 being proportional to u_*^4 during initial ripple growth. Once the threshold was exceeded sediment motion was found to be dependent on the changing bedform drag, varying in time with the mean flow. Finally, the balance of the local tidal dynamics with bottom friction was

considered.

An attempt was made by Soulsby and Dyer (1981) to correct the departure of velocity profiles, near the sea bed in accelerating flows, from the expected logarithmic form. By defining an acceleration length scale the possible form of the velocity profile in such conditions was derived. Using electromagnetic head and velocity profile data, collected in Start Bay and Weymouth Bay, a criterion for non-accelerating flow was derived. From this, and an estimate of von Karman's constant, λ compensating for accelerating effects, a value of $\kappa_0 = 0.40 \pm 0.014$ (von Karman's constant in non-accelerating flow) was arrived at. The value for the two areas was similar, despite the presence of considerable suspended sediment in Weymouth Bay, and comparable to laboratory values in oscillatory rough flows. Some evidence of a decrease in κ_0 with an increase in the ratio of the boundary-layer thickness to z_o was also noted.

Reynolds stress components, recorded over 4 hours at a depth of 42 m on the edge of the Skerries sand bank, were measured by Soulsby (1981), using electromagnetic heads. The ratios of the root mean square values of u,v and w to the friction velocity u_* were estimated, as was the ratio of $|\tau|$ to the turbulent kinetic energy. All were found to be comparable to atmospheric measurements. The Reynolds stress was observed to act at 6^o anticlockwise of the mean current 65 cm above the bed, apparently due to the veering of the mean current caused by the Skerries sand bank. It was further suggested that non-zero values of $-\overline{uv}$ observed during part of the experiment were associated with lateral shear created by the sand bank. Eddy scales contributing to the Reynolds stress were estimated as being in the range 5 - 500 m.

A comparison of turbulent laboratory and geophysical flows,

the latter of which utilised data from other workers in addition to that collected in the River Ouse over accelerating, steady and decelerating phases, was made by Anwar (1981). Values of C_{100} and z_0 determined from logarithmic profiles, appeared to be greatest during accelerating flows in some, but not all of the field measurements. Conversely, turbulence intensities were observed to be highest during decelerating flow in both field and laboratory experiments. An explanation of the latter was offered in terms of the existence of larger eddies in decelerating flow, evident in the higher energy spectra maxima for horizontal velocity and co-spectra in decelerating phases, and those maxima occuring at lower wavenumbers during that period. The duration between, and the frequency of events in the co-spectra was longer and slightly lower, respectively, in decelerating flow during laboratory and field experiments. Although, the interval between events, dependent on boundary layer thickness and mean velocity, appeared shorter in geophysical flows. Statistical properties of u'w', as represented by the probability distribution and the flatness factor, based on the correlation between u' and w' (Heathershaw, 1979), were similar in all flows.

Soulsby, Davies and Wilkinson (1983) summarised the results of an extensive study to examine the processes of sediment transport by tidal currents and surface waves in Start Bay and the Taw estuary. Observations outside periods of rapid acceleration, approximately one hour either side of slack water, indicated the majority of near bed velocity profiles fitted the logarithmic form and were valid to a greater distance from the bed at peak flows. The friction velocity u_* was observed to follow the form of U_{100}, suggesting the drag coefficient C_{100} to be Reynolds number independent, whilst z_0 increased gradually throughout the tide. Variations in z_0 appeared to

be uncorrelated with: changes in the bed geometry; saltation of grains, enhancing momentum transfer from the flow to the bed; suspended sediment, causing a deviation of the velocity profile from the logarithmic form. An examination of the bursting phenomenon showed that the amplitude, frequency and duration of the events increased with velocity and/or bed roughness, although the distribution of their spacing, size and type (bursts, sweeps, downdraught and updraught accelerations) remained roughly constant. Analysis of the flux angle distribution, defined as the proportion of the total Reynolds stress corresponding to water moving at a particular angle to the horizontal, indicated that the majority of the stress resulted from the burst and sweep events. An appreciable reduction in the turbulence intensity was observed during periods of sediment suspension, thought to be due to vertical density gradients inhibiting the production of turbulence as buoyancy fluxes had to be overcome. In addition, the influence of surface wave motion on sediment transport and the nature of the boundary layer formed, with a thickness of the order of millimeters for laminar and centimeters for turbulent flow, was studied in water of depth 6 m.

An experiment performed by McLean (1983) in a West German tidal inlet, known as the Jade, enabled comparisons of the Reynolds stress, obtained from uw fluctuations, to be made with u_*^2 from the mean velocity profile. Ducted impellors were employed to record the Reynolds stress at four positions and the velocity profile at three, within 2.2 m of the bed in a rectilinear flow of maximum velocity 65 cm s^{-1}. Despite a large scatter in the values of u_*^2 when plotted against $-\overline{uw}$, the trend indicated that both techniques gave comparable estimates of stress. The peak stress was found to lag the peak mean velocity (a hysteresis effect), which was explained in terms of the

time taken to distribute turbulent energy throughout the flow. The possible cause of a minimum in z_0 at peak flows was thought to be attributable to the smoothing of sand ripples by the flow as sediment was brought into suspension. As the velocity decreased particles fell out of suspension, reforming ripples and leading to a corresponding increase in z_0. Suspended sediment concentrations were thought too small to extract momentum from the flow and alter the form of the mean velocity profile. Several simple models of the flow and turbulence were considered and found to be in reasonable agreement with the measured data.

Using a primarily observational approach, drawn from marine studies, or laboratory and atmospheric examples when necessary, Soulsby (1983) outlined the principle features of the vertical current structure and turbulence properties in a variety of shelf sea boundary layers. Terms representative of the boundary layer and their inter relationships are defined. A subdivision of the geophysical boundary layer is presented and the nature of the flow in the bed layer (corresponding to the viscous sublayer in Fig. 1.1), logarithmic layer and outer layer is considered. Particular emphasis was placed on the form of z_0 for the varying hydrodynamic nature of the bed. Extending Bowden's (1978) classification, a number of outer layers are examined including: planetary boundary layers; oscillatory boundary layers; oscillatory boundary flow; stratified flow; depth limited flow; and flow over topography. In each case the dominant mechanism and its influence in the formation of the boundary layer was outlined. In addition, the current structure was derived and its variation throughout the layer considered, as was the nature of the turbulence throughout the layer. For each boundary layer considerable use of models and field data was made to illustrate the descriptions.

The measurement of turbulence spectra in shelf sea boundary layers was reviewed. Turbulence variation with tidal phase and topography was also considered. Finally, the nature of the bursting phenomenon was discussed and illustrated by measurements from Start Bay. The variation of the Reynolds stress structure with height, current speed and bottom roughness was summarised.

1.5 SUMMARY

In this chapter it has been attempted to provide an outline of the theory, as regards the generation of fully turbulent flow, in a constant density fluid, at a smooth boundary, in the presence of velocity shear. The composition of the boundary layer is presented in terms of the varying stress layers. A summary of the influence exerted on the flow by the variable nature of the roughness elements is given, followed by equations for the roughness length, boundary shear stress and drag coefficient, as utilised in the following chapters.

Finally, a review of previous experimental work, with particular relevance to the work presented in the ensuing chapters, is given. For a comprehensive review of the theoretical and experimental results relating to the benthic boundary layer, prior to 1978, the reader is referred to a paper by Bowden (1978). Finally, if a clear presentation of the nature of the bottom boundary layer of shelf seas is sought, a paper by Soulsby (1983), summarised at the end of Section 1.4, should be read.

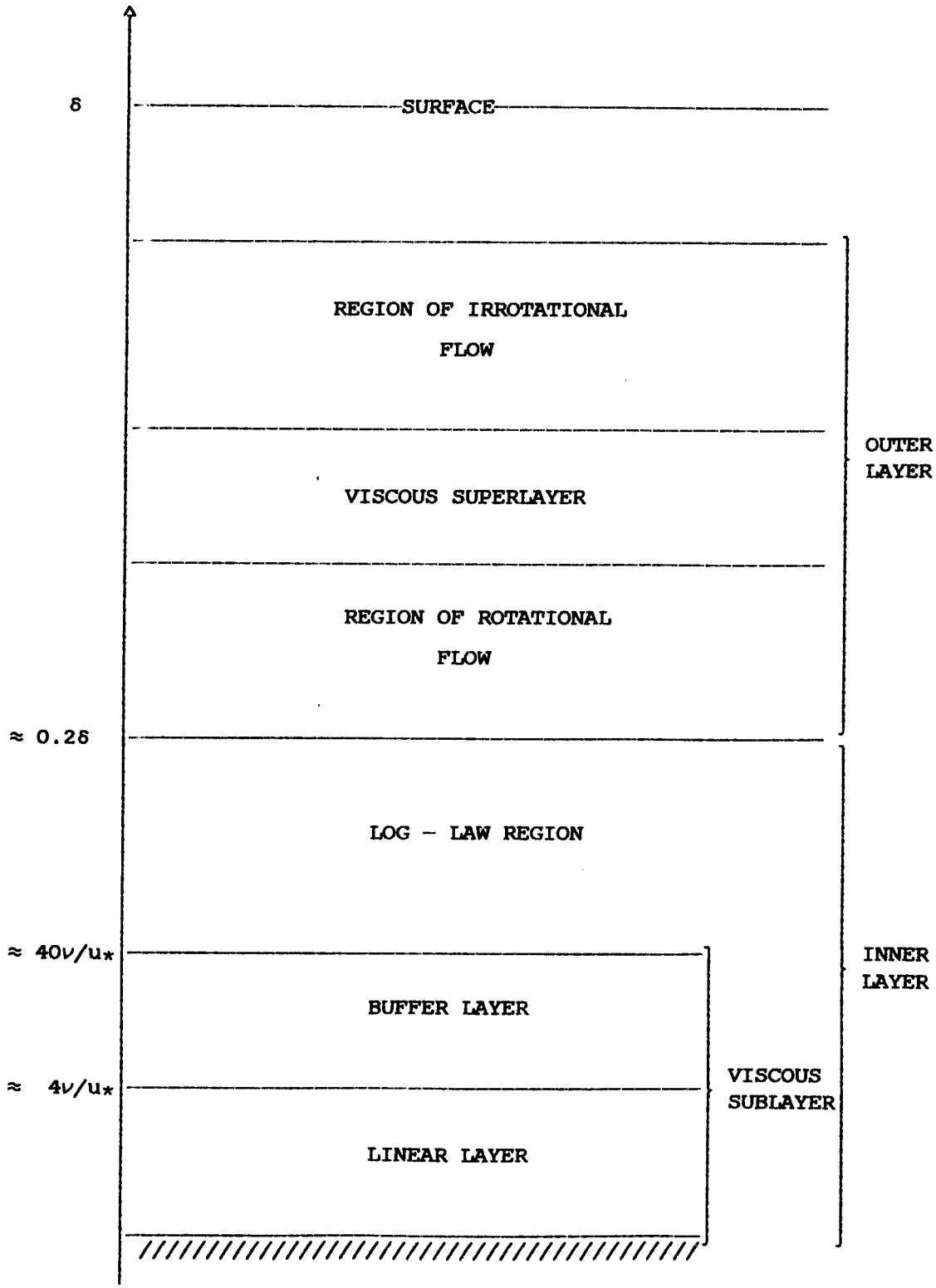

Fig. 1.1 Divisions of an idealised boundary layer (not to scale).

CHAPTER 2 - EXPERIMENTAL PROGRAMME

2.1 INTRODUCTION

The work detailed in the following chapters was an extension of an experimental programme initiated by Professor K.F. Bowden and implemented by Dr. S.R. Ferguson during the years 1975 to 1979. The results were presented by Bowden and Ferguson (1980) and Ferguson (1979). The aims of the programme , prior to 1980, had been to observe variations in turbulence levels over as much of the tidal cycle as possible. The dependence of turbulence characteristics on mean velocity were investigated and compared over the accelerating and decelerating phases of the tide. Simultaneous measurements of the uw components of Reynolds stress at three or four different positions in the boundary layer were made, in order to observe vertical gradients of Reynolds stress. Prior to 1979 data was recorded using an analogue system. A digitaly recording system under development was lost at sea in 1979.

When study for this thesis commenced in October 1980 the development of a replacment system was well advanced. Electromagnetic current meter heads (subsequently termed e.m. heads) to measure the uw component of Reynolds stress, attached to a redesigned turbulence rig, were to be deployed from the R.V. Sarsia on a cruise that month. Data from the cruise is not presented here as the rotors, to be used to measure the velocity profile at four points within 2 m of the sea bed, had yet to be constructed. The use of the e.m. heads and rotors is detailed later in this chapter, and their design and construction in Chapter 3.

2.2 EXPERIMENTAL AIMS

The aim of the experimental programme subsequent to 1980 was to develop a self-contained unit to record turbulent flow within 2 m of the sea bed over the full tidal cycle, in water of depth up to 60 m in the Eastern Irish Sea. It was proposed that measurements of the bottom shear stress should be obtained by the eddy correlation and log-law methods, using four e.m. heads and four rotors respectively. To achieve this an e.m. head and rotor were placed at the same level, with four such pairs spaced evenly above the sea bed as in Fig. 2.1. Initially, data was to be recorded on board ship on magnetic tape, with a tape recorder to be developed as part of the self contained unit on the final cruise. Data would then be transferred to this University's mainframe computer for analysis. Direct comparisons of the Reynolds stress, as measured by the two methods, were then possible. A photographic unit, as described in Section 3.3 and shown in Fig. 3.3, comprising a super 8 cine camera and flash was to be used in an attempt to correlate possible sediment motion with events in the u'w' time series. Several station positions were to be repeated on consecutive cruises to examine differences in turbulence characteristics, if any, over a period of time.

The remainder of this chapter outlines the sampling area, the construction of the turbulence rig, its method of deployment and associated problems, data recording and monitoring, data analysis and a summary of data collected.

2.3 SAMPLING AREA

All deployments of the turbulence rig were carried out in an area of the Eastern Irish Sea, bounded by the English and Welsh coasts to the east and south, and the lines of latitude 54° 0' N and

longitude 4^{o} 30' W to the north and west respectively. The chart given in Fig. 2.2 shows the area of interest,indicating turbulence stations (red figures) and Aanderaa current meter (blue figures) deployment positions as summarised in Tables A1.1 and 2.1 respectively. The combination of factors that contribute to the suitability of this intensively surveyed area for the study of turbulent flow were:

1) A diversity of sediment types and bedforms.

2) A relatively rectilinear flow (ratio of major to minor axis of the tidal ellipse 2.5 m above the sea bed close to station 10 being roughly 4:1 as recorded by an Aanderaa R.C.M. 4) allowing instruments to be deployed almost continuously throughout the tidal cycle without the response of the sensors falling to such a level (see Sections 3.2.2 and 3.4.1) as to necessitate frequent redeployment of the turbulence rig.

3) A periodic reversal of flow, with typical velocities in the range 5 cm s^{-1} to greater than 60 cm s^{-1}, giving accelerating, steady state and decelerating phases of the tidally induced flow.

4) The accessibility of the area combined with well documented characteristics. Added to this, a considerable number of turbulence studies had already been carried out in the area allowing comparisons with previous work to be readily made.

Prior to the deployments of the rig, at each chosen station, side scan sonar and echo sounder surveys were made along lines north to south, and east to west through the proposed station positions. An indication of the bed forms was obtained, with any suspected impediment to the flow in the immediate vicinity of the station leading to a relocation of the station.

Station depths varied from 7.5 m at stations 3 and 11 at low water to 50 m at station 19 at high water. Sediments varied from fine

sand to medium sand, broken shells and scallops north from stations 8 and 18 to station 16 and from thick mud to medium sand, broken shells and scallops west from station 11 to 15. A summary of the sediments obtained, using Shipek grab, and the depth range at each station is given in Table A1.1.

The use of side scan sonar to determine the wavelength and orientation of bedforms along the line of stations west of Blackpool (see Fig. 2.2) failed to indicate the presence of bedforms. This was possibly due to the poor quality of the helix and the generally poor state of repair of the equipment. Even at stations with obvious bedforms, as indicated by the echo sounder (Fig. 2.3a), the side scan failed to indicate bedforms during some periods. The absence of bedforms in the above area, though, was backed up by the echo sounder record from station 13 (Fig. 2.3b), typical of stations along this westward line, as well as stations 19 and 20. This form of record was shown along lines east - west and north - south through the stations. Conversely, the side scan surveys at stations clustered to north of Great Ormes Head and in Red Wharf Bay (Fig. 2.2) indicated bedforms of wavelength 5 to 20 m lying transverse to the tidal flow. The echo sounder record of station 8 indicated bedforms of height upto 2 m, when travelling east - west and, although an extreme example, indicates the type of bedforms present in the area. The short period ripples in Figs. 2.3a and 2.3b are due to wave induced motion acting on the ship. When the turbulence rig was deployed it was hoped to avoid siting it too close to the larger bedforms. This could not be guaranteed, but an indication of adverse topographical effects could be obtained from the signal given by the w channels of the e.m. heads as described in Section 2.5.

The differing bedforms are possibly due to the varying nature

of the sediment (see Table A1.1) between the two cases given above, combined with a less rectilinear flow to the west of Blackpool (the ratio of the major to minor axis of the tidal ellipse was typically 1.2:1) than to the north of Great Ormes Head.

Neil Brown C.T.D. profiles at each station indicated that the water column was well mixed through at least 70% of its depth above the sea bed. Figs. 2.4 and 2.5 give temperature, salinity and $\sigma_{s,t,0}$ profiles at stations 17 and 10 respectively. The salinity and density were calculated from the definitions of the practical salinity scale (UNESCO, 1981) and the International Equation of State of Seawater (UNESCO, 1981a) respectively. Station 17 exhibited the degree of stratification typically present at all the stations during the SH. 7/82 cruise. A summary of the three cruises undertaken during the experimental programme detailed here is given in Section 2.8. Station 10 was representative of all the stations during the J.M. 9/81 cruise. As the C.T.D. was unavailable during the J.M. 4/81 cruise no profiles are considered. There was a tendency for the group of stations to the north of Great Ormes Head to be stratified to a lesser degree than the stations in a line west of Blackpool during the SH. 7/82 cruise. The minimum $\sigma_{s,t,0}$ difference between surface and bottom was 0.446 x 10^{-3} g.cm^{-3} at station 18 and the maximum 1.395 x 10^{-3} g.cm^{-3} at station 13. Although stations along the line west of Blackpool were all within $\pm$ 0.120 x 10^{-3} g.cm^{-3} of the value for station 13. This situation did not exist during the J.M. 9/81 cruise, with no stratification evident at any station. Both cruises were at the same time of year (see Table A1.2 for dates) and over similar neap and spring tides. Simpson, Hughes and Morris (1977) have suggested that marginal stratification may exist in the area surveyed, during periods of low wind stress. Fig. 2.6 gives a plot of

the square of wind velocity (wind stress is proportional to (velocity^2)) for the periods from March to the 8th. August during 1981 and 1982. The data was collected at I.O.S. Bidston on the Wirral, and was assumed to be representative of the conditions prevailing in the area of interest. The build up of the thermocline generally begins during March or April, when the input of heat to the sea exceeds losses. With the exception of a period in April and May, the wind stress was lowest during 1982 when the thermocline was observed. In addition, weekly averages of wet bulb temperatures (Fig. 2.7) and hours of sunshine (Fig. 2.8) were greater during 1982, with the exception of a three week period of sunshine in June and July. This would suggest heat input was greatest in 1982. It would appear that the presence of stratification in 1982 was attributable to a combination of lower wind stress and higher surface heat input than in 1981, during the period discussed. None of the C.T.D. profiles extended to the sea bed to avoid damage to the instrument.

It is reasonable to assume that the final few metres of the water column are at least equally as well mixed as the column 5 m above the sea bed. If the local Richardson number, as defined by:

$$Ri = -\left[\frac{g}{\rho}\frac{\delta\rho}{\delta z}\right] \times \left[\frac{\delta u}{\delta z}\right]^{-2}$$

is ≤ 0.25 then stratification is insufficient to suppress turbulence (Simpson, 1975). Above this value the suppression of turbulent intensities occurs over a range, rather than an immediate "cut off". A number of workers (Heathershaw, 1979 and Soulsby, 1983) suggest Ri ≤ 0.03 to define neutrally stratified conditions. Considering the last metre of the C.T.D profiles (δz = 100 cm), the typical density ($\delta\rho$) and mean velocity (δu) differences were 4.0×10^{-6} g.cm^{-3} and 5 cm s^{-1} respectively. This gives a Ri of the order 0.02, well below the

value of 0.25 quoted for the suppression of turbulence and within the limit for neutral stratification. As the C.T.D. profiles only extended to within 4 m of the sea bed an over estimate of R_i is likely, as $\delta\rho$ will, in all probability, be a minimum in the 2 m above the sea bed. The value of δu was obtained from the velocity profiles within 2 m of the sea bed at a mean velocity of $\approx$ 25.0 cm s^{-1}. At peak velocities of $\approx$ 50.0 cm s^{-1} δu reaches values of 8.0 cm s^{-1} further reducing R_i.

Calibration of the temperature sensor, against a platinum resistance thermometer, and the conductivity sensor, against a Plessey Bench Salinometer, of the C.T.D. had previously been carried out in the Oceanography Department (Boxall, 1985). It was suggested that the above sensors were subject to some degree of drift, $\approx$ 0.0018 ^{o}C in temperature and $\approx$ 0.068 $^{o}/_{oo}$ in salinity over a four week cruise. In addition to this there was an offset from the calibration standard for temperature of +0.04 ^{o}C, which was applied to the data of Figs. 2.4 and 2.5. As one deployment of the C.T.D. took less than 5 minutes the effect of drift in the relative values during a deployment was negligible. The offset in temperature had also negligible affect ($\angle$ 0.01%) when calculating salinity and density over the maximum temperature range of 3.7^{o}C.

A string of Aanderaa R.C.M. 4 current meters were deployed from 'U'- shaped moorings, as shown in Fig. 2.9. For the purpose of this work the data obtained was used to give an indication of the tidal flow in the general deployment area. Table 2.1 gives the position and deployment duration for each mooring, the ratio of the major and minor axis of the tidal (M_2) ellipses at the bottom meter and the height of the meters above the sea bed. Velocities were obtained by inputing the Aanderaa data, previously transferred onto

paper tape, into the University's I.C.L. 1906S mainframe computer. Standard calibrations supplied by Aanderaa (1981) were then applied to give north and east components of velocity in cm s^{-1} and the direction of flow relative to magnetic north.

The ratios of the major to minor axis of the tidal ellipses were obtained by Fourier analysis on each station's data. As the deployments never exceeded 5 days (Table 2.1) there was insufficient data to apply harmonic analysis (Dronkers, 1964). Analysis on both the north (u) and east (v) components of velocity was carried out, yielding two equations of the form:

$$u = A_1 \cos 2\Theta + B_1 \sin 2\Theta$$

$$v = A_2 \cos 2\Theta + B_2 \sin 2\Theta$$

A_1, A_2, B_1 and B_2 are constants obtained from the analysis, representing the dominant semi - diurnal terms, $\Theta = nt/2$, where n = the speed of motion and t = the time taken from any assigned time origin. A plot of the resulting values of u and v, for the two equations, against one another yields an ellipse. This was representive of the dominant terms in the tidal motion, so giving an estimate of the complete tidal ellipse. An indication of whether the flow was rectilinear was obtained by the ratio of the major to minor axis of the tidal ellipse, a large major axis relative to the minor axis indicating an approximation to rectilinear flow.

The one exception to the above was CM5, which was deployed for 22 days. It had been intended that this station be occupied for no longer than 4 days. The batteries in the meters had not been changed, which was poor practice, and the recording was reliable for only 8 days. This was indicated by the reference number, recorded on channel one of the magnetic tape, varying by more than ±1 from its fixed value with a fully charged battery (see Aanderaa, 1981).

2.4 CONSTRUCTION OF THE TURBULENCE RIG

The rig was constructed as shown in Fig. 2.1, the frame of which consisted mainly of 2 inch aluminium scaffold tubing. All instrument packages were placed downstream of the sensors, with the exception of the camera, which was situated on the central pole above the sensors. Six 60 kg. lead weights, 2 per leg, were attached to prevent movement of the rig in the flow during deployment (see Fig. 2.1). Stainless steel struts of 1/4 inch diameter were attached from the top of the central pole to each foot to take the strain of flexing during lifting. The rig was lifted on a steel bridle hinged at two feet, with the third foot pointing downstream from which the electronics cable and the backup recovery rope were trailed. It was felt that this assisted the orientation of the rig in the desired direction by the flow.

2.5 DEPLOYMENT OF THE TURBULENCE RIG

The rig was deployed using a hydraulically controlled 'A'-frame and capstan. The two N.E.R.C. research vessels used were the 'R.R.S. John Murray' and the 'R.R.S. Shackleton' (see Section 2.8 for details). On the former, deployment was over the stern and on the latter, from the port side. Previous experience (Ferguson, 1979) had suggested that rather than try to maintain the vessel on station with several anchors, both fore and aft, it was simpler and as effective to use a single bow anchor. The rig was deployed as soon after slack water as possible, with the vessel orientated into the flow and swinging through an arc of no more than 60^{o}. A bridle, hinged at the base of the rig and attached by rope to the vessel, was used as a lowering point (Fig. 2.1). The backup rope and umbilical electric cable were kept reasonably taut when lowering to assist in

orientation. Once on the sea bed the orientation w.r.t. (with respect to) the flow was checked on chart recorders (see Section 2.6). This could only be done if one e.m. head was recording uv components of flow. Chapter 4 gives a fuller explanation, with Table A1.2 indicating on which deployments (or trials) and with which e.m. head uv was being recorded. If one leg of the rig was placed on an unusually large bedform this was indicated by high signal levels on the w channels. If either of the above occured the rig was redeployed until its position was acceptable. The logic unit was then switched on and the data recording commenced.

The approximate length of cable and rope between the ship and rig was equal to one and a half times the water depth, to guard against the swinging of the vessel at anchor dragging the rig. Despite this precaution and the regular visual checks on the cable and rope tension the rig moved a number of times. In the case of trial 182, two rotors were smashed and the stem of an e.m. head bent. If the above occured, or the angle of flow w.r.t. the rig became too great, the rig was redeployed after inspection.

The prevailing wind velocity relative to the tidal flow was one of the main factors which determined the deployment period. A steady wind from the ships bow, with the bow facing into the tidal stream, generally prolonged deployments, ocassionally beyond the turn of the tide. On the other hand, with a wind from the stern quarter deployments were shortened, both over the accelerating and decelerating phases of the tide.

Upon recovery the rig was, ideally, lifted vertically from the sea bed. If the wind was holding the ship away from the rig's position it was occasionally dragged along the sea bed. Generally little damage was caused, with the exception of trial 182 (see Section

2.8.3). Once out of the water the rig was lashed to the side of the vessel.

As was mentioned previously it was originally intended to deploy the rig as a self contained unit on the final cruise. Several power packs were constructed to power all the sensors and the photographic unit (described in Section 3.3) for up to 15 hours. Unfortunately the tape on the recorder occasionally ran off the spool when a flag, to indicate when to start recording on a new track, was ignored. It was decided to continue recording on board ship rather than risk the loss of data that may have resulted.

Despite this, several successful deployments and recoveries of the rig, stripped of all the sensors and recording equipment, with the exception of a pressure activated transducer for location and a buoyed rope for recovery, were performed. The advantage of such a rig would have been that periods of low stress close to slack water could have been recorded, although not during the period of highly variable current direction at slack water. Incidences of damage and breaks in the turbulence record would also have been reduced. The rig in its present form would have been of limited value in the less rectalinear region of flow to the west of Blackpool. To correct this the sensors would need to be orientated into the mean flow by means of some form of damped vane.

2.6 DATA RECORDING AND MONITORING

Following satisfactory deployment of the rig, data from the sensors, sampled 5 times a second, was recorded on a 9 track Kennedy 9800 tape recorder. In addition, analogue signals from the e.m. heads were monitored on four two-channel chart recorders. Irregularities in the attitude of the rig were readily detectable on these constantly

monitored records. Mean flow velocities from the rotors could be sampled periodically using four digital venner counters. A fuller description of the data formating and the recording electronics is given in Sections 4.2 and 3.5 respectively.

Upon recovery, end of file marks were inserted after each data file on the Kennedy recorder.

2.7 DATA PROCESSING

Initially, data was analysed on the University's I.C.L. 1906S mainframe computer, but the majority was analysed on an I.B.M. 4341 mainframe, introduced part way through this study. For the most part programmes were written by the author in FORTRAN.

Data was read from the 9 track Kennedy I.B.M. compatable tapes directly into the I.B.M. filestore. After code conversion, character manipulation and conversion to e.m. head voltage levels, the data was stored for future reference on the Computer Laboratory library tapes.

Data processing included: the application of flume calibrations for the rotors and e.m. heads (calibration procedures are described in Chapter 3) ; a determination of e.m. head offsets; the generation of turbulent time series; an attempt to verify that the idealised conditions for which the log-law of equation 1.11 is derived, could be said to exist; an examination of the effects of sensor misalignment; comparisons of stresses from e.m. heads and rotors; an investigation of possible variations in u_* and z_0 with tidal phase and station position; inspection of photographs in conjunction with the turbulent time series; and an investigation of the structure of the Reynolds stress.

A detailed discussion of the analysis is given in Chapters 4 to 8, inclusive.

2.8 DATA SUMMARY

The turbulence rig described here, was deployed in varying stages of development, during three cruises on N.E.R.C. research vessels in the Eastern Irish Sea.

Chronologically the cruises were:

1) John Murray cruise J.M. 4/81 in april 1981.

2) John Murray cruise J.M. 9/81 in july to august 1981.

3) Shackleton cruise SH. 7/82 in july to august 1982.

A summary of turbulence rig deployments is given in Table A1.2 indicating trial number, date and duration of the trial, the station at which the trial occured, useful record length, the tidal state (flood or ebb) during the trial, which e.m. head, if any, recorded uv components of flow rather than uw and the position on the rig of inoperative rotors. Following the summary the heights of each pair of sensors above the sea bed is also given. Table A1.1 summarises the position, water depth during trials and the bottom sediment characteristics of each station. Aanderaa deployment positions, as shown in Fig. 2.2 and denoted by CM1 to CM7, are summarised in Table 2.1. Mooring positions, dates and deployment durations, water depth, ratio of major to minor axis of the tidal ellipses and the heights of each rotor above the sea floor are given.

2.8.1 J.M. 4/81

In total 24 trials at 6 stations were carried out during J.M. 4/81 cruise. After only two trials a design fault in the lifting bridle caused the rig to free fall to the sea bed. Fortunately the problem had been spotted before the bridle parted and a rope and pellet floats attached. One full day's data (4 trials) was lost recovering and checking the rig. Subsequently, the rig was deployed

from an attachment point at the top of the central pole. Unfortunately data from trials 92 - 94 was overwritten, as the tape was stored in the wrong location and left unlabelled. During trial 98 at station 3, the shallowest station, surface wave noise masked turbulent fluctuations, with trials having to be continued during a period of calmer weather. Force 10 gales shortened the cruise by several days and the Aanderaa mooring (CM3) had to be abandoned, but was recovered by a group from I.O.S. Bidston approximately a month later. Throughout the cruise the orientation of the rig w.r.t. the flow was unknown, as not one of the e.m. heads was employed to record the uv components of flow.

2.8.2 J.M. 9/81

This cruise was blessed with exceptionally calm weather enabling 38 trials at 8 stations to be recorded. For trial numbers greater than 122 (Table A1.2) the second e.m. head from the sea bed recorded uv fluctuations allowing the orientation of the sensors w.r.t. the flow to be determined. During trial 139 the covering of the sea cable between the electronics and the ship became damaged, causing water to enter the electronics through a gland on the electronics casing. Only the circuitry of rotor three appeared to come in contact with the water, so rendering the rotor useless. The offending length of cable was removed between tides and no further data was lost. The reed switch for rotor 3 was flooded during trial 142, due to a break in the cable leading to the electronics. This was replaced for the following trial with out further data loss. On recovery of the 'U' - shaped mooring (CM5) from the second deployment, the meters had obviously been detached manually as the shackles had been removed, attaching the current meters to the anchor

clump and the subsurface bouy. This was possibly done by a trawler that was operating in the area if its trawl gear had become entangled with the mooring cables. The subsurface bouy was later found on the beach at Formby. This resulted in the loss of approximately 7 days data, which fortunately was not crucial to the experiment.

2.8.3 SH. 7/82

Despite less favourable conditions than the J.M. 9/81 cruise, 36 trials at 7 stations were achieved during the cruise. Two of the stations, 17 and 18, were chosen as they occupied the same positions as two stations, 8 and 14 (see Table A1.1 and Fig. 2.2 for cruises and positions), thus enabling comparisons between the two cruises to be made. Several stations of depth 45 m and greater were occupied, although the shortage of cable caused by splicing after previous breaks occasionally proved a limitation. On recovery after trial 162 the sea cable parted and the subsequent flood tide was missed whilst repairs were effected. For trials 167 - 177 inclusive, e.m. head 3 measured uv. For the remainder of the cruise e.m. head 1, unfortunately with a bent stem as there were no replacments, measured uv, whilst head 3 measured uw (see Table A1.2 for a summary). Upon recovery during trial 182 the sea cable was entangled in the rig, badly damaging two rotor frames and bending the stem of an e.m. head. The e.m. head was replaced whilst the two rotor frames were repaired during trial 183. The photographic unit was attached for trials 186 - 188, 192 and 193. It was originally designed to be powered from a rechargable battery pack available for use with the self contained rig. As this was not deployed, non-rechargable batteries, originally intended for testing the unit, were used, limiting the number of deployments to the trials given above. From trials 192 - 195

inclusive, the channels on the e.m. heads suffered offset problems for approximately the first half hour of the deployments. Throughout trials 194 and 195 rotor 4 was defective. These defects were attributed to the sea cable being badly worn with the protective covering being ruptured in several places. Fortunately it was not necessary to terminate the cruise, but further deployments from ship would have required a new length of cable.

2.9 SUMMARY

A total of 98 trials at 21 stations were made during the three cruises summarised in Section 2.8. In total 302 hours 11 minutes of data was recorded, of which 130 hours 24 minutes was considered to be of sufficiently high quality to be analysed fully (see Chapter 4 for details). There were 469 photographs taken with the flash functioning. Only 95, taken during trial 186, were examined in sufficient detail to present the results given in Chapter 8. Unfortunately the viewer and film were stolen before further trials could be examined.

In conclusion it can be said that the turbulence system performed well, within its limitations. The most serious of these being: the inability to align the sensors into the flow and so record over an entire half tidal period, especially in the low velocity region; it could not be deployed remotely so a full tidal cycle was not recorded and the research vessel was not freed for other work; the lack of power for the photographic unit and the inability to produce the desired number of photographs, as detailed in Section 3.3.

Despite the above limitations enough data, of a sufficiently high quality, was recorded to examine the characteristics of the

turbulent flow in the area detailed in Section 2.3. In particular, an extensive comparison of the stresses obtained by the eddy correlation and log-law methods was made over a number of different sediment types and the majority of the tidal cycle. Lastly, a degree of correlation between 'bursting' events in the turbulence spectrum and sediment motion as viewed by the photographic unit was made. These results are presented in further chapters.

The survey in the surrounding area of the turbulence stations could have been improved with the aid of a more reliable side scan sonar. Despite this the survey appeared to give sufficient information to position the rig satisfactorily. A reliable indication of the bedforms would have been of use in determining whether they had any discernible affect on the turbulence parameters.

The use of the C.T.D. indicated the assumption of non-stratified flow when analysing the data, quoted in the theory of Chapter 1, to be correct. The Aanderaa deployments gave an indication of the form of the tidal ellipses in the general area of each station. This suggested that even a self-contained rig in its present form would have been unsuitable for deployment in the area to the west of Blackpool. This also applied at periods of low tidal flow to the north of Great Ormes Head when current direction was highly variable. The modifications suggested in Section 2.5 would rectify this.

Fig. 2.1 Photograph of the turbulence rig. The rig, shown on the aft deck of the R.R.S. John Murray, was lifted from point A on the bridle, which is hinged at points B. The umbilical electrical cable was trailed from point C, assisting in the orientation of the rig. When situated on the sea bed the flow would ideally have come from the far side of the rig, as shown above. Cylinder D contained the recording electronics outlined in Section 3.5, whilst the three struts leading from the base to to the central pole provided rigidity during lowering and lifting, and hopefully minimised vibrations during deployment. Also indicated are the positions in which the camera and flash housings were placed.

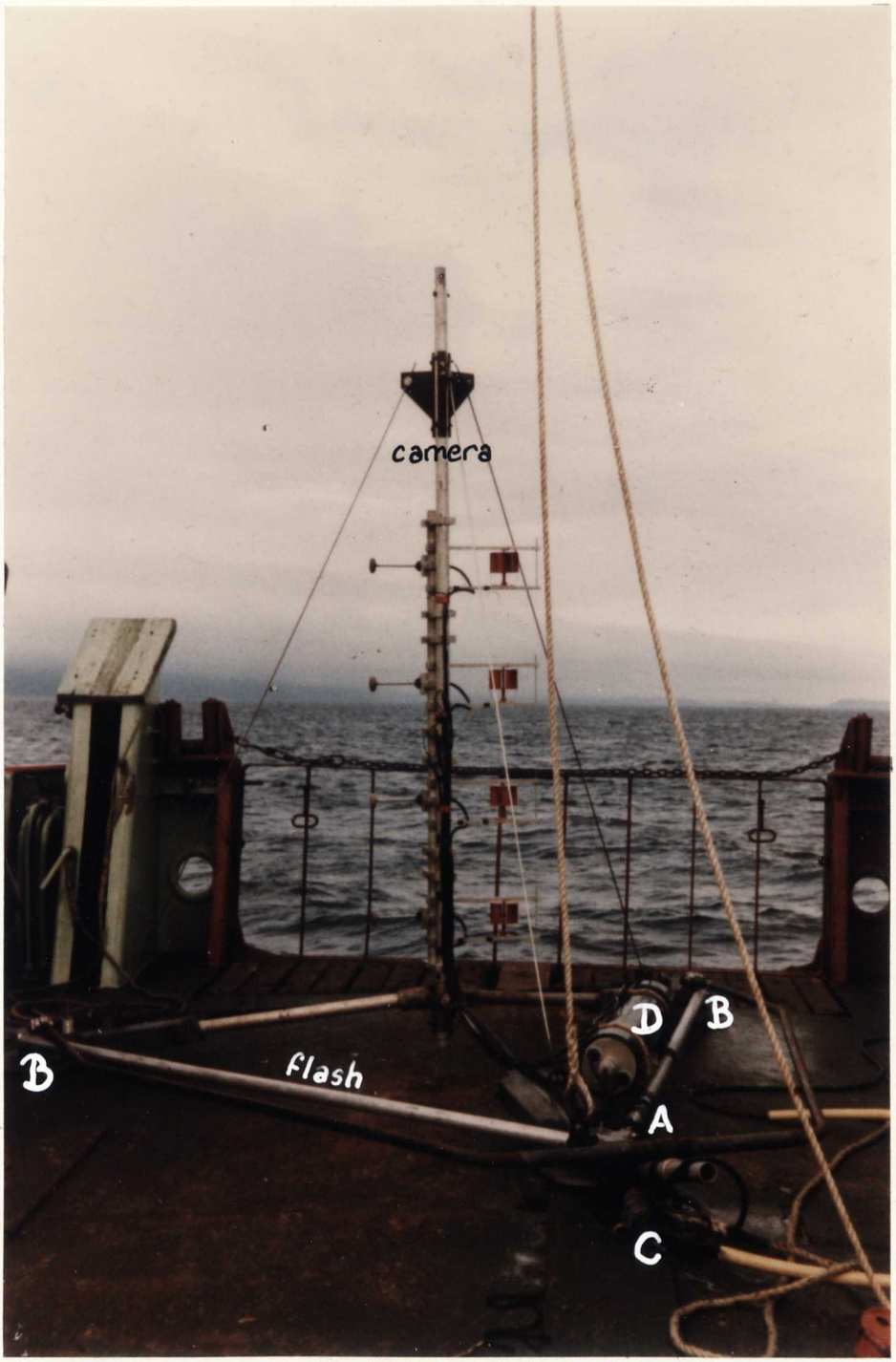
camera
D
B
B
flash
A
C

Fig. 2.2 A chart of the Eastern Irish Sea. Indicated, are the positions of the turbulence stations (red characters), Aanderaa deployments (blue characters) and relevent reference points. Contours are marked in fathoms, whilst the coast line is represented by the thick continuous line.

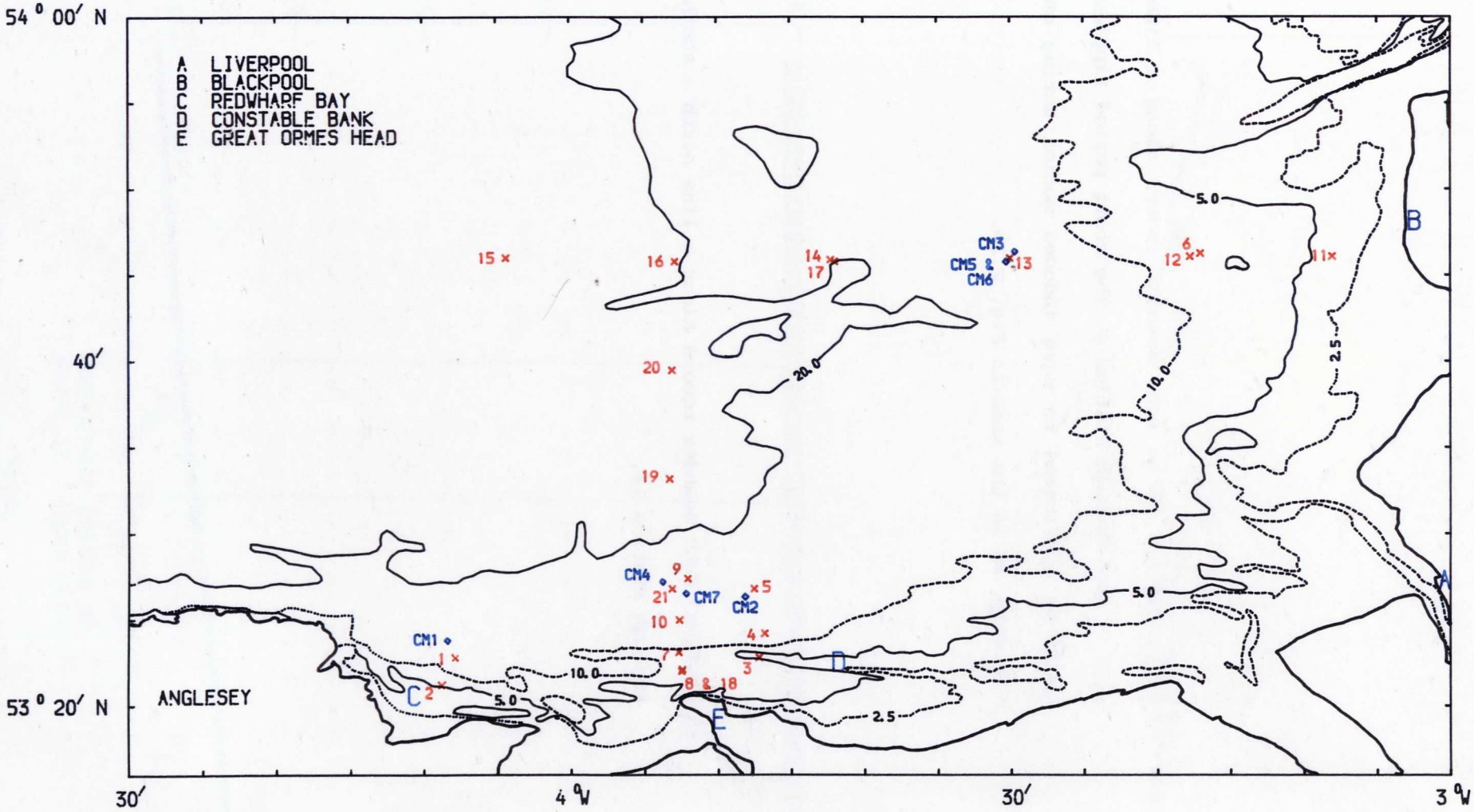
54° 00′ N
40′
53° 20′ N
30′
4°W
30′
3°W
A LIVERPOOL
B BLACKPOOL
C REDWHARF BAY
D CONSTABLE BANK
E GREAT ORMES HEAD
ANGLESEY
5.0
10.0
20.0
2.5
CM1
CM2
CM3
CM4
CM5 & CM6
CM7
1
2
3
4
5
6
7
8 & 18
9
10
11
12
13
14
15
16
17
19
20
21

Fig. 2.3 a) (TOP) Section of an echo sounder record along a line east - west through station 8. The short period ripples could be attributed to wave induced motion acting on the ship, as is the case in Fig. 2.3b.

b) (BOTTOM) Echo sounder record along a line north - south through station 13.

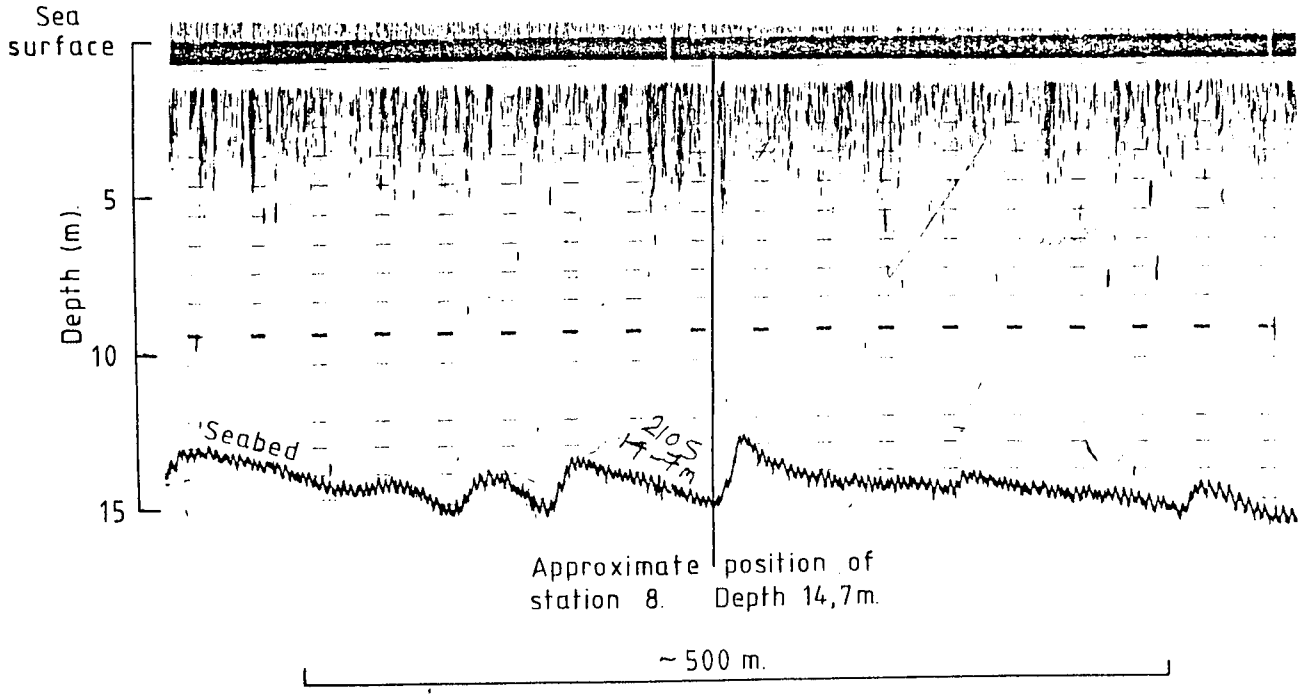
Sea surface
5
Depth (m)
10
15
Seabed
Approximate position of station 8. Depth 14,7m.
~ 500 m.

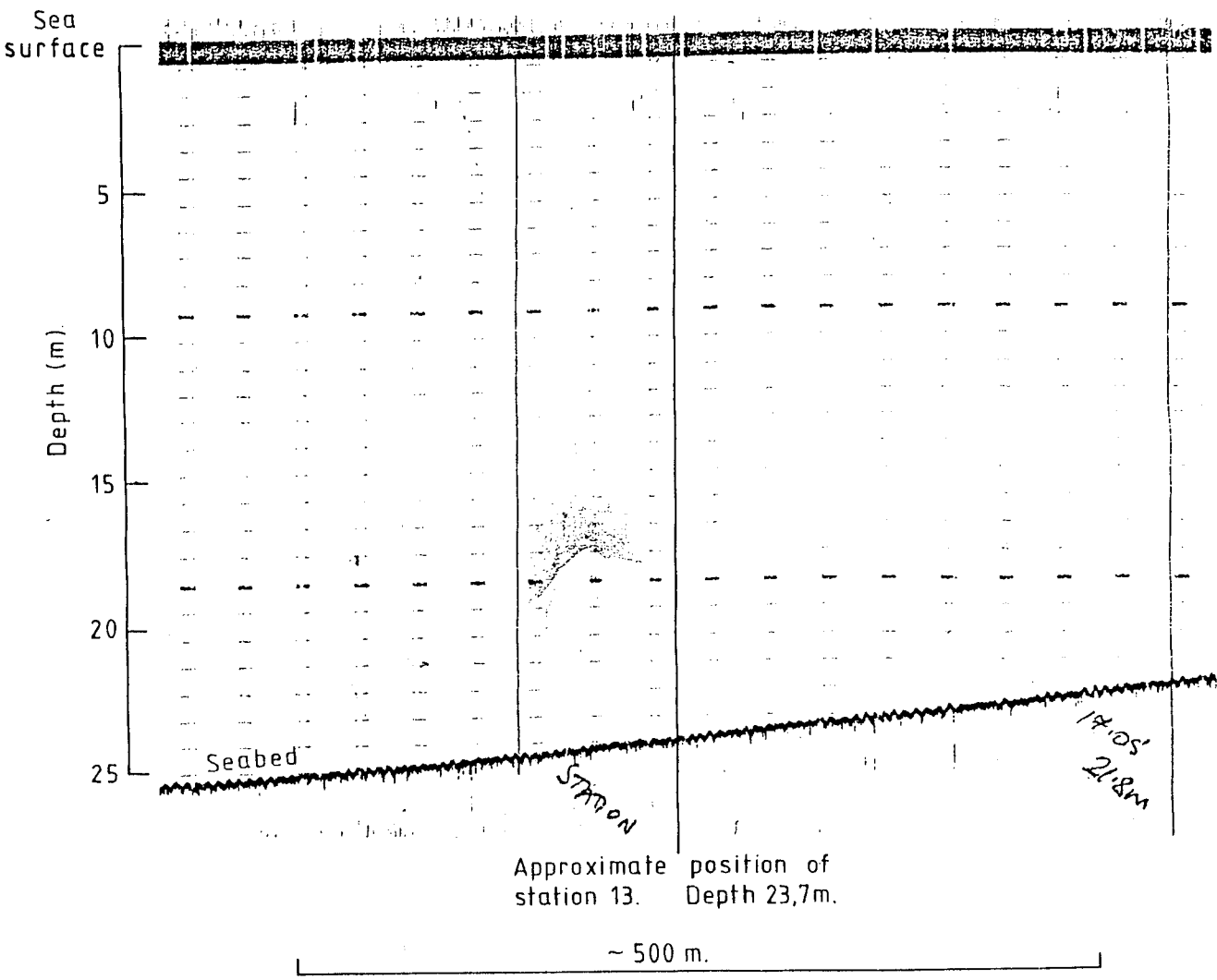
Sea surface
5
10
Depth (m)
15
20
25
Seabed
Approximate position of station 13. Depth 23,7m.
~ 500 m.

Fig. 2.4 A salinity, temperature and $\sigma_{s,t,p}$ profile at station 17. The water column was well mixed below the thermocline, present between the depths of approximately 5 and 10 m. Also of note was the wind mixed surface layer.

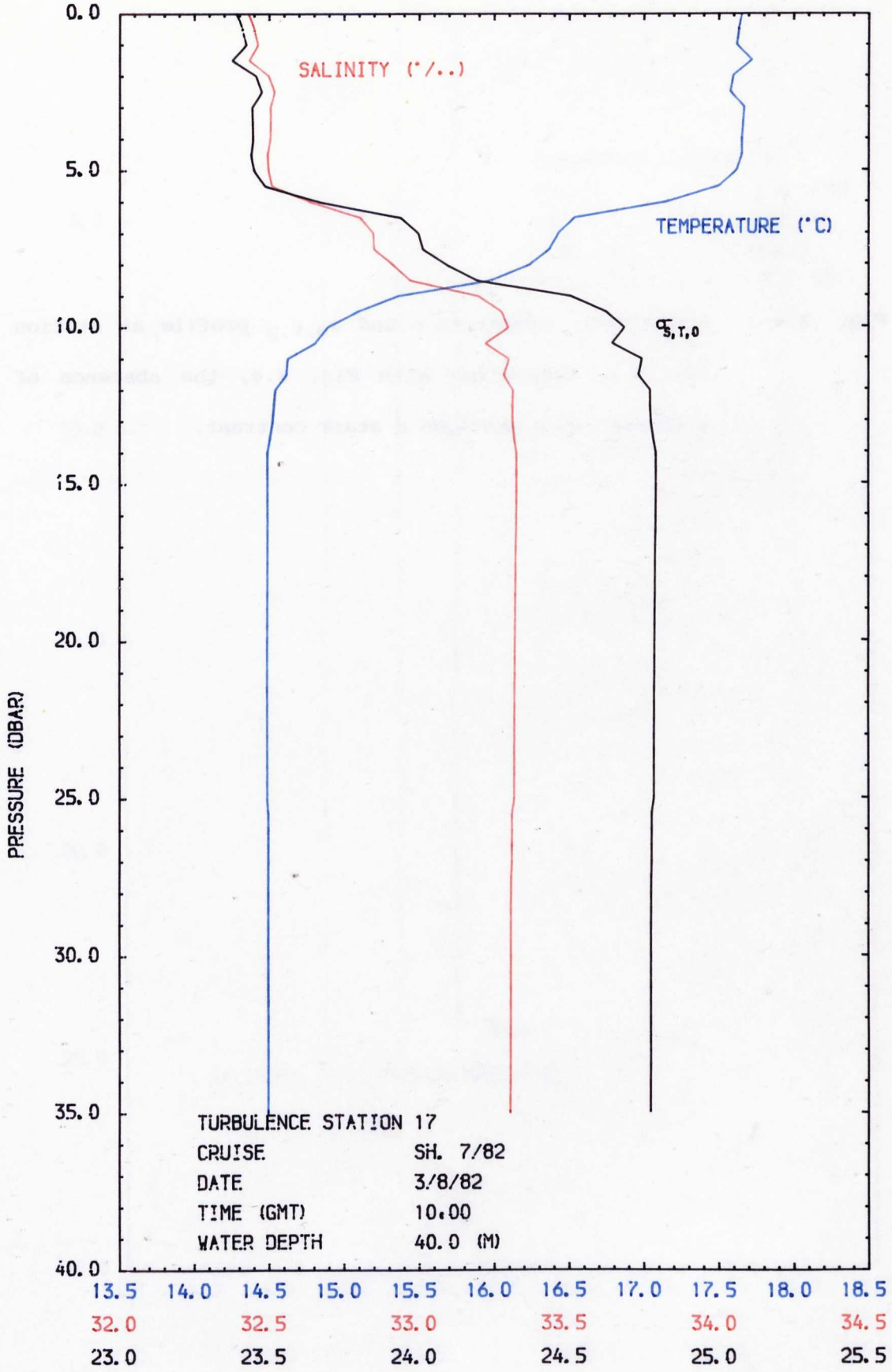
SALINITY (°/..)
TEMPERATURE (°C)
$\sigma_{S,T,0}$
PRESSURE (DBAR)
0.0
5.0
10.0
15.0
20.0
25.0
30.0
35.0
40.0
TURBULENCE STATION 17
CRUISE SH. 7/82
DATE 3/8/82
TIME (GMT) 10.00
WATER DEPTH 40.0 (M)
13.5 14.0 14.5 15.0 15.5 16.0 16.5 17.0 17.5 18.0 18.5
32.0 32.5 33.0 33.5 34.0 34.5
23.0 23.5 24.0 24.5 25.0 25.5

Fig. 2.5 A salinity, temperature and $\sigma_{s,t,p}$ profile at station 10. In a comparison with Fig. 2.4, the abscence of stratification provides a stark contrast.

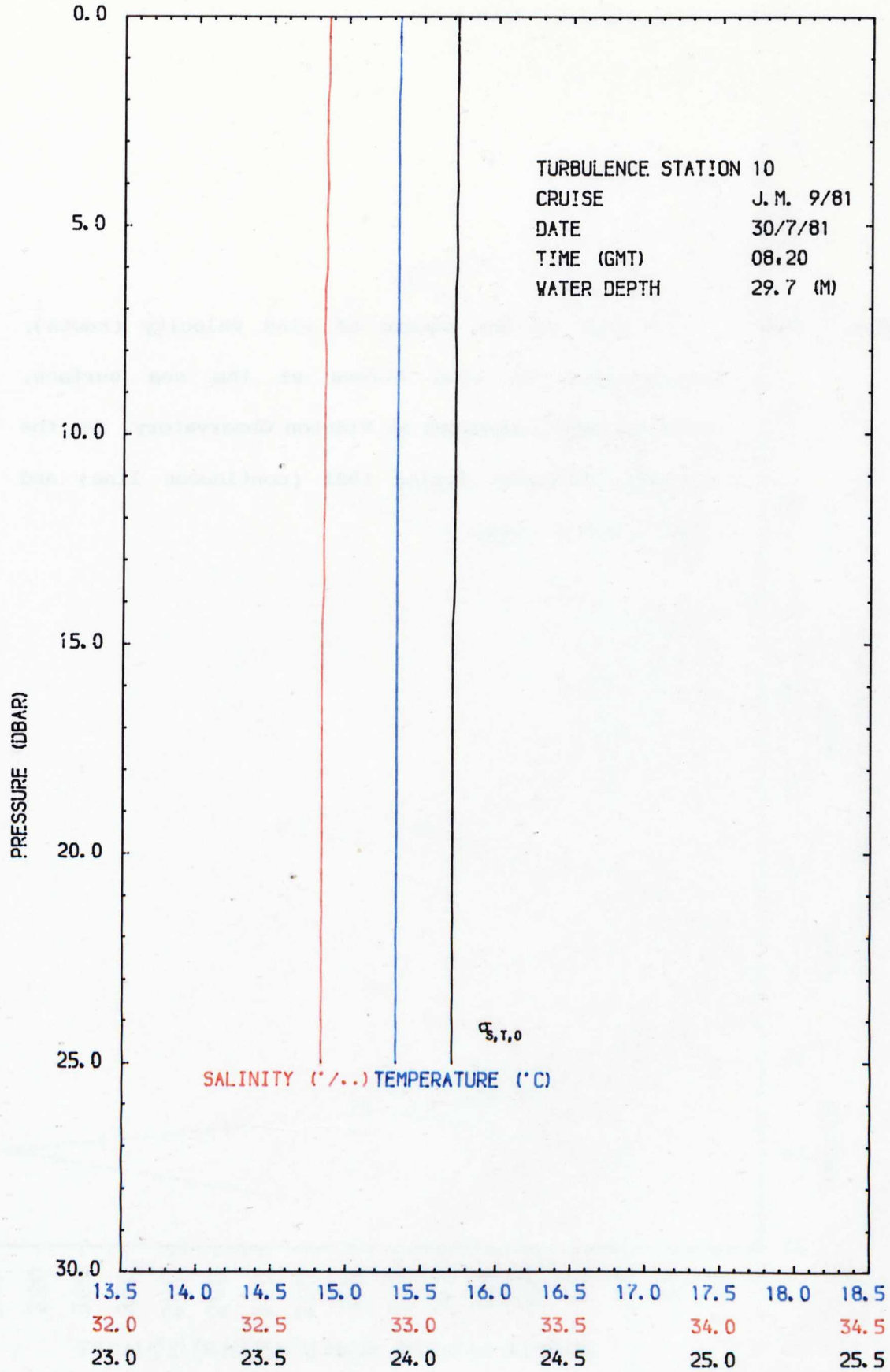
TURBULENCE STATION 10
CRUISE J. M. 9/81
DATE 30/7/81
TIME (GMT) 08.20
WATER DEPTH 29.7 (M)
PRESSURE (DBAR)
0.0
5.0
10.0
15.0
20.0
25.0
30.0
$\sigma_{S,T,0}$
SALINITY (‰) TEMPERATURE (°C)
13.5 14.0 14.5 15.0 15.5 16.0 16.5 17.0 17.5 18.0 18.5
32.0 32.5 33.0 33.5 34.0 34.5
23.0 23.5 24.0 24.5 25.0 25.5

Fig. 2.6 A plot of the square of wind velocity (knots), proportional to wind stress at the sea surface. Readings were collected at Bidston Observatory, for the periods indicated during 1981 (continuous line) and 1982 (broken line).

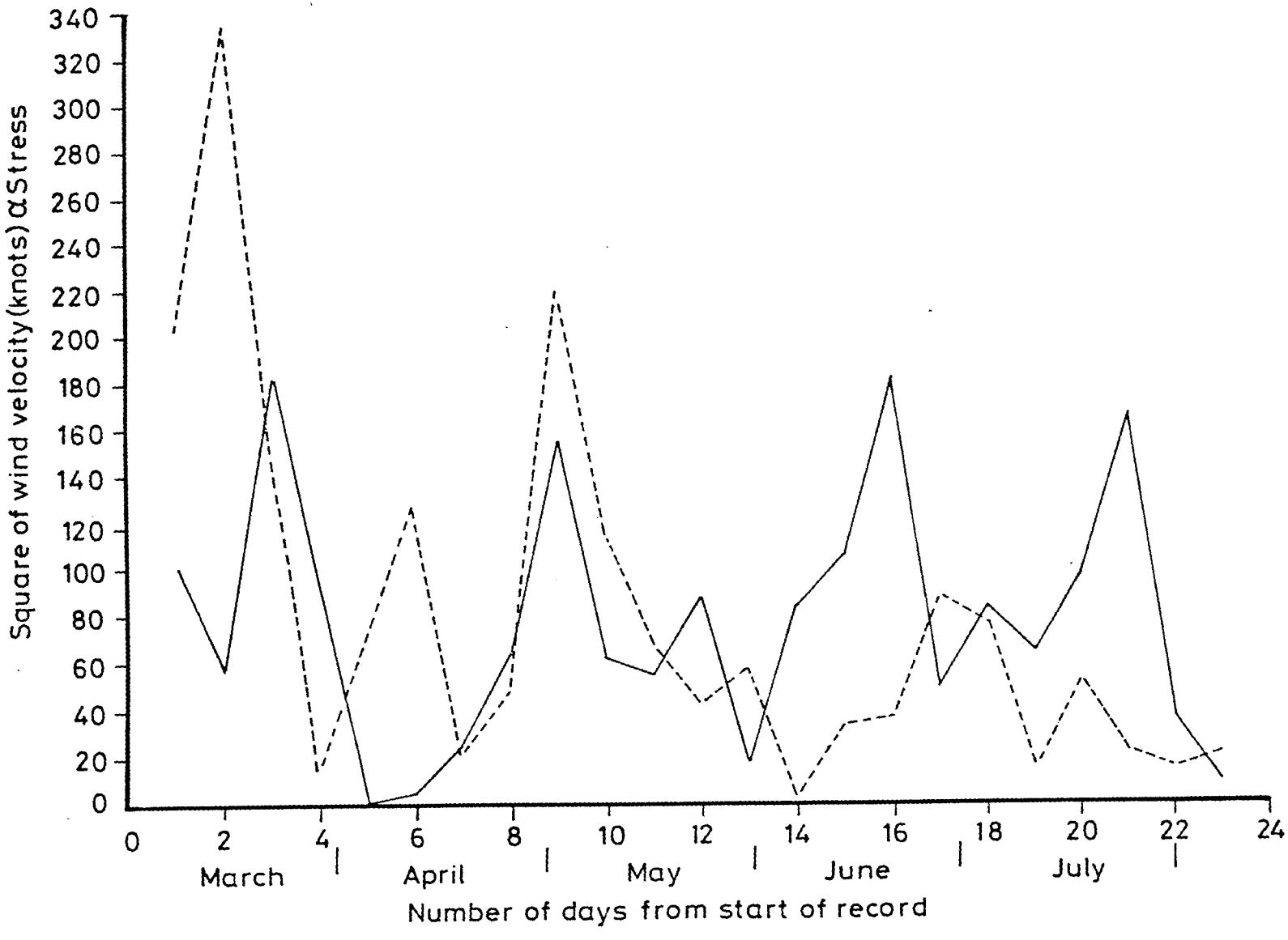
Square of wind velocity (knots) α Stress
340
320
300
280
260
240
220
200
180
160
140
120
100
80
60
40
20
0
0
2
4
6
8
10
12
14
16
18
20
22
24
March
April
May
June
July
Number of days from start of record

Fig. 2.7 A plot of wet bulb temperature (^{o}C). Data was recorded at Bidston Observatory for the periods indicated during 1981 (continuous line) and 1982 (broken line).

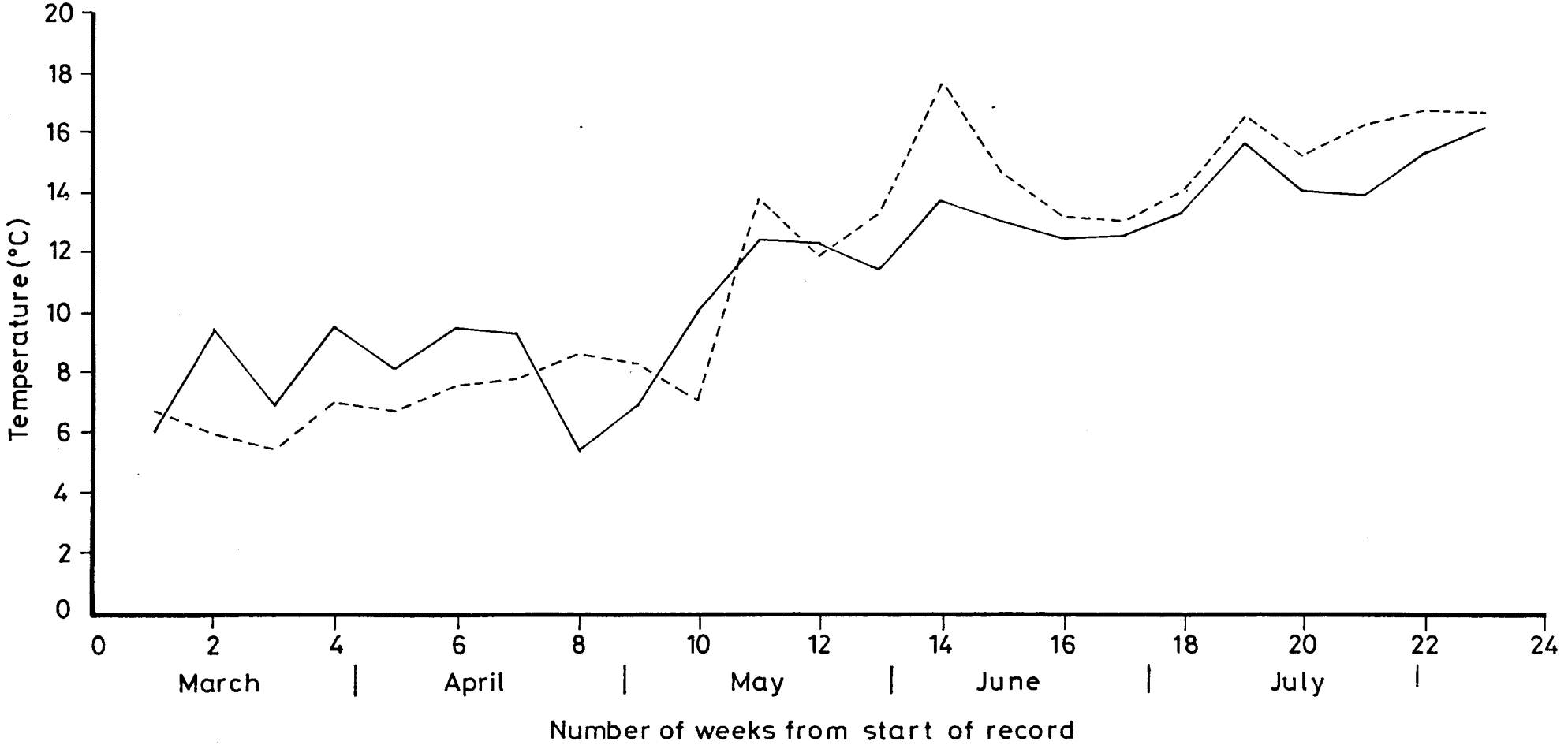
Temperature (°C)
20
18
16
14
12
10
8
6
4
2
0
0
2
4
6
8
10
12
14
16
18
20
22
24
March
April
May
June
July
Number of weeks from start of record

Fig. 2.8 A plot of hours of sunshine. Data was recorded at Bidston Observatory for the periods indicated during 1981 (continous line) and 1982 (broken line).

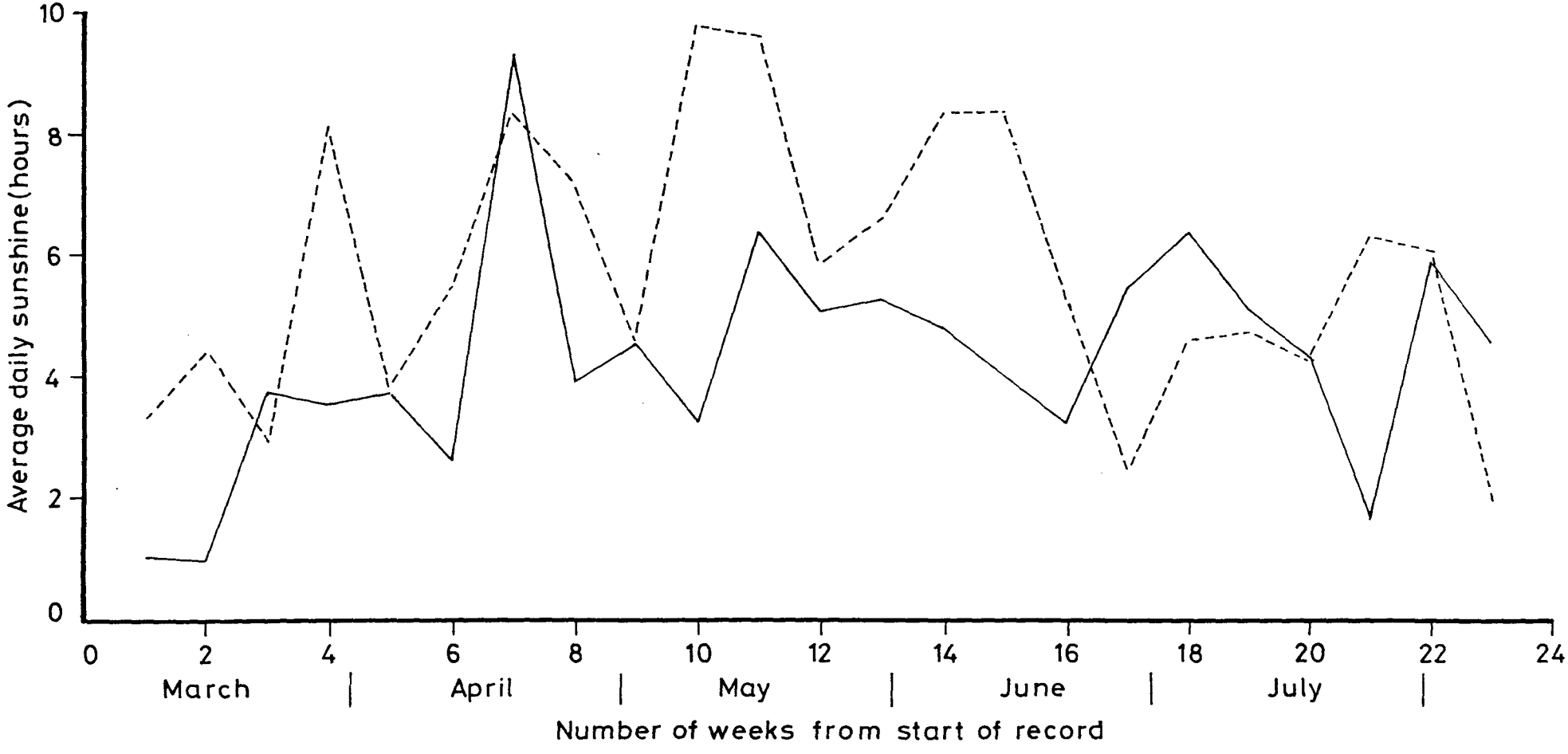
Average daily sunshine (hours)
10
8
6
4
2
0
0
2
4
6
8
10
12
14
16
18
20
22
24
March
April
May
June
July
Number of weeks from start of record

Fig. 2.9 The 'U' - shaped Aanderaa mooring. All connecting cables were of 13 mm steel wire, with the exception of those inter-connecting the meters (8 mm steel wire) and the 12 mm polypropelyne pellet float line. At all positions marked X, connections consisted of a 3 ton stainless steel swivel, connected via shackles to the respective cables. The shackles were rated from 15 cwt. to 2 ton breaking strain, depending on their position. All other connections were made via shackles.

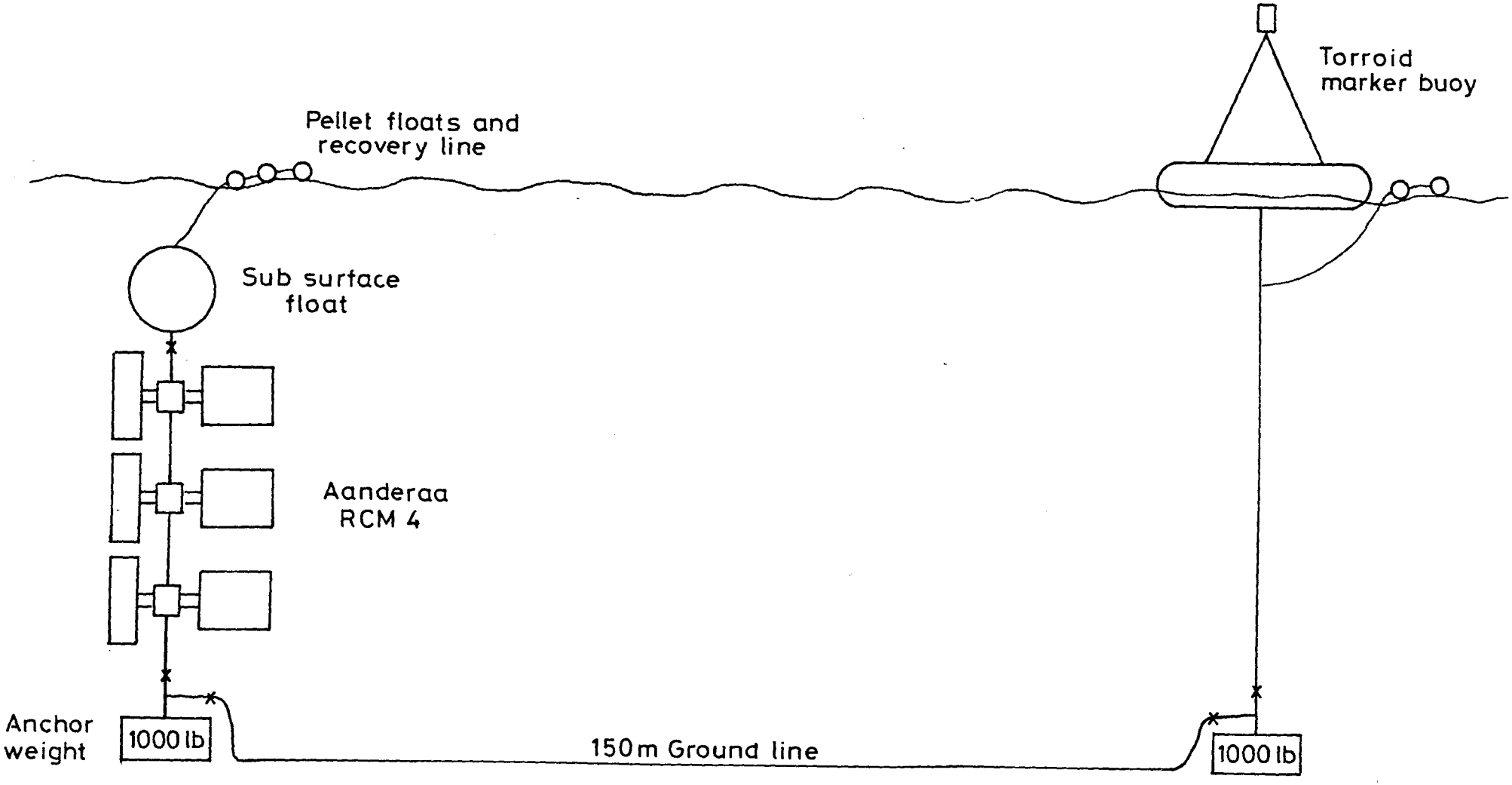
Torroid
marker buoy
Pellet floats and
recovery line
Sub surface
float
Aanderaa
RCM 4
Anchor
weight
1000 lb
150 m Ground line
1000 lb

TABLE 2.1 AANDERAA MOORING DETAILS

MOORING STATION	DATES AND TIMES (G.M.T.) OF DEPLOYMENTS	POSITION LATITUDE(N)	POSITION LONGITUDE(W)	RATIO OF MAJOR TO MINOR AXIS OF M_2 ELLIPSE AT LOWER METER	METER HEIGHT ABOVE BED (M) BOTTOM	CENTRE	TOP
	JOHN MURRAY 4/81						
CM1	15/4 08:24 - 19/4 09:04	53° 23.8'	4° 8.5'	4.6 : 1	2.5	7.5	14.5
CM2	19/4 17:10 - 23/4 07:43	53° 26.4'	3° 48.1'	4.2 : 1	2.5	7.5	14.5
CM3	23/4 10:20 - 14/5 13:55	53° 46.4'	3° 29.6'	1.1 : 1	2.5	7.5	14.5
	JOHN MURRAY 9/81						
CM4	25/7 17:20 - 30/7 05:00	53° 27.2'	3° 53.8'	3.9 : 1	2.5	7.5	15.5
CM5	30/7 17:20 LOST	53° 45.9'	3° 30.2'	———	2.5	6.5	13.5
	SHACKLETON 7/82						
CM6	28/7 17:58 - 3/8 08:15	53° 45.8'	3° 30.1'	1.2 : 1	2.5	6.5	13.5
CM7	3/8 16:20 - 8/8 18:30	53° 26.6'	3° 52.1'	4.1 : 1	2.5	7.5	17.5

CHAPTER 3 - INSTRUMENTATION

3.1 INTRODUCTION

This chapter concentrates on the design, construction and calibration of the profiling Aanderaa rotors and the photographic unit. There is also a summary of the calibration and performance of the e.m. heads, together with a brief description of the electronics unit. The electronics was designed by Dr. S.R. Ferguson in the Oceanography Department, to sample and digitise the signals from the turbulence sensors and then record the data on 9 track magnetic tape. The function and deployment of this equipment was described in Chapter 2.

The design, construction and calibration of the rotors and the photographic unit was carried out by the author, with much of the associated hardware being manufactured by Mr. R.H. Tennant in the Departmental work shop. In collaboration with Dr. S.R. Ferguson, the rotors and e.m. heads were calibrated by using the recirculating flume situated in the Department of Mechanical Engineering. The photographic unit which included a camera and flash unit, was tested in a 2 m square water tank in the Department of Oceanography.

3.2 CONSTRUCTION AND CALIBRATION OF THE ROTORS

The impellors were required to record the flow velocities parallel to, and at 4 heights above the sea bed, by the means discussed in Chapter 2. The velocities would then be integrated over periods of between one and fifteen minutes, as will be discussed in Chapter 4.

For this task Aanderaa rotors were chosen in preference to ducted impellors since:

1) They have a negligible response to the flow in the plane of the pivotal axis (Gaul, 1963).

2) They were relatively cheap and easily replaced.

3) They can record both components of the fluid velocity parallel to the sea floor without recourse to the use of vanes to align the impellor into the flow. This however was only true provided the angle of attack of the flow with respect to the rig was within limits discussed in Section 3.2.2.

The primary disadvantage of the Aanderaa rotors was that they suffer from inertia problems. That is to say in a situation where the flow is instantaneously switched on and then off, the time taken to achieve a constant rate of rotation from zero velocity, in a non-turbulent fluid, is less than the time taken to fall from that rate to zero. This inertia affect is particularly noticable in oscillatory flows, where it is often referred to as 'pumping', and the consequence of this on the rotor data will be discussed in Chapter 5. Ducted impellors, capable of responding to fluctuations with frequencies of up to 5hz. (Smith, 1974), would have greatly reduced this affect. Despite this, it was decided that 2) and 3) above, out-weighed this advantage, with any difference due to 1) being negligible. Also, part of the object of the comparison between the log-law and eddy correlation methods (see Section 2.2) was to provide an insight into the validity of previous measurements of the stress by the log profile, using low response impellors.

3.2.1 Construction.

The rotors were mounted between two parallel 1.27 cm (0.5 inch) square aluminium bars, their pivotal axis being approximately 16 cm from the vertical clamping supports attached to the main frame

of the turbulence rig (see Fig. 2.1). The bearings were mounted in two blocks attached to the parallel bars, with a reed switch encased in Araldite in the lower block below the rotor magnet. The reed switch was connected to the electronics unit via a two core wire. The switch remained on open circuit until closed by the passage of either magnetic pole, causing a pulse to be generated twice per revolution of the rotor. An R.C. circuit of time constant 1 ms, combined with a Schmidt trigger to form a square wave input to the digital electronics (see Section 3.5), was included. Spurious pulses originating from oscillations of the reed switch contacts were thus damped.

3.2.2 Calibration.

Calibration of both the rotors and the e.m. heads was carried out in a recirculating flume of approximate width 140 cm, depth 85 cm and working length 200 cm, with a capability of generating speeds in excess of 600 cm s^{-1}. During the calibration water velocities of up to 150 cm s^{-1} were used, supposedly accurate to ± 1% according to previous calibrations of the servo control potentiometer setting (Millward, 1973). In practice it was found that this absolute accuracy was subject to several factors which will be discussed later.

The rotor frames were clamped at mid-channel to a vertical pole, itself clamped to a cross member above the flume, firmly positioned on the bed of the channel. It was hoped that vibrations of the supporting pole induced by vortex shedding would then be reduced to a minimum. The velocity was considered to be uniform throughout the flume cross section at a distance of greater than 10 cm from the channel walls. Although, it should be noted that during an

examination of noise levels in the e.m. heads (Section 3.4.2) at 30 cm s^{-1}, a r.m.s (root mean square) value of turbulent intensity of 0.25 cm s^{-1} was recorded. This degree of turbulence was thought to be negligible in terms of inertia effects, as will be justified in Chapter 5.

Each rotor was calibrated individually over a velocity range of approximately 10.0 cm s^{-1} to 100.0 cm s^{-1}, in increments of 10.0 cm s^{-1}, with additional points at 125.0 cm s^{-1} and 150.0 cm s^{-1}. Pulses from the Reed switches were recorded for 2.5 minutes, subsequent to a 2.0 minute stabilization period following each new setting of the servo potentiometer. Interchanging components for different frames gave results well within the ± 1% uncertainty in the absolute value of the water velocities.

A number of calibrations were carried out between cruises, with no noticable effect of wear on the ageing components. Despite this, bearings and rotors were changed between cruises to avoid any such wear. On one occasion there was an apparent 4% increase in fluid velocity for equivalent settings of the servo potentiometer. This was eventually attributed to the removal of a baffle at one end of the flume channel, combined with a lowering of the fluid level. Upon recalibration of the flume the calibration curves for the rotors were satisfactorily reproduced.

For a large number of deployments at sea one e.m. head was used solely to record the uv components of the flow, enabling the direction of flow relative to the rig to be estimated, as discussed in Chapter 4. Accordingly, the directional response of the rotors was measured in increments of 5.0° through the range of 360° with an estimated uncertainty of ± 0.5°. The velocities were increased incrementally up to a maximum of 90.0 cm s^{-1} and the results are

presented in Fig. 3.1. The various troughs and peaks can be attributed to the respective shielding of, and eddy shedding onto the driving face of the rotor by frame supports. During the sea bed deployments, the angles of attack generally varied between 320° and 50° (see Chapter 4). The angles of flow with respect to the rotor frame are defined in Fig. 3.2 showing a diagram of the rotor and frame as deployed on the turbulence rig in Fig. 2.1.

Typical values of velocity, as experienced in the field, were in the range 20.0 to 60.0 cm s^{-1}. Consider these values, and also the range of angles of flow between 320° - 50°. It can be seen from Fig. 3.1, at the calibration velocity of 47.95 cm s^{-1}, that the ± 1% uncertainty previously stated was rapidly exceeded for positive angles. To compensate for this, the calibrations in Fig. 3.1 were applied to the field data, as detailed in Chapter 4.

Several threshold tests were carried out on the rotors. The velocity was increased in units of one (≈ 0.6 cm s^{-1}) on the servo potentiometer to approximately 6.5 cm s^{-1}, and held for 7.5 minutes at each level. This allowed the water velocity to reach a steady state. Similarly the velocity was decreased in units of one on the servo to 0 cm s^{-1}, from approximately 6.5 cm s^{-1}. As was expected, the threshold for accelerating flow (2.4 cm s^{-1}) was significantly different from the decelerating threshold (1.8 cm s^{-1}). This was partially due to the inertia of the rotors mentioned previously. In addition, a greater force is required to start a body from rest to a given velocity, to overcome friction, than if the body were already rotating. The thresholds were comparable to the specification for an Aanderaa meter of 2.0 ± 1.0 cm s^{-1} (Aanderaa, 1981). This was not surprising, since there is likely to be an equivalent flow geometry about the rotors at such low velocities. The minimum velocity that

could reliably be recorded in situ was approximately 15 cm s^{-1}, before the flow relative the rig exceeded the bounds of 330^{o} - 30^{o} as a result of the precessing of the tidal ellipse.

3.3 PHOTOGRAPHIC UNIT

As mentioned in Chapter 2 it was intended to use the unit in conjunction with the e.m. heads to correlate possible sediment motion with 'bursts' in the turbulence spectrum. Given the relative positions of the camera and flash, as indicated in Fig. 2.1, it was hoped to view an area of at least 2 m^2 upstream of the sensors. Initially the intention was to record every second for 5 minutes, switch off for 55 minutes and repeat this sequence throughout a deployment lasting up to 12 hours. It was assumed that a large number of photographs in a short period would enable the afore mentioned objective to be achieved, rather than the same number spaced over a longer period. A number of workers, including Heathershaw (1974), Ferguson (1979) and Soulsby, Davies and Wilkinson (1983), have observed events occuring with a period of the order of 5 to 100 seconds and duration 5 to 20 seconds. The above assumption was based on this time sequence.

Discussions with other workers led to a relatively cheap unit being developed, with readily available parts. Unfortunately the unit was not as flexible as had been hoped, for reasons which will be explained in Section 3.3.2..

3.3.1. The Camera.

A Sankyo EM 60XL super eight cine camera was chosen since it possessed the following essential features:

1) The ability to focus on any point from the lens face to

infinity. This property was necessary because of the nature of the water - perspex - air interface of the camera housing port, dealt with in Section 3.3.3.

2) A self timer, in this case capable of triggering at intervals of a 1/2, 15 and 60 seconds, which was necessary because the photographic unit was to be initially self contained during trials.

3) A flash synchronization, enabling the area of interest to be illuminated as the shutter opened.

4) Manual override of the automatic aperture control, to give the most suitable light intensity for distinguishing features on the sea bed.

5) Compactness, so minimising drag on the housing and ultimately the turbulence rig to which it was attached.

3.3.2 The Flash Unit.

A Vivitar 283 flash gun was chosen since it incorporated the following features:

1) A synchronization cord to the camera.

2) Variable power output, to be used in conjunction with the camera's override of the shutter, to control light intensity.

3) The ability of the flash window to lie flush with the body of the flash for compactness.

4) A short recycle time.

The last of these proved to be the biggest obstacle, with the flash recycling in approximately four seconds on full power. In most cases this was quicker than equivalent models comparable in price. The power packs originally intended for remote deployments on the rig were not available (as explained in Section 2.5) and non-rechargable batteries had to be used. As approximately only 90 flashes could be

obtained per set of batteries, the sampling rate was restricted to one frame a minute for the duration of each trial. Ideally a strobe would have been employed to illuminate the area at the desired intervals, but this was not budgeted for in the original grant application.

3.3.3. The Camera Housing Port.

The nature of the water - glass or perspex - air interface, generally used in underwater photography as a viewing port, can result in serious degradations of the object as seen by the camera. This is a result of the differing refractive indices of the mediums involved producing the following effects when using a plane port:

1) Curvature of the object as seen by the camera. This comes about as light not normally incident to the port is refracted by increasing degrees as the angle of incidence increases.

2) Chromatic aberrations, as a result of the various wavelengths of the non-normally incident light being diffracted by differing degrees. The aberration is manifest as a blurred object as seen by the camera, becoming increasingly severe with increasing angles of incidence.

3) Axial aberration, arising from refracted, non-normal rays from a point source failing to converge to a point after passing through the port. When seen as a virtual image from behind the port, the object appears blurred.

A further important effect of diffraction is to magnify the object as seen by the camera. In the case of perspex or glass the magnifying factor is 1.34.

A reduction in the f-stop (lens aperture), so excluding light

at greater angles of incidence, reduces the above effects. This unfortunately also reduces the field of view whilst increasing the depth of field, necessitating a compromise.

For a more comprehensive coverage of the above points the reader is referred to Mertens (1970) and Glover et. al. (1977).

A variety of lens systems exist to correct for the above distortions. The majority consist of a number of elements, for which the optical axes must coincide with one another and with that of the camera. In addition to being difficult to construct, a correspondingly longer camera housing is required. The choice of ports was arrived at after discussions with several firms manufacturing camera systems, in particular Osprey Electronics. An unpolished spherical port was purchased from them, manufactured to specifications dictated by the system, as discussed below. A port with a small radius of curvature would tend to give the same affect as a fish eye (wide angled) lens. There would be quite serious curvature of the edges of the image. Conversely, a large radius of curvature would extend the camera housing length, as the cameras focal point and the radius of curvature of the port must coincide. The port diameter should also be large enough so as not to decrease the field of view of the camera too greatly. Again a compromise was reached, resulting in a lens of diameter 13 cm, internal radius 13 cm and external radius 14 cm. Ideally the lens should be as thin as possible. The water pressure determines the thickness of the lens, with the particular lens used being several times stronger than is needed for the maximum depths (50 m) experienced in this experimental programme. The price of a polished lens was prohibitive, so the lens was polished in the Oceanography Department by the author, using materials readily available in the shops.

A spherical port has the advantage over a plane port, in that it is less susceptible to the effects of 1) and 2) above, whilst 3) is relatively minor in comparison to the others. The optical axes of the camera and port had still to coincide. With only the two elements, this was achieved easily by attaching the camera to a carriage capable of sliding along tracks rigidly attached to the lens housing. As the ratio of the apparent height of the object (virtual image formed by the port) to its distance from the cameras focal point, equalled that of the ratio of the actual object height and distance from the focal point, if viewed in air, the field of view of the camera was not reduced.

The spherical port obeyed the relationship given in equation 3.1 (from Jenkins and White, 1976), acting as a diverging lens producing a virtual image. This image then acts as an object for the camera.

$$\frac{n}{u} + \frac{n_2}{v} = \frac{n_1 - n}{r_1} + \frac{n_2 - n_1}{r_2} \quad , \qquad 3.1$$

where, in this application:

n = Refractive index of sea water = 1.34

n_1 = " " " perspex = 1.49

n_2 = " " " air = 1.00

r_1 = Radius of curvature of the outer face of the lens = 14 cm.

r_2 = " " " " " inner " " " " = -13 cm.

u = The distance of the object from the lens.

v = The virtual image (camera object) distance in front of the lens.

For example, for a value of u of 250.0 cm, as used in situ, the camera was focused on an object 23.2 cm in front of the port.

3.3.4. The Camera and Flash Housings.

The housings of the camera and flash units were constructed from 15.24 cm (6 inch) and 9.16 cm (4 inch) polyorc drainage tubing, respectively. Aluminium back plates sealed both tubes, into which were placed a four pin Marsh and Marine plug, from which the camera and flash were interconnected via four core cable. The camera port was secured in an aluminium plate, whilst the flash was housed behind a plane perspex port. Self-indicating silica gell was placed inside each housing in an attempt to prevent condensation forming on the ports. Fig. 3.3 shows the construction of the two units, along with their respective housings.

3.3.5 Photographic Unit Trials.

Trials to determine the optimum position of the camera relative to the port were carried out in a 2 m square tank of sides 2 m, in the Oceanography Department. A grid, of squares of sides one foot, was taped on the sides and base of the tank. Any degree of curvature of field was then detectable. The cameras optical axis coincided with that of the port. A carriage which could be screwed along this axis supported the camera. Photographs were taken for a combination of 5 f-stops, 5 focusing points and 36 positions relative to the port. The tank was blacked out, with the flash on full power in an attempt to simulate light conditions at greater than 25 m in the Irish Sea.

The optimum settings of the camera were with an f-stop of 2.0 and a focusing distance of approximately 35.0 cm. The camera lens to port separation was 6.6 cm. Taking the camera object to be 23.0 cm in front of the port and the focal point of the camera lens to be approximately 7.5 cm behind the camera lens face then :

Camera focusing point ≈ calculated object distance in front of the camera lens + camera focal point to camera lens separation.

3.4 THE E.M. FLOWMETERS

It is not intended to give a full description of the design and construction of the e.m. heads. This has been given by Tucker et. al. (1970), Tucker (1972), and Thorpe, Collins and Gaunt (1973). A brief description of the e.m. head performance and that of the electronics used is given below. A more detailed account of the performance was given by Griffiths, Collar and Braithwaite (1978).

E.m. heads were chosen in preference to sensors such as acoustic doppler shift current meters (Wiseman, Crosby and Pritchard, 1972), hot wire instruments (Grant, Stewart and Moilliet, 1962) and impellors (Cannon, 1971 and Smith, 1974) for the following reasons:

No moving parts, so preventing wear and clogging by extraneous material such as sand and weed; no inertia problems; robustness (important particularly during deployment and retrieval); each sensor measured two perpendicular components of flow; they were capable of fast response rates (5 hz. in this case); they were readily available commercially.

The e.m. heads used during the deployments considered here were manufactured by Colnbrook Instrument Electronics Ltd., under licence to I.O.S.. The power rating of the mark II e.m. heads was 2.5 watts, with a diameter of 5.5 cm, electrode separation 4.0 cm and a useful frequency range, which with suitable electronics could be extended up to 5 hz..

An assessment of their performance and calibration characteristics was carried out in the recirculating flume and also

in a still water tank. This was divided into three phases:

1) The measurement of flow parallel and at angles to the face of the e.m. head.

2) An estimation of the noise levels of the e.m. head and associated electronics.

3) A determination of the drift of the reference voltage as used to power the e.m. head.

3.4.1 The Velocity Calibrations.

Velocity calibrations were carried out with each e.m. head placed in mid channel of the flume and attached to a vertical pole, in the same manner as the rotors (Section 3.2.2). The servo control setting was varied in steps of twelve divisions ($\approx$ 7.5 cm s^{-1}) from 0 cm s^{-1} to 150 cm s^{-1}, and then similarly reduced back to 0 cm s^{-1}. Fluid velocities stabilized within two minutes of each new setting, after which the voltage output from the linear electronics (see Fig. 3.7) of the recording unit was sampled. For each e.m. head a 1.0 cm s^{-1} increment in fluid velocity was equivalent to an approximate 50 mv increase in the u channel and a 75 mv increase in v. A unique circuit board, with no interchanging of components, except in the case of failure, was used for each e.m. head. The angular response of the e.m. heads, as shown in Fig. 3.4 for six velocities, from -45^{o} to $+90^{o}$ was measured in increments of 5.0 $\pm$ 0.5^{o}, as for the rotors (Section 3.2.2). In Fig. 3.4 the ideal cosine response at each velocity is also given as a comparison. For angles less than -10^{o} the response was seriously impaired, resulting in the rejection of all field data below this value. Flow parallel to the face was referred to as 0^{o}, with the two electrodes measuring flow normal to a line along the flow direction. A negative angle refers to flow from behind the face,

whilst a positive angle corresponds to flow towards and across the face, as shown in Fig. 3.5. The main features of the curves have been previously reported (Tucker, 1972). Essentially, at negative angles the flow is rapidly restricted by the e.m. head itself.

The calibrations from 0 cm s^{-1} to 150 cm s^{-1} at 0^{o} yielded a linear relationship between velocity and the e.m. head output voltages, within ± 1%, when a least squares fit was applied. After the offsets on each e.m. head are taken into account (see Chapter 4 for details) the data shown in Fig. 3.4 can be employed to calculate voltage responses with changing velocity. Responses at each angle of flow were linear.

3.4.2 Noise Levels.

The noise level can be defined as a voltage level below which it is impossible to detect velocity fluctuations present in external flows. The velocity fluctuations are masked by voltage fluctuations generated internally by the measuring unit.

The noise levels of the e.m. heads were determined at a constant fluid velocity of 30.0 cm s^{-1}, using the flume, and at 0.0 cm s^{-1} by utilising a tank in the Oceanography Department. Fig. 3.6 shows the energy density spectra produced from trial 136, a fairly typical example of field data, and that during a run in the flume at a constant velocity of 30.0 cm s^{-1}. The r.m.s level of u ($(\overline{u^2})^{1/2}$), representing turbulent intensity, is given as 0.3 cm s^{-1} in the flume. There was a pronounced peak at frequencies of approximately 1.3 hz. This corresponded to the frequency of vortices shed from a cylinder of the same diameter as the pole which was used to support the e.m. heads in a flow of 30.0 cm s^{-1} (Schlichting, 1968). It would appear that the shedding excited the pole to vibrate at that

frequency also. This was attributed to the pole not being firmly placed on the bed of the flume. No evidence of any such excitation of the turbulence rig during deployments at sea was evident. Filtering of this peak reduces the r.m.s. level of u to 0.25 cm s^{-1}.

Geophysical values of r.m.s. u at 56.0 cm and 178.5 cm, the respective heights of the bottom and top sensor pairs above the sea bed during trial 136, are given as 8.5 cm s^{-1} and 4.5 cm s^{-1} respectively. This represents a level at 20% of u, whilst the flume value of r.m.s. u is only 0.8% of u. Still water trials over 17 hours gave a peak to peak noise level of 5.0 mm s^{-1} at a frequency of 10 hz. This was almost entirely due to the phase difference in frequency of the voltage powering the e.m. heads ($\approx$ 40 hz.) and that of the mains (50 hz.), which was not present at sea.

It is reasonable to assume that the noise level of the electronics at velocities of 30.0 cm s^{-1} should be comparable to that at 0.0 cm s^{-1}. This suggests that the value of r.m.s. u of 0.25 cm s^{-1} was almost completely due to turbulence generated in the flume. This arises as the fluid passes through a grid system intended to ensure uniform flow throughout the flumes cross section.

Similarly, the peak to peak noise level in the w channel was 5.0 mm s^{-1} in still water. This also suggests the r.m.s. value of w = 0.20 cm s^{-1} (0.17 cm s^{-1} upon filtering vibrations due to vortex shedding), shown in Fig. 3.6, resulted from the afore mentioned grid generated turbulence.

Digitising of the analogue voltage signals by the recording electronics results in an absolute minimum noise level of 0.1 mm s^{-1}. Input voltages to the digitiser were output in steps, each representing a resolution of 0.1 mm s^{-1} in velocity.

Compared to the geophysical noise levels, instrumental noise

can therefore be regarded as negligible.

3.4.3 D.C. Drift.

The original turbulence system built in the Oceanography Department (Ferguson, 1979) was subject to drifts in the d.c. offset, used as a reference to calculate absolute velocities, of up to 2.0 cm s^{-1} per hour. At a velocity of 50.0 cm s^{-1}, and over a period of 30 minutes, the present system was subject to a drift of only 2.0 mm s^{-1}. In still water over a period of 17 hours the long term drift was ± 1.0 mm s^{-1}. From in situ comparisons with the rotors over a two week cruise the drift did not exceed 3.5 cm s^{-1}, as detailed in Chapter 4.

3.5 OUTLINE OF THE RECORDING ELECTRONICS

It is not intended to present a full account of the electronics, which was designed and built by Dr. Ferguson, but since there is not yet a published account of this system, a brief outline is given below.

Fig. 3.7 shows a block diagram of the electronics, illustrating both the linear and digital sections. The linear electronics powers the e.m. heads, with the resulting signal being amplified and filtered before passing to the digital section. Here the linear signals were sampled and stored before being multiplexed and transferred serially to the Kennedy tape recorder.

3.5.1 Linear Electronics.

Each e.m. head was powered by a coil drive (C.D.) circuit. Voltages were switched across the coil at a frequency of approximately 40 hz. by the control oscillator to minimise contact

potentials between electrodes. The preamplifiers (P) amplified the weakly induced signals across the electrodes.

Sampling amplifiers (S) then extract that signal varying with the frequency of the switching voltage from the resulting waveform, which also includes a 'background' d.c. voltage generated by the electronics. Low pass filters (F) restricted the signal bandwidth from 0.0 to 2.5 hz. before the signals were passed to the digital electronics.

3.5.2 Digital Electronics.

The analogue signals from the eight e.m. head channels were sampled simultaneously by a buffer (S/H) every 0.2 seconds. This allows frequencies of up to 5 hz to be measured, which was considered to be sufficiently high to include the majority of the turbulent kinetic energy (Bowden, 1962 and Soulsby, 1977 and 1980). Signals were held until switched sequentially by a multiplexer (MX) through an analogue to digital converter (ADC). Data from the ADC was then combined with rotor counts, time data from a clock and header flags. This was transferred serially via the connecting cable to the research vessel and the Kennedy recorder.

3.6 SUMMARY

This chapter has given an account of the design, construction and calibration of the rotor frame work and photographic unit. Factors influencing the choice of components have been discussed. Included, is an account of the e.m. head calibration combined with a brief description of the flowmeter electronics.

The Aanderaa type rotor and associated components were capable of measuring the velocity profile at four positions within 2 m of the

sea bed. In stationary, unstratified and what can be considered non-turbulent flow, the velocity for each rotor could be determined with an uncertainty of ± 1% over the maximum range of velocities (10.0 - 70.0 cm s^{-1}) expected during the field experiments. This applied for velocities incident to the rotor through an arc of at least ± 30° about 0° as described in Section 3.2.2.. The threshold of the rotors (≈ 2.0 cm s^{-1}) was well below the expected minimum velocity. It should be noted that conditions in situ are obviously not as outlined above and rotors are influenced by inertia as discussed in Section 5.3.3.

The photographic unit, utilising a spherical port to reduce aberrations, was capable of recording an area of sea bed of 2.5 m^2 upstream of the velocity sensors. The optimum setting of the camera was with an f-stop of 2.0 and focused at approximately 35.0 cm. Due to insufficient power, in situ photographs had to be limited to one per minute. With favourable visibility the unit was thought to be capable of giving an indication of bedforms, sediment types and possible sediment motions.

The e.m. heads could record events occurring with frequencies of up to 5 hz, with an estimated resolution of at least 5.0 mm s^{-1}, as dictated by the noise level. The stability of the d.c. offset over a time interval equivalent to one trial was well within the ± 1% uncertainty in the flume calibration. The poor response outside the angles of flow relative to the rig of -10° to +30° imposed limitations on the flows that could be measured with confidence.

The complete system was capable of the simultaneous measurement of the boundary stress by the eddy correlation and log-law techniques, making a direct comparison of the two methods possible. In addition, it was possible, using the photographic unit and e.m. heads, to gain an indication of the bedforms and the motion

of sediment as related to events in the Reynolds stress. Finally, with a sampling rate of 5 hz an investigation of the Reynolds stress structure can be made.

Fig. 3.1 Calibration curves for the rotors. The abscissa gives the angle of attack of the flow to the rotor, as defined in Fig. 3.2. The ordinate axis gives the number of counts in the calibration interval of 2 minutes, whilst the velocities on the right indicate the fluid speed in the flume during each calibration. The two parallel lines at the calibration velocity of 47.95 cm s^{-1} represent the ± 1% uncertainty in flume velocity. The troughs, from left to right and denoted S, resulted from shielding by the rotor frame support, main rig frame and spacer, the latter visible to the right of the rotor in Fig. 2.1. The peaks, from left to right and denoted ES, were caused by eddy shedding from the rotor frame support, a combination of rotor frame and main frame supports and the main frame support.

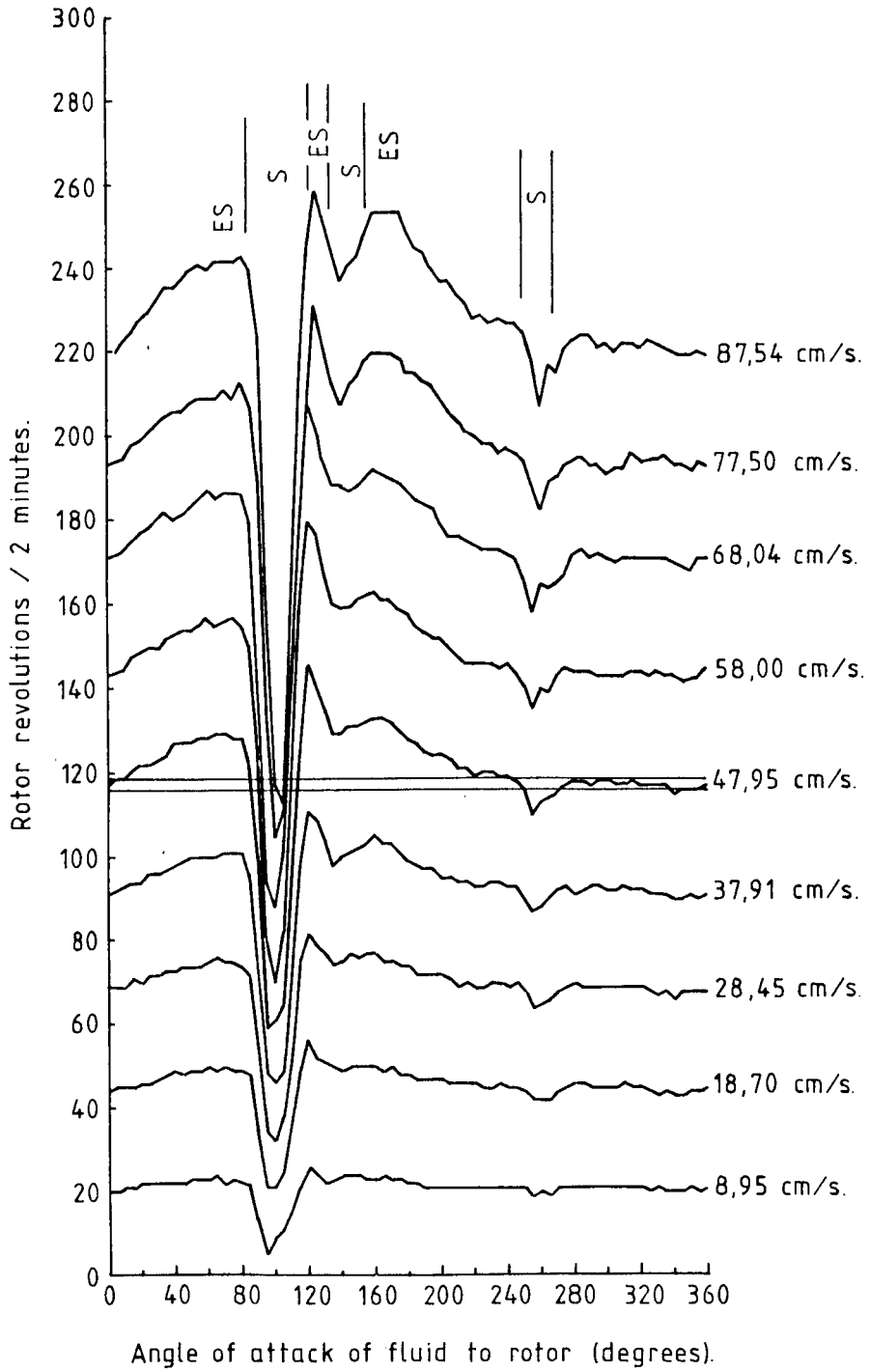
300
280
260
240
220
200
180
160
140
120
100
80
60
40
20
0
ES
S
ES
S
ES
S
87,54 cm/s.
77,50 cm/s.
68,04 cm/s.
58,00 cm/s.
47,95 cm/s.
37,91 cm/s.
28,45 cm/s.
18,70 cm/s.
8,95 cm/s.
Rotor revolutions / 2 minutes.
0 40 80 120 160 200 240 280 320 360
Angle of attack of fluid to rotor (degrees).

Fig. 3.2 Definition of the angles of flow with respect to the rotor frame. The rotor is viewed from above.

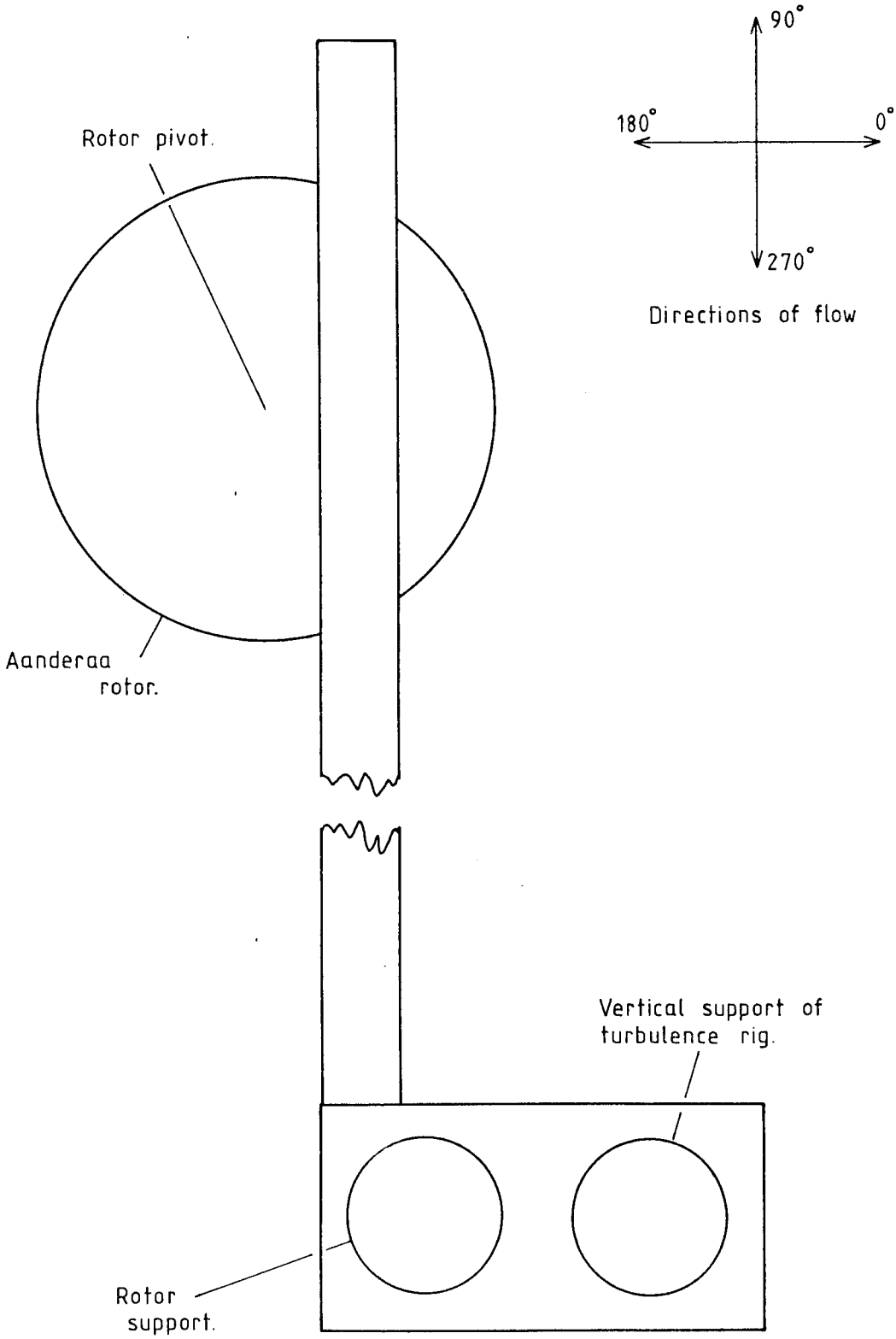
90°
180°
0°
270°
Directions of flow
Rotor pivot.
Aanderaa rotor.
Vertical support of turbulence rig.
Rotor support.

Fig. 3.3 Photograph of the camera and flash beside their respective pressure housings.

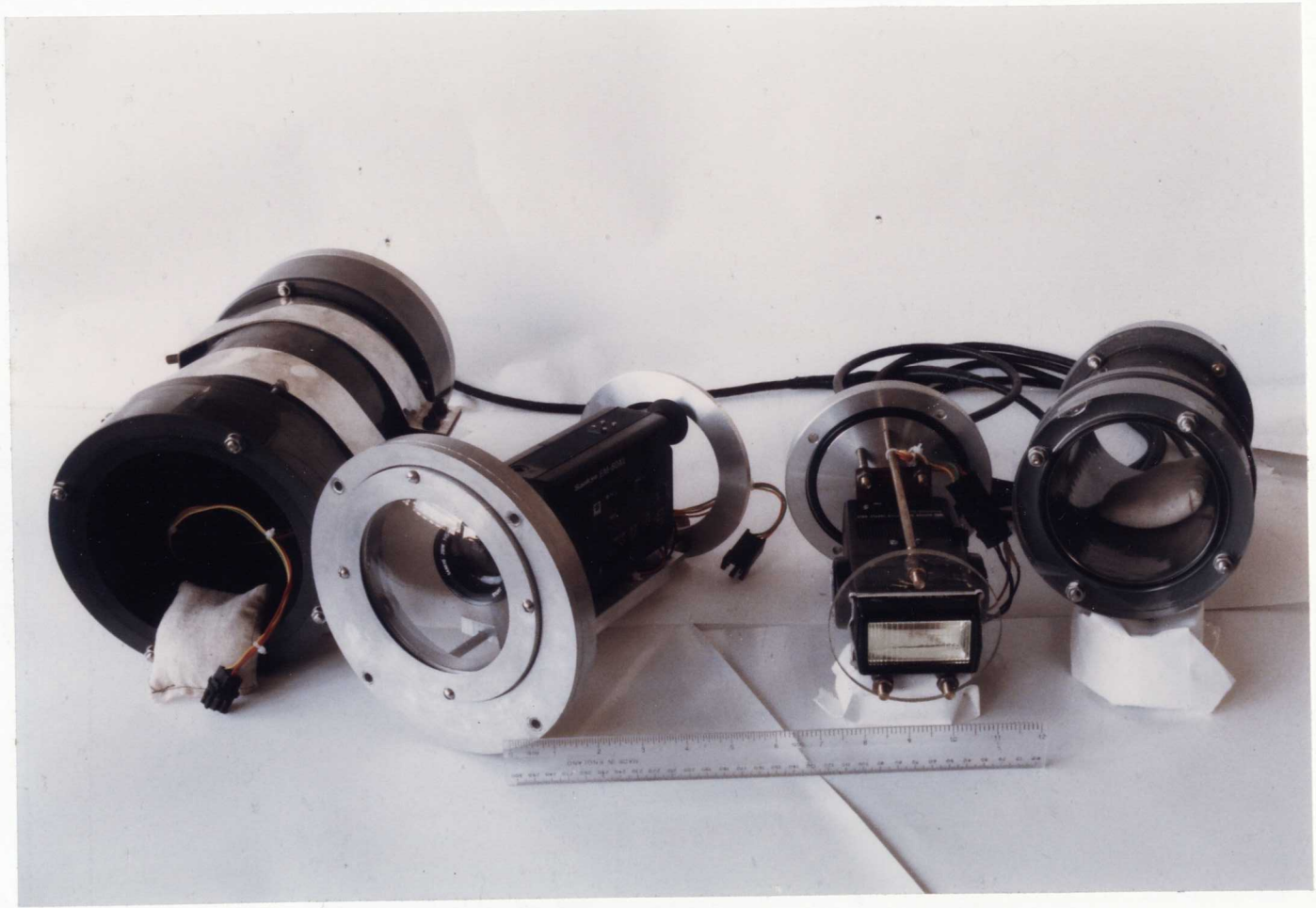

Fig. 3.4 Angular calibration curves for the e.m. heads. The ordinate axis represents voltage levels (mv) across the electrodes at the given velocities. The broken lines indicate the ideal cosine response. The rapid drop in response for angles of less than -10^{o}, as defined in Fig. 3.5, is evident.

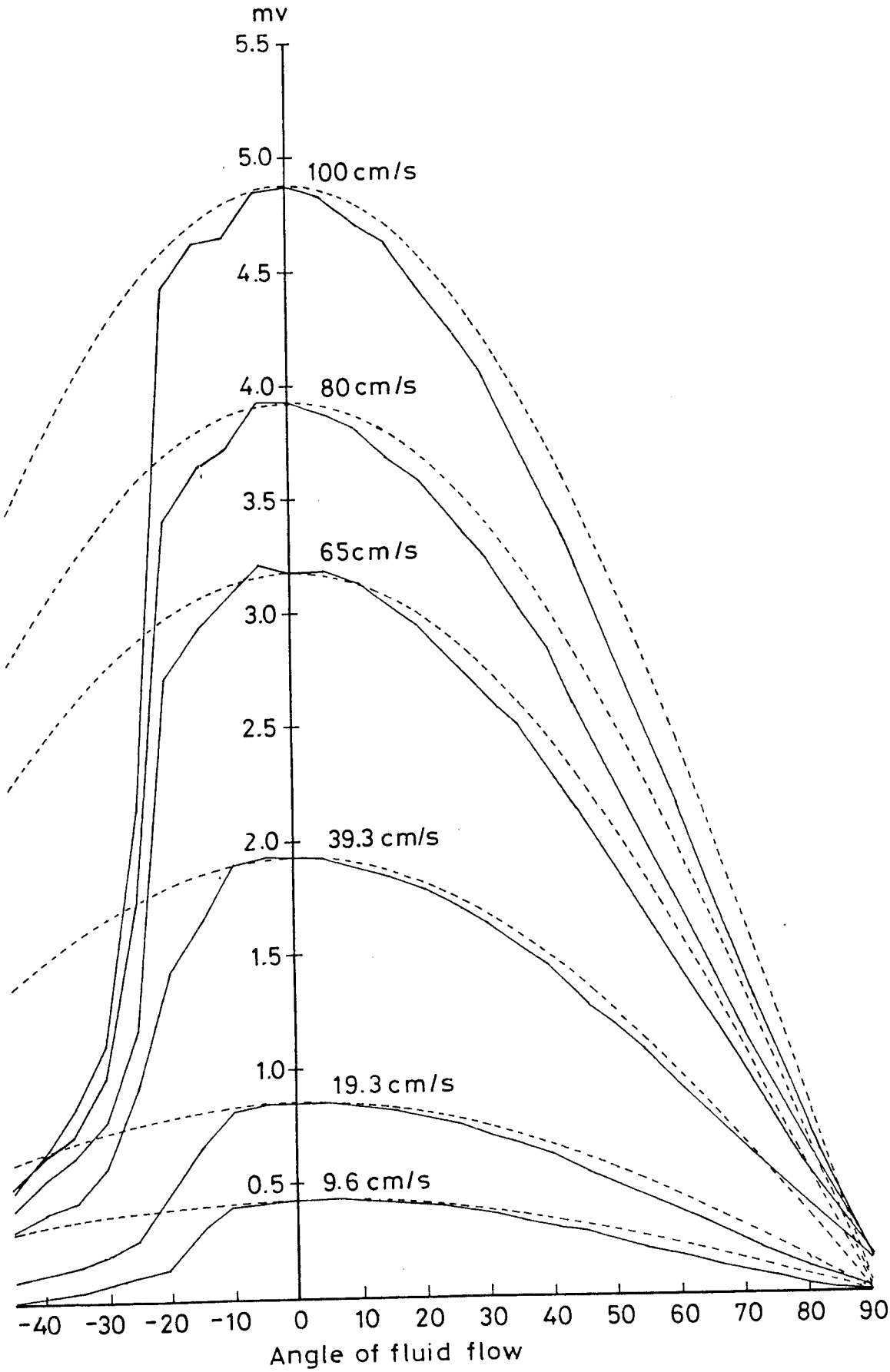
mv
5.5
5.0
4.5
4.0
3.5
3.0
2.5
2.0
1.5
1.0
0.5
100 cm/s
80 cm/s
65 cm/s
39.3 cm/s
19.3 cm/s
9.6 cm/s
-40 -30 -20 -10 0 10 20 30 40 50 60 70 80 90
Angle of fluid flow

Fig. 3.5 Definition of the angles of flow given in the angular calibration curves of Fig. 3.4. It is obvious that the electrodes were rapidly shielded by the epoxy resin of the e.m. head for increasingly negative angles.

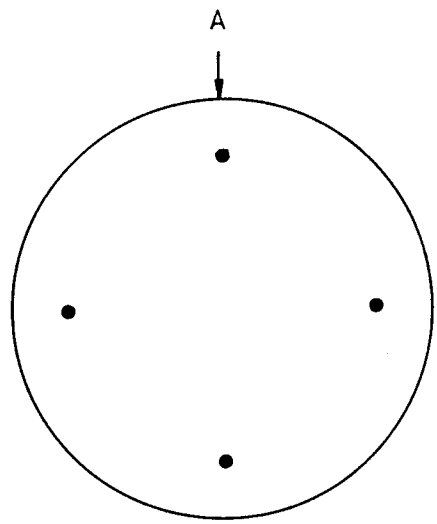

Front view of
5,5 cm. diameter
E.M. head.

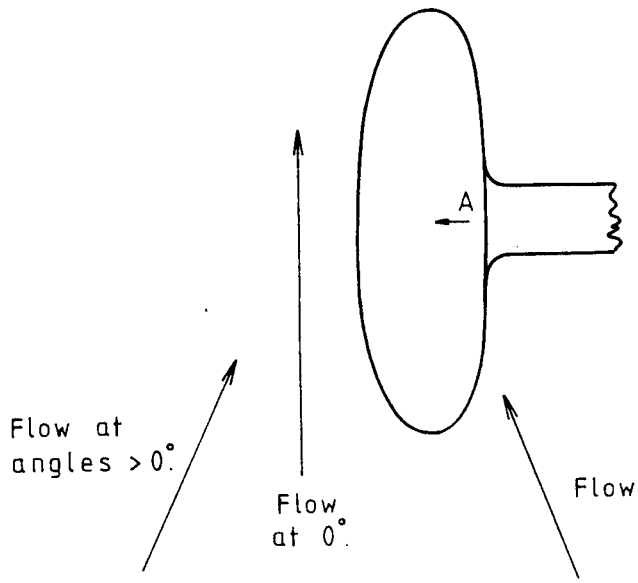

View looking down
from position A.

Fig. 3.6 Energy density spectra. Spectra for u and v, from geophysical flows (top 2 curves) is compared with that from a calibration run in the flume at 30 cm s^{-1} (bottom curve). The flume calibrations show a pronounced peak at frequencies of approximately 1.3 hz. This can be attributed to the excitation of the supporting pole by vortex shedding. The vibrations were not apparent in the the geophysical measurements. The root mean square level of turbulent intensity measured in the flume can be attributed almost entirely to turbulence generated by the flume.

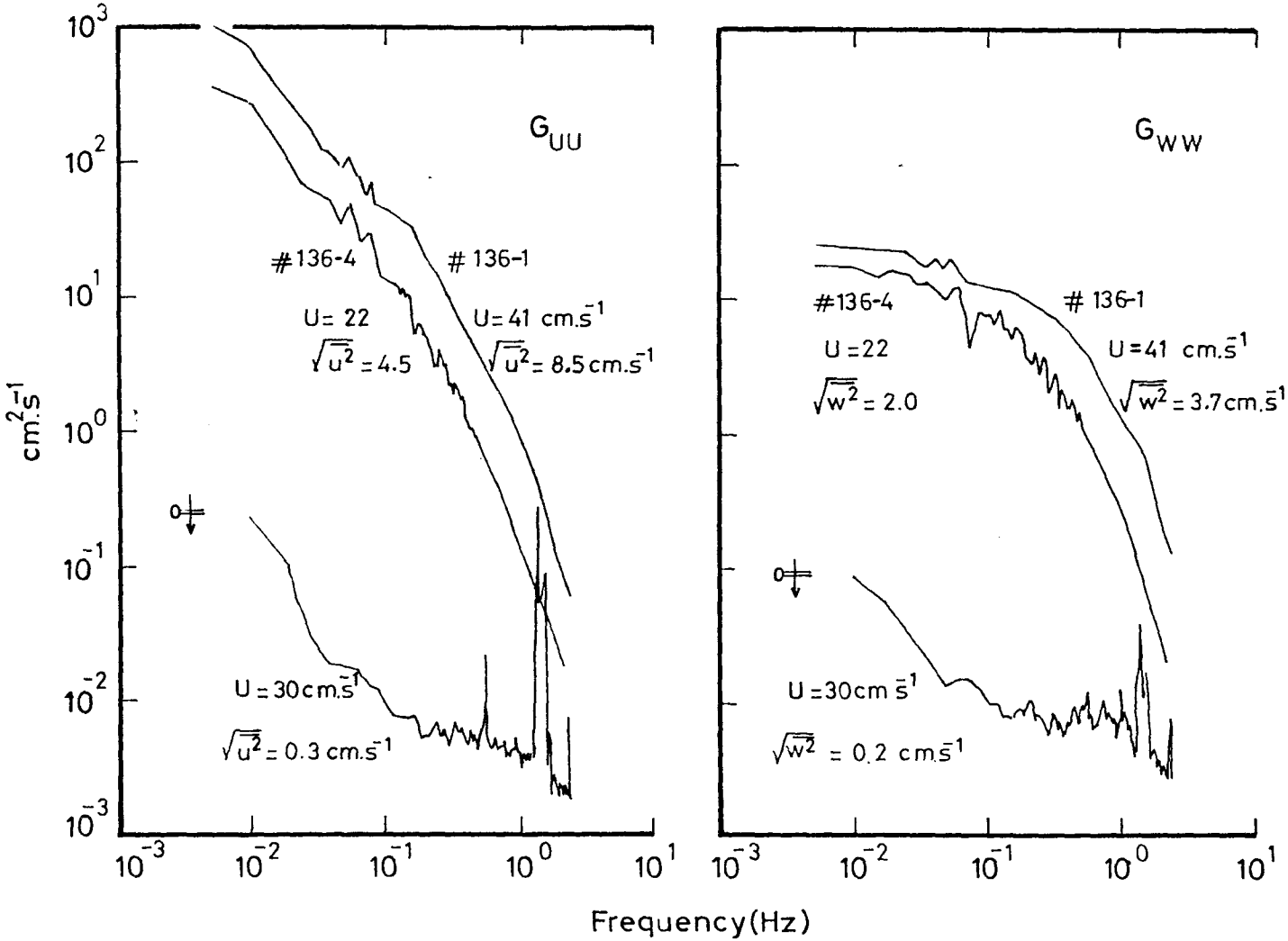
G_{UU}
G_{WW}
#136-4
# 136-1
U= 22
$\sqrt{\overline{u^2}}$ = 4.5
U= 41 cm.s^{-1}
$\sqrt{\overline{u^2}}$ = 8.5 cm.s^{-1}
U = 30 cm.s^{-1}
$\sqrt{\overline{u^2}}$ = 0.3 cm.s^{-1}
#136-4
# 136-1
U =22
$\sqrt{\overline{w^2}}$ = 2.0
U =41 cm.s^{-1}
$\sqrt{\overline{w^2}}$ = 3.7 cm.s^{-1}
U =30 cm s^{-1}
$\sqrt{\overline{w^2}}$ = 0.2 cm.s^{-1}
cm^2.s^{-1}
Frequency (Hz)

Fig. 3.7 Block diagram of the recording electronics, used to sample and digitise flow velocities.

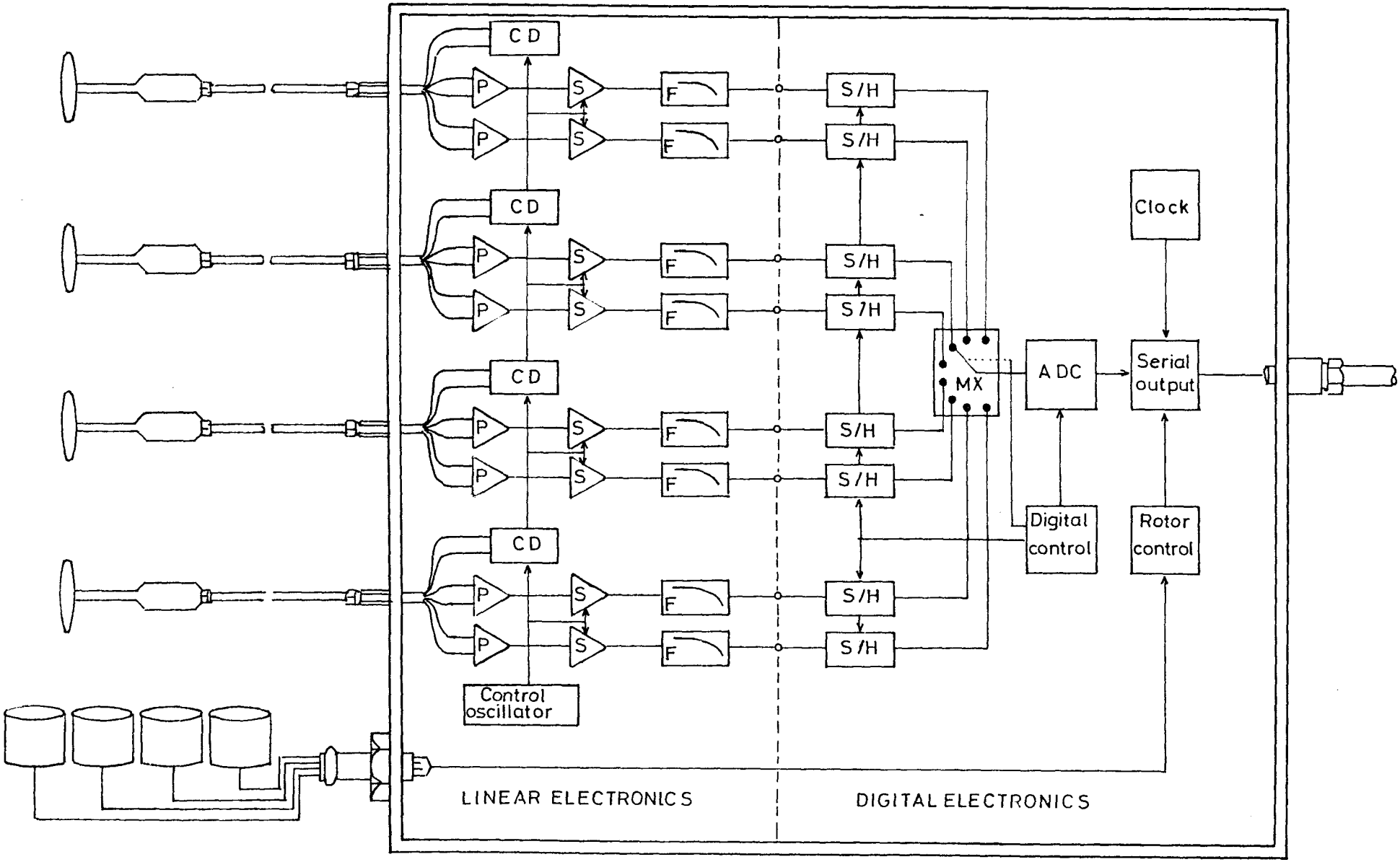
CD
P
S
F
S/H
MX
ADC
Clock
Serial output
Digital control
Rotor control
Control oscillator
LINEAR ELECTRONICS
DIGITAL ELECTRONICS

CHAPTER 4 - PRELIMINARY DATA ANALYSIS

4.1 INTRODUCTION

This chapter covers the analysis of data from the digital form, as recorded by the Kennedy tape recorder, to the production of initial estimates of turbulence parameters, both by the log - law (rotors) and eddy correlation (e.m. heads) methods. To begin with some analysis was performed using the University's I.C.L. 1906S mainframe computer, but for the majority, an I.B.M. 4341 mainframe was utilised. Graphical presentations of the various parameters were plotted on a Calcomp plotter associated with the computers. Plots of small data sets (e.g. d.c. offsets on the e.m. heads) were carried out using the Oceanography Departments H.P. 85 micro and associated flatbed plotter.

Processing began with the digitised turbulence data being transferred from the 9 track I.B.M. compatible Kennedy magnetic tapes, via the Computer Laboratory tape reader, to the filestore of the I.B.M.. This was followed by a code conversion and manipulation of the characters in the data file. Calibration data for the rotors and e.m. heads, obtained using the recirculating flume (see Chapter 3), were then applied. This enabled outputs for each channel of the e.m. heads, in terms of mv/cm s^{-1} averaged over one minute, to be calculated. An estimate of the d.c. offset on each u channel of the e.m. heads was made by comparisons with the corresponding rotors. In addition, the d.c. offsets on the w channels were also estimated. Following this, an estimate of the angle of flow of the current w.r.t the sensors was made, provided one e.m. head was recording the uv components of flow. Calibration data, as shown in Figs. 3.1 and 3.4, were applied, yielding velocities corrected for the varying angles of

flow relative to the rig. Finally, initial estimates of turbulence parameters were made. Plots of 12 minute running averages of rotor velocity ($\bar{R}$), e.m. head velocities for each channel ($\bar{U}$, $\bar{W}$ and $\bar{V}$), r.m.s. of u ($(\overline{u^2})^{1/2}$), r.m.s. of w ($(\overline{w^2})^{1/2}$), $\bar{U} - \bar{R}$ for each sensor pair, Reynolds stress ($-\overline{u'w'}$), friction velocity (u_*) and roughness length (z_0) were produced. It was then possible to get an indication of the data quality as given in Table A1.2 and summarized in Section 2.9.

The remainder of this chapter describes the above, leading to the production of initial estimates of turbulence parameters. As a result of this analysis the assumptions upon which the log-law of equation 1.11 were based were examined. The parameters obtained from the velocity profiles were examined in Chapter 7. This included the influence of accelerating effects and the variation of the parameters with tidal phase and the nature of the sea bed. Chapter 6 considers the comparison of Reynolds stress obtained by using eddy correlation and log-law techniques. The variation with tidal phase, height above the sea bed and differing bed compositions is also examined. Finally, Chapter 8 examines the structure of the Reynolds stress and attempts to investigate possible correlations between events in the turbulence spectrum and sediment motion.

4.2 DATA RECORDING AND TRANSFER

Digitised data from the flowmeter electronics, sampled every 0.2 seconds, consisted of 28, 8 bit bytes. These 28 bytes were divided into: 2 for the header to the e.m. head data; 2 each for the eight e.m. head channels; 2 for the header to the rotor and time data; 4 for the time data; one each for the four rotors.

The Kennedy recorded data as blocks of 512 bytes, each

represented 3.66 seconds of data at the above sampling rate. The input to the Kennedy had two buffers, one of which received data until 'filled' with 512 bytes, upon which the data was spewed to the second buffer. The first continued receiving data, whilst the data in the second was transferred onto magnetic tape.

Each tape was attached to a tape reader in the Computer Laboratory from which data was transferred directly to I.B.M. filestore. The resulting data was coded in ASCII(1). The 8 bits of each byte were reversed when recorded on the Kennedy tape. By cross referencing an ASCII character with the corresponding EBCDIC (2) code character from a table, the data was converted to a form acceptable to the I.B.M.. Upon the change of code, the bits of each byte were reversed, replacing the data in the order it was transferred from the flowmeter electronics.

4.3 ESTIMATION OF THE D.C. OFFSETS

For each e.m. head channel the data, as obtained in the previous section, was converted to voltage outputs in mv, averaged over a choice of intervals from 1 to 30 minutes, in 1 minute increments. For the turbulence time series, required to examine bursting as discussed in Chapter 8, the data could be output prior to the averaging routine in the program. Time series of u'w', sampled at 5hz over a 12 minute period during trial 186, are shown in Fig. 8.1. Having obtained the voltage levels, flume calibrations at an angle of 0^{o}, as discussed in Chapter 3 and shown in Fig. 3.4, were applied. Voltages of approximately 47 mv and 75 mv in the u and w

(1) ASCII ≡ American Standard Code for Information Interchange.

(2) EBCDIC ≡ Extended Binary Coded Decimal Interchange Code.

(or v if the e.m. head is recording uv) channels respectively, represented a fluid velocity of 1.0 cm s^{-1}. Rotor calibrations were also applied at 0^{o}, as shown in Fig. 3.1 and detailed in Chapter 3.

It was assumed that the d.c. offsets for each channel remained constant throughout a trial, as discussed in Chapter 3. In addition, the 12 minute averaged u component ($\bar{U}$) for each channel could never exceed the similarly averaged rotor velocity ($\bar{R}$). The reasons for a 12 minute averaging interval are given in Section 4.7. A positive value of $\bar{U} - \bar{R}$, for each sensor pair at 0^{o}, represented a positive offset in the u channel and a negative value indicated a negative offset. The difference at 0^{o} was represented by a peak in the $\bar{U} - \bar{R}$ time series. The shift in terms of cm s^{-1} required to place the peak at 0.0 cm s^{-1} was representative of the d.c. offset on each e.m. head. As the flow w.r.t. the rig was found to be 0^{o} at some time during approximately 96% of the trials this was possible. For the remaining trials the rig was badly orientated and the overall record was poor, resulting in the rejection of entire data sets.

The offset in the w channels was estimated by assuming negligible residual flow perpendicular to the sea bed, hence 12 minute averages of w ($\bar{W}$) should have had approximately zero means. The difference in the actual mean and the zero was representative of the d.c. offset. During the two week cruises the w offsets varied by no more than $\pm$ 0.6 cm s^{-1}, with what was considered zero drift.

The d.c. offsets in the u and w channels for e.m. head 2, over the two week cruise SH. 7/82, are shown in Fig. 4.1. A least squares fit to the offsets in w indicates no drift, but the u channels always appeared to be subject to drift. The d.c. offsets for the u channel in Fig. 4.1 show a drift of up to 3.4 cm s^{-1} over the two weeks. The

spike for trial 163 was removed as there was insufficient data (30 minutes) for an estimate of an offset. The method of least squares used in the next section to estimate the rig orientation tends to validate the above method for calculating the offsets in u. There was no obvious explanation for there to be drift in only the u channels. The drying of the e.m. head epoxy resin, in which the electrodes are embedded, whilst on deck between deployments and the build up of material due to electrochemical action should affect both channels equally. As mentioned in Section 3.2, ageing of the rotor components did not appear to alter the calibrations, so this too was discounted. The ± 1% uncertainties in the calibrations of the rotors and e.m. heads could account for approximately 1.0 cm s^{-1} of the drift at 30.0 cm s^{-1}. At most the 'pumping' of the rotors could account for 0.5 cm s^{-1}, with the angle of 0^{o} was always found at velocities greater than 25 cm s^{-1}. This effect is discussed in Section 5.3.3. These uncertainties still fail to account for the trend in u as shown in Fig. 4.1, which has to be attributed to long term instability in the electronics unit.

The estimation of the d.c. offsets was completed with the aid of graphics screens associated with the I.B.M.. This enabled the data to be viewed more readily, although the screen could not give the same degree of resolution as the hard copy plots.

4.4 ESTIMATING THE ORIENTATION OF THE RIG

Having estimated the offsets in the u and w channels, an estimate of the offset in the v channel and the orientation of the sensors w.r.t. the flow was made, given that one sensor was recording uv. Both the rotors and the e.m. heads recording uv were assumed to be sampling flow parallel to the sea bed. Then:

$$(\bar{U} + u_0)^2 + (\bar{V} + v_0)^2 = \bar{R}^2 \quad , \qquad 4.1$$

where : $\bar{U}$ = 12 minute averaged velocity in the x direction.

u_0 = d.c. offset in the u channel.

$\bar{V}$ = 12 minute averaged velocity in the y direction.

v_0 = d.c. offset in the v channel.

$\bar{R}$ = 12 minute averaged rotor velocity.

The x axis is taken as being in the direction of flow at 0^o to the sensors. The co-ordinates used are a mutually orthogonal right handed cartesian system.

A plot of the right and left hand terms of equation 4.1 should yield a straight line. The displacment of each point from the line can be represented by:

$$e_i = y_i - (a + bx_i) \quad , \qquad 4.2$$

where: a = y axis intercept.

b = gradient.

then:

$$\sum_{i=1}^{N} e_i = \sum_{i=1}^{N} (\bar{U}_i + u_0)^2 + (\bar{V}_i + v_0)^2 - \bar{R}_i^2 \quad , \qquad 4.3$$

N = number of independent 12 minute averages in each trial.

The line of best fit is that for which $\Sigma\, e_i^2$ is a minimum. The differentials of $\Sigma\, e_i^2$ by u_0 and v_0 result in two cubic equations given below, the solutions of which yield u_0 and v_0.

$$\frac{\delta\left(\sum_{i=1}^{N} e_i^2\right)}{\delta u_0} = \sum_{i=1}^{N} 4\left[u_0^3 + 3\bar{U}_i u_0^2 + (v_0^2 + 2\bar{V}_i v_0 + (\bar{V}_i^2 + 3\bar{U}_i^2 + \bar{R}_i^2))u_0 + v_0^2\bar{U}_i + 2\bar{V}_i v_0 \bar{U}_i + \bar{U}_i(\bar{U}_i^2 + \bar{V}_i^2 + \bar{R}_i^2)\right] \quad , \quad 4.4a$$

$$\frac{\delta\left(\sum_{i=1}^{N} e_i^2\right)}{\delta v_0} = \sum_{i=1}^{N} 4\left[v_0^3 + 3\bar{V}_i v_0^2 + (u_0^2 + 2\bar{U}_i u_0 + (\bar{U}_i^2 + 3\bar{V}_i^2 + \bar{R}_i^2))v_0 + u_0^2\bar{V}_i + 2\bar{U}_i\bar{V}_i u_0 + \bar{V}_i(\bar{V}_i^2 + \bar{V}_i^2 + \bar{R}_i^2)\right] \quad , \quad 4.4b$$

Substituting 12 minute averages of $\bar{U}_i$ and $\bar{V}_i$ into equations 4.4a and 4.4b and utilising a N.A.G. (Northern Algorithms Group) library routine, available from the Computer Laboratory, yielded up to nine roots for each equation. The roots were found by iteration about estimates of u_0 and v_0 input by the programmer. Values of u_0 and v_0 were estimated from substitution in equations 4.4a and 4.4b, in increments of one from −20 to +20, in conjunction with the measured values of $\bar{U}_i$, $\bar{V}_i$ and $\bar{R}_i$. Contours of u_0 and v_0 were plotted with the aid of a library routine, with the crossing point of the zero contours representing a root. Fig. 4.2 shows one such a plot for trial 175 . Roots were indicated at approximately $u_0 = 0.9$ and $v_0 = -6.5$ and $u_0 = -4.3$ and $v_0 = -20.0$. If nine roots did exist the remainder were outside the values given on the axis and were not representative of a minimisation of equation 4.2. Considerably smaller intervals of u_0 and v_0 would have given an accurate root in place of the N.A.G. routine, but the system time and storage required on the computer proved prohibitive. These roots were substituted into equation 4.3, with lowest value of $\sum e_i^2$ taken to be the u_0 and v_0 estimates.

Values of u_0, as plotted in Fig. 4.3 for those trials with a uv head, had previously been estimated as described in Section 4.3. The points should therefore be close to zero. In the majority, u_0 is within ± 1.0 cm s^{-1} of zero. That is allowing a 1.5% uncertainty in e.m. head velocities at 40.0 cm s^{-1}, the velocity typically experienced at an angle of 0.0°, due to a ± 3.0° orientation uncertainty in aligning the sensors. For trials 128, 139, 146 and 155 the error in u_0 can be attributed to the fact that an angle of flow w.r.t. the rig of 0° was never experienced. This gave rise to an over estimate of the d.c. offsets and a correspondingly large negative u_0. Trials 129 and 134 can be accounted for by an incorrect estimate of $\bar{U} - \bar{R}$. Poor estimates of u_0 for trials greater than 177 were in all probability caused by an e.m. head with a bent stem being used to record uv. The angle of the sensor was such that it recorded flow coming from slightly behind the head instead of that in the plane parallel to the sea bed.

The final estimates of the angle of flow w.r.t. the rig were given with an uncertainty of approximately ± 4°.

4.5 ESTIMATING FLOW CHARACTERISTICS AND TURBULENCE PARAMETERS

The results obtained here were primarily to determine the quality of the data collected, using the assumptions of a constant stress layer and non-accelerating flow, as discussed in Chapter 1. By applying the calibrations, made in increments of 5.0° and shown in Fig. 3.1, and given an estimate of the angle of flow w.r.t. the rig, corrected rotor velocities were obtained. The corrections were made by interpolating between the counts at the 5.0° calibration points preceding and following the estimated angle for each velocity. An individual calibration curve for each angle was calculated by

applying a least squares fit to the resulting points. Corrected rotor velocities were then obtained from this curve. Turbulence parameters z_0, u_* and C_{100} were found as a result of applying a least squares fit to values of $\bar{U}$ and lnz in equation 1.11, for four heights, with d assummed to be $\ll z$, and then employing equation 1.13.

Twelve minute averaged values of u were initially calculated with d.c. offsets applied, but without angular correction. Calibrations as shown in Fig. 3.4 were applied, interpolating in the same manner as the rotors, with voltage levels in mv replacing rotor counts. The 12 minute averaged velocity ($\bar{U}$) was substituted into the resulting calibration equations for the estimated angle and 0^o. A ratio of the voltages at the former angle and 0.0^o gave a factor by which the measured velocity was corrected for angle. Twelve minute averages of w ($\bar{W}$) were also obtained, assuming that channel to be recording the flow perpendicular to the sea bed (i.e. 90.0^o). The possible effects of sensor misalignment is discussed in Section 5.3.

Turbulent components of the velocity time series, u' and w', were obtained by subtracting 12 minute averaged u and w values respectively, from u and w recorded every 0.2 seconds. A least squares fit was applied to the resulting time series of u', enabling trends to be removed. An average of the term by term product of u' and w' over 12 minutes gave the Reynolds stress $-\overline{u'w'}$. Angular corrections were then applied to the resulting $-\overline{u'w'}$ values using the factors obtained above. The u'w' time series, shown in Fig. 8.1, was generated from the term by term product of u' and w'.

All the velocities and turbulent parameters, as listed in Section 4.1, were plotted as time series. Poor quality data was readily evident in these plots, as shown in Figs. 4.4a, 4.4b and 4.4c

and detailed in the following section.

4.6 DATA QUALITY

Due to the high volume of data collected it was felt that the criterion for the rejection of data could be fairly rigorous. This led to the rejection of all the data from trials not employing a uv recording e.m. head. Although, in most cases preliminary estimates of velocity and turbulence parameters were made.

The primary reason for rejection in the remaining data was poor orientation of the sensors w.r.t. the flow. This was due to initial misalignment of the rig on deployment, or to the precessing of the tidal ellipse throughout the trial. Data recorded when angles exceeded the bounds of -10^{o} and $+30^{o}$ for the e.m. heads and $\pm$ 30^{o} for the rotors were regarded with suspicion, and the data rejected within the computer programs.

Fig. 4.4c shows a plot of 12 minute running averaged values of $\bar{W}$ and $\bar{V}$ (- - - -) for trial 138. The discontinuity in the v channel represents a redeployment of the rig, as is the case in all the records in Figs. 4.4a and 4.4b for the rotors and e.m. heads respectively. If Figs. 4.4a and 4.4b are compared after 120 minutes it can be seen that e.m. head velocities decayed faster than the rotors and that the top two e.m. head velocities overlap. This indicates that the flow w.r.t. the rig is beyond $+30^{o}$ and that redeployment of the rig was necessary. This is also evident in Fig. 4.4c were the v channel velocity becomes increasingly large. The irregular record at the end of each graph indicates the rig being lifted from the sea bed.

Redeployment of the rig during trials resulted in data gaps, evident as a time interval between successive readings of greater

than the sampling interval of 0.2 seconds. The Kennedy recorder and logic unit were offline during redeployment, with the exception of the logic unit clock which continued counting. When recording recommenced, the time difference between the last reading before redeployment and the first reading after redeployment represented the redeployment duration. Such data gaps were rejected in the preliminary programs by examining the difference in the time intervals between the start and the end of the data blocks being averaged over the time interval. If the difference was outside the bounds of the averaging interval ±1 second, then the difference between the time interval plus one minute was examined, until the difference was within the bounds previously stated. When the logic unit was switched back on rotor count pulses often started at greater than zero before being reset at the next sampling interval. Also, the logic unit may have been switched off part way through the final minute of an averaging interval, which is not detectable by the above method. By investigating the averaging interval plus one minute, in the same manner as above, this was detected and the next data block, starting at the time of the averaging interval plus one minute into further into the data, was examined.

Trials with one inoperative e.m. head, rotor or both at one height, assuming it was not a uv recording sensor, were included in the analysis by considering the remaining sensor pairs only.

In total 130 hours 24 minutes of data was considered suitable for further analysis, representing 43% of the total data collected.

4.7 AVERAGING INTERVAL

Strictly speaking the data should be ensemble averaged, but due to the oscillatory nature of the flow this was impossible and time

averages were taken, with stationarity being assumed over each averaging interval. Aside from sensor response, both in the high frequency region of the spectrum and the spatial scales to which it can resolve, the averaging interval is dictated by a desire to average over as long a period as possible. The majority of the turbulence energy can then be included, with the proviso that the flow remains as near stationary as possible.

Soulsby (1977) suggested that a plot of energy spectra as a function of a dimensionless wave number ($kz = 2\pi zf/U$) was representative of the contribution of the various frequencies to the total turbulence flow energy. Here, z is a scaling length equivalent to the height of the measuring sensor above the sea bed and f is frequency in the turbulence spectra.

The lowest frequency observable in a record of length T is approximately T^{-1}. The highest is dictated by the Nyquist frequency, taken to be half the digitising rate of 5 hz.

Considering typical values as experienced in the Eastern Irish Sea, z = 180.0 cm and 12 minute averaged velocity extremes of 15.0 to 60.0 cm s^{-1}, values of kz of 0.1 and 0.03 respectively are given for low frequencies. Whereas for high frequencies and a z = 50.0 cm, the lowest sensor height, kz is 52 and 13.

The greatest percentage loss in the high and low frequency spectra of $-\overline{u'w'}$ (Soulsby, 1980) is given as 1% and 6% respectively for the above values. In practice the latter is an over estimate for the data considered in this study, as the final 5 to 10% of the trial is generally rejected. Here velocities of less than 25.0 cm s^{-1} (kz = 0.6) are often outside the previously defined limits of the angle of flow w.r.t. the rig.

Soulsby (1980) suggests that beyond 8 minute averages $\bar{U}$

becomes non - stationary. This represents an unacceptable loss in the low frequency end of the $\overline{u'w'}$ spectra of almost 30%. Alternatively 12 minute averaged values of $\overline{u'w'}$ are considered stationary. This was also found to be so for $\bar{U}$ recorded during this experimental programme, using the technique discussed in Section 5.2.

Twelve minute averages were taken so that either of the assumptions of stationarity and the inclusion of the entire energy spectra did not become too liberal.

4.8 SUMMARY

This chapter has dealt with the processing of the data from its recording on magnetic tape at sea to estimates of data quality and preliminary turbulence parameter values.

Comparisons of 12 minute time averaged $\bar{R}$ and $\bar{U}$ show that the long term drift of the d.c. offset during a two week cruise was no greater than 3.4 cm s^{-1}. During the same period the d.c. offset on the w channel was stable within ± 0.6 cm s^{-1}. Angles of flow w.r.t. the rig were estimated with an uncertainty of ± 4^{o} by a least squares technique. That suggested d.c. offsets in the u channels were within ± 1.0 cm s^{-1} of their true value. Sudden loss of response experienced at angles of less than -10^{o} for the e.m. heads, estimated by the above method, corresponded well with the responses measured in the flume (Chapter 3).

Although a large proportion of the collected data was rejected for the various reasons given in this chapter, the remaining 130 hours 24 minutes of data represented approximately 650 independent 12 minute averages.

A discussion of the various features of the turbulence and

velocity time series are left until the following chapters, although typical examples are shown in Figs. 5.6, 5.7, 7.3, 7.4 and 8.1.

Fig. 4.1 D.C. offsets for the u and w channels of e.m. head 2, during the trials of the SH. 7/82 cruise.

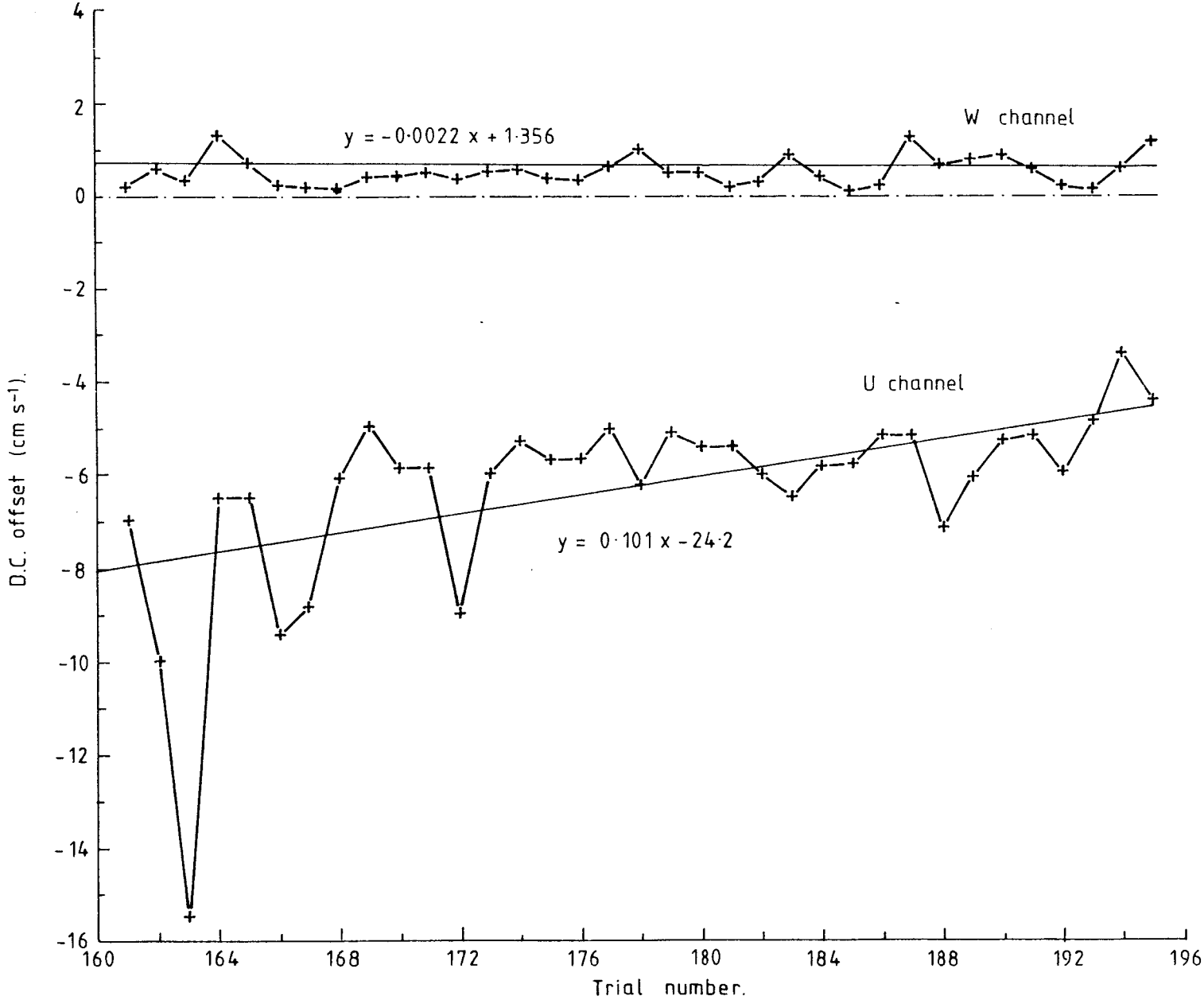
W channel
y = -0·0022 x + 1·356
U channel
y = 0·101 x - 24·2
D.C. offset (cm s⁻¹).
Trial number.
4
2
0
-2
-4
-6
-8
-10
-12
-14
-16
160
164
168
172
176
180
184
188
192
196

Fig. 4.2 Contour plot of d.c. offsets in the u and v channels of e.m. head 3 , during trial 175

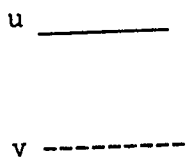

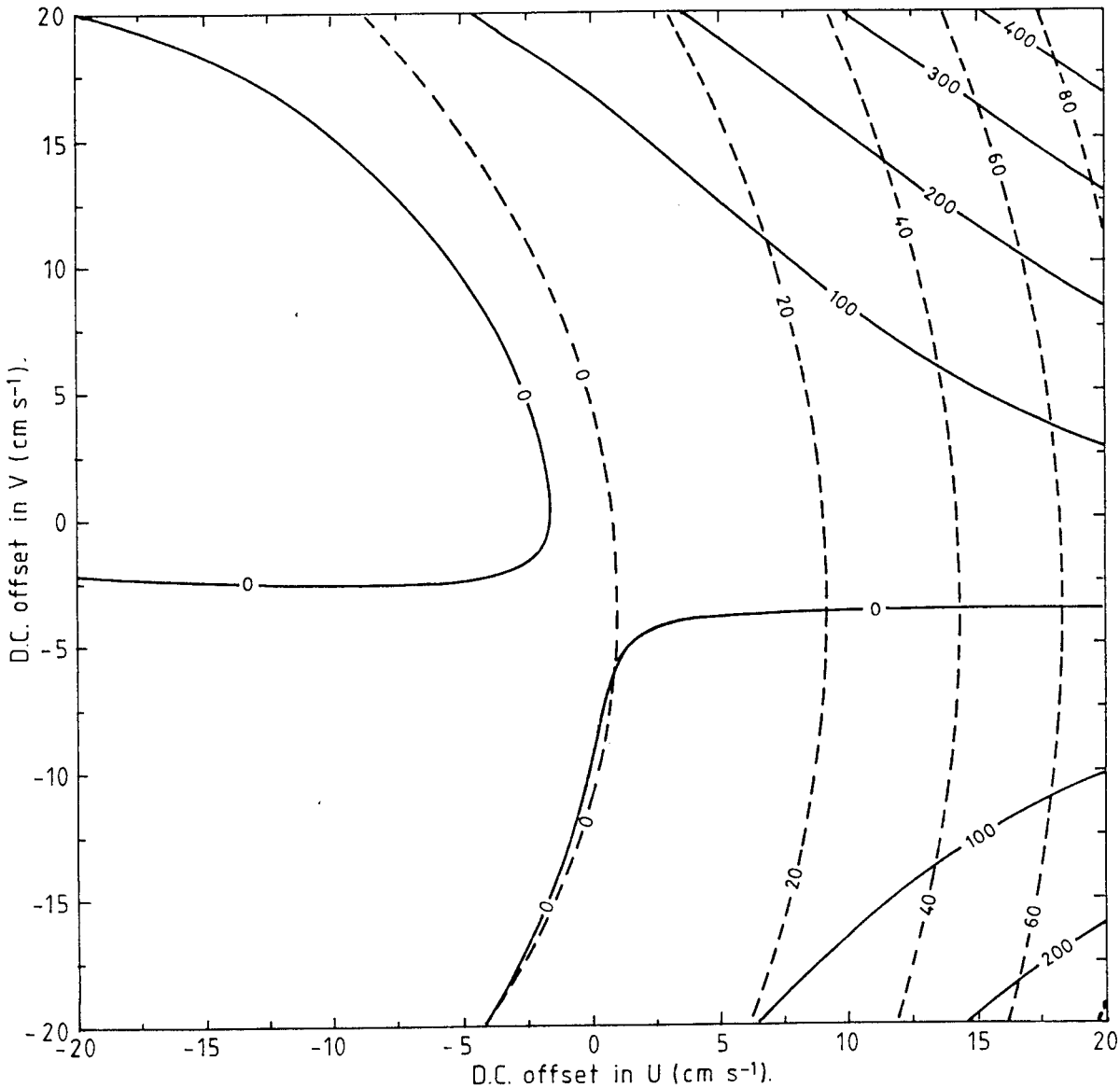
D.C. offset in V (cm s⁻¹).
D.C. offset in U (cm s⁻¹).
20
15
10
5
0
-5
-10
-15
-20
-20
-15
-10
-5
0
5
10
15
20
0
0
0
0
0
0
20
20
40
40
60
60
80
100
100
200
200
300
400

Fig. 4.3 Corrected u offsets. The parallel lines at ± 1 cm s^{-1} represent a ± 1.5% uncertainty in e.m. head velocities at 40 cm s^{-1}.

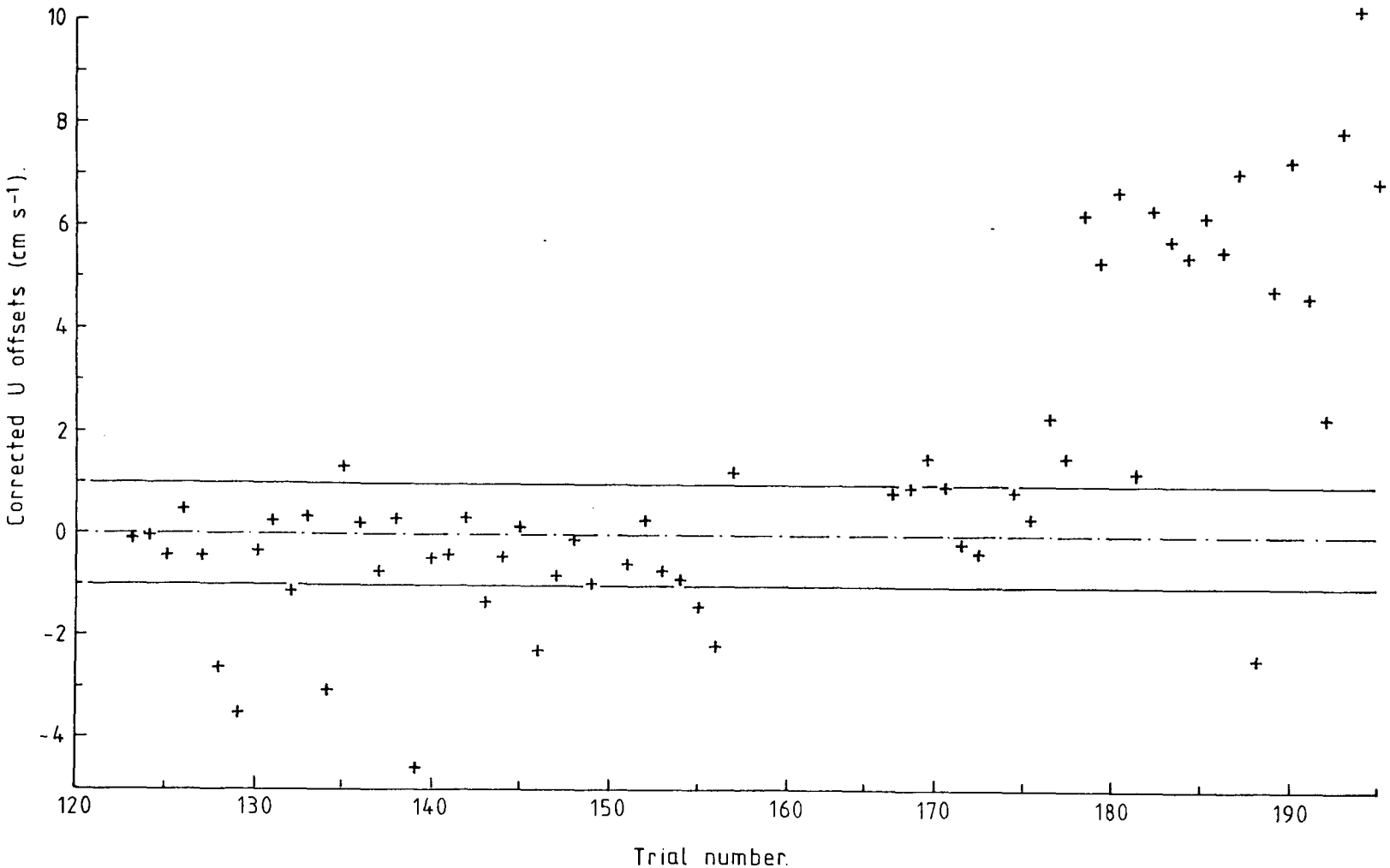
Corrected U offsets (cm s⁻¹).
10
8
6
4
2
0
-2
-4
120
130
140
150
160
170
180
190
Trial number.

Fig. 4.4 Preliminary estimates of velocities for trial 138.

a) 12 minute averaged velocities recorded by the rotors (TOP).

b) 12 minute averaged velocities from the u channels of the e.m. heads (CENTRE).

c) 12 minute averaged velocities from the w channels of the e.m. heads (BOTTOM).

———— Sensor height = 56.0 cm

– – – – Sensor height = 96.5 cm

– · – · Sensor height = 138.0 cm

····· Sensor height = 178.5 cm

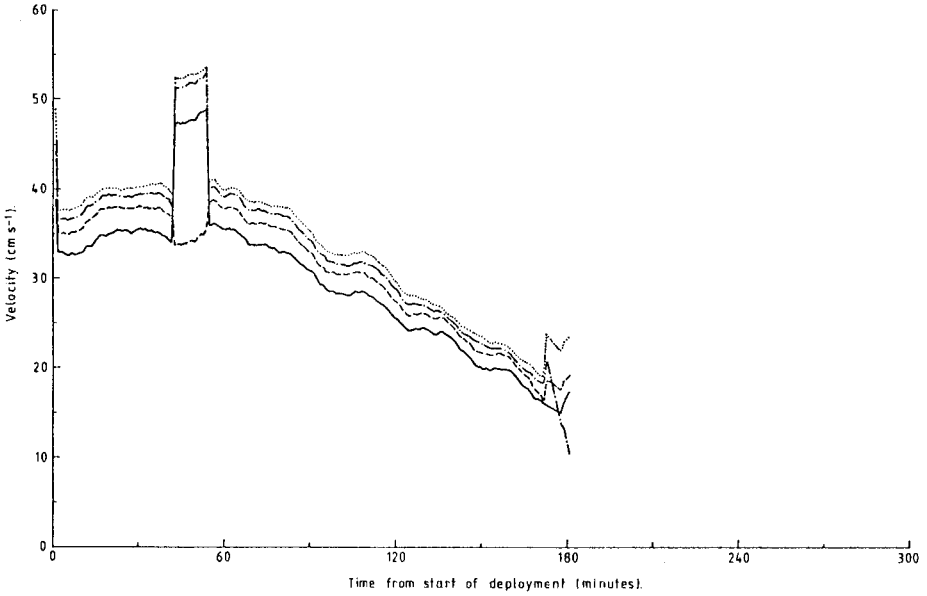
Velocity (cm s⁻¹).
60
50
40
30
20
10
0
0
60
120
180
240
300
Time from start of deployment (minutes).

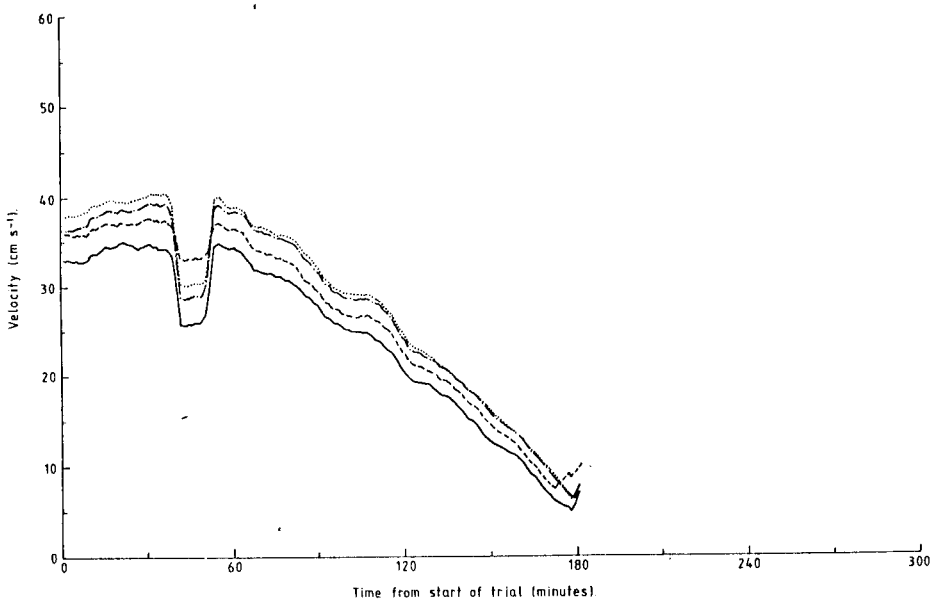
Velocity (cm s⁻¹).
60
50
40
30
20
10
0
0
60
120
180
240
300
Time from start of trial (minutes).

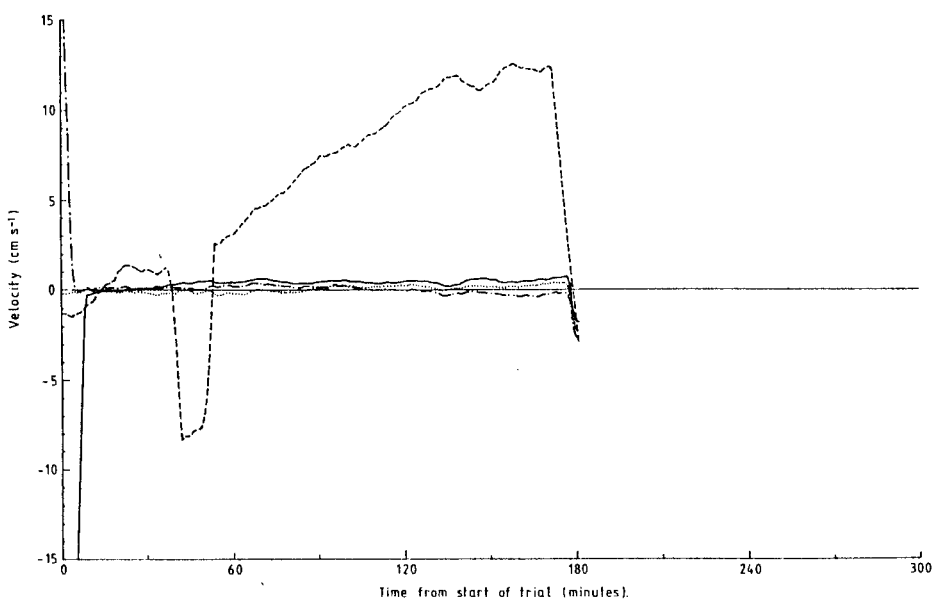
Velocity (cm s⁻¹)
15
10
5
0
-5
-10
-15
0
60
120
180
240
300
Time from start of trial (minutes).

CHAPTER 5 - FACTORS INFLUENCING THE DERIVATION OF TURBULENCE PARAMETERS FROM THE LOG-LAW

5.1 INTRODUCTION

In a study of turbulence in the benthic boundary layer it is a commonly accepted practice to evaluate the turbulence parameters u_*, z_o and C_{100} from equations 1.11 and 1.13 (see Section 1.3), reproduced below.

$$\frac{\bar{U}}{u_*} = \frac{1}{\kappa_0} \ln \left[\frac{z - d}{z_0} \right] \quad , \qquad 1.11$$

$$C_{100} = \left[\frac{u_*}{U_{100}} \right]^2 = \left[\frac{1}{\kappa_0} \ln (z/z_0) \right]^{-2} \quad , \qquad 1.13$$

These equations are derived for the idealised conditions of non-accelerating (statistically stationary) and non-rotational flow over a hydrodynamically rough surface, neutral stratification and in a layer of constant Reynolds stress close to the water-sediment interface. Due to the nature of the flow in the marine environment, particularly in the area of this study, some, or possibly all of these conditions may not be satisfied.

This chapter examines possible departures from the above conditions, particularly those concerning a constant stress layer, non-accelerating flow and a hydrodynamically rough boundary. An estimate of surface wave effects is made and the possibility of some degree of stratification is considered, which might be due to suspended sediments or temperature and salinity variations. In addition, the effects on the parameters of sensor misalignment, relative to one another and as a result of bedforms, and rotor inertia are also considered.

The data analysed in this and the following chapters were collected during the trials listed in Table 5.1, unless otherwise

stated. This data was considered to be of sufficiently high quality having been assessed according to the criteria outlined in Chapter 4. Data for which the angle of flow with respect to the sensors was outside the limits specified in Chapter 3, ±30° for the rotors and -10° and +30° for the e.m. heads, were removed during the application of the FORTRAN programmes.

The assumption of non-rotational flow was considered in Section 1.3 and was taken to be valid throughout the ensuing analysis.

5.2 THE CONSTANT STRESS LAYER

In Section 1.2.3 it was stated that the log-law applied in a region of constant stress close to the boundary. Monin and Yaglom (1971) state that this layer typically occupies 10 - 20% of the boundary layer, where vertical profiles of the mean dynamic variables are only slightly sensitive to the variation of boundary stress (τ_0). A model to predict the boundary layer thickness (δ), discussed in a paper by Soulsby (1983), suggests that δ is depth limited in the area of this study. The model was based on data collected in May before an appreciable thermocline might be formed. As discussed in Section 2.3, the thermocline in our case extended to a maximum depth of 10m along the line of stations to the west of Blackpool during the SH. 7/82 cruise. If δ can be taken to extend from the sea bed to the bottom of the thermocline, then δ will be approximately 28 m. At station 18, see Fig. 2.2, the minimum recorded depth was 17.0 m. The thermocline was considerably thinner at this station, being only 3 m thick. Taking the figures of 10 - 20% quoted above, a constant stress layer could possibly exist beyond the height of the top sensor at all these stations.

Due to the highly variable nature of the Reynolds Stress (Heathershaw and Simpson, 1978; Gordon and Witting, 1977; Soulsby, 1980) it is difficult to determine with confidence the relationship between stresses recorded at various heights. The least squares technique detailed in Appendix 2 was applied to the data analysed in this section. This enabled a statistical significance to be placed on the gradient and intercept which, within the confidence limits, will be equal to unity and zero respectively for a plot of stresses at two heights, if a constant stress layer should exist. An additional advantage of this technique to determine the slope m, where

$$m = \frac{\Sigma (x_i - \bar{X})(y_i - \bar{Y})}{\Sigma (x_i - \bar{X})^2} ,$$

was that lower values of x (stress at the lowest uw recording head) were given less weighting. These values have proportionally greater sampling errors (Heathershaw and Simpson, 1978) than stresses of greater magnitude. Using a simple average the values may significantly affect estimates of m.

Before the comparison of stresses was made it was attempted to exclude statistically non-stationary data to a level of confidence of 95%. The test, given by Bendat and Piersol (1971), was based on the number of crossings of the median value of the 12 individual one minute averaged stress values which constituted a 12 minute averaged value of Reynolds stress. Less than 3% of the values appeared non-stationary as a result of this test. Those that were occurred randomly throughout the records as well as with position above the sea bed, and were removed from the data.

Table 5.1 presents the results of the comparisons, showing trial number, the gradient (m) and intercept (c) of the plots with 95% confidence limits (the gradient is effectively the ratio), the number

of 12 minute averages in the trial and the station number. In addition, the two right hand columns present the gradient and intercept, with 95% confidence limits for each station. There were only two values of m and c per trial since one head recorded uv. All the values of m marked * indicate that a constant stress layer existed within the 95% confidence limits.

Consider first the 22 trials analysed from the data collected during the J.M. 9/81 cruise. The uw recording heights were 56.0, 138.0 and 178.5 cm above the sea bed. In all but two trials (144 and 152) the stress at height 178.5 cm was found to be comparable to that at height 56.0 cm, within the 95% confidence limits. When heights 56.0 and 138.0 cm were compared, 7 trials (125, 127, 131, 132, 138, 144 and 148) indicated that the values of stress were not equivalent. Grouping the data for each station, all stations indicated a constant stress layer in comparisons between heights 56.0 and 178.5 cm. Alternatively, only station 14 suggested a constant stress layer from the ratios of heights 56.0 and 138.0 cm. In every instance where the ratios failed to indicate a constant stress layer within the confidence limits, the stress at 56.0 cm was greatest.

During the SH. 7/82 Cruise sensors at heights 47.5, 100.0 and 172.5 cm recorded uw up to and including trial 177. Of these comparisons, only that between heights 47.5 and 100.0 cm, during trials 170 and 174, suggested a departure from the constant stress layer. From trial 178 onwards the e.m. heads of interest were at 100.0, 138.0 and 172.5 cm. Only one trial (186) indicated that the stress layer was not constant between the heights 100.0 and 138.0 cm. Again departures were when comparing the lowest e.m. head with the central of the three, with the greatest stress at the central one for trials 170 and 186 and at the bottom for 174. Grouping the data

showed that the stresses from station 16 were not comparable when considering heights 47.5 and 100.0 cm, with the latter recording the greater stress. The remaining comparisons indicated a constant stress layer.

In every case, when the value of m indicated a constant stress layer, the intercept equaled zero within the 95% confidence limits. It would be expected that if the stress at one height equaled zero, then throughout the water column this would also be true. For trials 148, 170 and 174 and station 16, comparing the bottom and central sensors gave a value of c not equal to zero, in accordance with the value of m, which also indicated a departure from the constant stress layer. This also applied for trials 144 and 152 between the bottom and top sensors.

When grouping the trial data for each station, possible local variations in bedforms should not be significant. The least squares technique simply compared ratios of stress, which if a constant stress layer existed, should have been independent of bedform.

Ferguson (1979) recorded similar results to those obtained at stations 16 and 17, from work in the Eastern Irish Sea. He suggested that the bottom sensor, which was 50.0 cm above the bed, may have been shielded by bedforms. This may have been possible as the data was collected in the same area as station 8 (see Fig. 2.2), where quite considerable bedforms were observed (Fig. 2.3a). Similar results were obtained by Smith and McLean (1977) from work in the Columbia River, where the Reynolds stress was observed to increase from the bed to 200.0 cm. This was also attributed to bedforms. The data collected by the latter workers fitted the form presented by a model for flow over bedforms.

The results of station 16 cannot be explained by the presence

of bedforms. The station was situated along the line of stations to the west of Blackpool, where the bed was as featureless as that shown in Fig. 2.3b. Neither can the observations of the J.M. 9/81 cruise be explained in these terms, as the stress minimum was consistantly observed at the central e.m. head.

The systematic nature of the above anomalies, combined with the fact that the central sensor alone departed from the constant stress layer, suggest that sensor misalignment rather than the effects of accelerating flow, was responsible. This possibility is explored in the following Section.

It should be noted that Heathershaw and Simpson (1978) have suggested that any variation from the constant stress layer may be accounted for by the inherent sampling variability of the Reynolds stress. The uncertainty of ± 45% quoted in a single 12 minute averaged value, represents ± 64% in a comparison of stresses at two heights. Taking trial 125 as an example, the ratios between heights 56.0 and 138.0 cm varied between 0.59 and 1.37. With an uncertainty of ±64%, all the ratios would be within the limits for a constant stress layer, contrary to the value of 0.694 ± 0.215 given in Table 5.1. This approach would suggest that in the majority of cases the comparisons presented in Table 5.1 represented a constant stress layer.

5.3 SENSOR MISALIGNMENT AND ROTOR INERTIA

Up to this point, the only corrections applied have been to compensate for the misalignment of the sensors with respect to the mean flow, as discussed in Chapter 4. No account has been taken of the influence of possible topographic features, or sensor misalignment when attached to the turbulence rig.

5.3.1 E.m. Heads.

In the case of the e.m. heads the covariance ($\overline{uw}$) obtained from the recordings of such a sensor is sensitive to the orientation errors of the sensor. Heathershaw (1979) gave an expression for the calculated covariance as

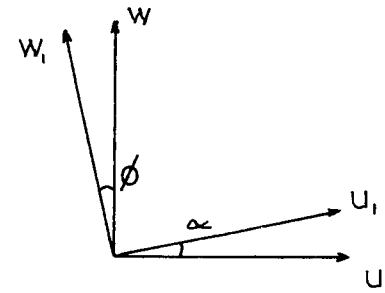

$$\overline{u_1 w_1} \approx \overline{uw}\left[1 + \alpha\left(\frac{\overline{w^2} - \overline{u^2}}{\overline{uw}}\right)\right] ,$$

where the sensor had been rotated through a small angle α ($\alpha = \phi$), measured in radians, with respect to the co-ordinate axis so as to measure u_1 and w_1 (see sketch). It was suggested, from consideration of observed data, that errors arising from this may be typically ± 10% per degree. In addition, misalignment of the electrode pairs, not accurately perpendicular, would give a similar expression for the apparent covariance of

$$\overline{u_1 w_1} \approx \overline{uw}\left[1 - \alpha.\phi + \left(\frac{\overline{w^2}\alpha - \overline{u^2}\phi}{\overline{uw}}\right)\right]$$

This error was estimated to be between ± 2% and ± 7%.

Throughout the analysis of the data collected during this study, the assumption has been made that the mean flow streamlines parallel to the sea bed were being recorded. No account has been taken of possible deviations of the central sensor support (see Fig. 2.1) from the perpendicular with respect to the bed. In the areas where bed forms existed, the rear foot (that from which the cables trail in Fig. 2.1) of the turbulence rig may have lain upon a raised feature, or in a trough. Such a feature need only deviate approximately ± 3 cm from

the general level of the bed to tilt the central support ± 1° from the vertical. This would be equivalent to rotating the sensor ± 1° with respect to the co-ordinate axis discussed above. If either of the other two feet rested on, or in, a feature, the vertical component w would have been wrongly sampled. A feature of approximately ± 2 cm would tilt the central support ± 1° from the vertical. If the tilt exceeded ± 10°, equivalent to a feature of ± 18 cm, the response of the sensors would have been severely restricted, as discussed in Section 3.4.1 and shown in Figs. 3.4 and 3.5. An inclinometer was not deployed in this study, but data from one used by Heathershaw (1979), in approximately the same area in which the bedforms of station 8 were observed (see Fig. 2.3a and Section 2.3 for details), indicated a tilt of the order of 2.5°. This would result in an error in $-\overline{uw}$ of up to ± 30%.

In Chapter 4, the use of one sensor to record the orientation of the rig with respect to the flow was discussed. The presence of bedforms would affect the response of the e.m. head in the same manner as the deviation from the vertical affects the w channel. A tilt of ± 2.5° would give an uncertainty well within the ± 1% uncertainty of the absolute velocity from the flume calibrations. The uncertainty of ± 4%, quoted in Section 4.4, in measuring the direction still therefore applies.

5.3.2 Rotor Misalignment.

The influence of tilt on Aanderaa type Savoniuos rotors was examined by Serkin and Kronengold (1974). A reduction by 5% in the number of revolutions of the rotor was observed for a tilt of ± 10° from the vertical axis of the rotor. For a tilt of 2.5° the discrepency becomes camparable with the uncertainty in the flume

calibrations for this study of ± 1%, discussed in Section 3.2.

5.3.3 Rotor Inertia ('pumping').

Work completed by Hammond and Collins (1979), indicated that the superposition of an oscillatory current upon a unidirectional flow gave an apparent increase in velocity when recorded by Aanderaa rotors. The increase was independent of the period of the oscillations, between the experimental values of 5 and 15 seconds, and entirely dependent on the maximum velocity of the oscillations and the magnitude of the unidirectional flow. This behaviour, often referred to as 'pumping', resulted from the inertia of the rotor, giving the characteristic of a rapid response to positive accelerations in comparison to negative. The effect of inertia was partially responsible for the higher starting threshold (2.4 cm s^{-1}) than stopping threshold (1.8 cm s^{-1}) in this work, detailed in Section 3.2.2.

Fig. 5.1 shows a 12 minute time series of u', and an expanded 100 second extract, from trial 186. The record was recorded at 100.0 cm above the bed during a period when U_{100} = 32.88 cm s^{-1}. The peak to peak velocity fluctuations, marked X in Fig. 5.1, were taken to be 9 cm s^{-1}, and considered dominant in inducing 'pumping'. The fluctuations were approximated to a wave of peak velocity 4.5 cm s^{-1}, about a mean current, and period (2π/frequency) ≈ 60s. Although this period was significantly greater than the maximum value of 15s investigated by Hammond and Collins (1979), it was assumed that the apparent increase in $\bar{U}$ was still independent of period at this value. At $\bar{U}$ = 20 cm s^{-1} and a peak velocity fluctuation of ± 4.5 cm s^{-1}, $\bar{U}$ would be overead by 1 cm s^{-1}. A typical velocity

difference between the top and bottom rotors, at the above value of $\bar{U}$, was 4 cm s^{-1} (see e.g. Fig. 4.4a), with the top rotor overeading by approximately 0.5 cm s^{-1}. With these values, u_* and z_0 could be underestimated by up to 12.5% and 70% respectively.

The above estimates can be regarded as maximum values, as peak to peak fluctuations below $\bar{U}$ = 32.88 cm s^{-1} would be smaller. Above $\bar{U}$ = 30.0 cm s^{-1} the increase in $\bar{U}$ due to 'pumping' can be considered negligible (Hammond and Collins, 1979).

5.3.4 Sensor Misalignment in the Constant Stress Comparisons.

What appeared to be a systematic error in the comparisons of stress in Section 5.2 can be attributed to sensor misalignment. Sensors need only be misaligned by 1^{o} relative to one another to produce a systematic error of 10%. An error of this magnitude could account for the apparent departures from the constant stress layer, discussed in Section 5.3. Although the deviation of the central support from the vertical was systematic for one trial, it would be predominantly random over a number of trials. Throughout this work the measured $\overline{uw}$ has been taken to be a correct measure of the Reynolds stress, but subject to certain possible sources of error, which unfortunately could not be corrected. This should be borne in mind when considering the results presented in the following Chapters.

5.4 THE HYDRODYNAMIC NATURE OF THE FLOW

In the analysis of pipe flow experiments it is common to define a roughness Reynolds number $R_r = u_*d/\nu$, in the manner of Nikuradse (1933), where d is the scale of the roughness elements and ν = kinematic viscosity. Three regimes of flow have been observed,

described as hydrodynamically smooth ($R_r \angle 5$), transitional ($5 \angle R_r \angle 70$) and fully rough ($R_r \triangle 70$). Observations of geophysical flows have indicated a full range of these regimes to be present.

When the magnitude of the viscous stress is comparable with the Reynolds stress the flow is termed smooth. Under this regime the roughness elements are submerged in the viscous sublayer and can be considered to have no influence on the flow above this layer. Such conditions were discovered by Caldwell and Chriss (1979), using a hot thermistor current meter in 200 m of water on the Oregon continental shelf. Transitional flow occurs when the influence of the viscous forces is comparable to that provided by the roughness elements that protrude partially from the viscous sublayer. When the elements protrude well beyond the viscous sublayer, and it is only their interaction with the fluid motion that determines the nature of the flow, then the regime is termed rough. Sternberg (1968) suggested that in geophysical flows the boundary from transitional to rough flow was characterized by a decrease in the dispersion of the drag coefficient (C_{100}) when plotted against $R_e = \bar{U}_z z/\nu$, where z = 100 cm. Re was estimated as approximately 1.5×10^5 at the boundary between the two regimes.

For the log-law of equation 1.11 to apply, the flow was assumed to be hydrodynamically rough. For such flow over a fixed bed the drag coefficient C_D can be defined from the quadratic stress law of equation 1.12 as $C_D = \tau_0/\rho\bar{U}_D^2$. For each station given in Table 5.1, three separate estimates of C_D were made. Figs. 5.2a, 5.2b and 5.2c give plots of C_D versus Re, in the manner of Sternberg (1968), for station 12, where ν was taken as 0.014 $cm^2\ s^{-1}$ (10°C, 35 °/oo). The line through the values of C_D represents the mean, whilst the error bar indicates the ± 45% uncertainty that could be expected due to the

variability of the Reynolds stress (Heathershaw and Simpson, 1978). The height of each sensor in the plots is given in Table 5.2. Also drawn on each plot is the Karmann - Prandtl smooth flow relationship, where

$$C_D = \left[\frac{1}{\kappa_0} \ln \bar{U}_* z/\nu + 5.2 \right] \quad , \qquad 5.1$$

Table 5.2 presents, for each station analysed, the average C_D for each sensor, with a 95% confidence limit, the number of 12 minute averages in each estimate, the nature of the bed and the hydrodynamic nature of the flow.

When estimating the nature of the flow it was immediately obvious from Figs. 5.2a, 5.2b and 5.3c that the regime was either transitional or rough. To determine in which category the flow could be placed, the dispersion of C_D over a range of Reynolds numbers was examined. Fig. 5.3 gives the 95% confidence limits on C_D for intervals of 2×10^5 in Reynolds number for station 12. There was no evidence of an increase in dispersion of C_D at lower Reynolds numbers, said to characterize the boundary between rough and smooth flow (Sternberg, 1968). The situation shown at station 12 was typical of all stations, with the flow estimated as rough regardless of bottom type, mean velocity or height above the bed.

5.4.1 Relation of Drag Coefficient to the Nature of the Sea Bed.

A comparison of C_D at the top sensor for all the stations appeared to reflect the varying roughness of the sea bed. From Table 5.2 and Fig. 2.2 it can be seen that the average values of C_D at the top sensor, for the stations lying along the line west of Blackpool, was in the range $(1.028 - 1.910) \times 10^{-3}$. The remaining southerly stations gave averages in the range $(2.877 - 3.338) \times 10^{-3}$. Bottom

topography at the southern stations was more varied (see Section 2.3). Combined with this, stations 18 and 8 had the same sediment characteristics as 16, but gave significantly greater values of C_D, suggesting the above statement to be valid. Stations 19 and 20, although practically devoid of bedforms, consisted of coarser roughness elements, possibly providing an explanation for the higher average C_D.

A decrease in C_D would be expected with height in a constant stress layer. At stations 8 to 14 the minimum at the central sensor tended to belie this, but was probably a result of the supposed misalignment discussed in Section 5.3. A similar explanation could be forwarded for the the peak C_D at the central sensor of station 16. The peak in C_D at the central sensor for stations 18 - 20 cannot be explained in this manner. Within the 95% confidence limits C_D may be distributed as expected. This could also apply in the cases of the other stations, so a firm conclusion was difficult to reach.

5.5 BOUNDARY LAYER CURRENTS INDUCED BY SURFACE WAVES

It was stated in Chapter 2 that a sea state corresponding to winds greater than force 5 on the Beaufort scale (17 - 21 knots, or 8.5 - 10.5 m s^{-1}) was sufficiently severe to prevent deployment of the turbulence rig. Surface wave heights expected under such conditions are given on the Beaufort scale as 1.25 - 2.5 m (Beer, 1983). There was a possibility that such waves may have induced velocities close to the sea bed of the order of the tidal velocities, especially during periods close to slack water at the shallower stations. As a result u_* and z_0, from the log profiles, and $\overline{uw}$, from the e.m. heads, may have been considerably modified.

Daily averages of wind velocity collected at Bidston

Observatory during the periods of the J.M. 9/81 and SH. 7/82 cruises are presented in Table 5.3. By utilising these readings and applying linear surface wave theory, extreme values of the horizontal (u) and vertical (w) components of surface wave induced velocities were estimated at the boundary (e.g. see Bowden, 1983).

For waves in water of finite depth, the velocity components at a height z above the bed, due to a wave of wavenumber k and angular frequency σ, travelling in the x direction, are:

$$u = a\sigma \frac{\cosh(k(h + z))}{\sinh(kh)} \cos(kx - \sigma t) \quad , \qquad 5.2$$

$$w = a\sigma \frac{\sinh(k(h + z))}{\sinh(kh)} \sin(kx - \sigma t) \quad , \qquad 5.3$$

where a is the amplitude of the vertical displacement of the sea surface, and h the water depth.

If we consider station 8, the water depth was relatively shallow (17.5 m at low water) and the wind speed a maximum (8.0 knots $\approx$ 4.1 m s^{-1}) during measurements. Fig. 5.4 gives graphs, derived by Carter (1982), to predict the significant wave height (H) and zero up-crossing period (T), given wind speed and fetch, or if not fetch, the duration of the wind blowing from a constant direction. (The significant wave height = the average of the heighest 1/3 of the waves in a given time interval. The zero up-crossing period = the number of up-crossings of the mean height in a given time interval. These terms were explained more fully by Tann, 1976). For a wind velocity of 4.1 m s^{-1} and maximum possible fetch of ~200 km (see Fig.2.2 for station position), given the westerly wind recorded in the ships log, and using Fig. 5.4, H $\approx$ 40 cm and T $\approx$ 3s.

Using equations 5.2 and 5.3 and a = H/2 $\approx$ 20 cm, $\sigma = 2\pi/T \approx$ 2.07 s^{-1} and $k = \sigma^2/g \approx 0.0044$ $cm^{-1}s^{-1}$, the maximum values of u and w

at 180 cm above the bed were ≈ 0.05 cm s^{-1} and 0.03 cm s^{-1} respectively.

The maximum value of u that could have been induced by surface wave action was approximately 0.25% of the minimum 12 minute averaged value of u, used in the analysis, of approximately 20 cm s^{-1}. This would have been undetectable within the ± 1% uncertainty in calibrations.

It would be inappropriate to compare directly surface wave induced values of w and the minimum in the 12 minute averaged value of w. The average w represents an average of the fluctuations about zero, which at any instant may be typically in the range ± 10 cm s^{-1}. For this reason the approach of Bowden and Ferguson (1980) was adopted. The wave energy was taken to be detectable in the root mean square (r.m.s.) turbulence level for a given component, when r.m.s. wave amplitude ∧ r.m.s. turbulence level (α). α was taken to be due to shear alone. It was observed by the authors that

$$\overline{u^2}^{1/2} = 0.17\, U_{100}$$

$$\overline{w^2}^{1/2} = 0.08\, U_{100}$$

and this was independent of height for z ∠ 200 cm. Similar values were given by Soulsby, Davies and Wilkinson (1983) and Gordon and Dohne (1973).

From equations 5.2 and 5.3 wave energy would only be detectable in u and w r.m.s. values when

$$U_{100} \angle \frac{a\sigma}{0.17\sqrt{2\alpha}} \frac{\cosh(k(h+z))}{\sinh(kh)} \quad , \qquad 5.4$$

$$U_{100} \angle \frac{a\sigma}{0.08\sqrt{2\alpha}} \frac{\sinh(k(h+z))}{\sinh(kh)} \quad , \qquad 5.5$$

Substituting the extreme values of a, σ and k previously calculated, the right hand terms of equations 5.4 and 5.5 equal 4.2 cm s^{-1} and 2.7 cm s^{-1} respectively, with α = 10% (typical uncertainty in r.m.s. u and w (Bowden and Ferguson, 1980)). At the lowest value of U_{100} ($\approx$ 20 cm s^{-1}) considered in this study, the wave energy was considered undetectable.

The above calculations indicate that the influence of surface wave induced velocities was negligible in the analysis of data collected during this study.

5.6 BOUNDARY LAYER STRATIFICATION

The extent of the near bottom stratification induced by variations in temperature and salinity was discussed in Section 2.3. Neil Brown C.T.D. profiles indicated that the water column within 5 m of the bed was neutrally stratified, as defined by the local Richardson number (Ri $\angle$ 0.03), for all stations.

The absence of suspended sediment concentrations in this study provided the greatest uncertainty in the estimates of the degree of stratification. Adams and Weatherly (1981), using a numerical model, have suggested that sediment in suspension could lead to an apparent reduction in κ_0 of up to 15%. This would be manifest as a 15% over estimate of u_*, when using the log-law of equation 1.11, as κ_0 remains constant. A resulting over estimate of u_*/κ_0 leads to z_0 being underestimated. Theoretical velocity profiles for a variety of concentrations (Taylor and Dyer, 1977) have shown the velocity profile to be unaffected only when all the sensors are situated in neutrally stratified flow (i.e. sediment transport is by bed load only, or non-existent).

Soulsby (1983) presented diagramatically (Fig. 5.5), for known

values of u_* and sediment grain diameter (d_i), a method to predict the degree of stratification above an unrippled bed with uniform sediment dimensions. It was based on a theoretical expression for z/L (z = height above the bed and L = Monin-Obukhov length) derived from several existing expressions for sediment concentration profiles. The diagram suggests that sediment movement would be completely absent, for all d, for only a very restricted range of relatively low u_*.

Unfortunately values of d were not ascertained during this work, as the grab samples were inadvertantly discarded. A programme of extensive grab sampling in the Eastern Irish Sea (Pantin, 1977) reflected the nature of the sediment characteristics presented in Table A1.1. Values of d at all stations, excepting 6, 11, 12 and 13 (see Fig. 2.2), were observed to be of the order of 1000 - 2000 μm. The remaining stations indicated d to be in the range 250 - 1000 μm. Considering these estimates of d in conjunction with Fig. 5.5, and a peak value of $u_* \approx 4.0$ cm s^{-1} from the trials, it would appear to be reasonable to assume that sediment transport was chiefly as bed load. This was to some extent supported by the film from the photographic unit, deployed at station 20, where the suspended sediment concentration appeared low (see Section 8.2). In this case readings were unlikely to be influenced. There was a possibility that large amplitude events in the turbulence spectrum may have briefly brought sediment into suspension.

It seems reasonable to assume that the water column can be regarded as neutrally stratified during this study. Inexplicably large values of the confidence limits on u_* and z_0 (see Chapter 7) may indicate the presence of stratification.

5.7 THE INFLUENCE OF TIDALLY ACCELERATING FLOW

Consecutive 12 minute averages of rotor velocity for trial 127 are presented graphically in Fig. 5.6, combined with a plot of $|d\bar{U}/dt|$ (average in velocity differences over the averaging interval at all four rotors ÷ time interval of 720 seconds). Evidently the flow was experiencing constant variations in velocity, with no obvious period of zero acceleration. The test for statistically stationary flow, discussed in Section 5.2, suggested non-stationarity during the final 72 minutes of the flow only. It existed in only ten of the possible twenty four 12 minute averages. The situation observed during trial 127 was representative of the majority of the trials listed in Table 5.1. Rapid accelerations, such as the peak at approximately 17:00 hours in Fig. 5.6, were often found to be statistically stationary. This suggested the need for the more rigorous approach to define accelerating flow, discussed below.

5.7.1 Soulsby and Dyer (1981) Criterion for Accelerating Flow.

An acceleration length $\Lambda = u_*|u_*|/\dot{u}_*$, where $\dot{u}_* = du_*/dt$, was defined by Soulsby and Dyer (1981) to correct for the effects of accelerating flow, when deriving turbulence parameters from the velocity profile. The log-law of equation 1.11 was expressed as,

$$\bar{U} = \frac{u_*}{\kappa_0}\left[\ln\frac{z - z_0}{z_0} - \frac{z - z_0}{\gamma\Lambda}\right] \quad , \qquad 5.6$$

where the usual annotation applies, γ = constant and z_0 can be considered $\ll z$. When applied to data collected in Start Bay it was estimated that u_* and z_0 may be underestimated by 20% and 60% respectively during the initial accelerating phase. Conversely,

during the deceleration u_* and z_0 could be overestimated by 20% and 83% respectively. These figures underline the importance of applying equation 1.11 to non-accelerating flow only.

Values of u_* and z_0, considered in the following Chapters were derived from equation 1.11 and in the manner of Soulsby and Dyer (1981). To use the latter technique γ and κ_0 had to be estimated. This was achieved using velocity profile measurements in conjunction with simultaneous measurements of u_* from the e.m. heads. In the main, the procedure described by Soulsby and Dyer (1981) was followed, but with an attempt to define a criterion for non-accelerating flow.

Values of τ_0, and hence u_*, were estimated from,

$$\tau_0 = \frac{z_A z_B}{z_B - z_A}\left[\frac{\tau_A}{z_A} - \frac{\tau_B}{z_B} + \frac{\partial}{\partial t}\left(\overset{\Delta}{U}_B - \overset{\Delta}{U}_A\right)\right] , \qquad 5.7$$

derived from the equation of motion in a uniform, non-rotating unstratified fluid, where

$$\overset{\Delta}{U}(z) = \frac{1}{z}\int_0^z U(z')\,dz'$$

The above form of τ_0 is intended to correct for accelerating flow, with τ_A and τ_B obtained at e.m. heads 1 and 4 , at heights z_A and z_B respectively. The central sensor was not included because of the probable misalignment discussed in Sections 5.2 and 5.3. Losses due to cut off in the cospectral content, at frequencies corresponding to the record length and digitizing rate, were corrected for by the following procedures described in Soulsby (1980). In that work the expected percentage loss in the cospectrum was presented graphically over a range of the dimensionless wavenumber kz of 1×10^{-4} to 1×10^{4}. The lowest and highest values of

kz observed in the present work were in the ranges of 0.1 - 0.03 and 13.0 - 52.0 respectively, as discussed in Section 4.7. By taking 10 points, equally spaced over the ranges of kz, 10 corresponding values of the percentage loss were obtained. In the computer programs, values of kz were calculated for each value of stress. The percentage loss was taken as that corresponding to the closest of the 10 values of kz above. The corrections for the high frequency loss was typically in the range 0.2 to 0.6%, and as such relatively insignificant. In the low frequency range corrections were typically 3% to 10%. These losses were systematic, which if not corrected for would have led to considerable underestimates of τ_0.

Having estimated τ_0, u_* and hence Λ were calculated for the 12 minute averages. Using equation 5.8, rotor velocities and u_* from the e.m. heads, three estimates of the apparent value of von Karmann's constant ($\tilde{\kappa}$), not accounting for accelerating flow, were made for each 12 minute average. From equation 5.9 a plot of $\tilde{\kappa}^{-1}$ versus z/Λ yielded three values of γ and κ_0 per trial

$$\tilde{\kappa} = \frac{u_*}{z}\left[\frac{\partial U}{\partial z}\right]^{-1} \quad , \qquad 5.8$$

$$\tilde{\kappa}^{-1} = \kappa_0^{-1}\left[1 - \frac{z}{\gamma\Lambda}\right] \quad , \qquad 5.9$$

Only those points in the range $|z/\Lambda| < 0.02$, exhibiting a linear relationship, were considered. From the trials listed in Table 5.1, 101 estimates of γ were made. In several cases insufficient points (< 3) were available, as the above criterion was not satisfied, so the maximum 108 estimates was not possible. A mean value of $\gamma = 0.066$, with a standard deviation of $\pm$ 0.117, was given. This value is comparable with that given by Soulsby and Dyer (1981) of

0.04, based on 7 estimates.

Time series of τ_0, Λ^{-1} and $\tilde{\kappa}$ for trial 127 are presented in Fig. 5.7. There was no dependence of $\tilde{\kappa}$ on height, contrary to the results of Soulsby and Dyer (1981), who attributed it to the differing performances of the Braystoke rotors. There appeared to be an increase in $\tilde{\kappa}$ with time, but the converse situation, or steady values were found on other trials, suggesting this to be not significant. Fig. 5.8 gives a plot of $\tilde{\kappa}^{-1}$ versus $|z/\Lambda| < 0.02$, for which a linear relationship was found.

5.7.2 Estimate of von Karmann's Constant (κ_0).

Soulsby and Dyer (1981) estimated κ_0 from equation 5.9 by taking the averages of those values in the arbitrarily defined range $|z/\Lambda| < 0.005$. Flow was termed non-accelerating, representing a departure of the velocity gradient by at most 13% from the steady value. For the estimates of κ_0 made in this work an attempt has been made to define the non-accelerating range of $|z/\Lambda|$ from the collected data. The plot of $|d\bar{U}/dt|$, given in Fig. 5.6, indicates a period of relatively low acceleration, bounded by periods of greater acceleration at the beginning and end of trial 127. This situation was typical of the trials given in Table 5.1. A total of 434 values of $|d\bar{U}/dt|$ from the trials were plotted on the histogram of Fig. 5.9. It seemed a reasonable assumption that the relatively uniform number of occurrences of $|d\bar{U}/dt| < 0.004$ cm s^{-2} represented an approximation to non-accelerating flow. Taking the relationship $C_D = (u_*/\bar{U}_D)^2$, and a mean value of C_D from Table 5.2 of 2.4×10^{-3}, then $u_* \approx \bar{U}_D/20$ and

$\dot{u}_* \approx \dot{\bar{U}}_D/20$. Assuming $\dot{\bar{U}}_D = 0.004$ cm s^{-2} to define the limit of non-accelerating flow, $\dot{u}_* \approx 2.0 \times 10^{-4}$ cm s^{-2}. Taking u_* to be typically 2.25 cm s^{-1}, then $\Lambda = u_*|u_*|/\dot{u}_* \approx 25312.5$ cm. Given $z \approx 100.0$ cm, $|z/\Lambda| \approx 0.004$, comparable to the value of 0.005 used by Soulsby and Dyer (1981).

Table 5.4 presents the values of κ_0 derived from equation 5.9 for each station, where $\gamma = 0.066$ and $|z/\Lambda| \angle 0.005$. Included is the standard error on κ_0 and the values used in each estimate. There was a considerable variation in the estimates of κ_0, but only stations 16, 17 and 19 were found to give a value which departed, within the standard error, from the widely accepted value of 0.4. Of these, doubt must be cast on the values at stations 16 and 19, as the estimates were based on 4 and 2 points only. For the entire data set of 298 points the weighted mean $\kappa_0 = 0.379 \pm 0.098$ (excluding stations 16 and 19). This compares quite well with the value of $\kappa_0 = 0.398 \pm 0.012$ obtained by Soulsby and Dyer (1981) for 81 points at several stations in Start and Weymouth Bays. It is in even closer agreement with the work of Smith and McLean (1977), who estimated $\kappa_0 = 0.38$ from velocity profiles above bed forms, both with and without the presence of suspended sediment, in the Columbia river. Caldwell and Chriss (1979) estimated $\kappa_0 = 0.415 \pm 0.020$, based on flow measurements in the viscous sublayer over a hydrodynamically smooth bed on the Oregon continental shelf.

Alternatively, all stations, with the exceptions of 10, 16 and 19, gave a value of κ_0 which could be said to be equal to 0.35, suggested by Businger et. al. (1970) and Schotz and Panofsky (1980) for atmospheric work. Such a large discrepency in κ_0 would give estimates of Reynolds stress that differed by 27%. In the light of

this it was difficult to draw a firm conclusion on the value of κ_0. Possible departures from the values of unity in the ratios of u_*^2 to $-\overline{u'w'}$, in Chapter 6, may indicate which value is closer.

5.7.3 The Use of $|z/\Lambda|$ in Favour of $|d\bar{U}/dt|$.

In the following Chapters values of u_* and z_0 were corrected for the effects of accelerating flow, using equations from the work of Soulsby and Dyer (1981). If $|d\bar{U}/dt|$ can be used in place of $|z/\Lambda|$ considerable time and effort would be saved. Of the 434 values analysed from the 36 trials given in Table 5.1, only 107 (24.9%) could be termed non-accelerating as defined by $|z/\Lambda| < 0.005$. This contrasted with the 332 as defined by $|d\bar{U}/dt| < 0.004$ cm s^{-2}. If the criteria are to be considered equally valid the proportions should be approximately equal.

The estimation of $|z/\Lambda|$, based on $|d\bar{U}/dt| < 0.004$ cm s^{-2} in Section 5.7.2, included a number of fairly generous approximations. By varying the values of C_D and u_* from the collected data, the $|z/\Lambda|$ estimate may lie between 0.002 and 0.012. The number of values in the non-accelerating range $|z/\Lambda| < 0.01$ was increased to 236 (54.3%). Taking the above into consideration there was still a considerable discrepency which could not be accounted for.

To define non-accelerating flow with a reasonable degree of confidence, when determining u_* and z_0, it is perhaps wiser to use the criterion $|z/\Lambda| < 0.005$. This gives a measure of the degree of departure of the velocity gradient from a steady value. The range $|d\bar{U}/dt| < 0.004$ cm s^{-2} should only be applied for a coarse estimate of accelerating flow.

5.8 SUMMARY AND CONCLUSIONS

In this Chapter the flow conditions upon which the log-law of equation 1.11, used to determine u_* and z_0, is based were examined. Measurements were assumed to be in non-accelerating, neutrally stratified and non-rotational flow, over a hydrodynamically rough bed in a layer of constant stress. The magnitude of the surface wave induced velocities, possible sensor misalignment and rotor inertia were also considered.

A total of 12 stations, including 36 trials (103 hours 11 minutes of data), were tested for the existence of a constant stress layer. Comparisons between the bottom and central e.m. heads at stations 8 to 13 and 16 suggested a departure from a constant stress layer. The remaining comparisons indicated the Reynolds stress to be constant within 180 cm of the bed. The systematic nature of the departures from constant stress suggested that sensor misalignment, rather than accelerating effects, may have been responsible.

From the work of Heathershaw (1979), it was deduced that a 1^{o} misalignment of the co-ordinate axis of two e.m. heads relative to one another, would be sufficient to result in the observed departure from a constant stress layer. Further more, a tilt of the turbulence rig in the xz plane of $\pm$ 2.5^{o}, equivalent to a bedform of $\pm$ 10 cm, may have resulted in $\overline{uw}$ being in error by $\pm$ 30%. Such a tilt in the yz plane was thought unimportant. Similarly the performance of the Aanderaa rotors would be unaffected by a tilt of this magnitude in either plane. By simplistically considering the fluctuations in u (u') to be a current superimposed on a unidirectional flow ($\overline{U}$), inertial overeading was examined. Comparisons with laboratory work of Hammond and Collins (1979), where such an effect was examined, suggested that overeading was negligible above U_{100} = 30 cm s^{-1}.

Although at $U_{100} \approx 21$ cm s^{-1}, u_* and z_0 may be underestimated by up to 12.5% and 70% respectively. The error decreases in significance to 30 cm s^{-1}.

An absence of an increase in the dispersion of the drag coefficient (C_D) with decreasing Reynolds number, implied that the flow was hydrodynamically rough at all the stations. A C_D minimum at the central sensor at stations 8 to 14, and a maximum at 16, was attributed to sensor misalignment. It was thought that the values of C_D for each station accurately reflected the varying roughness of the bed.

From a consideration of linear surface wave theory and wind data, collected during the period of turbulence data recording, it was estimated that surface wave energy was negligible at the boundary. Maximum surface wave induced velocities were ≈ 0.05 cm s^{-1}, too low to induce 'pumping' of the rotors.

C.T.D. measurements of the water column showed it to be neutrally stratified ($Ri < 0.03$) within 5 m of the bed. The nature of the sediment in the area of study, combined with a diagramatic prediction for sediment motion (Soulsby, 1983), suggested sediment transport to be as bedload only. It was considered unlikely that the form of the velocity profiles would be influenced, although z_0 may have been altered in the presence of bedload transport.

A criterion suggested by Soulsby and Dyer (1981), defining non-accelerating flow to be in the range $|z/\Lambda| < 0.005$, showed only 25% of the 434 values collected from 36 trials to be non-accelerating. The constant $\gamma = 0.066 \pm 0.117$, based on 101 estimates, was comparable with the value of 0.04 given by the afore mentioned workers. A weighted mean value of $\kappa_0 = 0.379 \pm 0.098$ for all stations was found from 298 estimates in the range $|z/\Lambda| < 0.005$. For

individual stations κ_0 varied from 0.292 ± 0.068 to 0.591 ± 0.193, with no tangible dependence on sediment characteristics. It was not possible to draw a conclusion to whether κ_0 was representative of the value increasingly used in the atmosphere (0.35), the value used in marine and laboratory flows (0.40 - 0.42) or a value midway between the two. The variation of κ_0 may

show up in the comparisons of $-\overline{u'w'}$ and u_*^2 in Chapter 6. Finally, it was decided that it was inadvisable to use values of $|dU/dt|$ to define non-accelerating flow, except for rough estimates.

Summarising, it can be concluded that during this study, measurements were made in a neutrally stratified layer of constant stress, above a hydrodynamically rough bed, where the influence of surface waves was negligible. The exception to the idealised conditions assumed in the derivation of equation 1.11 was in the case of non-accelerating flow. Corrections for this were applied when deriving u_* and z_0 in Chapters 6 and 7. Some doubt was also cast on the correct orientation of the central e.m. head during deployments at stations 8 - 13 and 16. This should be bourne in mind in the analysis contained in Chapter 6.

Fig. 5.1 A 12 minute time series of u' and expanded 100 second extract. Data was recorded during trial 186 at the e.m. head 100.0 cm above the bed. Below, in the expanded section, X represents what were considered the dominant peak to peak fluctuations in inducing 'pumping' of the rotors.

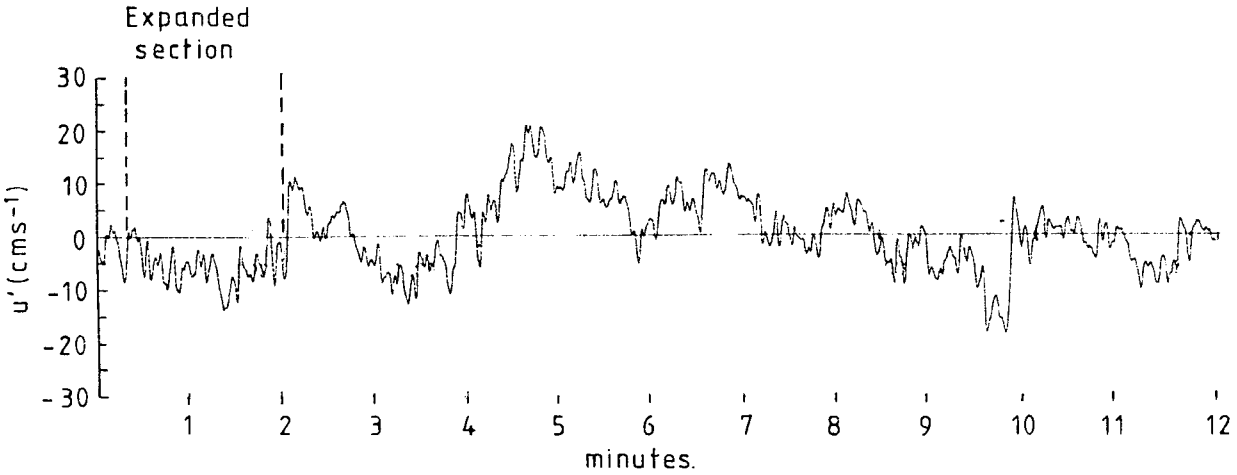

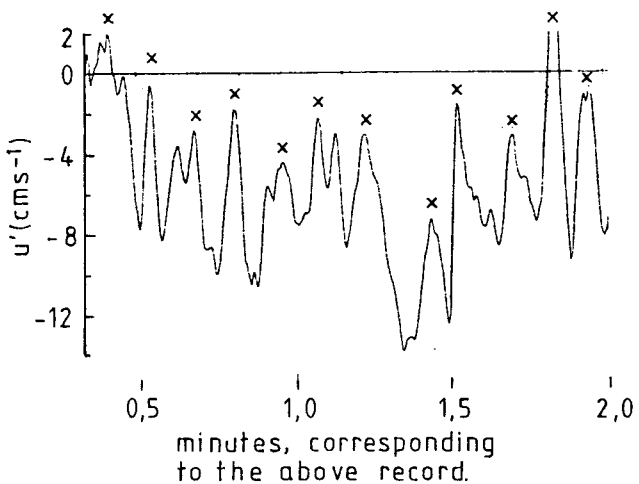

$\bar{u}$ = 32,88 cms^{-1}

Fig. 5.2 Plots of drag coefficient (C_D) against Reynolds number (R_e). Data was collected at each e.m. head during deployments at Station 12. The line through the points gives the mean and the error bars for 95% confidence limits. The Karmann-Prandtl smooth flow relationship is also included.

a) C_D at the e.m. head 56.0 cm above the bed.

b) C_D at the e.m. head 138.0 cm above the bed.

c) C_D at the e.m. head 178.5 cm above the bed.

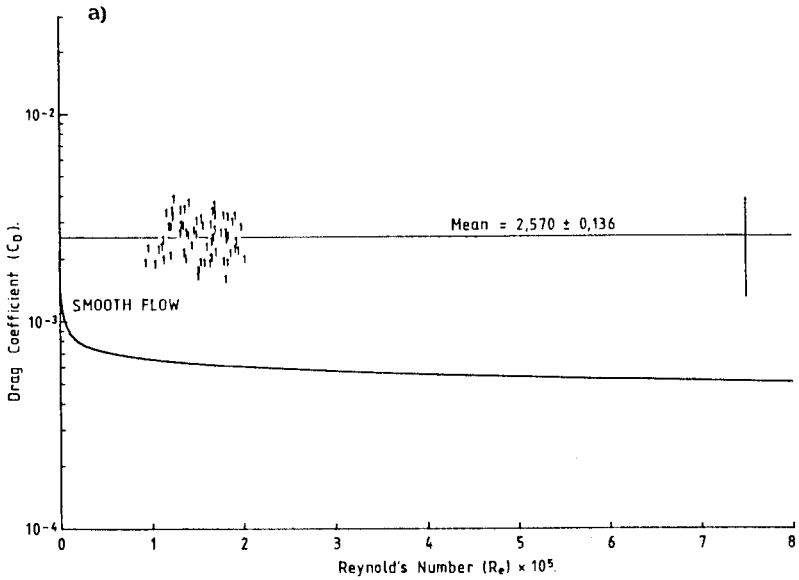
a)
Mean = 2,570 ± 0,136
SMOOTH FLOW
Drag Coefficient (C_D).
Reynold's Number (R_e) × 10^5.

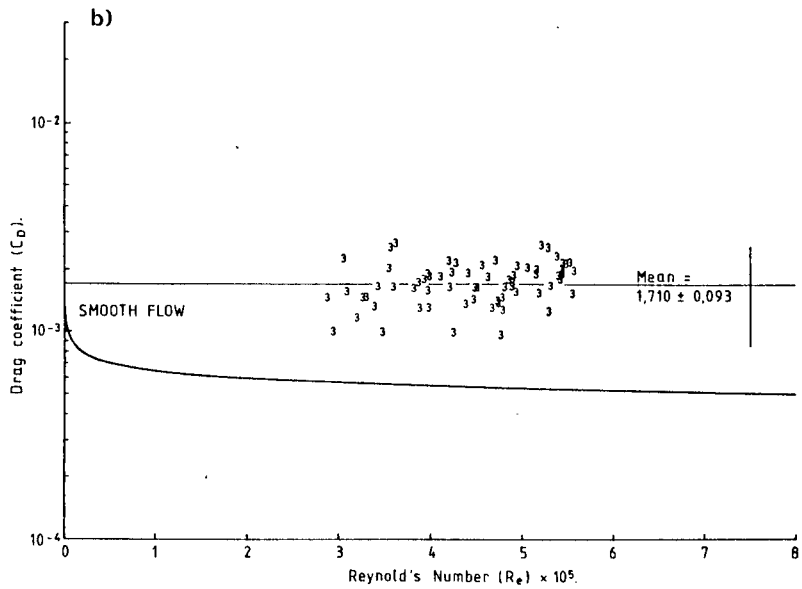
b)
Mean =
1,710 ± 0,093
SMOOTH FLOW
Drag coefficient (C_D).
Reynold's Number (R_e) × 10^5.

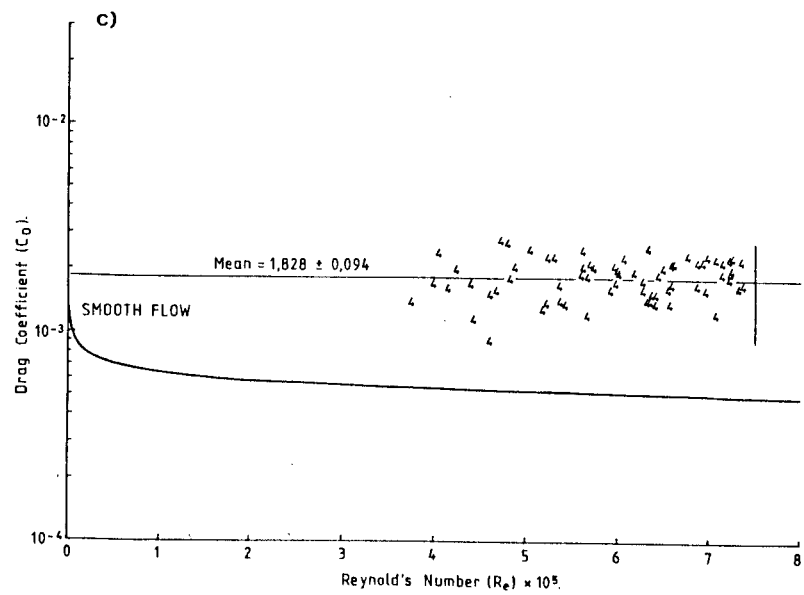
c)
Mean = 1,828 ± 0,094
SMOOTH FLOW
Drag Coefficient (C_D).
Reynold's Number (R_e) × 10^5.

Fig. 5.3 Graph of the 95% confidence limits on C_D, over the range of Reynolds numbers recorded in the data of Fig. 5.2, in intervals of 0.2×10^5. Vertical lines represent the +ve value of the uncertainty, above which is given the number of points each estimate was based on. There was no evidence of an increase in the dispersion of C_D at lower values of R_e.

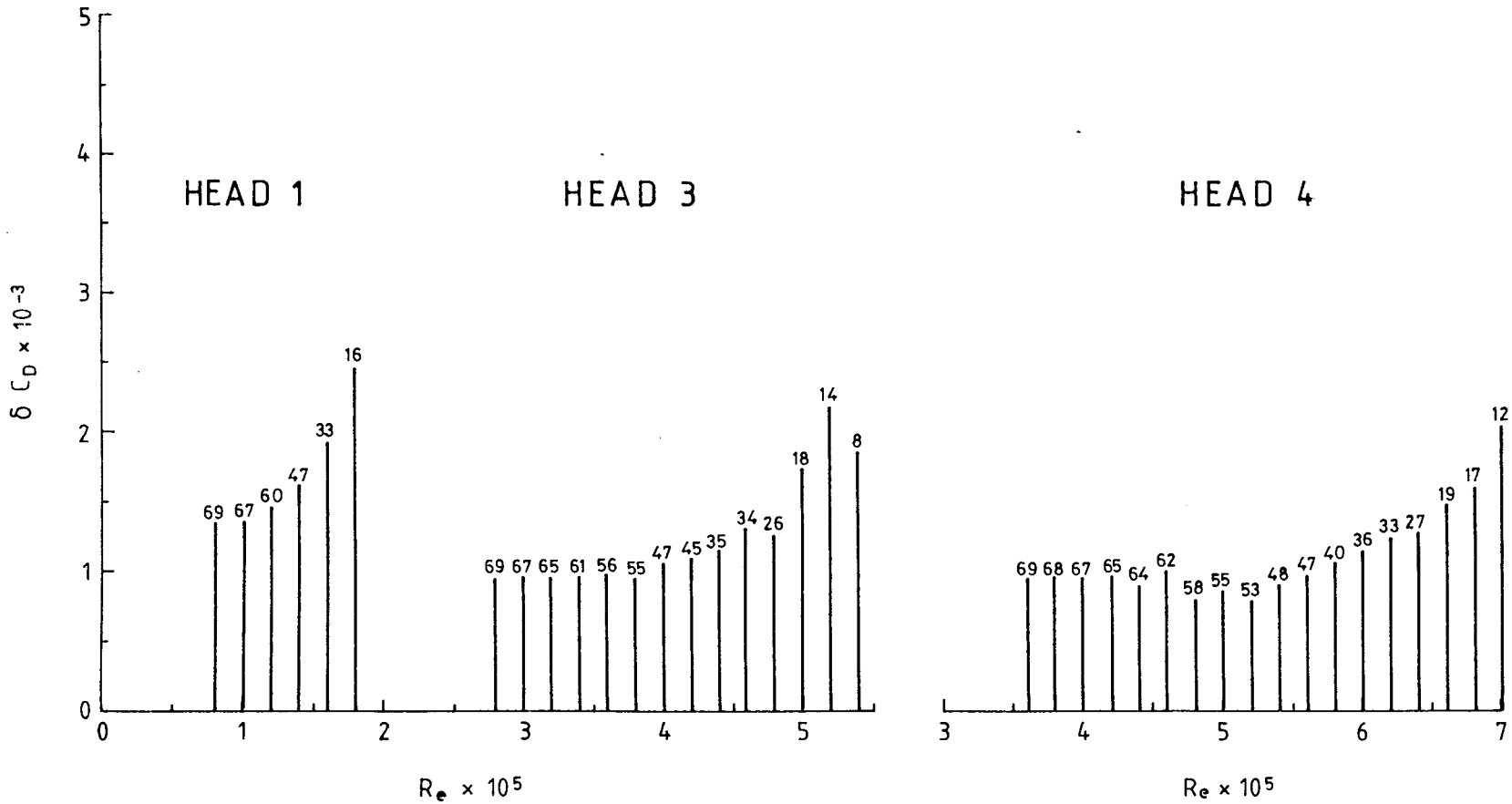
HEAD 1
HEAD 3
HEAD 4
δ C_D × 10^-3
Re × 10^5
Re × 10^5
0
1
2
3
4
5
69 67 60 47 33 16
69 67 65 61 56 55 47 45 35 34 26 18 14 8
69 68 67 65 64 62 58 55 53 48 47 40 36 33 27 19 17 12
3
4
5
6
7

Fig. 5.4 Wave prediction graphs, given by Carter (1982) from the JONSWAP results.

a) Significant wave height prediction graph. (Enter with wind speed at left-hand side, move across till the limiting fetch or duration is reached, then move down the curve to the scale height.) (TOP)

b) Zero up-crossing wave period prediction graph. (Enter with wind speed at left-hand side, move across till the limiting fetch or duration is reached, then move down the curve to the period scale.) (BOTTOM)

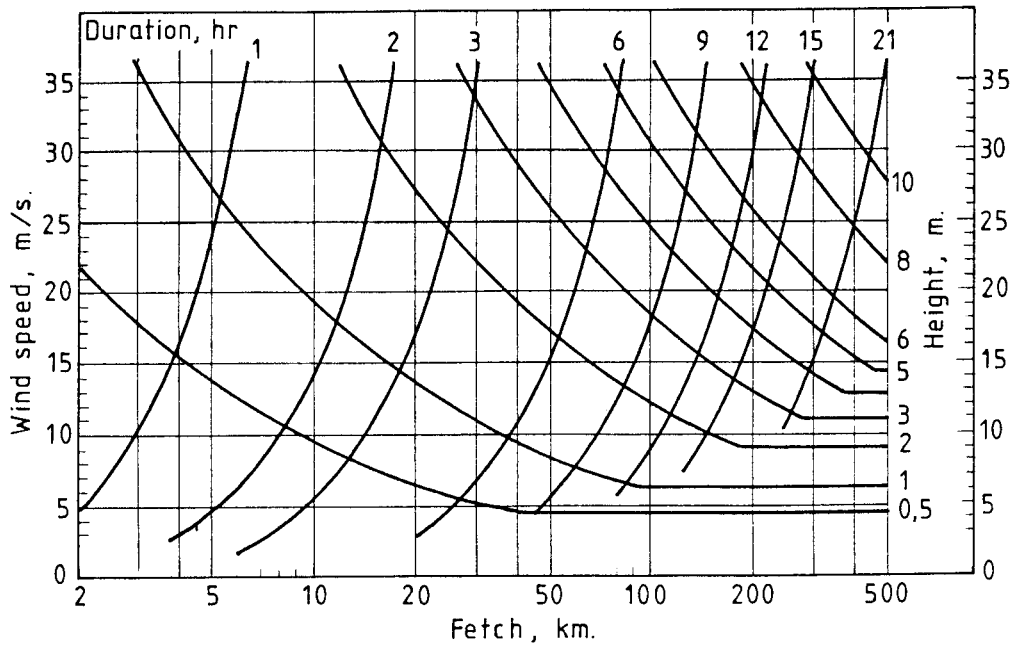
Duration, hr
1
2
3
6
9
12
15
21
Wind speed, m/s.
Height, m.
Fetch, km.
0
5
10
15
20
25
30
35
2
5
10
20
50
100
200
500
10
8
6
5
3
2
1
0,5

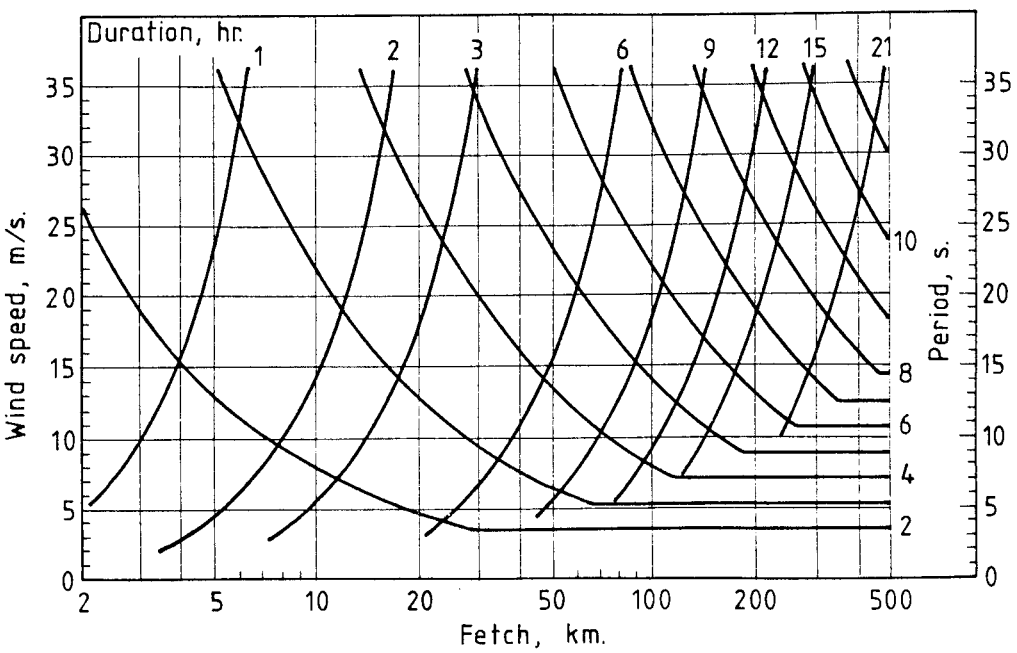
Duration, hr
1
2
3
6
9
12
15
21
Wind speed, m/s.
Period, s.
Fetch, km.
0
5
10
15
20
25
30
35
2
5
10
20
50
100
200
500
10
8
6
4
2

Fig. 5.5 Diagramatic prediction of the gravitational stability of the water column. The sediment grain diameter (d) and friction velocity (u_*) are required (Soulsby, 1983).

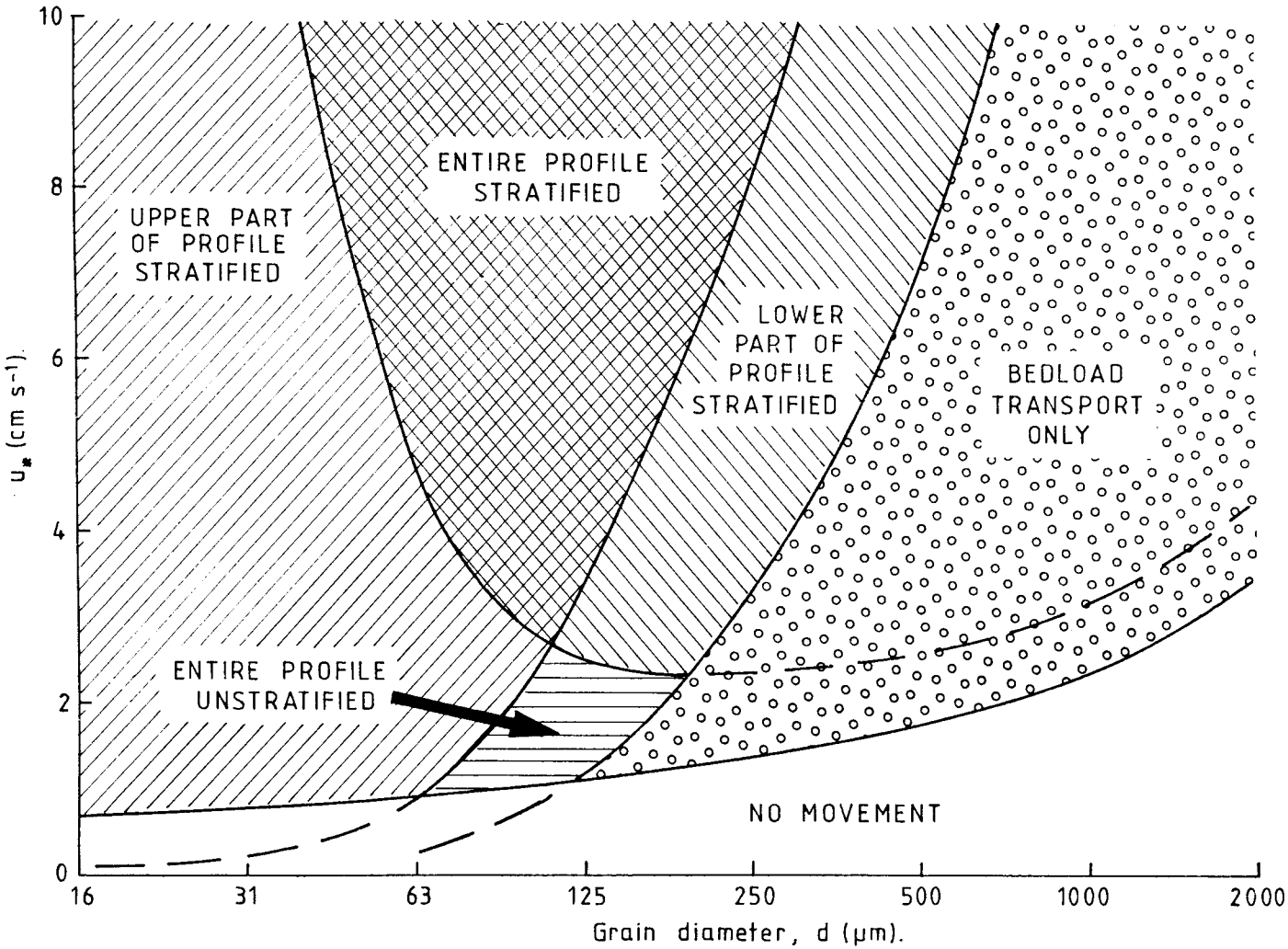
10
8
6
4
2
0
u_* (cm s^{-1}).
ENTIRE PROFILE STRATIFIED
UPPER PART OF PROFILE STRATIFIED
LOWER PART OF PROFILE STRATIFIED
BEDLOAD TRANSPORT ONLY
ENTIRE PROFILE UNSTRATIFIED
NO MOVEMENT
16
31
63
125
250
500
1000
2000
Grain diameter, d (μm).

Fig. 5.6 a) 12 minute averaged rotor velocities ($\bar{U}$), recorded during trial 127. Velocities increase with height above the bed. (TOP)

b) $|d\bar{U}/dt|$ for trial 127. $d\bar{U}$ represents the difference in values of $\bar{U}$ between consecutive 12 minute averages, then averaged over the 4 heights. dt = 720 seconds. (BOTTOM)

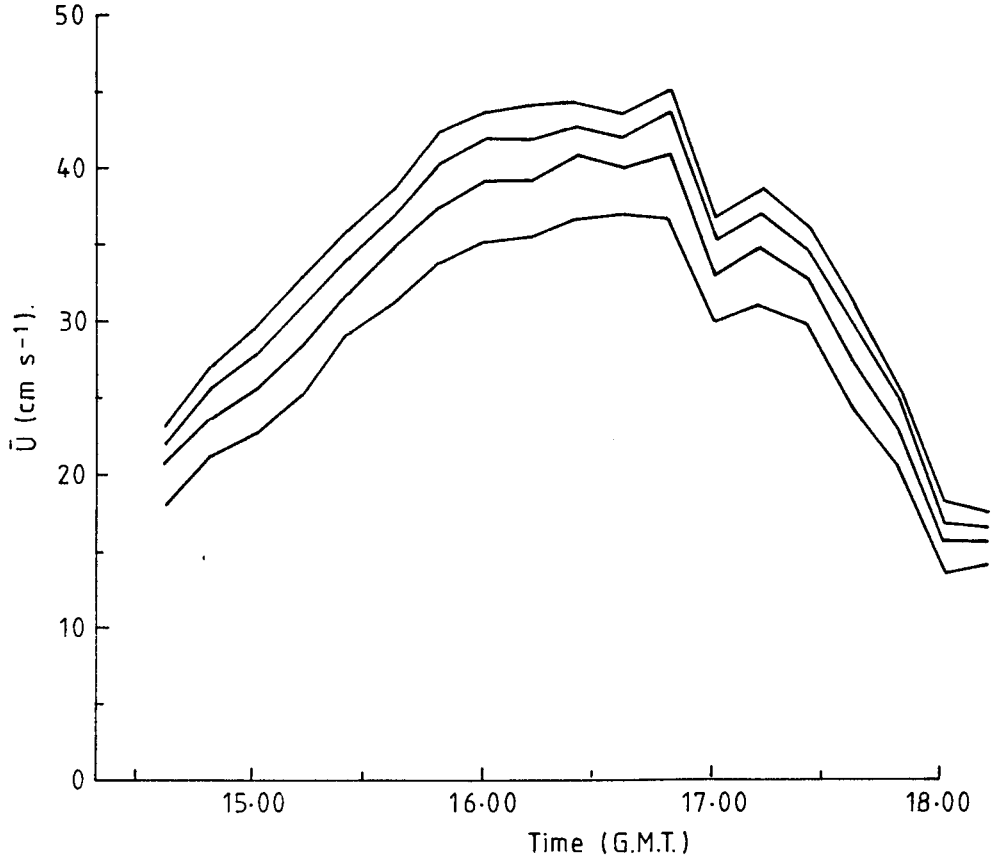
50
40
30
20
10
0
Ū (cm s⁻¹).
15·00
16·00
17·00
18·00
Time (G.M.T.)

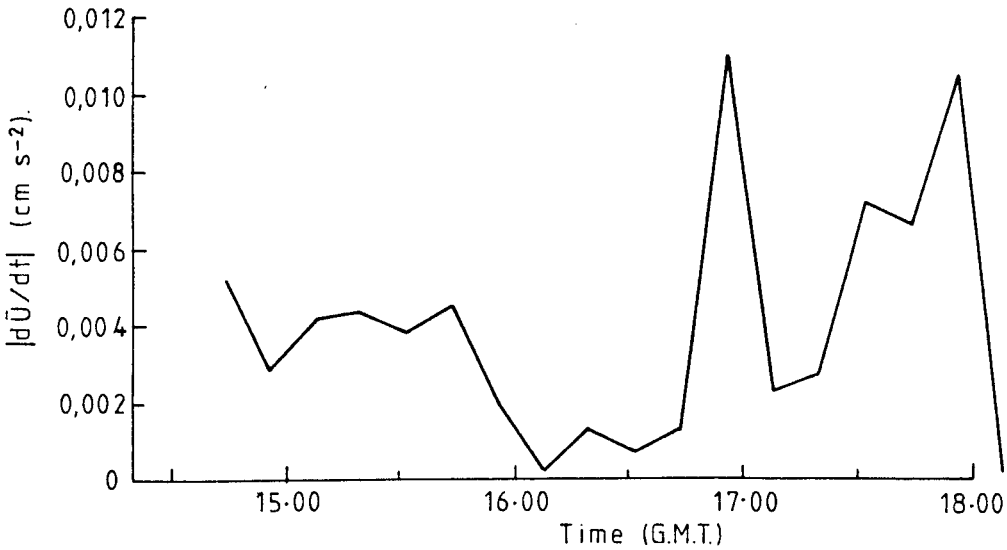
0,012
0,010
0,008
0,006
0,004
0,002
0
|dŪ/dt| (cm s⁻²).
15·00
16·00
17·00
18·00
Time (G.M.T.)

Fig. 5.7 Graphs of τ_0, Λ^{-1} (acceleration length) and $\tilde{\kappa}$ (apparent value of von Karmann's constant) for trial 127.

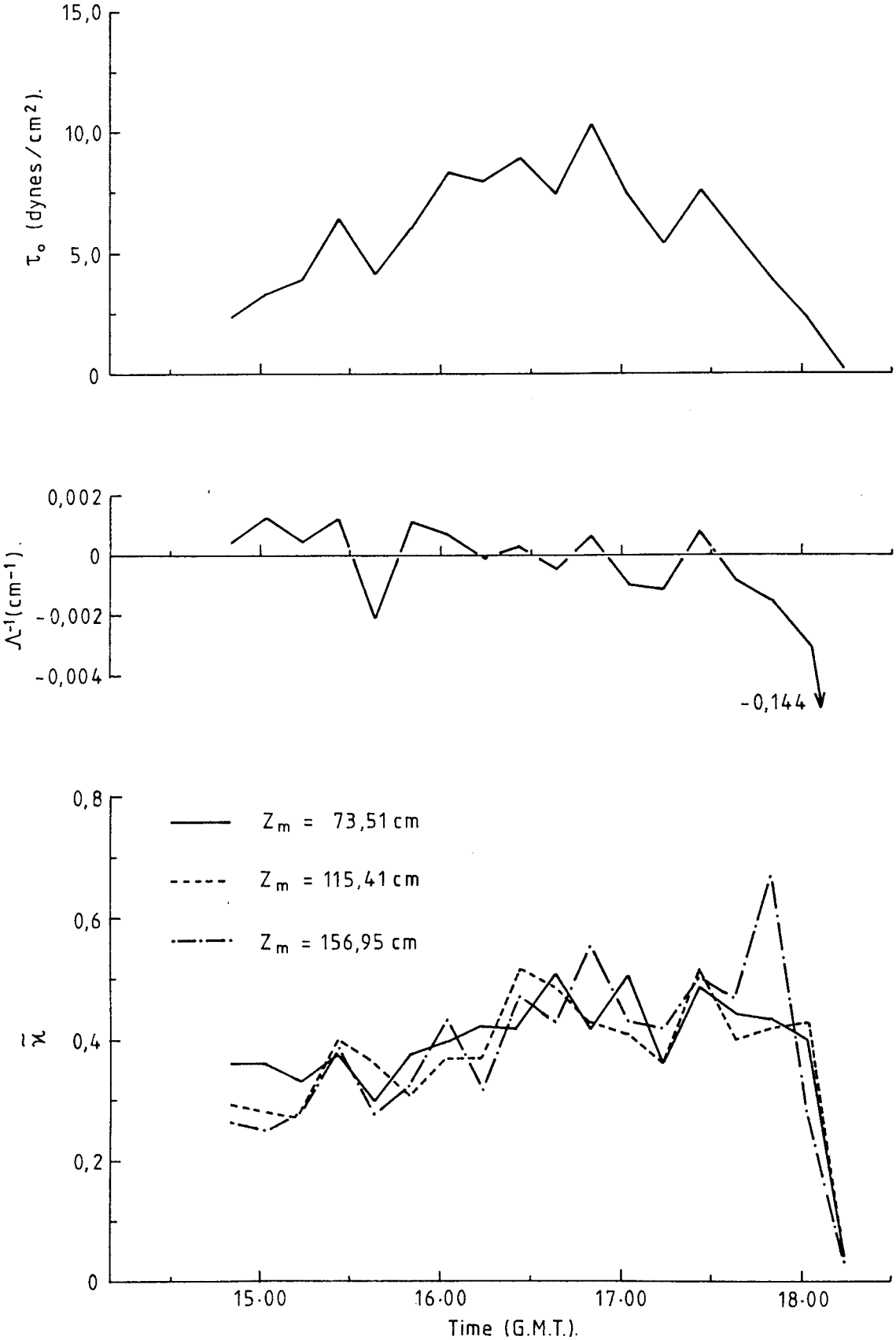
15,0
10,0
5,0
0
τ_o (dynes / cm^2).
0,002
0
-0,002
-0,004
Λ^{-1}(cm^{-1}).
-0,144
0,8
0,6
0,4
0,2
0
$\tilde{\varkappa}$
Z_m = 73,51 cm
Z_m = 115,41 cm
Z_m = 156,95 cm
15·00
16·00
17·00
18·00
Time (G.M.T.).

Fig. 5.8 Values of z/Λ plotted against $\tilde{\kappa}^{-1}$. The three lines represent least squares fits to the data at the heights given, in the range $|z/\Lambda| < 0.02$ over which graphs were linear.

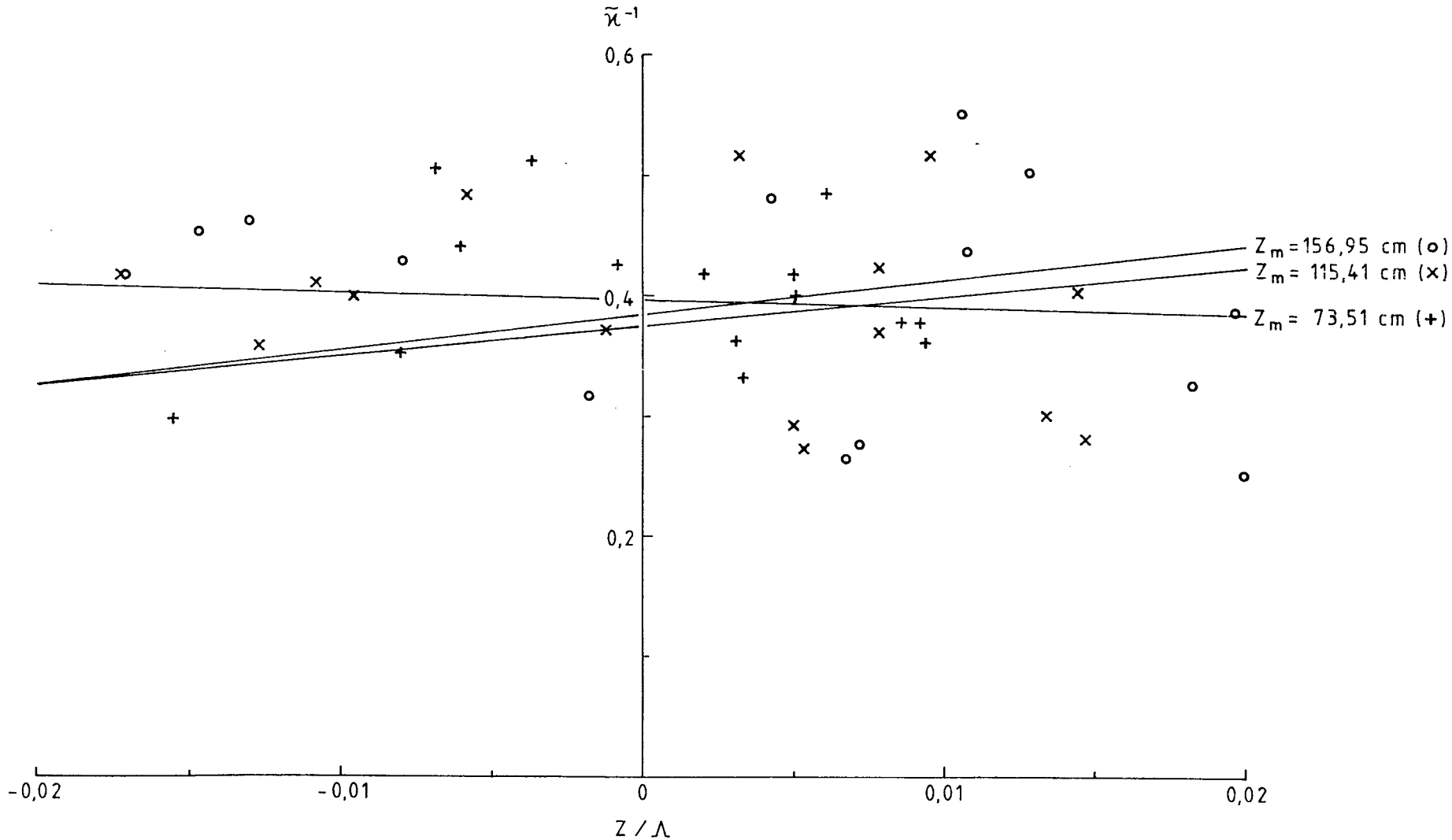
$\tilde{\varkappa}^{-1}$
0,6
0,4
0,2
Z_m = 156,95 cm (o)
Z_m = 115,41 cm (×)
Z_m = 73,51 cm (+)
-0,02
-0,01
0
0,01
0,02
Z / Λ

Fig. 5.9 Histogram of the number of occurrences of $|\bar{dU/dt}|$ for the given ranges. Values were taken from 434 estimates during the 36 trials given in Table 5.1.

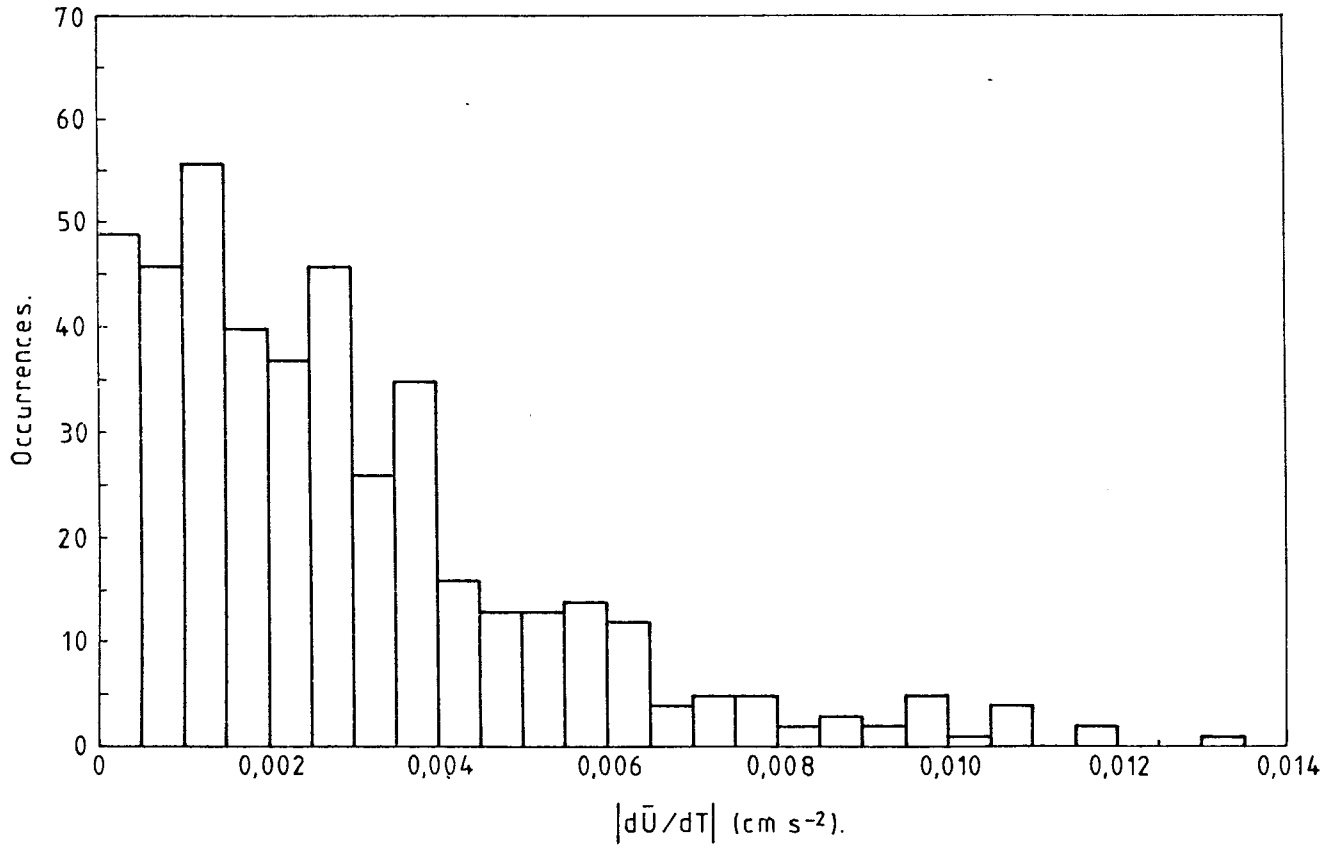
70
60
50
40
30
20
10
0
Occurrences.
0
0,002
0,004
0,006
0,008
0,010
0,012
0,014
|dŪ/dT| (cm s⁻²).

TABLE 5.1 COMPARISONS OF REYNOLDS STRESSES WITHIN 180.0 CM OF THE BED (In columns 2, 3, 6 & 7, from the left, the upper value refers to m and that below to the intercept.)

TRIAL	$\tau_{138} = m\,\tau_{56}$ INTERCEPT	$\tau_{178.5} = m\,\tau_{56}$ INTERCEPT	NUMBER OF POINTS USED	STATION	$\tau_{138} = m\,\tau_{56}$ INTERCEPT	$\tau_{178.5} = m\,\tau_{56}$ INTERCEPT
125	0.694 ± 0.215	0.786 ± 0.349 *	17			
	-1.269 ± 1.303	-1.114 ± 2.116				
126	0.768 ± 0.416 *	0.818 ± 0.400 *	14	8	0.721 ± 0.141	0.799 ± 0.281 *
	-0.151 ± 2.228	-0.568 ± 2.142			-0.589 ± 0.795	-0.584 ± 0.914
127	0.601 ± 0.239	0.753 ± 0.274 *	19			
	-0.768 ± 1.232	-0.891 ± 1.413				
131	0.684 ± 0.276	0.860 ± 0.500 *	8	9	0.684 ± 0.276	0.860 ± 0.500 *
	-0.551 ± 1.245	-0.452 ± 2.255			-0.551 ± 1.245	-0.452 ± 2.255
132	0.764 ± 0.234	1.038 ± 0.318 *	18			
	-0.616 ± 1.055	-0.479 ± 1.434		10	0.800 ± 0.154	0.972 ± 0.166 *
134	0.803 ± 0.241 *	0.970 ± 0.250 *	20		-0.531 ± 0.764	-0.606 ± 0.824
	-0.531 ± 1.478	-0.563 ± 1.533				
137	0.793 ± 0.424 *	0.890 ± 0.500 *	13			
	0.372 ± 1.127	0.393 ± 1.330		11	0.678 ± 0.189	0.775 ± 0.299 *
138	0.599 ± 0.270	0.703 ± 0.427 *	9		0.021 ± 0.447	0.033 ± 0.707
	-0.202 ± 0.501	-0.190 ± 0.792				

TRIAL	$\tau_{138} = m\,\tau_{56}$ INTERCEPT	$\tau_{178.5} = m\,\tau_{56}$ INTERCEPT	NUMBER OF POINTS USED	STATION	$\tau_{138} = m\,\tau_{56}$ INTERCEPT	$\tau_{178.5} = m\,\tau_{56}$ INTERCEPT
141	0.748 ± 0.384 *	0.715 ± 0.300 *	9			
	−0.844 ± 1.716	−1.337 ± 1.341				
143	0.747 ± 0.453 *	0.584 ± 0.480 *	13			
	−1.682 ± 2.158	−2.081 ± 2.287				
144	0.631 ± 0.140	0.585 ± 0.200	23	12	0.752 ± 0.113	0.927 ± 0.128 *
	−0.434 ± 0.573	−0.982 ± 0.818			−0.192 ± 0.488	−0.492 ± 0.553
145	0.863 ± 0.660 *	0.687 ± 0.603 *	14			
	−0.632 ± 3.202	−2.117 ± 2.925				
146	0.752 ± 0.510 *	1.047 ± 0.557 *	10			
	−0.482 ± 1.593	0.036 ± 1.740				
147	0.608 ± 0.441 *	0.678 ± 0.485 *	10			
	−0.724 ± 1.651	−1.023 ± 1.934				
148	0.582 ± 0.324	0.567 ± 0.451 *	16	13	0.804 ± 0.098	0.660 ± 0.418 *
	−1.039 ± 0.981	−1.379 ± 1.465			−0.257 ± 0.348	−0.337 ± 0.465
149	1.154 ± 0.583 *	0.543 ± 1.134 *	9			
	1.357 ± 2.407	−1.773 ± 4.683				
152	0.606 ± 0.985 *	0.234 ± 0.670	9			
	−1.194 ± 3.202	−2.611 ± 2.178				

TRIAL	$\tau_{138} = m\,\tau_{56}$ INTERCEPT	$\tau_{178.5} = m\,\tau_{56}$ INTERCEPT	NUMBER OF POINTS USED	STATION	$\tau_{138} = m\,\tau_{56}$ INTERCEPT	$\tau_{178.5} = m\,\tau_{56}$ INTERCEPT
153	0.908 ± 0.356 *	1.044 ± 1.833 *	10			
	−0.154 ± 1.152	−0.353 ± 5.930				
154	0.242 ± 0.975 *	0.356 ± 1.011 *	9			
	−1.950 ± 2.926	−2.001 ± 3.034				
155	0.832 ± 0.261 *	0.963 ± 0.469 *	10	14	0.873 ± 0.129 *	1.003 ± 0.187 *
	−0.449 ± 0.773	−0.824 ± 1.389			−0.249 ± 0.388	−0.265 ± 0.562
156	0.945 ± 0.513 *	0.907 ± 0.397 *	5			
	0.132 ± 1.262	0.111 ± 0.977				
157	0.796 ± 0.794 *	0.391 ± 1.027 *	8			
	−0.649 ± 2.445	−2.155 ± 3.163				

	$\tau_{100} = m\,\tau_{47.5}$ INTERCEPT	$\tau_{172.5} = m\,\tau_{47.5}$ INTERCEPT			$\tau_{100} = m\,\tau_{47.5}$ INTERCEPT	$\tau_{172.5} = m\,\tau_{47.5}$ INTERCEPT
169	1.243 ± 0.952 *	0.829 ± 0.426 *	10			
	−0.277 ± 0.874	−0.208 ± 0.391				
170	1.251 ± 0.188	1.097 ± 0.292 *	12	16	1.237 ± 0.165	1.080 ± 0.174 *
	−0.301 ± 0.299	−0.280 ± 0.464			−0.341 ± 0.206	−0.194 ± 0.217
171	0.640 ± 0.425 *	0.703 ± 0.390 *	9			
	−0.848 ± 0.859	−0.503 ± 0.788				

TRIAL	$\tau_{100} = m\ \tau_{47.5}$ INTERCEPT	$\tau_{172.5} = m\ \tau_{47.5}$ INTERCEPT	NUMBER OF POINTS USED	STATION	$\tau_{100} = m\ \tau_{47.5}$ INTERCEPT	$\tau_{172.5} = m\ \tau_{47.5}$ INTERCEPT
173	0.939 ± 0.176 *	0.813 ± 0.384 *	14			
	−0.320 ± 0.546	−0.235 ± 0.537				
174	0.702 ± 0.177	0.635 ± 0.392 *	18			
	−0.832 ± 0.313	−0.610 ± 0.694		17	0.817 ± 0.227 *	0.796 ± 0.327 *
175	0.713 ± 0.549 *	0.441 ± 1.084 *	9		−0.417 ± 0.471	−0.363 ± 0.569
	−0.937 ± 1.183	−1.113 ± 1.546				
177	0.648 ± 0.597 *	0.362 ± 0.736 *	14			
	−0.960 ± 0.966	−1.217 ± 1.228				

	$\tau_{138} = m\ \tau_{100}$ INTERCEPT	$\tau_{172.5} = m\ \tau_{100}$ INTERCEPT			$\tau_{138} = m\ \tau_{100}$ INTERCEPT	$\tau_{172.5} = m\ \tau_{100}$ INTERCEPT
179	0.828 ± 0.410 *	0.782 ± 0.372 *	21			
	−1.330 ± 1.740	−1.583 ± 1.879		18	0.993 ± 0.192 *	0.985 ± 0.181 *
180	1.036 ± 0.224 *	1.039 ± 0.216 *	17		−0.799 ± 0.931	−0.927 ± 1.071
	−0.748 ± 1.233	−0.859 ± 1.189				
185	0.919 ± 0.238 *	0.785 ± 0.392 *	16	19	0.919 ± 0.238 *	0.785 ± 0.392 *
	−0.985 ± 1.217	−1.106 ± 1.234			−0.985 ± 1.217	−1.106 ± 1.234

TRIAL	$\tau_{138} = m\ \tau_{100}$ INTERCEPT	$\tau_{172.5} = m\ \tau_{100}$ INTERCEPT	NUMBER OF POINTS USED	STATION	$\tau_{138} = m\ \tau_{100}$ INTERCEPT	$\tau_{172.5} = m\ \tau_{100}$ INTERCEPT
186	1.452 ± 0.333 *	1.302 ± 0.646 *	9			
	0.326 ± 2.233	-0.952 ± 4.332				
187	0.933 ± 0.411 *	0.601 ± 0.439 *	9			
	-1.600 ± 2.428	-2.094 ± 2.593				
189	1.244 ± 0.327 *	1.242 ± 0.353 *	15	20	1.103 ± 0.162 *	1.060 ± 0.215 *
	0.301 ± 1.630	0.419 ± 1.760			-0.970 ± 1.131	-1.156 ± 1.190
191	0.969 ± 0.364 *	1.000 ± 0.441 *	11			
	-1.786 ± 1.788	-1.423 ± 2.166				

TABLE 5.2 THE DRAG COEFFICIENT (C_D) AND HYDRODYNAMIC NATURE OF THE FLOW

STATION	CHARACTER OF THE BOTTOM SEDIMENT (DEFINED OVERLEAF)	AVERAGE $C_D \times 10^{-3}$ WITH 95% CONFIDENCE LIMITS			NUMBER OF POINTS	HYDRODYNAMIC NATURE OF THE FLOW		
		1	2	3		1	2	3
8	MSSP	5.541 ± 0.394	3.126 ± 0.241	3.254 ± 0.286	55	ROUGH	ROUGH	ROUGH
9	FCS	4.231 ± 0.891	2.566 ± 0.588	2.934 ± 0.634	8	ROUGH	ROUGH	ROUGH
10	FCS	3.527 ± 0.454	2.609 ± 0.321	3.033 ± 0.368	42	ROUGH	ROUGH	ROUGH
11	SM	1.765 ± 0.159	0.948 ± 0.125	1.028 ± 0.151	23	ROUGH	ROUGH	ROUGH
12	SM	2.570 ± 0.134	1.710 ± 0.093	1.828 ± 0.094	69	ROUGH	ROUGH	ROUGH
13	TMS	2.729 ± 0.189	1.785 ± 0.175	1.910 ± 0.169	46	ROUGH	ROUGH	ROUGH
14	MSS	2.201 ± 0.150	1.623 ± 0.125	1.763 ± 0.158	43	ROUGH	ROUGH	ROUGH
16	MSSP	2.401 ± 0.336	2.919 ± 0.391	1.901 ± 0.257	27	ROUGH	ROUGH	ROUGH
17	MSS	2.348 ± 0.202	2.223 ± 0.216	1.795 ± 0.264	56	ROUGH	ROUGH	ROUGH
18	MSSP	3.304 ± 0.280	3.660 ± 0.462	3.219 ± 0.262	40	ROUGH	ROUGH	ROUGH
19	SG	3.194 ± 0.763	4.398 ± 1.688	3.338 ± 0.690	16	ROUGH	ROUGH	ROUGH
20	SG	2.606 ± 0.235	3.103 ± 0.301	2.877 ± 0.310	45	ROUGH	ROUGH	ROUGH

Up to and including station 14	1 = e.m. head at	56.0 cm
	2 = e.m. head at	138.0 cm
	3 = e.m. head at	178.5 cm
Stations 16 and 17	1 = e.m. head at	47.5 cm
	2 = e.m. head at	100.0 cm
	3 = e.m. head at	172.5 cm
Stations 18 onwards	1 = e.m. head at	100.0 cm
	2 = e.m. head at	138.0 cm
	3 = e.m. head at	172.5 cm

For the bottom sediment character the following apply:

FCS ≡	Fine Clean Sand	SG ≡	Sand and Gravel
MSS ≡	Medium Sand and Shells	SM ≡	Sand and Mud
MSSP ≡	Medium Sand, Shells and Pebbles	TMS ≡	Thick Muddy Sand

TABLE 5.3 AVERAGE DAILY WIND VELOCITIES AT BIDSTON OBSERVATORY DURING THE J.M. 9/81 AND SH. 7/82 CRUISES

J.M. 9/81			SH. 7/82		
DATE	WIND VELOCITY		DATE	WIND VELOCITY	
	KNOTS	M S^{-1}		KNOTS	M S^{-1}
25/7	8.4	4.3	28/7	2.6	1.3
26/7	8.0	4.1	29/7	1.9	1.0
27/7	6.1	3.1	30/7	5.7	2.9
28/7	2.6	1.3	31/7	4.5	2.3
29/7	7.5	3.9	1/8	0.6	0.3
30/7	2.1	1.1	2/8	1.1	0.6
31/7	4.4	2.3	3/8	1.5	0.8
1/8	4.1	2.1	4/8	0.8	0.4
2/8	1.4	0.7	5/8	4.1	2.1
3/8	5.0	2.6	6/8	5.0	2.6
4/8	1.1	0.6	7/8	9.4	4.8
5/8	1.5	0.8	8/8	4.6	2.4
6/8	4.3	2.2	9/8	4.8	2.5
7/8	3.8	2.0	10/8	6.4	3.3
8/8	1.3	0.7			

(1 KNOT = 0.514 m s^{-1})

TABLE 5.4 VALUES OF VON KARMANN'S CONSTANT (κ_0), DERIVED BY THE METHOD OF SOULSBY AND DYER (1981)

STATION	κ_0	STANDARD DEVIATION	NUMBER OF POINTS ESTIMATE BASED ON
8	0.395	0.067	45
9	0.411	0.096	7
10	0.581	0.195	19
11	0.382	0.065	21
12	0.366	0.068	65
13	0.367	0.089	52
14	0.398	0.082	20
16	0.302	0.019	4
17	0.292	0.068	29
18	0.355	0.052	25
19	0.207	0.043	2
20	0.341	0.107	15

Weighted mean κ_0 = 0.379 ± 0.098 for 298 points (stations 16 and 19 excluded as estimates were based on too few points).

CHAPTER 6 - COMARISONS OF REYNOLDS STRESS WITH u_*^2

6.1 INTRODUCTION

In the study of turbulent geophysical flows it has been common practice to assume that the measurement of $-\overline{u'w'}$, by eddy correlation techniques, yields the same value as u_*^2, derived from the log-law of equation 1.11. If this assumption proved invalid, values of C_D, z_0 and boundary stress, necessary in determining design criteria for underwater structures, often via equation 1.11 for simplicity, may be significantly in error. Results from the Eastern Irish Sea, reported by a number of workers and given in Table 6.1, show a considerable range of z_0 and C_{100} when determined by the above techniques. It is perhaps difficult to explain in terms of differing bed roughness alone. For example, the values of z_0 given by Heathershaw (1979), using eddy correlation techniques, were significantly lower than those from Charnock (1959) and Bowden, Fairbairn and Hughes (1959), using the log-law. Similarly, C_{100}'s given by Heathershaw (1979), using the log-law, were considerably smaller than those of Bowden and Ferguson (1980), using eddy correlation.

This chapter compares u_*^2, from the Aanderaa rotor profiles, with $-\overline{u'w'}$, from the e.m. heads, for different tidal conditions and station positions. Accelerating effects on the velocity gradient, and hence u_*, are also corrected for. From this point $-\overline{u'w'}$ is referred to as the Reynolds stress, strictly $-\overline{\rho u'w'}$, but density ρ can be considered as a scaling factor.

6.2 PREVIOUS COMPARISONS

To the author's knowledge there has been no concerted effort

to compare the two techniques from simultaneous measurements in marine flows. McLean (1983) presented a somewhat cursory comparison from work in the Jade. It was suggested the two techniques were comparable within a very large degree of uncertainty, provided by the inherent variabilty of the Reynolds stress. Ducted impellors were used for both methods, the response of which is considerably better than the traditionally used Aanderaa and Savonious rotors or propellor sensor. Different results may be yielded by the log-law in the present study because of this. McPhee and Smith (1976) examined the boundary layer below pack ice, driven by wind at velocities of approximately 24 cm s^{-1}. The relative flow was found to be stationary and neutrally stable within 4 m of the under surface of the ice.

Values of $-\overline{u'w'}$, derived from the mean momentum equation, were found to be comparable with u_*^2 from the log-law. There must be some doubt about the validity of the values of u_*, as the layer in which the velocities were measured appeared not to be one of constant stress. To determine u_* a value of $\kappa_0 = 0.35$ was also used. Finally, Miyake et. al. (1970) compared u_* from wind velocity profiles (log-law), with the stress $-\overline{u'w'}$ derived from velocity component fluctuations (eddy correlation), measured above the surface of a lake. It was concluded that the techniques were comparable within the experimental errors, although they were not stated.

6.3 A DETERMINATION OF THE FLOOD AND EBB PERIODS

It is desirable to have as large a data set as possible when examining $u_*^2/-\overline{u'w'}$ over a tidal period, to increase confidence in the results. This also applies for the tidal variations of u_* and z_0 which will be investigated in chapter 7. To achieve this, data sets of approximately the same flood and ebb duration at each station were

combined. The length of a flood or ebb was estimated by analysing the bottom current meter records of the Aanderaa moorings that were deployed during the turbulence measurements.

Since the second Aanderaa mooring of the J.M. 9/81 cruise was not recovered, the analysis was based on stations CM4, CM6 and CM7 (see Fig. 2.2 for positions and Table 2.1 for deployment details). The duration of a flood or ebb was determined by the time between velocity minima. However because the meters were set to record once every four revolutions, rather than more frequently, and since the turn of the tide occured over approximately one hour, during which the velocity remained relatively constant, the minima were difficult to define. In an attempt to gain a better definition of the turning points the number of counts per minute were squared. A Fourier analysis was than performed on the resulting time series for a deployment (counts/minute, referred to as counts rather than velocity, were used to greatly reduce the analysis period and storage required on the computer). One such turning point is shown in Fig. 6.1 for the bottom meter (2.2 m above the bed) at station CM7. The minimum of the $(\text{counts})^2$ could reasonably occur between 16:55 and 17:15, this being by no means the least well defined turning point of the data collected.

A time series x(t), of N points, may be expressed in terms of the Fourier series given by equation 6.1 (Bendat and Piersol, 1971).

$$x(t) = A_0 + \sum_{q=1}^{N/2} A_q \cos\left[\frac{2\pi qn}{N}\right] + \sum_{q=1}^{N/2-1} B_q \sin\left[\frac{2\pi qn}{N}\right] \quad , \qquad 6.1$$

where $$A_0 = \frac{1}{N} \sum_{n=1}^{N} x_n = \bar{x} = 0$$

$$A_q = \frac{1}{N} \sum_{n=1}^{N} x_n \cos\left[\frac{2\pi qn}{N}\right] \qquad q = 1,2,\cdots\cdots, N/2-1$$

$$B_q = \frac{1}{N} \sum_{n=1}^{N} x_n \sin\left[\frac{2\pi qn}{N}\right] \qquad q = 1,2,\cdots\cdots, N/2-1$$

$$x_n = x(t)$$

Averaging $(\text{counts})^2$ over 15 minute intervals (meters recorded once a minute) for 111.75 hours, the coefficients A_0, A_q and B_q were obtained for each meter deployment. Taking $q = 1,2,\cdots\cdots,72$, the coefficients of the tidal constituents with periods down to 3.102 hours, including the dominant M_2 constituent of period 12.408 hours, were found. By substituting the coefficients into equation 6.1, a smoothed version of the time series of $(\text{counts})^2$ was obtained. This resulted in a better definition of the minimum, as shown by the solid line in Fig. 6.1.

It was felt that the above method gave a more accurate representation of the local conditions than would have been possible by inferring minima from a secondary port and co-tidal charts. A comparison of the lengths of the ebbs and floods for the three stations, determined by the two methods (given in Table 6.2), suggest this to be so.

At all three stations the ebb was consistently longer than the flood, when determined from the tide tables. This pattern was accurately reflected by the in situ data of CM4 and CM6, but not of CM7. At stations CM4 and CM6 the bottom meters gave erratic results, with the ebb tide often appearing severely truncated. It was possible that the short strop (2 m) between the anchor clump and the bottom meter (see Fig. 2.9) may have been trapped beneath the anchor on

deployment. If this were the case the meters were possibly shielded from the flow on one phase of the tide, giving the anomalous results. It was therefore necessary to analyse the central current meter records, where the meters were 6.5 m and 7.5 m above the bottom at stations CM4 and CM6 respectively. This may explain why the length of the flood ≈ length of the ebb at CM7, but was not the case at the other stations. For trials 179 onwards (CM7) it would appear to be reasonable to group all data for each turbulence station, on both the ebb and flood, together. For the other trials it was decided to group only data recorded on comparable phases of the tide. It was assumed that the latter was reasonable for the trials recorded when the Aanderaa deployment at CM5 was lost.

6.4 RATIOS OF u_*^2 TO $-\overline{u'w'}$

Before presenting the comparisons, a summary of the principal errors in the recording of the stress by the two methods, discussed in Chapter 5, is given below.

Misalignment of electrode pairs, which may not be accurately perpendicular, can lead to a systematic error in $-\overline{u'w'}$ for each trial of a cruise, of ± 2% - ± 7%. A 2.5° tilt of the rig from the perpendicular, in relation to the bed, was feasible if the rig had been situated on a bedform. As a result of such a tilt a systematic error in $-\overline{u'w'}$ of the order of ± 30% may have been present during individual trials. Considering these two errors alone, it is conceivable that the ratio may vary between 1.58 and 0.73 while the two methods are actually recording the same value of Reynolds stress. Superimposed on this is the inherent variability of the stress which introduces an additional uncertainty. Rotor inertia at U_{100} ≳ 30 cm s^{-1} was thought to have a negligible effect, but at U_{100} ≈ 21 cm s^{-1}

it could result in a u_* underestimate of 12.5% ($\approx$ 17.7% in u_*^2). For this reason, only values of $U_{100} \geq 28$ cm s^{-1} ($\approx$ 4% error in u_*^2) have been considered.

The possible variation in κ_0 between stations, as discussed in Section 5.7.2, may also be an important factor in the comparisions.

In the following comparisons, the losses due to cut off in the cospectral content were corrected for, as detailed in Section 5.7.1.

6.4.1 Comparisons (u_*^2 Uncorrected for Acceleration)

It was originally intended to apply the least squares technique of Appendix 2 to determine the ratios, in the same manner as the investigation of the constant stress layer in Section 5.2. In a number of trials the data set was relatively small and recorded over a comparatively short time interval. Fig. 6.2 illustrates such a case for trial 154. Applying the least squares fit of Appendix 2 yielded a gradient of -0.416 and an intercept 5.53, which is obviously totally unrepresentative of the physical processes occurring at the boundary. Alternatively, for other trials (see Fig. 6.3 for trial 125) it appeared reasonable to apply the technique.

One possible approach was to take simple averages of the ratios and obtain a standard deviation. The disadvantage of this would be in the distribution of the ratio, which would probably be very asymmetrical (e.g. if the mean ratio is 1.2, say, individual ratios cannot fall below zero, but could become very large if u_*^2 is large and $-\overline{u'w'}$ is small). The approach adopted here was to apply a least squares technique, but to constrain the intercept to pass through $u_*^2 = 0.0$ and $-\overline{u'w'} = 0.0$. This would yield a straight line of the form

$$y = m_1 x$$

where $$m_1 = \Sigma x_i y_i / \Sigma x_i^2 = \text{ratio}$$

$$y \equiv u_*^2$$

$$x \equiv -\overline{u'w'}$$

In Chapter 5 it was concluded that the boundary layer within 180.0 cm of the bed comprised a region of constant stress. Combining the data from the three e.m. heads and comparing it with each estimate of u_*^2 to give only one ratio reduces the uncertainty in the results. Fig. 6.4 gives ratios for the 36 trials dealt with in Chapter 5. Bracketed below the trial numbers are the number of points (NP) in each estimate. (NP = number of e.m. heads x number of 12 minute averages.) Only 3 trials (143, 153 and 155) indicated a ratio of one within the confidence limits. Results given in Table 5.1 showed the central sensor failed to compare with the top and bottom sensors for trials 125, 127, 131, 132, 138, 148, 152, 170, 174 and 186, possibly attributable to sensor misalignment. Fig. 6.5 presents the ratios for these trials, but omitting the central sensor. Trials 127 and 131 then compare. Of the remaining trials little difference was made to the value of the ratio. In Figs. 6.4 and 6.5, 28 of the 36 trials lay between the extreme limits (dashed lines in the Figs.), within the 95% confidence limits. Trials 132 and 134 had ratios << 1, and were outside the extreme value previously quoted of 0.73. The results were obtained at station 10 where the presence of bed forms was observed (see Fig. 2.2 and Section 2.3). It is feasible that the rig may have been situated so as to produce a tilt of greater than 2.5^{o} Alternatively trials 169 - 171, 173 - 175 and 177 had ratios considerably greater than one. Only three trials 170, 173 and 175 were within the extreme limits previously quoted. It was difficult to accept that this could be attributed to consecutive misalignments

of the turbulence rig in the same sense. The results were from stations 16 and 17, where the bed was observed to be featureless (see Fig. 2.2 and Section 2.3). A possible explanation could be the misalignment of all three e.m. heads relative to the rig, and in the same manner. This would fail to be detected in the constant stress comparisons, but may be sufficient to be apparent in comparisons with u_*^2.

6.4.2 Comparisons (u_*^2 Corrected for Acceleration)

In Chapter 5 it was shown that the flow was undergoing continuous acceleration. Soulsby and Dyer (1981) suggested that this could be corrected for by using equation 6.2, below.

$$\tilde{u}_* = u_* \left[1 - \frac{z}{\gamma \Lambda} \right]^{-1} \quad , \qquad 6.2$$

Where u_* = apparent friction velocity derived from equation 1.11, γ = constant = 0.066 (see Section 5.7.1) and z/Λ = Soulsby and Dyer (1981) criterion for accelerating flow. Ratios were examined in the range $|z/\Lambda| < 0.015$, representing a 29% positive correction in u_*^2 for accelerating flow and a 19% negative correction for deceleration. (From this point u_* refers to $\tilde{u}_*$ in 6.2.)

The ratios for each trial are presented in the same manner as the uncorrected data. Fig. 6.6 gives the combined data for the three sensors, with Fig. 6.7 showing the data with misaligned sensors omitted. Trials 156 and 169 had only one 12 minute average during which $|z/\Lambda| < 0.015$ and this data was not considered significant. In the main, the results were similar to those for the uncorrected ratios. Minor positive or negative shifts occurred depending on whether the majority of the data points were collected during accelerating or decelerating flows. The exceptions to these were

trials 155, 189 and 191, where the corrected ratios were approximately 50% greater, and trials 171 and 175, where corrected ratios were approximately 50% lower. Trials 171 and 175 were recorded during predominantly decelerating flow. From equation 6.2 a negative correction would be expected. Trials 155 and 189 were recorded during accelerating flow. Trial 191 was based on 6 points (two 12 minute averages) with individual averages ranging from 1.1 to 3.0. This dispersion was reflected in the large standard deviation on each estimate of the ratio.

Seven trials (143, 153, 154, 157, 185, 187 and 191) indicated a ratio of one within the standard deviations. When the supposedly misaligned e.m. heads were ignored, trials 131 and 186 also compared. Of the uncorrected ratios, trials 155 and 127 compared, but they failed when using corrected values. This difference for trial 155 was attributed above, to recording during accelerating flow. Using corrected values of u_*^2 for trial 127 gave a ratio increase by approximately 12%, also attributable to the measurements being recorded during predominantly accelerating flow. Four trials (132, 149, 174 and 189) failed to compare within the previously quoted extremes. In the cases of trials 132 and 189 this could conceivably be attributed to misalignment by bedforms. For the two other trials the bed was apparently featureless (see Section 2.3). Profiles were apparently logarithmic so gravitational stratification does not provide an explanation. Possibly there existed localised bedforms, not revealed by the survey of the bed discussed in Chapter 2.

The effect of using corrected values of u_*^2 was probably most evident for the trials presented in the range 170 to 177. Resulting ratios indicated that sensor misalignment was extremely

improbable and showed the advisability of using corrected values of u_* in estimates from the log-law.

To increase the data sets further, corrected ratios were calculated for each station and are presented in Fig. 6.8. The data omitting the possibly misaligned sensors was plotted on the lower axis. Before this, the ratios for each station on the ebb, or flood tides, were plotted to test for tidal variations. The reasoning for this and the definition of the turning points of the tide was discussed in Section 6.3. Two such plots for trials 132 and 134, and 179 and 180 , are given in Fig. 6.9a and 6.9b respectively, representing two of the larger data sets spanning as much of the tide as possible. In these plots there was no justification for suggesting the ratio varied with the tidal phase. This situation existed in every other data set examined with the exception of trials 125 and 127 considered in Section 6.4.4. If this were not the case then it would be incorrect to group the data as shown in Fig. 6.8.

6.4.3 Variation of Ratio with κ_0

In Section 5.7 it was suggested that the ratios for each station might reflect possible variations of κ_0 for different stations, apparent in Table 5.4. Values varied from 0.581 ± 0.195 to 0.292 ± 0.068. If κ_0 does vary, a low value would result in a correspondingly lower ratio and vice versa. This situation would be expected to be most prevalent at stations 10, 12, 13, 17, 18 and 20. In all cases, with the exception of station 10, the ratios should be low. In fact the converse was true, with every ratio being greater than one, with the exception of that for station 10. This was also true when the misaligned sensors were omitted. With the inclusion of the misaligned sensor only station 19 indicated a ratio of one within

95% confidence limits. Omitting the sensor gave a ratio of one at station 9 also. Stations 11 and 17 failed to fall within the previously stated extremes. It might also be expected that the extreme values would be reduced by a combination of up to 5 trials at each station. Although, with so few occurrences it would be rather optimistic to assume that the turbulence rig would be tilted in opposite senses for equal numbers of trials, so the reduction in the extremes may well be small. In the cases of stations 11 and 17 the bottom was observed to be featureless, so the extremes would be less than the values given. The data from the remaining stations would appear to fall within even reduced extremes.

Taking the entire data set yielded a ratio of 1.287 ± 0.043 for 765 points. For the data omitting misaligned sensors the ratio was 1.268 ± 0.049, for 577 points. These values are equivalent to a κ_0 of 0.353 and 0.355 respectively, and are comparable with the value of 0.379 given in Table 5.4, for which a ratio of 1.114 would be expected. A possible explanation for the discrepancy is an underestimate of the stress recorded by the e.m. heads, resulting from spectral loss at the high and/or low frequency ends. Inadequate correction could have resulted in a lower estimate of κ_0. It is improbable that such an explanation gives such a large difference between 0.355 and 0.4. Apparently, from the comparisons, the value of κ_0 lies closer to that of 0.35, suggested by Businger *et al* (1970) and Schotz and Panofsky (1980) for atmospheric work. This is apposed to 0.40, suggested by Soulsby and Dyer (1981) and Caldwell and Chriss (1979), or even the value of 0.38 given by Smith and Mclean (1977).

6.4.4 Variation of Ratio with Bed Character

It may have been possible that the ratio would vary with

bottom roughness or sediment type. Fig. 6.10 gives a plot of values of C_{100} against ratios for a number of trials and stations. Data was taken from Table 7.2. Where several trials were used for an estimate of C_{100} the data was combined and treated as before. From this plot the ratio was apparently independent of bed roughness.

In Table 7.2 it can be seen that C_{100} varied from (7.87 - 3.78) x 10^{-3} for the combined data of trials 125 and 127. This was attributed to the possible streamlining of sand ripples during the tide (see Chapter 7). A plot of the ratios from trials 125 and 127 (Fig. 6.11) apparently indicates a decrease in ratio with bed roughness (see Fig. 7.4a for comparison). Initially the bed was considerably rougher than at other stations. It may have been that the dependence was relatively weak and the range of C_{100} , (2.17 - 4.17) x 10^{-3}, was insufficient to have revealed the dependence. The values of the ratio after 90 minutes appear to reach values comparable with the ratios observed during the remaining trials in Fig. 6.8.

It is improbable that the initially high ratios arose directly from the variation of bed roughness. A greater displacement height (d) in equation 1.11 would be expected to give an increase in u_*^2, but not of the order of the 100% increase shown in Fig. 6.11. Adams and Weatherly (1981) have indicated that the existence of sediment stratification may result in an apparent increase in u_*. This was also accompanied by a damping in turbulent intensity as the kinetic energy is reduced. Assuming sediment from steep faces of ripples at the start of the tide (see Section 7.4) is initially brought into suspension, such an apparently high ratio may be possible. It seems unlikely that this would only occur during the initial stages, with lower ratios occurring at greater velocities, as

indicated by the time of peak velocity in Fig. 6.11. The presence of stratification would then appear improbable.

6.5 SUMMARY AND CONCLUSIONS

In this chapter an attempt has been made to compare the Reynolds stress measured by the eddy correlation technique, with simultaneous measurements of u_*^2 by the log-law. Prior to this, comparisons from previous results were reviewed, all of which suggested that the techniques would give comparable values. Only the work of McLean (1983) was carried out in the benthic boundary layer, based on 104 profiles at one location, using averaging intervals of between 9 - 20 minutes. The application of Fourier analysis to the Aanderaa records to determine the turning points of the tide at each station enabled the possible dependence of the ratios on tidal phase to be investigated.

The major obstacles to reliable comparisons were the large uncertainties imposed by possible sensor misalignment and the inherent variability of the stress. Comparisons, with u_*^2 uncorrected for the effects of accelerating flow, suggested that during only 5 trials were the techniques comparable, and that was after the removal of misaligned sensor data. Of the 36 trials considered, 28 had ratios within the extreme limits imposed by sensor misalignment. Of the remaining trials, two had ratios considerably less than 1.0 and the others were considerably greater. Applying a correction to u_*^2 for the effects of accelerating flow, (Soulsby and Dyer, 1981), and removing misaligned sensor data, produced seven trials with consistent ratios. Thirty trials lay inside the extreme values. Of the remaining, one was less than 1.0 and the others greater.

Based on the absence of a variation of the ratios with tidal

phase, comparisons at the 12 stations failed to suggest any dependence of ratios on differing values of κ_0, as obtained in Chapter 5. Taking the entire data set, including and excluding apparently misaligned sensors, the values of κ_0 were 0.353 and 0.355 respectively. These values could be said to be comparable with the value of 0.379 obtained in Chapter 5. The difference was possibly due to inadequate correction for spectral loss from the e.m. heads.

A plot of C_{100} against the ratio for various trials and stations failed to indicate a variation in the ratio with bed roughness. Combined data for trials 125 and 127 suggested that high ratios were correlated to initially high values of z_0. Possibly the variation in bed roughness for the C_{100} versus ratio plot was insufficient to distinguish variations.

In conclusion, it can be said that on the whole the log-law technique would appear to overestimate the Reynolds stress by approximately 26%. This may be due to using a value of κ_0 of 0.4 to determine u_*^2. The data indicates a value of κ_0 closer to the atmospherically applied value (0.35) than the laboratory and previously used marine value (0.40 - 0.42). The need to correct for losses due to cut off in the cospectral content was evident when determining the Reynolds stress by eddy correlation. For the log-law, the importance of correcting for accelerating flows was highlighted. There was no evidence of κ_0 varying with bedform or sediment distribution. Over an apparently immobile bed the ratios were independent of tidal phase. There was a suggestion that the ratios may increase at higher values of bed roughness.

Fig. 6.1 Plot of (the number of counts recorded per minute)^2 from the bottom Aanderaa meter (6145) at station CM7, between 15:35 and 18:36 on 4/8/82. The solid line represents a smoothed version of the data resulting from the Fourier analysis of 111.75 hours of data at this station. The turning point of the tide was taken as being at ~ 17:06.

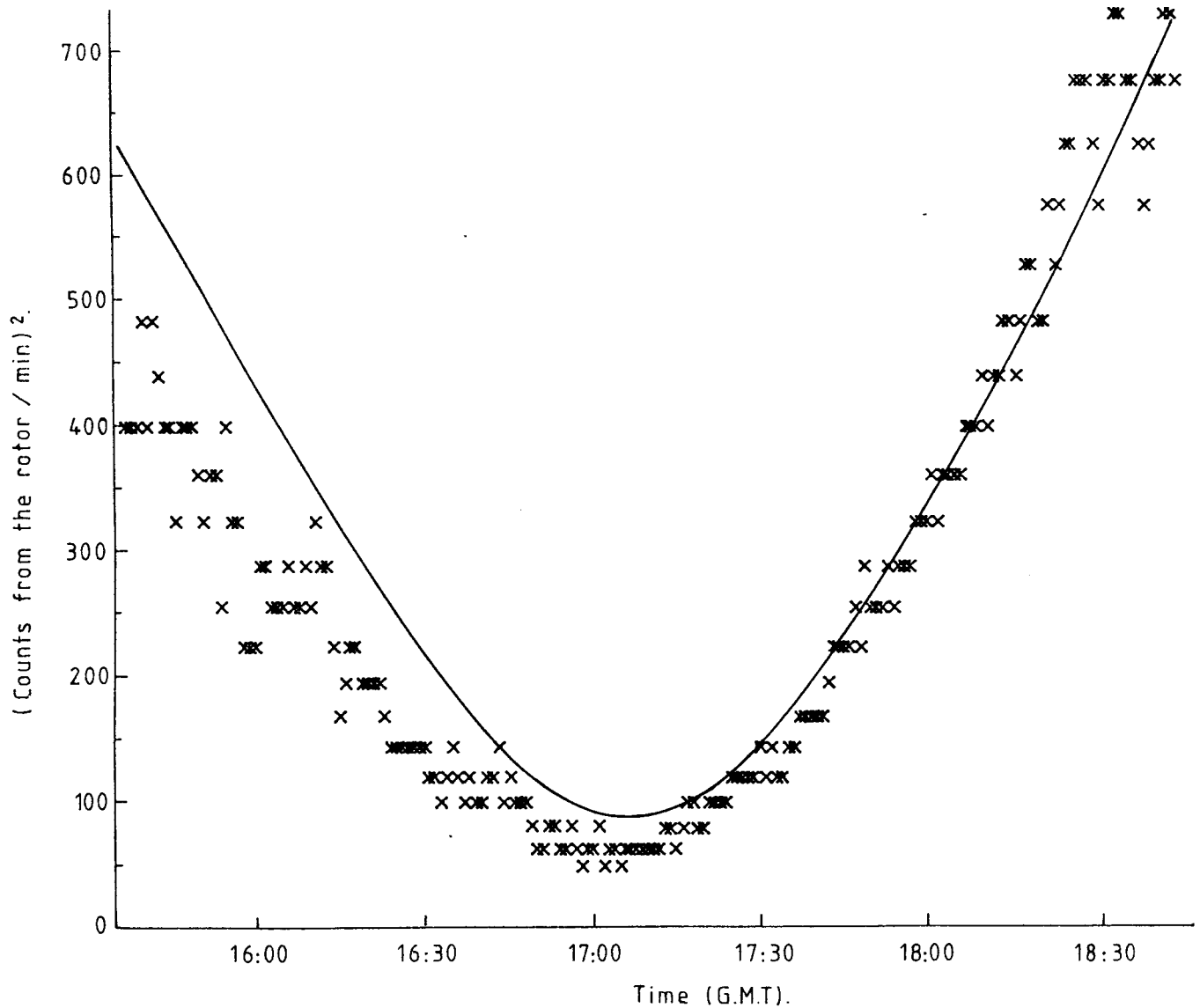
700
600
500
400
300
200
100
0
(Counts from the rotor / min.)².
16:00
16:30
17:00
17:30
18:00
18:30
Time (G.M.T).

Fig. 6.2 $\overline{-u'w'}$ .v. u_*^2 (corrected) for trial 154. Shown are are the lines for $u_*^2 = \overline{-u'w'}$, that from the least squares technique of Appendix 2 and $u_*^2/\overline{-u'w'} = 1.34$ with 95% confidence limits (dashed), when the line was constrained to pass through the origin.

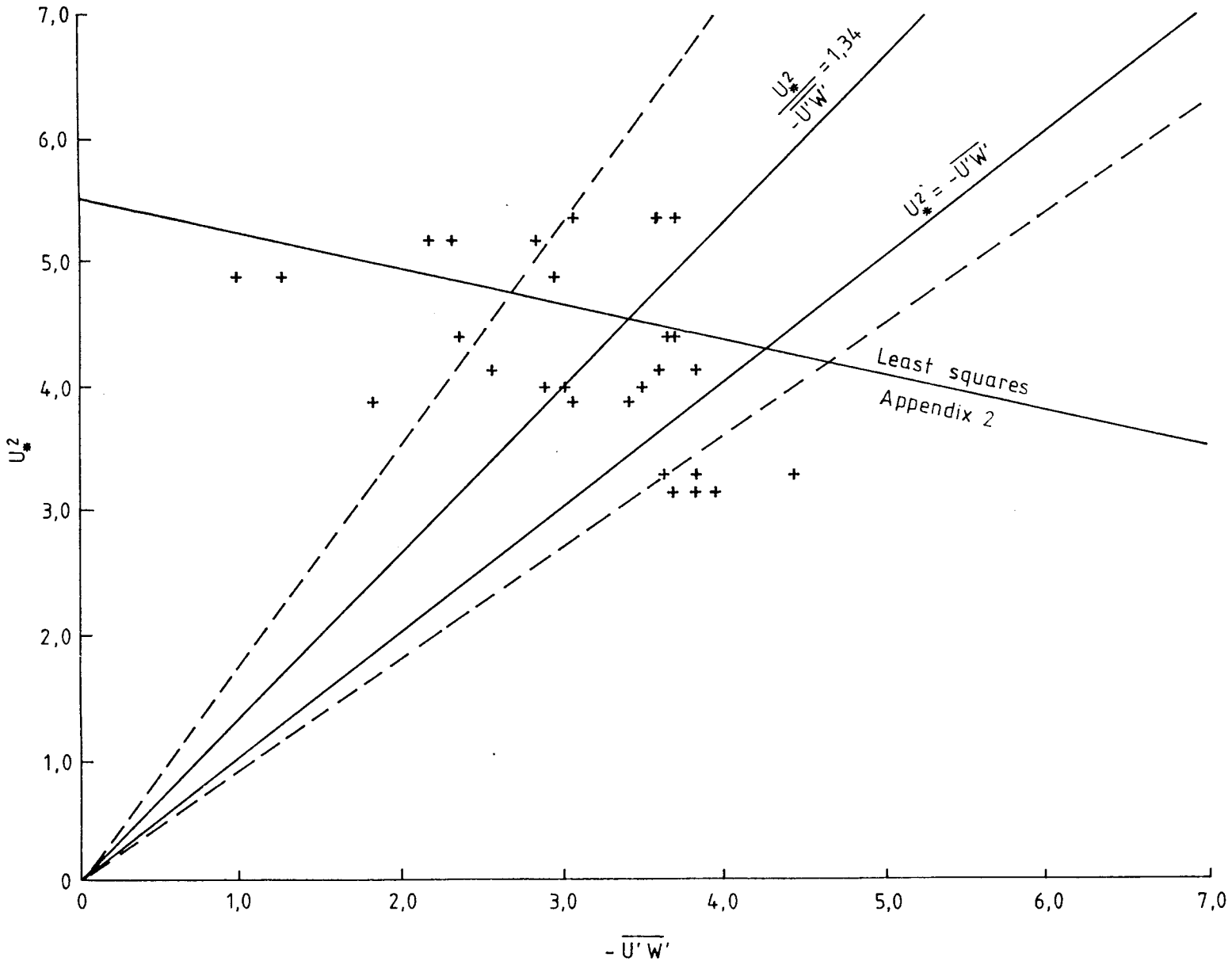
7,0
6,0
5,0
4,0
3,0
2,0
1,0
0
U_*^2
0
1,0
2,0
3,0
4,0
5,0
6,0
7,0
$-\overline{U'W'}$
$\frac{U_*^2}{-\overline{U'W'}} = 1{,}34$
$U_*^2 = -\overline{U'W'}$
Least squares
Appendix 2

Fig. 6.3 $-\overline{u'w'}$ .v. u_*^2 (corrected) for trial 125. Shown are lines for $u_*^2 = -\overline{u'w'}$, that obtained using the least squares technique of appendix 2 and $u_*^2/-\overline{u'w'} = 1.47$ with 95% confidence limits (dashed), with the line constrained to pass through the origin.

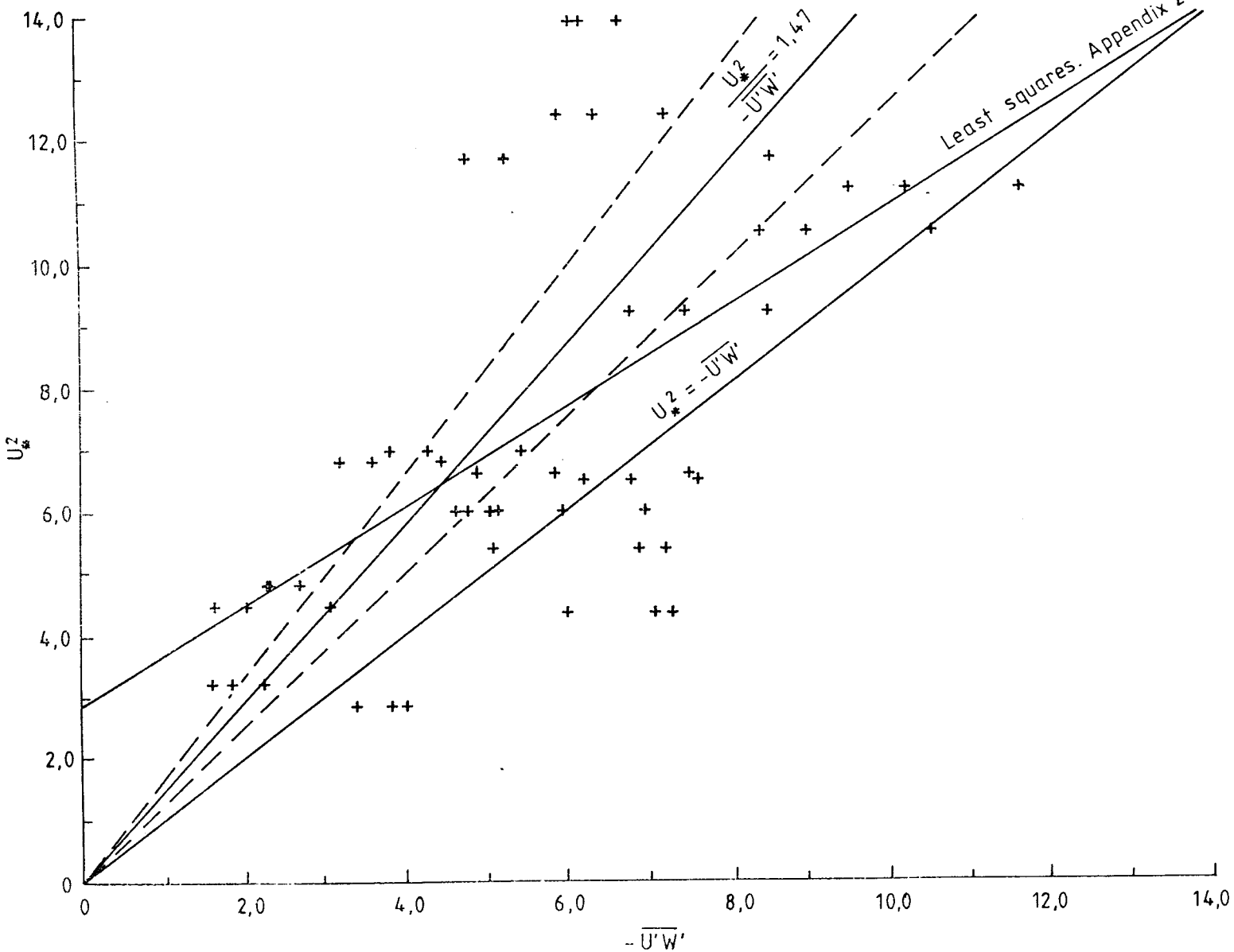
14,0
12,0
10,0
8,0
6,0
4,0
2,0
0
U_*^2
0
2,0
4,0
6,0
8,0
10,0
12,0
14,0
$-\overline{U'W'}$
$\frac{U_*^2}{-\overline{U'W'}} = 1,47$
Least squares. Appendix 2
$U_*^2 = -\overline{U'W'}$

Fig. 6.4 $u_*^2/-\overline{u'w'}$ for the 36 trials judged suitable for analysis, uncorrected for acceleration. Bracketed below each trial number are the number of points each estimate was based on. The 95% confidence limits are given by the error bars. Dashed lines represent extreme values of the ratio that might be expected due to sensor misalignment and the ratio still be considered one.

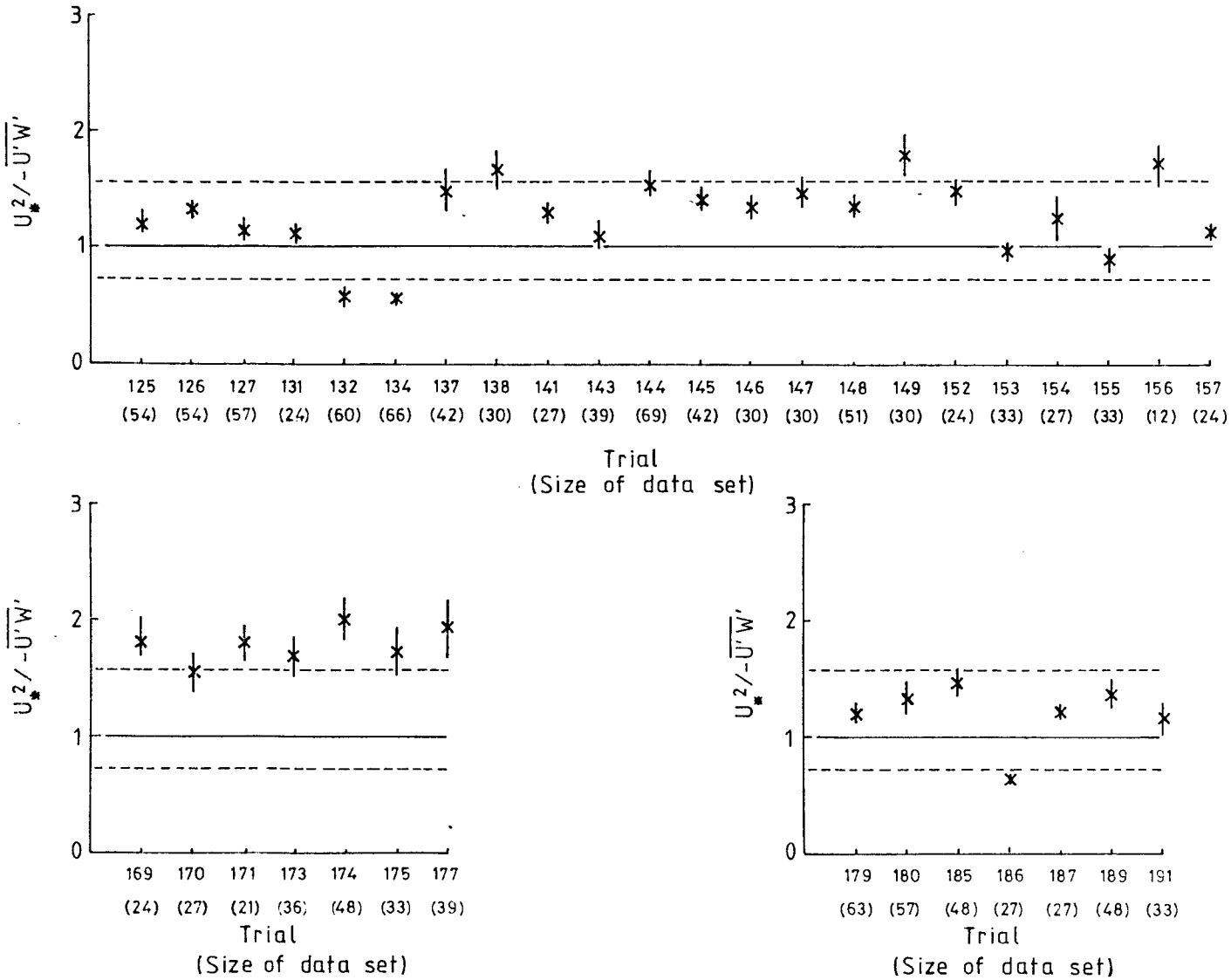
$U_*^2/-\overline{U'W'}$
3
2
1
0
125 126 127 131 132 134 137 138 141 143 144 145 146 147 148 149 152 153 154 155 156 157
(54) (54) (57) (24) (60) (66) (42) (30) (27) (39) (69) (42) (30) (30) (51) (30) (24) (33) (27) (33) (12) (24)
Trial
(Size of data set)
169 170 171 173 174 175 177
(24) (27) (21) (36) (48) (33) (39)
Trial
(Size of data set)
179 180 185 186 187 189 191
(63) (57) (48) (27) (27) (48) (33)
Trial
(Size of data set)

Fig. 6.5 $u_*^2/-\overline{u'w'}$, uncorrected for acceleration, but omitting misaligned sensors. The legend of Fig. 6.4 explains the graph more fully.

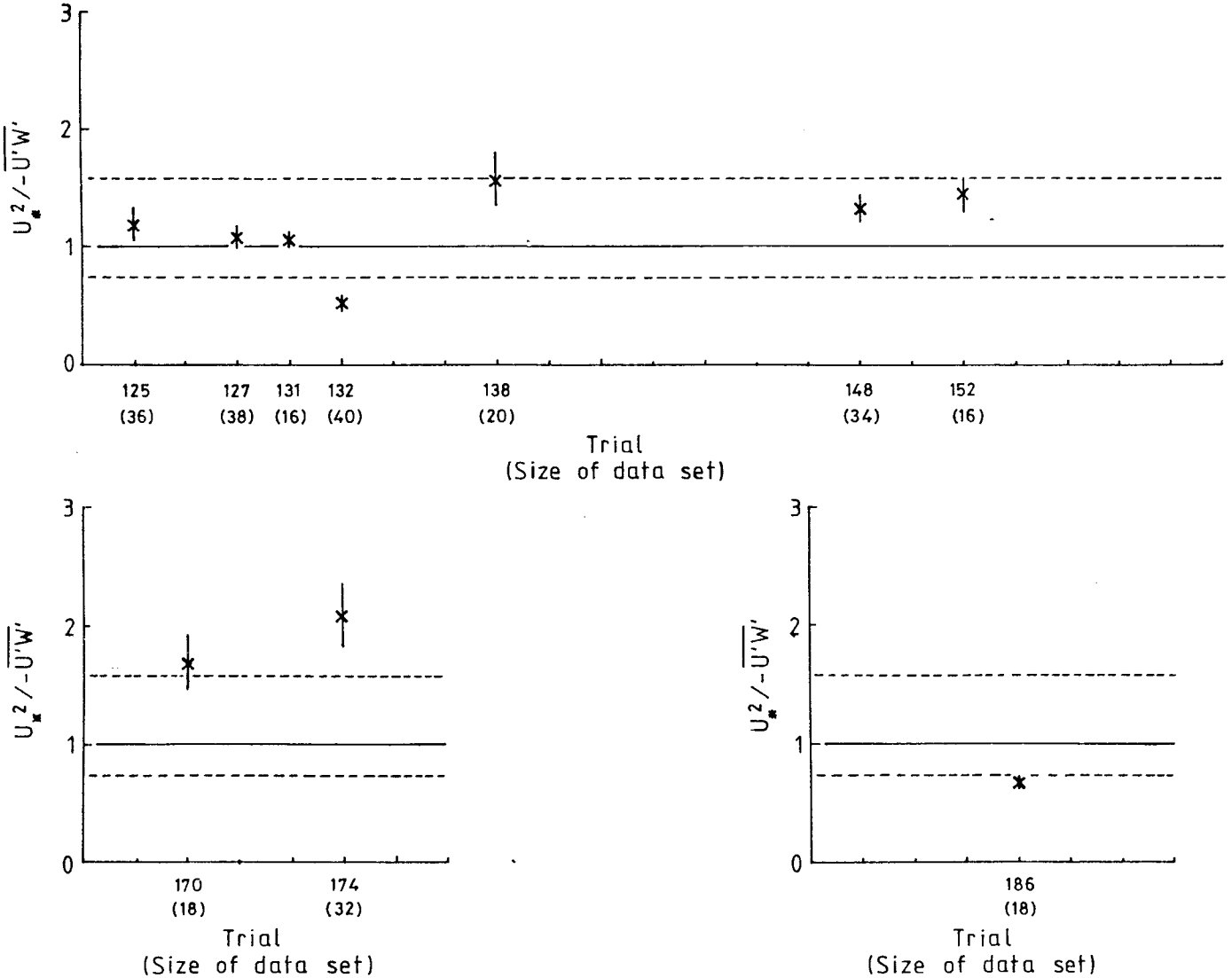
3
2
1
0
$U_*^2/-\overline{U'W'}$
125 (36)
127 (38)
131 (16)
132 (40)
138 (20)
148 (34)
152 (16)
Trial
(Size of data set)
170 (18)
174 (32)
186 (18)

Fig. 6.6 $u_*^2/-\overline{u'w'}$, corrected for acceleration. The legend of Fig. 6.4 explains the graph more fully.

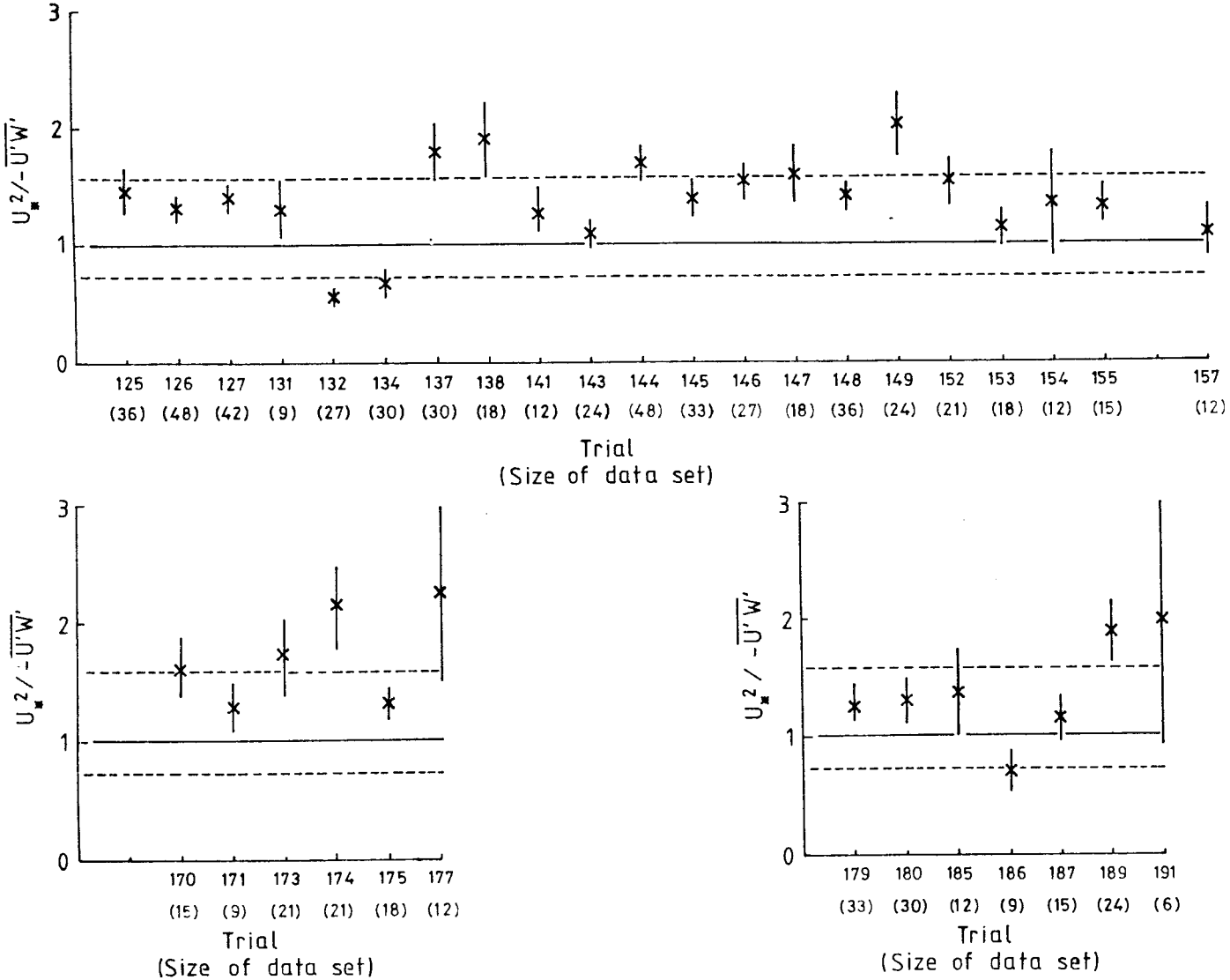
$U_*^2/-\overline{U'W'}$
3
2
1
0
125 126 127 131 132 134 137 138 141 143 144 145 146 147 148 149 152 153 154 155 157
(36) (48) (42) (9) (27) (30) (30) (18) (12) (24) (48) (33) (27) (18) (36) (24) (21) (18) (12) (15) (12)
Trial
(Size of data set)
$U_*^2/-\overline{U'W'}$
3
2
1
0
170 171 173 174 175 177
(15) (9) (21) (21) (18) (12)
Trial
(Size of data set)
$U_*^2/-\overline{U'W'}$
3
2
1
0
179 180 185 186 187 189 191
(33) (30) (12) (9) (15) (24) (6)
Trial
(Size of data set)

Fig. 6.7 $u_*^2/-\overline{u'w'}$, corrected for acceleration, but omitting misaligned sensors. The legend to Fig. 6.4 explains the graph more fully.

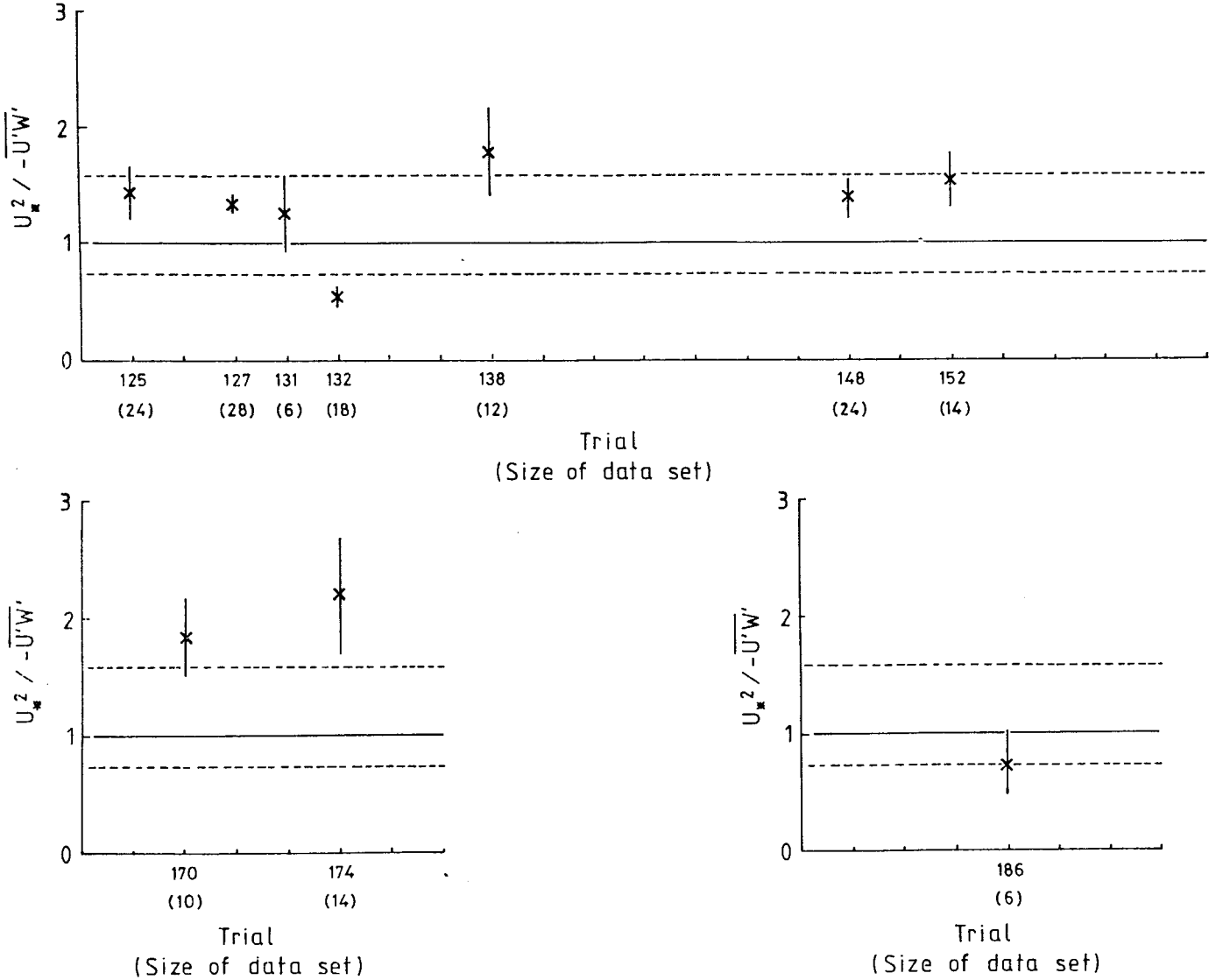
3
2
1
0
$U_*^2 / -\overline{U'W'}$
125
(24)
127
(28)
131
(6)
132
(18)
138
(12)
148
(24)
152
(14)
Trial
(Size of data set)
3
2
1
0
$U_*^2 / -\overline{U'W'}$
170
(10)
174
(14)
Trial
(Size of data set)
3
2
1
0
$U_*^2 / -\overline{U'W'}$
186
(6)
Trial
(Size of data set)

Fig. 6.8 $u_*^2/\overline{-u'w'}$ for stations. The upper axis represents values including possibly misaligned sensors, whilst in the lower they were omitted. The remaining features are detailed in the legend to Fig. 6.4.

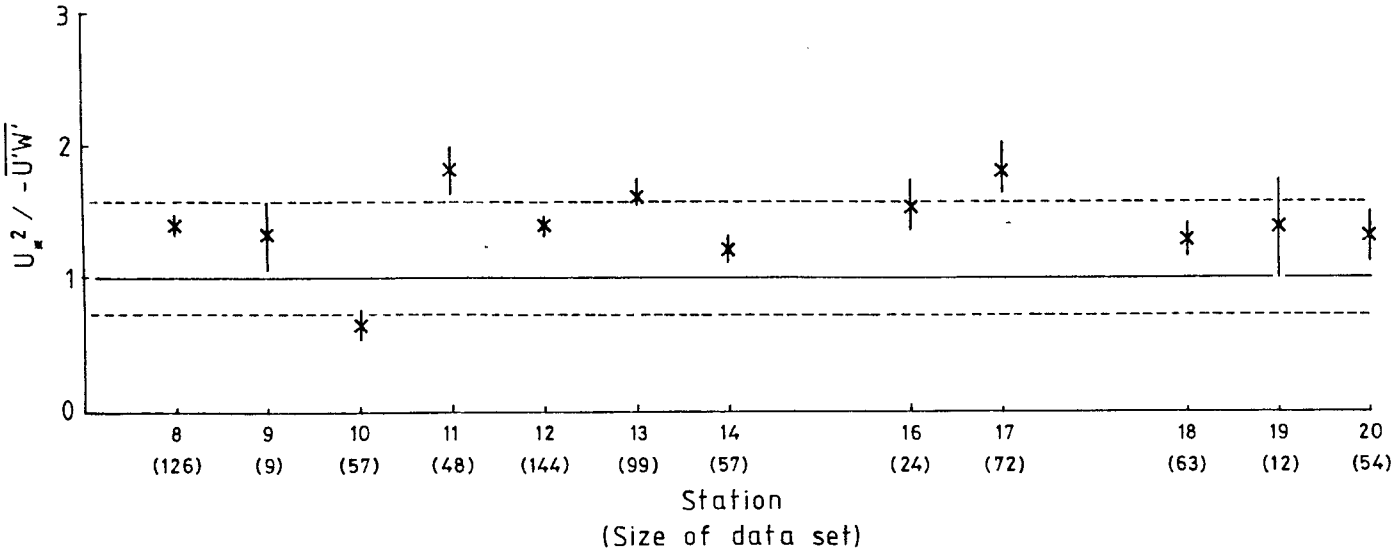
3
2
1
0
$U_*^2 / -\overline{U'W'}$
8 (126)
9 (9)
10 (57)
11 (48)
12 (144)
13 (99)
14 (57)
16 (24)
17 (72)
18 (63)
19 (12)
20 (54)
Station
(Size of data set)

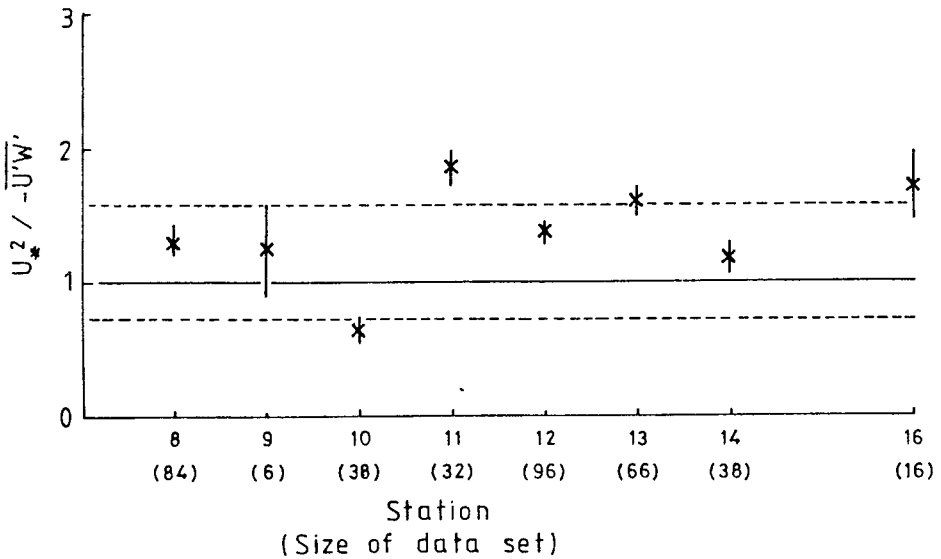
3
2
1
0
$U_*^2 / -\overline{U'W'}$
8 (84)
9 (6)
10 (38)
11 (32)
12 (96)
13 (66)
14 (38)
16 (16)
Station
(Size of data set)

Fig. 6.9 $u_*^2/-\overline{u'w'}$ .v. time from slack water.

a) For trials 132 (X) and 134 (0) (TOP)

b) For trials 179 (X) and 180 (0) (BOTTOM)

The start of the ebb phase is marked SE on the abscissa.

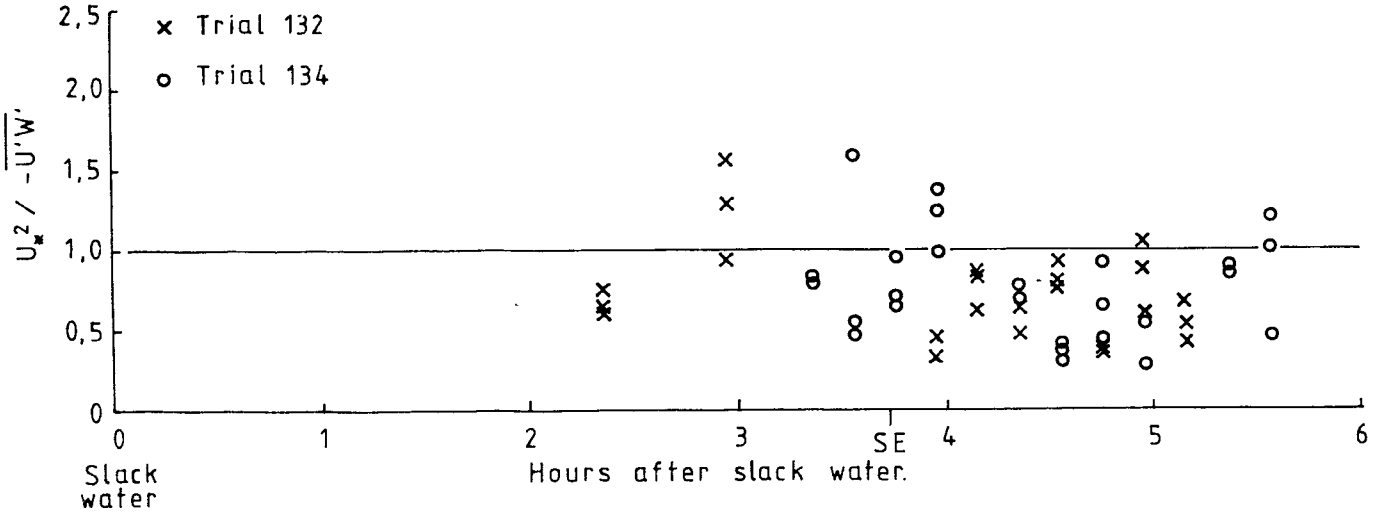
Trial 132
Trial 134
$U_*^2 / -\overline{U'W'}$
2,5
2,0
1,5
1,0
0,5
0
0
1
2
3
SE
4
5
6
Slack water
Hours after slack water.

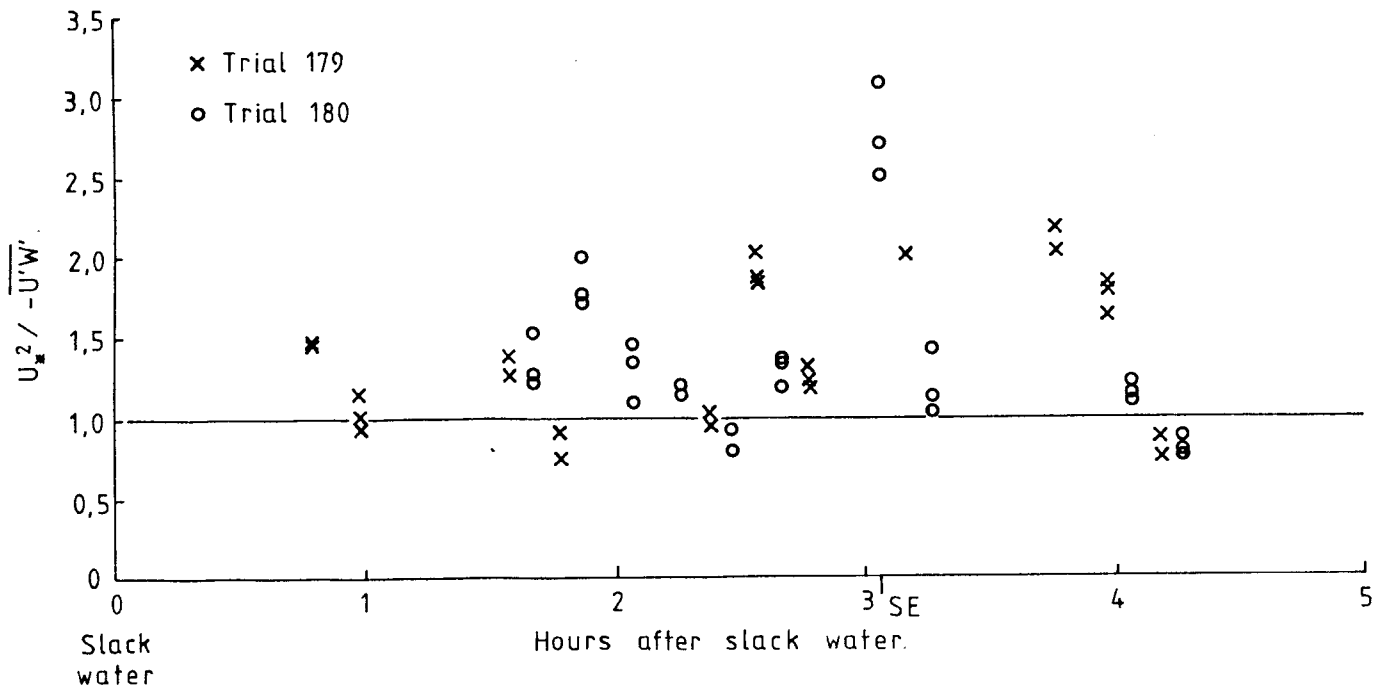
Trial 179
Trial 180
$U_*^2 / -\overline{U'W'}$
3,5
3,0
2,5
2,0
1,5
1,0
0,5
0
0
1
2
3
SE
4
5
Slack water
Hours after slack water.

Fig. 6.10 $u_*^2/-\overline{u'w'}$ against C_{100}. Adjacent to each point are the trials (or station) from which the data was drawn.

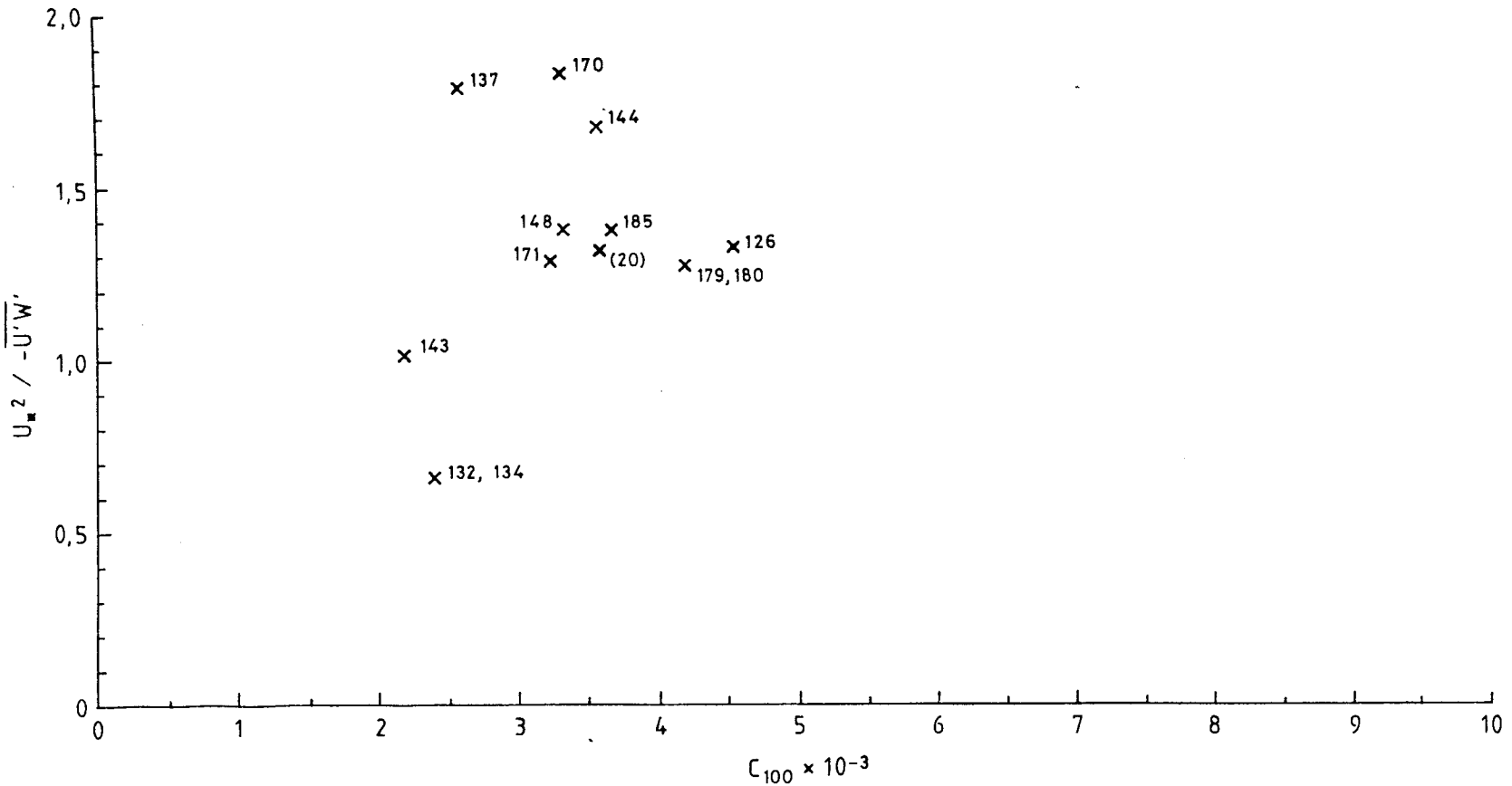
2,0
1,5
1,0
0,5
0
0
1
2
3
4
5
6
7
8
9
10
$U_*^2 / -\overline{U'W'}$
$C_{100} \times 10^{-3}$
137
170
144
148
185
171
(20)
126
179, 180
143
132, 134

Fig. 6.11 $u_*^2/-\overline{u'w'}$ with time from slack water for trials 125 (X) and 127 (O). PV marked on the abscissa represents the time of peak velocity 100.0 cm above the bed.

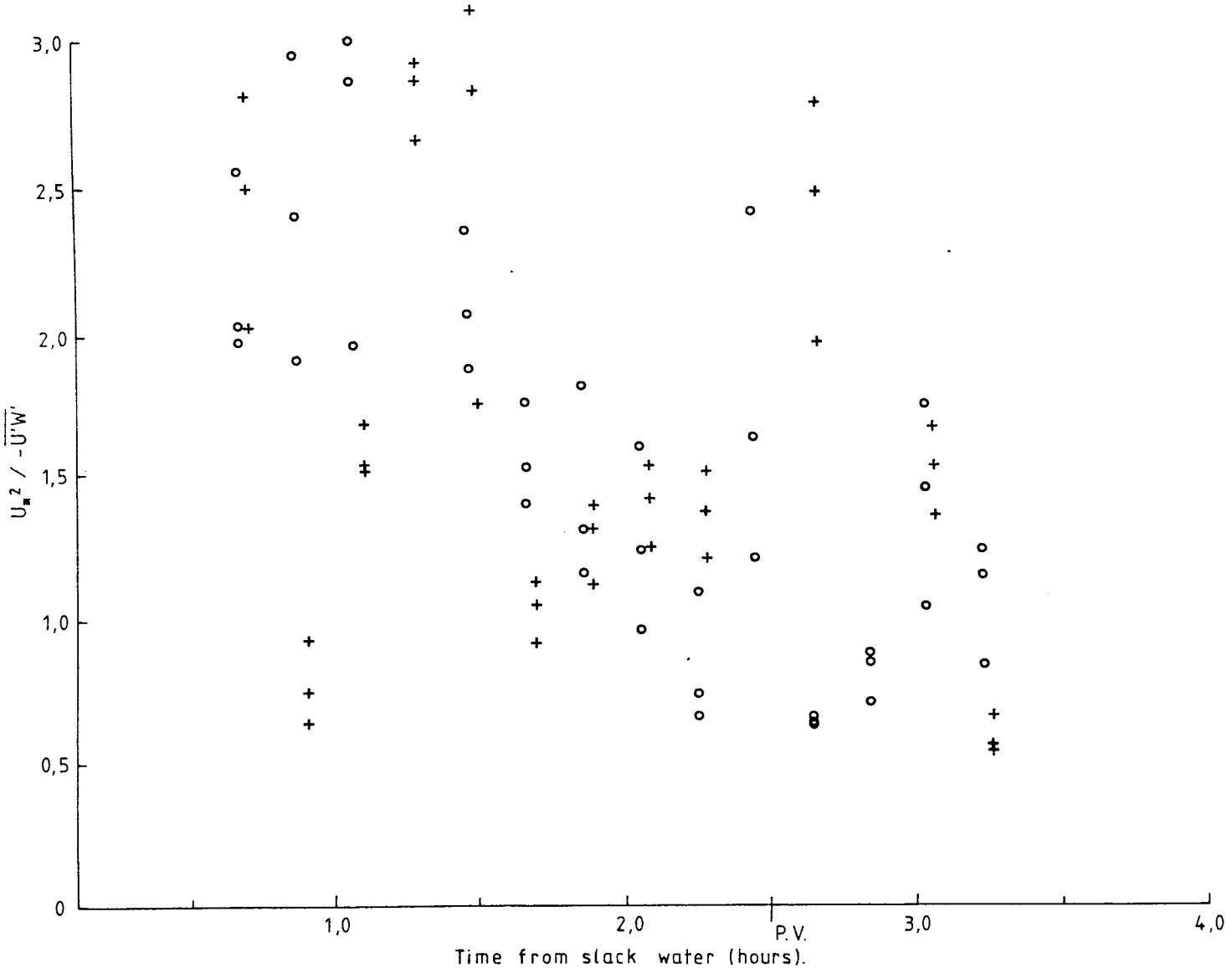
3,0
2,5
2,0
1,5
1,0
0,5
0
$U_*^2 / -\overline{U'W'}$
1,0
2,0
P.V.
3,0
4,0
Time from slack water (hours).

TABLE 6.1 VALUES OF z_0 AND C_{100} RECORDED BY PREVIOUS WORKERS IN THE EASTERN IRISH SEA

LOCATION LAT.(N) LONG.(W) OR LOCATION	SEDIMENT TYPE	z_0 (cm)	C_{100} $x10^{-3}$	METHOD OF DETERMINATION
RED WHARF BAY [a]	S	—	3.23	EDDY CORRELATION
RED WHARF BAY [b]	S	0.1 - 0.3	3.7 - 4.3	LOG-LAW
RED WHARF BAY [c]	S	0.16	—	LOG-LAW
53° 40' 3° 50' [d]	MSP	0.027	1.8	
53° 40' 4° 10' [d]	GS	0.017	1.5	
54° 0' 3° 50' [d]	MS	0.020	2.3	
54° 0' 4° 10' [d]	MSP	0.072	1.7	
54° 0' 4° 20' [d]	GS	0.00046	0.87	
54° 0' 4° 30' [d]	SSh	0.006	1.4	
RED WHARF BAY [d]	S	0.4	5.0	
53° 27' 3° 40' [e]	S	—	5.29	EDDY CORRELATION
53° 25' 4° 8' [e]	S	—	4.30	EDDY CORRALATION

[a] Bowden (1962) [b] Charnock (1959)
[c] Bowden et. al. (1959) [d] Heathershaw (1979)
[e] Bowden and Ferguson (1980)

Values of z_0 and C_{100} were determined by eddy correlation and the log-law respectively in the case of [d].

S ≡ Sand MSP ≡ Medium Sand and Pebbles
GS ≡ Gravel and Sand MS ≡ Muddy Sand
SSh ≡ Sand and Shingle

TABLE 6.2 COMPARISONS OF FLOOD AND EBB DURATIONS (HOURS AND MINS.) FROM TIDE TABLES AND IN SITU MEASUREMENTS

STATION CM4 J.M. 9/81 FROM ~00:35 26/7 TO ~21:50 29/7		STATION CM6 SH. 7/82 FROM ~22:55 28/7 TO ~04:20 2/8		STATION CM7 SH. 7/82 FROM ~22:10 3/8 TO ~00:30 8/8		FLOOD(F) OR EBB(E)
TABLES	IN SITU	TABLES	IN SITU	TABLES	IN SITU	
6.11	5.42	5.57	6.08			F
6.30	6.57	6.48	7.27	6.35	6.18	E
6.11	5.44	5.52	5.48	5.46	6.07	F
6.29	6.47	6.30	6.35	6.23	6.06	E
6.02	5.23	6.04	6.00	5.50	6.16	F
6.39	7.02	6.41	7.03	6.34	6.00	E
5.59	5.48	6.01	5.56	5.43	6.16	F
6.38	6.40	6.27	6.45	6.27	6.06	E
5.52	5.32	6.04	5.52	5.47	6.12	F
6.40	7.03	6.31	6.31	6.38	5.56	E
5.53	5.39	5.59	5.58	5.40	6.24	F
6.40	6.56	6.30	6.44	6.29	6.00	E
5.46	5.37	6.00	5.48	5.48	6.09	F
6.39	6.53	6.26	6.54	6.38	6.15	E
5.43	5.37	5.58	5.22	5.41	6.06	F
		6.29	7.10	6.29	5.51	E
				5.48	6.25	F

CHAPTER 7 - VARIATIONS OF u_*^2 AND z_0

7.1 INTRODUCTION

In the past, a number of workers have observed a hysteresis between the boundary shear stress and velocity. Peak values of Reynolds stress were observed by McLean (1983) to lag peak velocities 214 cm above a level bed. Stress on the decelerating phase of the tide was found to be significantly greater than the accelerating phase for equivalent velocities. Gordon (1975) observed a similar situation, with $z/\delta \lesssim 0.5$ (z = height of the sensor above the bed and δ = boundary layer thickness). Conversely, Bowden and Ferguson (1980) reported no such hysteresis at $z/\delta \lesssim 0.1$. It was shown that the effect would only be expected to be evident when adverse pressure gradients enhanced the Reynolds stress for $z/\delta \gtrsim 0.2$. It should be noted that McLean's (1983) results were taken for $z/\delta \approx 0.1$, apparently contradicting the previous statement.

Other workers have suggested that z_0 varies during a tide, most probably as a result of sediment motion, and hence bedform adjustments. Vincent and Harvey (1976), and Harvey and Vincent (1977) observed z_0 to decrease with increasing mean flow over a static bed. When comparing theoretical stress profiles with data from the Columbia River, Smith and McLean (1977) found z_0 to increase with the sediment concentrations as τ_0 increased. Dyer (1980) reported an initial increase in z_0 with U_{100}, decreasing with the onset of sediment motion. During the decelerating phase of the tide, z_0 was observed to decrease rapidly, after a brief increase before the cessation of sediment motion. Anwar (1981) reported z_0 to be greatest during accelerating flows. Conversely, Soulsby, Davies and Wilkinson (1983), and Wilkinson (1984) found an increase in z_0 during the

decelerating phase of the tide. Lastly, McLean (1983) observed z_0 to increase and decrease with velocity.

In this chapter, possible variations in stress and z_0 with tidal phase and sediment types are investigated. In particular, this may help to resolve the apparent uncertainty in the response of z_0 to mean flow. The drag coefficient (C_{100}) and z_0 are also compared with values from past work, for a range of sediment types.

7.2 DERIVATION OF u_*^2 AND z_0

Values of u_*^2 and z_0 were derived from equation 1.11, using the least squares technique of Appendix 2, from which 95% confidence limits were derived. In this section von Karmann's constant κ_0 was taken to equal 0.4. Comparisons of $-\overline{u'w'}$ and u_*^2 in Section 6.4.3 indicated a degree of uncertainty in this value. In this chapter it is not important to examine absolute values of stress. Also in the determination of z_0 (= exp(intercept/gradient)) the absolute value is unaffected by uncertainty in κ_0. Values of C_{100} presented in Section 7.5 are subject to the greatest degree of uncertainty due to κ_0. Possibly values are overestimated by up to 25%.

An interesting feature of the log profiles was that almost wthout exception they were linear to a level of 98% confidence (i.e. the Students t parameter for N-2 degrees of freedom was less than 6.97, where N = 4). This would suggest that at no time was there appreciable stratification of the water column by suspended sediment, as discussed in Section 5.6.

When investigating the possible hysteresis of the stress, u_*^2 has been examined rather than $-\overline{u'w'}$. In the latter, different attitudes of the turbulence rig, if situated on bedforms, may have a marked effect for the data combined from several trials. Subsequent

over, or underestimates, of the stress may conceal hystereris effects. Using the square of the friction velocity will also amplify differences in the stress for equivalent velocities on the accelerating and decelerating phases of the tide. In the analysis, 12 minute averaged velocities from the top rotor were used to achieve a value of z/δ as close to the range 0.1 - 0.2 as possible.

Values of z_0 were examined uncorrected and corrected for accelerating flow. In the case of the latter, the correction suggested by Soulsby and Dyer (1981), given in a rearanged form in equation 7.1 below, was employed.

$$z_0 = \exp\left[\ln \tilde{z}_0 + \frac{\ln z/\tilde{z}_0 - 1}{\gamma\Lambda/z} \right] \quad , \qquad 7.1$$

Where $\tilde{z}_0$ = apparent value of z_0 from the log-law of equation 1.11, γ = a constant = 0.066 (see Section 5.7.1) and z/Λ = Soulsby and Dyer (1981) criterion for accelerating flow.

7.3 TIDAL HYSTERESIS OF STRESS

In this and the following section, grouping of the data from the various trials was based on the Fourier analysis of the Aanderaa records, described in Section 6.3. Trials at each station were grouped separately into data sets covering ebbs and floods. The exceptions to this were for trials 179 onwards, where the durations of the floods and ebbs were comparable. As in Section 6.4.2., values of u_*^2 were examined in the range $|z/\Lambda| \angle 0.015$. In a number of cases insufficient data was available over the flood or ebb period. This was in part due to adverse weather conditions delaying or curtailing deployments, as discussed in Chapter 2. In addition, the angle of the mean flow with respect to the rig lay outside the bounds of $\pm 30^{\circ}$ (see

Section 4.4). In total, 15 plots of u_*^2 against velocity were examined. The details of these are listed in Table 7.1, which includes the station at which the data was collected, the number of points available, whether there was evidence of hysteresis, the range of z/δ and pertinent comments relating to the data.

Only the plots for trials 144 and 146 at station 12, given in Fig. 7.1a, displayed any evidence of hysteresis. The data was recorded on the ebb tide, X representing accelerating flow and o decelerating flow. A plot for trials 141, 143 and 145, over the flood at the same station failed to reveal any evidence of the effect (see Fig. 7.1b). This may be attributable to the lack of data on the decelerating phase.

Excepting station 11, z/δ was a maximum at station 12, between 0.12 and 0.08 at low and high water respectively. δ was taken as the depth of the water column that was neutrally stratified, as detailed in Section 2.3. Bowden and Ferguson (1980) suggested that in the range of $z/\delta = 0.1 - 0.2$ hysteresis may become evident. This would appear to be so in Fig. 7.1a. There was no evidence of hysteresis at the only other station (11) within the above limits, where $z/\delta = 0.24 - 0.11$. This can be partially attributed to the comaparable values of the major to minor axes of the tidal ellipse, resulting in a rather poorly defined velocity maxima, as shown by the grouping of the points between 35 and 42 cm s^{-1} in Fig. 7.2a, for trial 137. In addition, the relatively short record length made interpretation difficult. Trial 138 had too little data to be useful.

At the remaining stations there was no evidence of a hysteresis effect, with the situation typical of that shown in Fig. 7.2b for trials 125 and 127. Values of u_*^2 appear to be randomly distributed for a given mean velocity on positive and negative

accelerations. This would be expected, with all values of z/δ below 0.1, if the results of Bowden and Ferguson (1980) were applied.

In Section 6.4.4 it was suggested that the ratio $u_*^2/-\overline{u'w'}$ might be significantly greater over the roughest bed forms examined in this study during trials 125 and 127. Values of u_*^2 in Fig. 7.2b may have been overestimated during the accelerating phase. If this were so then hysterisis may well have been present. The cause of the high ratios was not clear. Therefore possible hysterisis may not result from Reynolds stress enhancement by adverse pressure gradients, but to an increase in the gradient (u_*/κ_0) from the log profile for some reason.

7.4 TIDAL VARIATIONS IN z_0

Values of z_0, uncorrected for the influence of accelerating flow, are plotted against time from slack water in Figs. 7.3a, to 7.3g. Included in the plots are the 95% confidence limits on each individual point, the typical magnitude of which varied from ± 20% to ± 120% of z_0. An interesting feature of the limits was their increase often found at the beginning and end of the records. This can most probably be attributed to the influence of accelerating flow, manifest as a slight departure of the log-law from the linear form. The uncertainties given here were comparable to those presented by Wilkinson (1984), employing the same least squares technique, but using six rotors. It would be expected that the results of the latter would give smaller uncertainties, as the Students t parameter decreases for larger data sets (see Appendix 2). This suggests that the results of the present study gave a closer fit to the log-law, possibly because there was less suspended sediment. Soulsby, Davies and Wilkinson (1983) have reported a degree of suspended sediment in

Start Bay, where Wilkinson's (1984) data were collected. Uncertainties of such magnitude have a tendency to conceal the trends in z_0. Despite this, trends were observable in a number of cases, especially in data extending over a large part of a tidal cycle.

The data sets in which trends were most evident were given in Figs. 7.3a to 7.3e, the data of which were collected during the trials indicated in the plots. Table 7.2 summarises the data considered in this section, at which station it was recorded, the sediment type and whether there was evidence of a change in z_0 for uncorrected and corrected values. Whenever there was evidence of a variation in z_0, a minimum existed during periods of maximum velocity (central portion of the plots). These results were comparable to those of McLean (1983), where z_0 minima were also observed at peak tidal flows. Soulsby and Dyer (1981) suggested that z_0 would be overestimated during periods of accelerating flow. The above results would appear to be at variance with this, if the trends were due to acceleration alone.

In a number of cases, the most notable of which are given in Figs. 7.3f and 7.3g, it appeared that z_0 was constant over the tide. This was perhaps a little surprising as the records were long enough to show the influence of acceleration on the velocity profiles.

In an attempt to clarify the situation, values of z_0 were corrected for the effects of accelerating flow according to equation 7.1.

Plots corresponding to those given in Fig. 7.3, but accounting for the effects of accelerating flow, are presented in Figs. 7.4. The major drawback in using the values of z_0 derived from equation 7.1, was the large increase in the uncertainty of the values. The uncertainty in γ was $\pm$ 0.117 (see Section 5.7.1), and in the

uncorrected z_0 was typically ± 70%. Applying standard error analysis techniques, the uncertainties increased by approximately an order of magnitude. Because of this, the error bars have been omitted in Figs. 7.4. This must also cast some doubts on the validity of the results. Despite this, it was felt that it might prove instructive to examine the data in the corrected form. Only values of z_0 in the range $|z/\Lambda| < 0.015$ were considered, which led to considerably depleted data sets in a number of instances.

In the case of Fig. 7.4a, and possibly Fig. 7.4c, the upward trend during the decelerating phase appears to be have been removed, although the initial decrease in z_0 was still evident. The upward trend during the final stages of the remaining plots in Figs. 7.4b, 7.4d and 7.4e would also appear to be absent, and also no trends were evident during the initial stages of these plots. In the cases of Figs. 7.4b and 7.4d this was to be expected since the accelerating phase was not sampled fully. For Figs. 7.4f and 7.4g there was no trend evident.

The eradication of the upward trend from the decelerating phase of the records, if present, suggests this was due to accelerating effects only. An explanation for initially high values of z_0, seen most readily in Fig. 7.4a, was forwarded by McLean (1983). Using a high frequency echo sounder, capable of resolving to ± 1 mm over a 6 m long track, it was found that ripples on the bed had relatively steep faces orientated into the flow immediately after the turn of the tide. As the tidal cycle proceeded these faces became gradually more streamlined, with the steep faces eventually orientated downstream. From in situ T.V. pictures, Dyer (1980) reported a similar change in the ripple forms. The increase in z_0 occurred at the onset of the suspension of sediment, with a

corresponding rise in the ripple height. This was unfortunately impossible to verify from the photographs taken during the present study, as over the area of deployment the bed consisted of predominantly gravel and sand, devoid of ripples (see Chapter 8). This would also explain the absence of a trend in Figs. 7.4e and 7.4f. The magnitude of the roughness elements would be expected to remain constant throughout the tide, as the majority of the sediment was too large to be advected.

It is difficult to provide an explanation for the absence of any evidence to support the results of Fig. 7.4a, in the remaining trials. A large proportion of the trials were recorded at stations with similar sediment types. Perhaps the precession of the tidal ellipse at the stations in a line west of Blackpool (see Section 2.3) resulted in a constant change in the orientation of the bedforms, precluding the development of bed forms of any magnitude and direction. At the remaining stations it might be that the velocity was below the threshold for sediment motion. This may have been possible, as discussed in Section 5.6, where it was thought sediment motion was as bedload or non-existent. Why there should be motion at only one station, where the velocities were comparable to the other stations, cannot be readily explained. Perhaps the large degree of uncertainty in values of z_0 masks the effects, which may not bave been quite as pronounced as those of Fig. 7.4a.

7.5 VARIATIONS IN z_0 AND C_{100} WITH SEDIMENT TYPE

Soulsby (1983) presented a table of typical values of z_0 and C_{100} for different bottom types, which is reproduced in Table 7.3. The data was drawn from 18 sources, at a variety of locations. Values of z_0 were expressed as geometric means. Included is a variation

factor, which if multiplied by, or divided into the mean, corresponds to one standard deviation either side of the mean. C_{100} was determined from the expression

$$C_{100} = \left[\frac{\kappa_0}{\ln(100/z_0)} \right]^2 ,$$

where κ_0 was taken as 0.4.

To enable comparisons with this work, the corrected and uncorrected values of z_0 and C_{100} in Table 7.2 have been dealt with in the same fashion. The number of points in each estimate of z_0 is given in brackets. Where there was evidence of tidal variations in z_0 a range of values is given. The range corresponds to the initial maximum, central minimum and final maximum values of z_0, taken from the apparent trends of Figs. 7.3 and 7.4.

It was immediately obvious from the values of z_0, presented in Table 7.2, that the use of the corrected data in favour of uncorrected, results in no significant changes in the z_0 estimate. It is possible that any such changes may have been masked by the large variability. It follows from the above expression, that this statement also applied to C_{100}.

The mean values of z_0 fall into two main groups:

A $z_0 \sim 0.02 - 0.05$: Station 10, 11, 12 : $C_{100} \sim (2 - 3) \times 10^{-3}$.

B $z_0 \sim 0.10 - 0.20$: Station 8, 13, 16, 18, 19, 20 : $C_{100} \sim (3 - 4) \times 10^{-3}$.

Values for station 8 and 12 are very variable, but the minimum values of z_0 would put 8 in group A and the maximum put 12 in group B.

Comparing the results with Table 7.3, group A corresponds approximately with the values of z_0 for mud, unrippled sand and the

various sand combinations. Group B values of z_0 are of the same order as, but somewhat less than that for gravel and for rippled sand.

Comparable values of z_0 were obtained from the data collected during trial 126 (station 8) and that collected at station 18. Both stations were in approximately the same position (see Fig. 2.2), suggesting relatively stable long term conditions.

The variation of z_0 for similar sediment types, but over rippled and unrippled beds, indicates that it was the form drag, rather than the localised skin friction that was recorded. Values of C_{100}, ranging from approximately (2.5 - 8.0) x 10^{-3} over beds of varying roughness, illustrate the inadvisability of using one estimate for all beds. It would appear that in regions where the sediment was relatively fine and unrippled, values of C_{100} in group A are applicable. With an increase in sediment particle size, or progressive rippling of the bed, values of C_{100} in group B appear to be appropriate. Even at a single station, one value of C_{100} should only be applied with care, as shown by the value at station 8 varying from approximately 3.78 x 10^{-3} to 7.87 x 10^{-3}, and possibly dependent on the steepness of the ripple faces.

7.6 SUMMARY AND CONCLUSIONS

In this chapter the possible variations of stress and z_0 with tidal phase have been examined. Values of z_0 and C_{100} were also compared with previous work.

In order to increase the data set, values of u_*^2 (corrected for accelerating effects) were examined in preference to $-\overline{u'w'}$ for combinations of trials at one station. Sensor misalignment due to bedforms was thought likely to mask possible hysteresis effects in the data obtained using the e.m. heads. Hysteresis was observed at

one station only, where $z/\delta \geq 0.1$. At the only other station where this value was exceeded, the poorly defined velocity maximum, and a relatively short record length, may have masked the effect. At all other stations $z/\delta < 0.1$, hysteresis was not observed. These results support the work of Bowden and Ferguson (1980), who suggested that tidal hysteresis would become evident in the range $z/\delta = 0.1 - 0.2$.

Values of z_0, uncorrected for accelerating flow, indicated a variation with tidal phase at a number of stations, characterised by a minimum in z_0 at peak velocities. A number of stations failed to show a dependence. When corrected for accelerating flow, z_0 varied at one station only, exhibiting a maximum at the start of the tide. This could possibly be best explained by the steep faces of the bed ripples facing upstream initially, but becoming streamlined as the threshold of sediment motion was exceeded. At the remaining stations all evidence of variations in z_0 was eradicated. Despite a large degree of uncertainty in the corrected z_0's, it would appear that tidal variations, recorded by previous workers may have been due, in some instances, to non-removal of accelerating effects. There was no evidence of a sharp decrease in z_0 during the decelerating period, as reported by Dyer (1980), after the cessation of sediment motion. This suggested that gravitational stability of the water column was near neutral, and so little sediment was in suspension.

Both corrected and uncorrected values of z_0 and C_{100} compared well with the values collated from previous studies. Differences may have been partly explained by the large degree of variability in the results. The range of C_{100} ($\sim 2.2 - 8.0 \times 10^{-3}$) indicated the danger of assumming a standard value of C_{100} for all stations. Values may be up to 25% lower due to the uncertainty in κ_0, as discussed in Chapter 6. Lower values should be applied for relatively fine and unrippled

sediment. For coarser sediment and heavily rippled beds, values toward the higher end of the range should be applied.

Fig. 7.1 Values of u_*^2 (corrected for acceleration) .v. velocity (recorded 178.5 cm above the bed), X ≡ accelerating flow, O ≡ decelerating.

a) For trials 144 and 146. The continuous line represents the possible trend of u_*^2 against velocity (hysteresis effect)

b) For trials 141, 143 and 145. There is no evidence of a hysteresis.

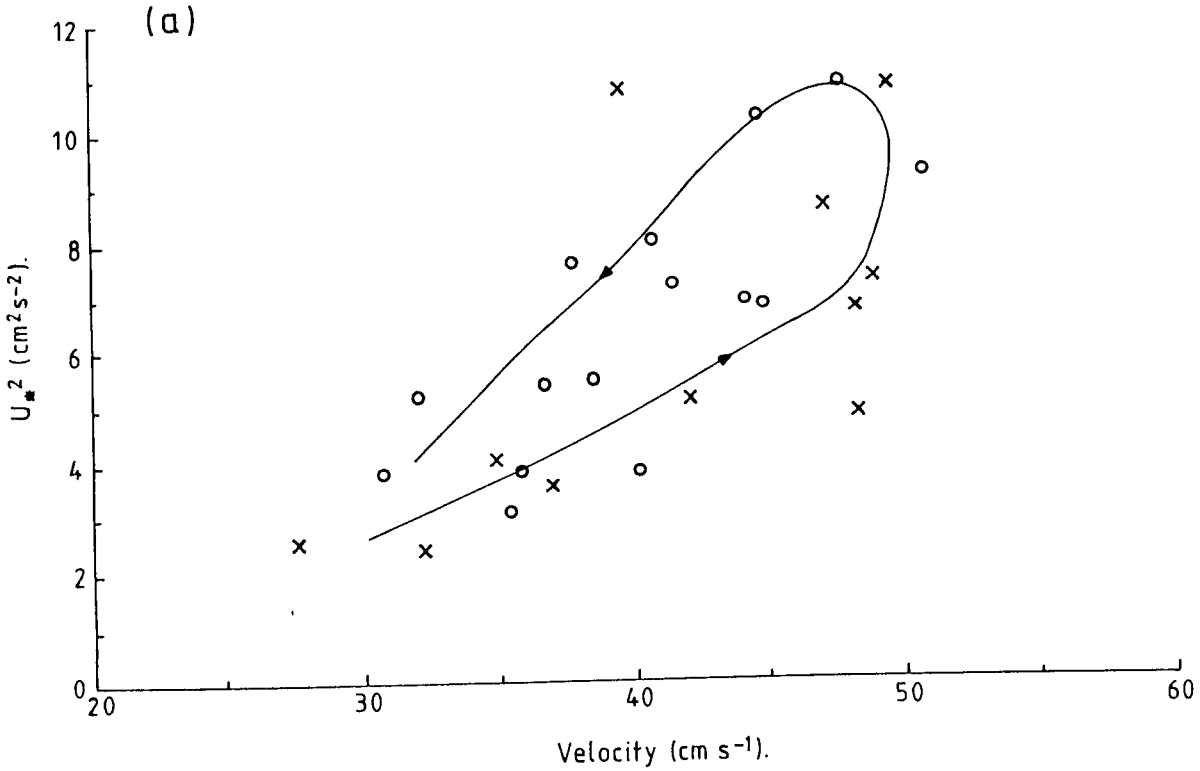
(a)
12
10
8
6
4
2
0
20
30
40
50
60
U_*^2 (cm^{2}s^{-2}).
Velocity (cm s^{-1}).

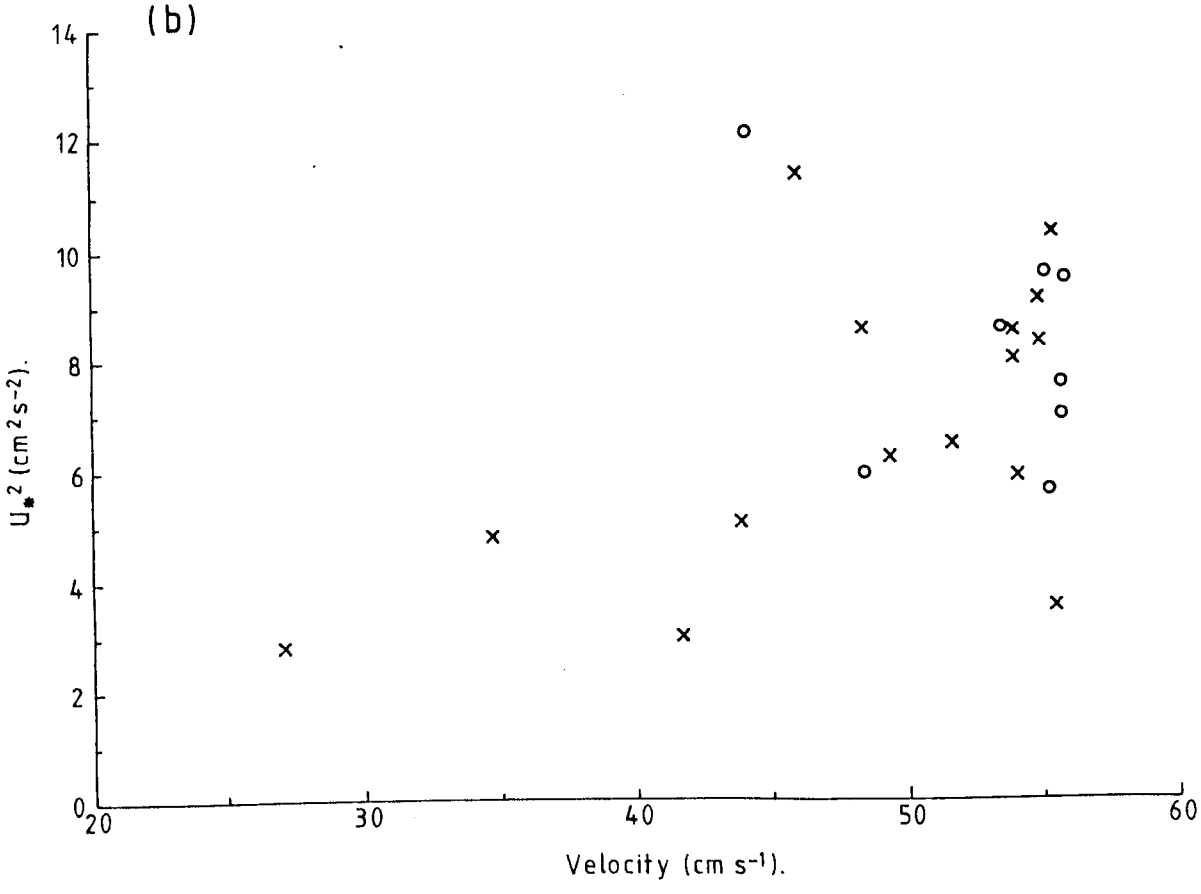
(b)
14
12
10
8
6
4
2
0
20
30
40
50
60
U_*^2 (cm^{2}s^{-2}).
Velocity (cm s^{-1}).

Fig. 7.2 Values of u_*^2 (corrected for acceleration) .v. velocity (recorded 178.5 cm above the bed), X ≡ accelerating flow, O ≡ decelerating.

a) For trial 137. Evidence of hysteresis may be concealed by the poorly defined velocity maxima, manifest as a grouping of the data, and relatively short record length.

b) For trials 125 and 127. The random distribution of data implies no hysteresis.

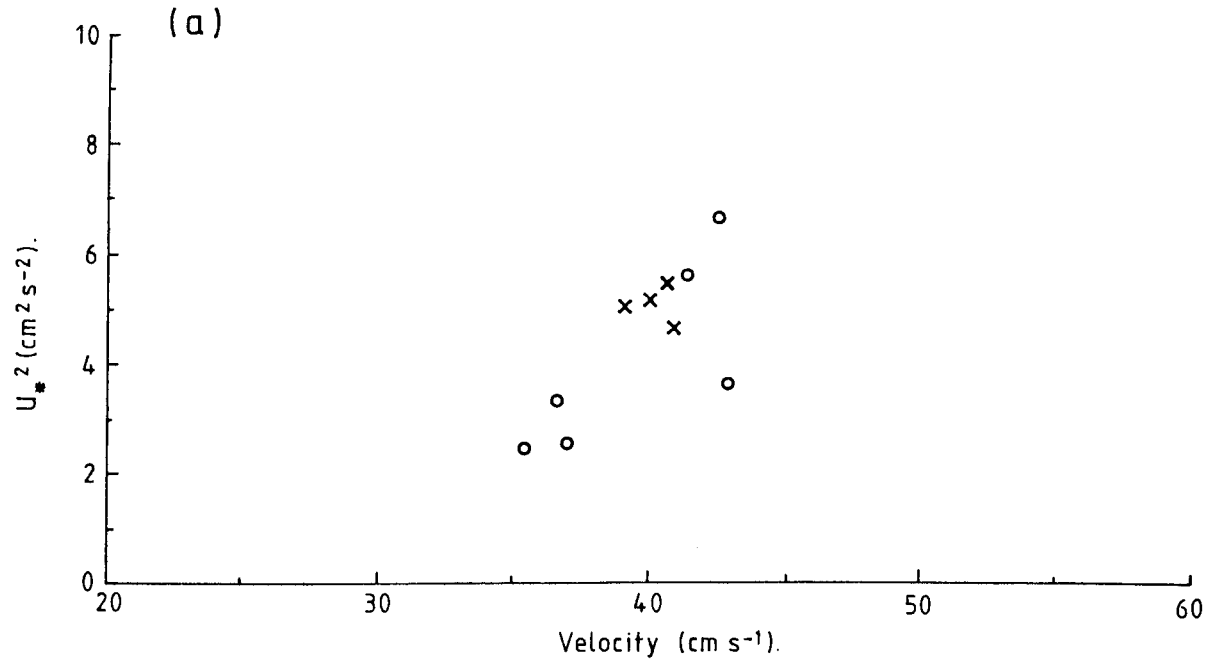
(a)
10
8
6
4
2
0
20
30
40
50
60
U_*^2 (cm^2 s^{-2}).
Velocity (cm s^{-1}).

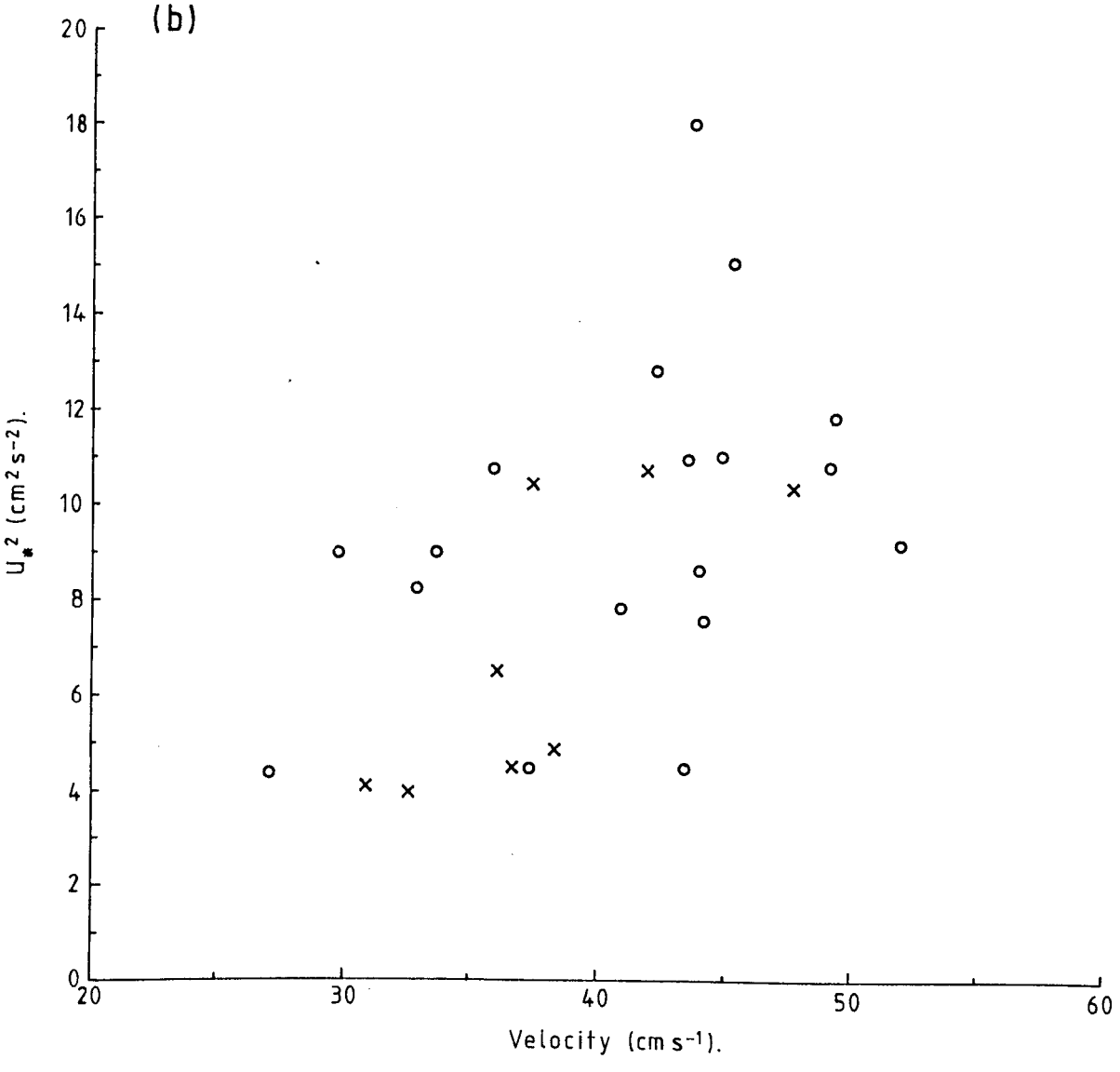
(b)
20
18
16
14
12
10
8
6
4
2
0
20
30
40
50
60
U_*^2 (cm^2 s^{-2}).
Velocity (cm s^{-1}).

Fig. 7.3 z_0 (uncorrected for acceleration) .v. time. All records are plotted relative to slack water (excepting Fig. 7.3c), where no reliable estimate was available. Error bars represent 95% confidence limits and the solid line, up to and including Fig. 7.3e, the trend. In Figs. 7.3f and 7.3g the solid line represents the geometric mean with the standard deviation given by the error bar.

a) Trials 125 and 127.

b) Trial 137.

c) Trial 145.

d) Trials 169 and 171.

e) Trials 179 and 180.

f) Trials 132 and 134.

g) Trial 185.

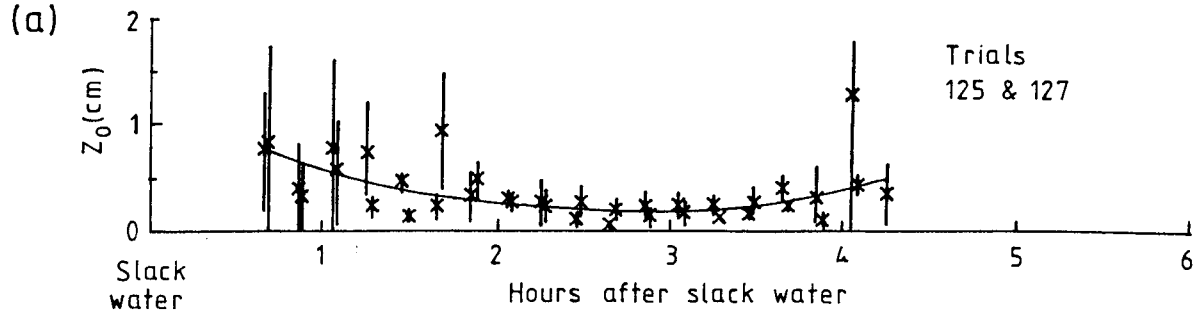

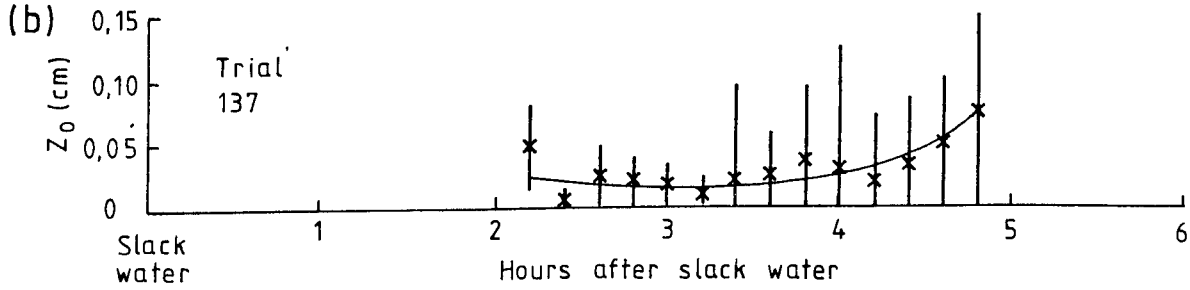

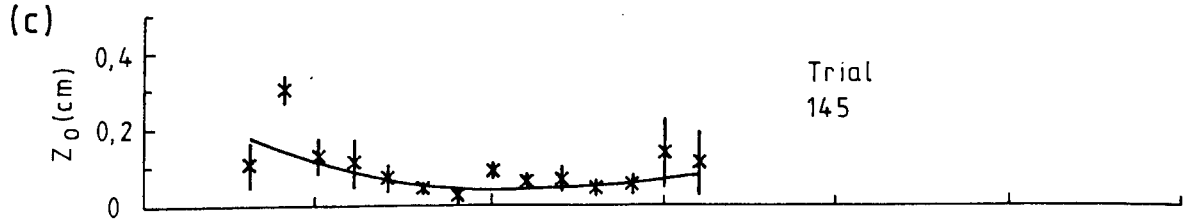

Divisions in hours (no reliable reference to slack water).

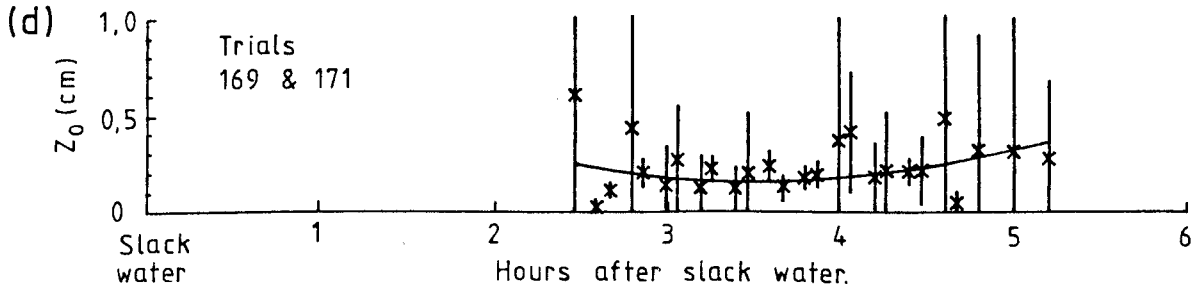

(e)

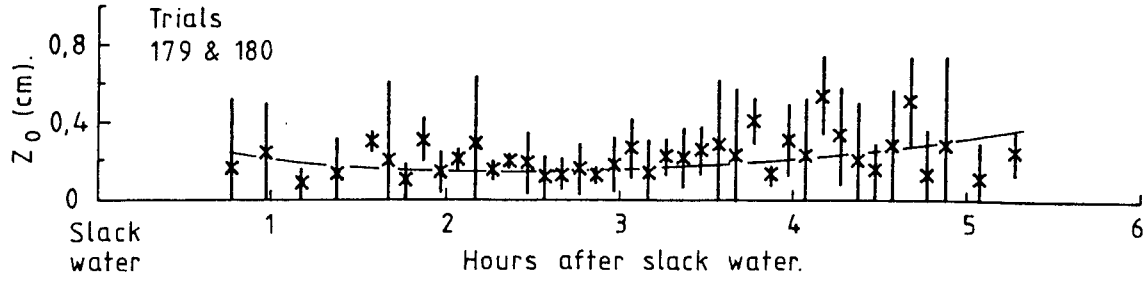
Trials
179 & 180
0,8
0,4
0
Z_0 (cm).
Slack
water
1
2
3
4
5
6
Hours after slack water.

(f)

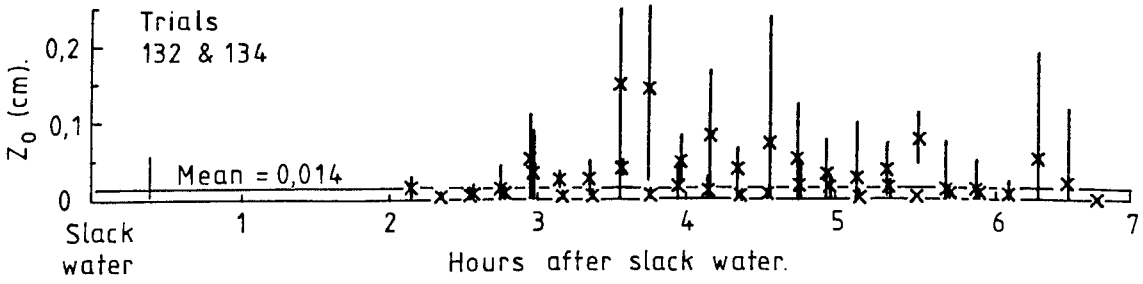
Trials
132 & 134
0,2
0,1
0
Z_0 (cm).
Mean = 0,014
Slack
water
1
2
3
4
5
6
7
Hours after slack water.

(g)

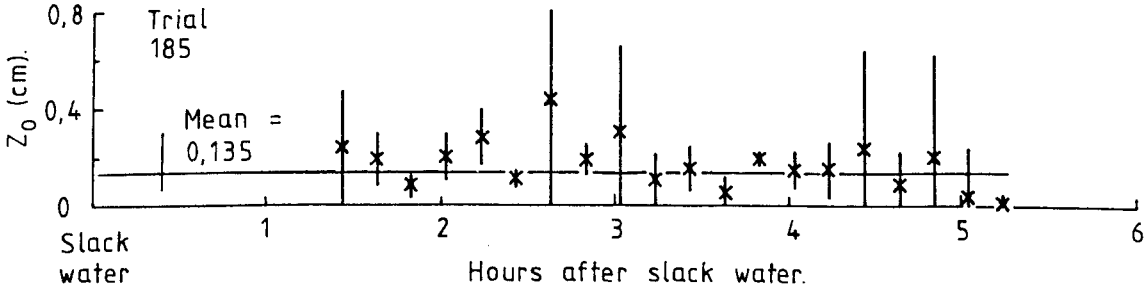
Trial
185
0,8
0,4
0
Z_0 (cm).
Mean =
0,135
Slack
water
1
2
3
4
5
6
Hours after slack water.

Fig. 7.4 z_0 (corrected for acceleration) .v. time. In all but Fig. 7.4a and 7.4c the solid line represents the geometric mean with the standard error. No estimate of the trend in Fig. 7.4c is given as this was unclear. a) to g) correspond to the trials of Fig. 7.3.

(a)

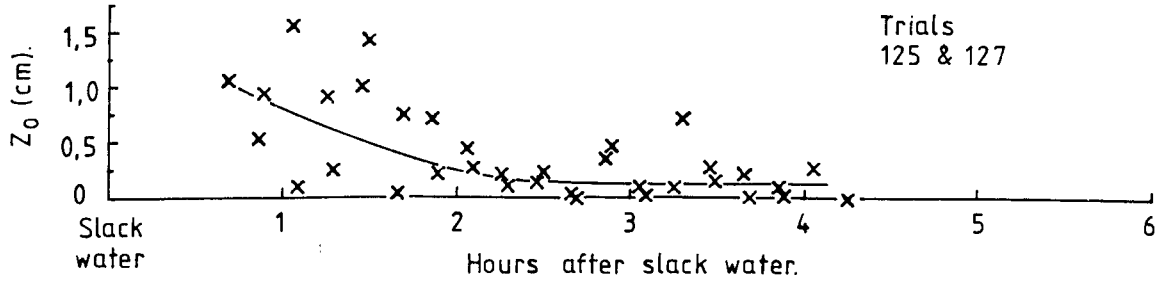

(b)

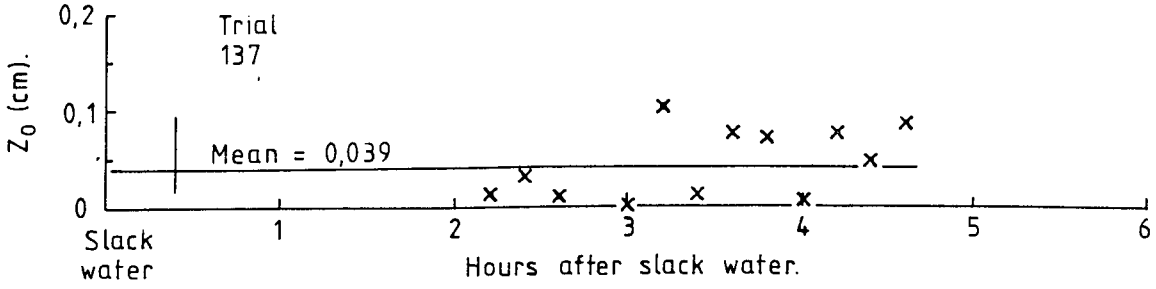

(c)

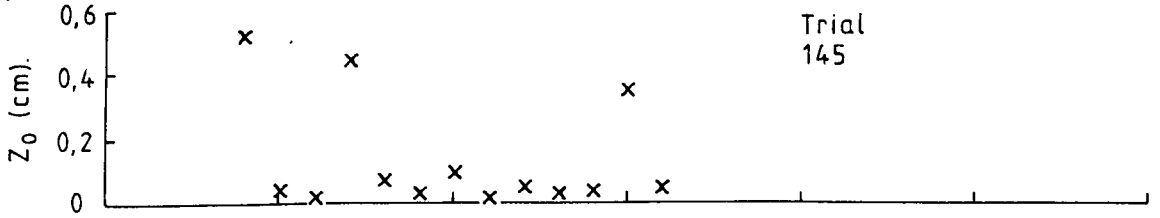

Divisions in hours (no reliable reference to slack water).

(d)

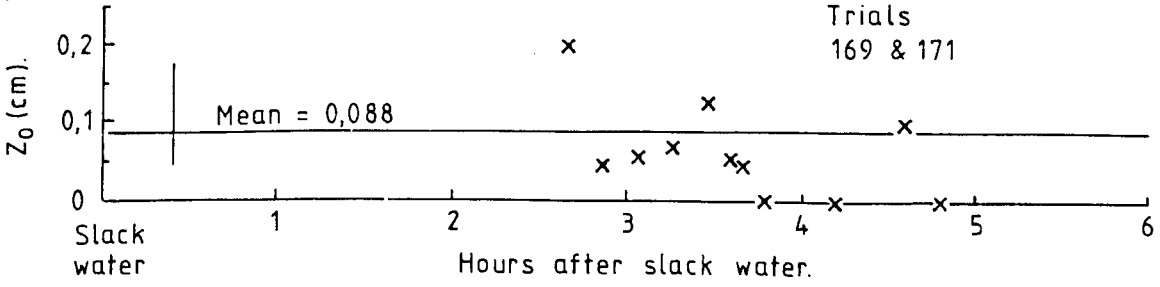

(e)

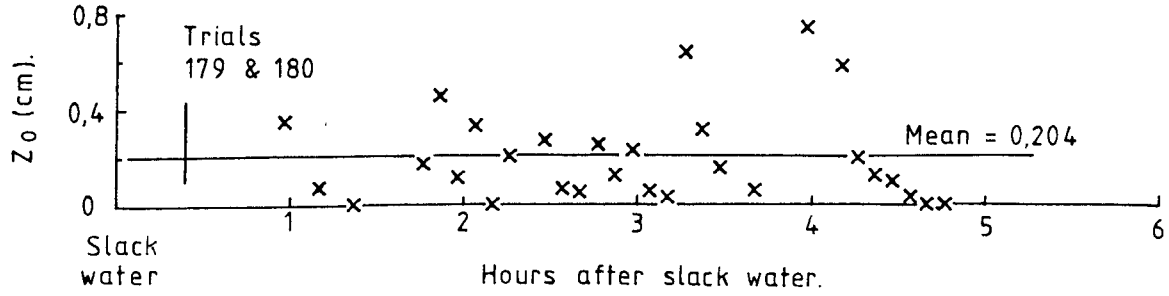
0,8
0,4
0
Z_0 (cm).
Trials
179 & 180
Mean = 0,204
1
2
3
4
5
6
Slack
water
Hours after slack water.

(f)

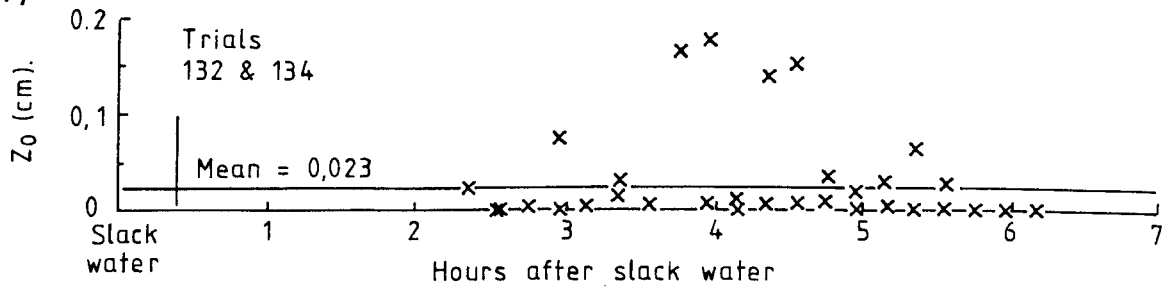
0.2
0,1
0
Z_0 (cm).
Trials
132 & 134
Mean = 0,023
1
2
3
4
5
6
7
Slack
water
Hours after slack water

(g)

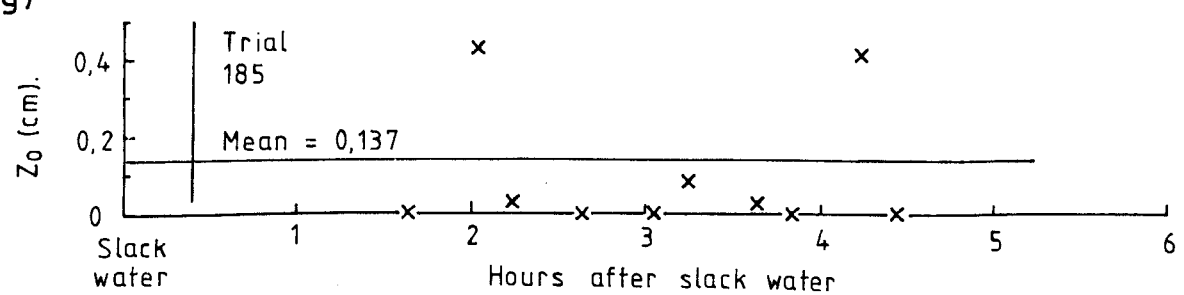
0,4
0,2
0
Z_0 (cm).
Trial
185
Mean = 0,137
1
2
3
4
5
6
Slack
water
Hours after slack water

TABLE 7.1 SUMMARY OF DATA USED TO DETERMINE THE POSSIBILTY OF HYSTERESIS IN THE STRESS

TRIALS COMPRISING DATA SET	STATION	RANGE OF z/δ	NUMBER OF POINTS	COMMENTS
125, 127	8	0.10 - 0.08	26	POSSIBLE HYSTERISIS CAUSE UNCERTAIN
126	8	0.10 - 0.08	16	
132, 134	10	0.08 - 0.06	20	
137	11	0.24 - 0.11	10	
138	11	0.24 - 0.11	6	INSUFFICIENT DATA
141, 143, 145	12	0.12 - 0.08	23	DATA CONCENTRATED AROUND PEAK VELOCITIE
144, 146	12	0.12 - 0.08	26	EVIDENCE OF HYSTERESIS
147, 149	13	0.08 - 0.06	14	
148, 152	13	0.08 - 0.06	18	
153, 155, 157	14	0.05 - 0.04	13	
154, 156	14	0.05 - 0.04	5	INSUFFICIENT DATA
169, 171	16	0.06 - 0.05	5	INSUFFICIENT DATA
173, 175, 177	17	0.06 - 0.05	13	MAJORITY OF DATA FROM ACCELERATING PHASE
179, 180	18	0.12 - 0.09	11	
186, 187, 189, 191	20	0.06 - 0.05	26	

The remaining trials had too few points to obtain meaningful results.

TABLE 7.2 SUMMARY OF THE DATA USED TO DETERMINE POSSIBLE TIDAL VARIATIONS IN z_0

TRIALS COMPRISING DATA SET	STATION	SEDIMENT TYPE	EVIDENCE OF TIDAL VARIATIONS IN z_0		z_0 (cm)		$C_{100} \times 10^{-3}$	
			UNCORRECTED	CORRECTED	UNCORRECTED	CORRECTED	UNCORRECTED	CORRECTED
125, 127	8	MSSP	YES	YES	0.75 0.20 0.45	1.10 0.15 0.15	6.68 4.14 6.46	7.87 3.78 3.78
126	8	MSSP	NO	NO	0.306 1.48(18)	0.265 2.00(16)	4.77	4.55
132, 134	10	FCS	NO	NO	0.014 4.03(42)	0.023 4.20(19)	2.04	2.29
137	11	SM	YES	NO	0.03 0.01 0.07	0.039 2.47(10)	2.43 1.89 3.03	2.60
143	12	SM	?	NO	0.0059 – 0.1238	0.019 4.48(8)	1.69 – 3.57	2.17
144	12	SM	NO	NO	0.103 1.52(23)	0.124 2.23(16)	3.38	3.57
145	12	SM	YES	?	0.18 0.05 0.08	0.20 0.03 0.03	4.01 2.77 3.15	4.14 2.43 2.43
148	13	TMS	NO	NO	0.090 2.48(22)	0.098 2.20(12)	3.25	3.33
169, 171	16	MSSP	YES	NO	0.25 0.15 0.32	0.088 2.00(4)	4.46 3.78 4.85	3.24
170	16	MSSP	NO	NO	0.182 2.29(13)	0.099 2.72(5)	4.02	3.34
179, 180	18	MSSP	YES	NO	0.22 0.15 0.35	0.204 2.13(21)	4.27 3.78 5.00	4.17
185	19	SG	NO	NO	0.135 2.22(20)	0.137 3.93(4)	3.67	3.68
186, 187, 189 & 191	20	SG	NO	NO	0.083 2.45(52)	0.127 3.22(18)	3.18	3.60

A range of values of z_0 and C_{100} are given when there was evidence of tidal variation, otherwise the geometric mean, variation factor and (number of points) in the estimate are given. See Table A1.1 for sediment definition.

TABLE 7.3 TYPICAL VALUES OF z_0 AND C_{100} FOR DIFFERENT SEDIMENT TYPES (FROM SOULSBY, 1983)

BOTTOM TYPE	z_0 (cm)	VARIATION FACTOR	$C_{100} \times 10^{-3}$	NUMBER OF OBSERVATIONS
MUD	0.02	—	2.2	1
MUD/SAND	0.07	4.1	3.0	3
SILT/MUD	0.005	—	1.6	1
SAND (UNRIPPLED)	0.04	2.0	2.6	7
SAND (RIPPLED)	0.6	1.3	6.1	6
SAND/SHELL	0.03	4.5	2.4	2
SAND/GRAVEL	0.03	6.7	2.4	7
MUD/SAND/GRAVEL	0.03	3.0	2.4	2
GRAVEL	0.3	1.6	4.7	4

The 'number of observations' takes no account of the quantity of data comprising an individual observation and no account was taken of the hydrodynamic roughness regime.

CHAPTER 8 THE BURSTING PHENOMONEN AND ITS INFLUENCE ON SEDIMENT MOTION

8.1 INTRODUCTION

It has been established from laboratory (Corino and Brodkey, 1969; Willmarth and Lu, 1972; Praturi and Brodkey, 1978) and geophysical (Gordon, 1974; Heathershaw, 1974; Gordon and Witting, 1977) measurements that the Reynolds stress ($-\rho\overline{u'w'}$) consists of a series of intermittant events. Fig. 8.1 shows a 12 minute time series of the u'w' products for trial 186, 100.0 cm, above the bed. The record consists of short periods when the amplitude is many times greater than the long term mean stress. Each of these periods, or events (shaded), lasts several seconds. Interspersed between them are longer quiescent periods.

Each individual stress measurement can be classified as one of four events, depending on the sense of u' and w', shown in the sketch below. Bursts are ejections of near bed fluid into the flow ($w' > 0$) and their velocity is lower than the surrounding fluid ($u' < 0$). Sweeps carry higher velocity fluid ($u' > 0$) toward the bed ($w' < 0$). Both type of events make negative contributions to the Reynolds stress. Up-accelerations ($u' > 0$, $w' > 0$), up-acc, and down-decelerations ($u' < 0$, $w' < 0$), d-dec, make positive contributions to the Reynolds stress. Soulsby (1983) found that bursts and sweeps contributed approximately 50% each to the net Reynolds stress, whilst up-accs and d-decs contributed a value of only 5% of the net Reynolds stress. The net Reynolds stress was

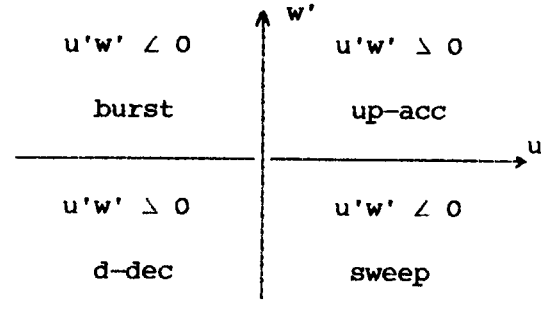

defined as 90% of the total stress. The amplitudes of each event were found to be comparable, but the duration and number of the negative contributions were considerably greater than the positive. The weaker nature and more frequent occurence of the latter, results in the overall negative Reynolds stress values when long term averages are considered (12 minutes in the present study).

It was originally intended that during this study an attempt would be made to examine possible correlations of the above events with sediment motion, observed by the photographic unit. Unfortunately the films were stolen before much more than a cursory examination could be made. The data from trial 186 had been examined more fully than the remainder, and this will be discussed in the following section.

8.2 EXAMINATION OF THE EVENTS IN THE u'w' TIME SERIES IN CONJUNCTION WITH THE PHOTOGRAPHS

In Section 3.3, where the design, construction and trials of the photographic unit were described, it was stated that the original intention was to take photographs once a second for 5 minutes, repeating this hourly throughout a trial. Regretably this could not be achieved, as explained in Section 3.3.2. Instead a sampling rate of one frame per minute for the lifetime of the flash batteries (~ 90 flashes) was adopted. As a result of the theft of the film only 93 frames were examined, corresponding to the first 93 minutes of the u'w' records from trial 186.

The u'w' time series, as shown in Fig. 8.1, was generated by a term by term product of the u' and w' series, as detailed in Section 4.5. Corrections for the angle of flow with respect to the rig, derived from 12 minute averaged velocities only, were applied to

individual u'w' values in each time series. McLean and Smith (1979) and Ferguson (1979) suggest there is little vertical correlation between events. It would therefore be dangerous to use instantaneuos values of u' and v' to estimate angles of flow at each sensor height.

8.2.1 Film Analysis.

When developed, the super 8 cine film was viewed on an Agfa viewer. Each frame could be viewed individually, or at 18 frames per second (corresponding to normal projection speed). The images were projected onto the inside of a 15.24 x 20.32 cm (6 x 8 inch) translucent screen, attached so as to protrude from the projector. To enable a greater accuracy in the charting of particle movements during the interval between the recorded frames, the screen was divided into a grid, as shown in the sketch below.

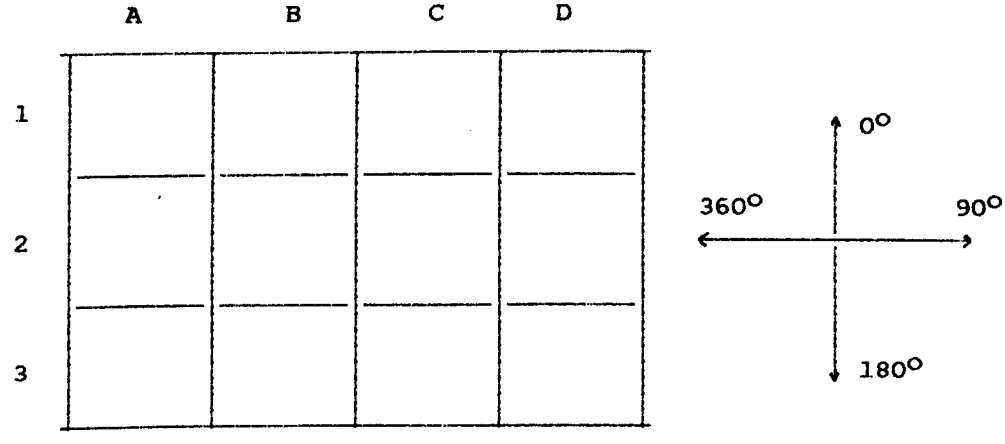

The mean flow direction was defined as being towards the top of the page.

Films were taken during deployments at station 20 only (see Fig. 2.1 for position), where the bed consisted largely of gravel and pebbles, with some sand. This type of bed produced occasional movement of particles, which resulted in a number of frames appearing cloudy. This was presumed to be due fine sediment in suspension.

Several of the 'particles' were observed to move consistently against the flow, and although not positively identified as such in trial 186, may have been marine life. In addition, a number of hermit crabs were observed to move across the bed on several occasions.

Table 8.1 summarises variations in the character of the bed, which took place in the sectors defined in the above sketch. Only those frames in which the changes occured in relation to the preceding frame are given. The frame number represents the time from the start of the turbulence rig deployment. Frame one corresponds to the beginning of the u'w' record. Also included is the supposed nature of the particle and an estimate of the direction of motion, as depicted in the above sketch.

8.2.2 Events in the u'w' Time Series.

Mclean and Smith (1979) produced u'w' time series at four levels between 35 cm and 215 cm above the bed. Lagged cross-correlations suggested events to be of limited vertical extent. The minimum spacing between the bottom sensor and that above was 26 cm. Ferguson (1979) presented visual comparisons of three u'w' time series of duration 12 minutes, recorded at heights of 50, 100 and 200 cm above the bed. In a number of instances it was thought that events could be correlated between two adjacent sensors, but rarely between three.

The above work, especially the former, casts doubt upon whether events would extend from the sea bed to even the lowest sensor, 100 cm above the bed in this study, with the bottom sensor recording u'v' in this trial. If true, then it would be impossible to correlate sediment motion with events in the u'w' time series of this study. A further difficulty arises from the relatively infrequent

nature of the photographs. When attempting correlations, it is likely that only relatively active periods of the u'w' time series would show correlation between frames where sediment was observed to move. It is probable that correlations will only be found when considering the lowest sensor.

An examination of separate 12 minute time series of u'w' for trial 186 was carried out before attempting correlations. Calculations of the amplitudes and durations of the events comprising 90% of the stress followed the definitions given by Soulsby (1983). To determine these events the largest single value of |u'w'| in a 12 minute record was located. By following the time series forwards and backwards until |u'w'| had decayed to 10% of the maximum value, the duration of the event was determined. The record was searched for the next highest peak of |u'w'|, and the process repeated until the value of the sum of u'w' comprising the events ÷ total number of points equaled 90% of $-\overline{u'w'}$ for the 12 minutes. Amplitudes of the events comprising 90% of the stress are shown in Fig. 8.2, for a 12 minute record of trial 186. The record for the lower sensor corresponds to that of the u'w' time series in Fig. 8.1. The amplitude of an event was defined as the mean of u'w' over the duration of the event. In Fig. 8.2 the amplitude of the event is given at the time the peak value of u'w' was measured. Events are classified as: 1 = up-acc; 2 = sweep; 3 = d-dec; 4 = burst.

A closer examination of the records in Fig. 8.2, reveals that in a number of instances events of the same nature occur at the same time (± 1 second) in all three records. This would indicate that the events (marked ↑ on the bottom axis) were of greater vertical extent than suggested by McLean and Smith (1979). In their work, correlations were made between each height for all the values of u'w'

in each record. Such correlations would appear to yield a low value in the records of Fig. 8.2 also. Coherent events were generally those of larger amplitude. Such events would be more energetic, and could therefore reasonably be expected to be detectable further from their point of origin. In the majority, these events comprise bursts or sweeps, probably reflecting the greater proportion of negative to positive contributions made to the Reynolds stress by such events (Soulsby, 1983). This pattern was typical of the other eight 12 minute records analysed from trial 186. The number of coherent events varied from 9 to 14, apparently independent of the magnitude of the U_{100} (see Table 8.3). If the records are examined for coherent events between only two heights, then there is a significant increase in the number. It would appear from the results presented, that an examination of the u'w' records as high as 180 cm from the bed, in conjunction with short interval time lapse photography, may reveal some degree of correlation between events and sediment motion, if the latter existed.

For each record there was a tendency for bursts (4) and d-decs (3) to occur together in groups of between 5 and 20 events. Similar groupings were evident for the sweeps (2) and up-accs (1). Soulsby (1983) also reported such groupings. This pattern was at variance with the laboratory work of Corino and Brodkey (1969), who reported a cycle of events in the sublayer, with sweeps being followed by bursts. The results may be more in accord with the work of Praturi and Brodkey (1978). It was suggested that the appearance of a high speed front into a region of lower velocity was the mechanism by which the events were triggered. As a result of the high shear across the front instabilities develop, leading to the formation of vortices. Ejections of fluid (bursts) then occur from the wall region along the

front. Sometimes the ejections were observed to extend as continuous events well into the outer region, and may occur in groups. As the stronger ejections passed from the low-speed to the high-speed region of the fluid, some may be advected with the fluid, possibly as up-accs. As the region of high shear diminishes the vortices grow in size, eventually drawing in fluid from above, which at this stage is moving with a higher velocity. This results in a downward flow, which in the earlier stages may be in the form of d-decs and in the latter as sweeps. Obviously it is dangerous to compare the rather idealised laboratory flows with geophysical flows. Despite this, it appears that there may be some similarities.

8.2.3 Comparison of the u'w' Time Series and Photographs.

Comparisons were attempted using the amplitude plots of the events contributing 90% of the stress, measured at 100.0 cm above the bed. As photographs were taken at intervals of one minute, such plots should give a reasonable representation of the degree of turbulence activity during each frame. Two such plots are given in Figs. 8.3a and 8.3b. On each record the interval during which the sediment motion was observed, as summarised in Table 8.1, is marked. From Fig. 8.3a it would appear that sediment motion occured during periods of relatively high event intensity. In both cases the marked events (↑) appeared to show coherence with those recorded by the upper sensors. Fig. 8.3b presents a somewhat contradictory picture. Motion observed in frames 39 and 40 and 42 to 44 apparently corresponds to a relatively quiescent period. Although during frame 39, the lone event exhibited coherence with the other levels, with a relatively high amplitude of 105 cm^2 s^{-2} at the central sensor recording u'w'. In frame 42 no events contributing to 90% of the stress were recorded.

During frame 43 there was only one event, although the motion observed was manifest as a cloudy picture. This was possibly as a result of events upstream of this point, the intensity of which had decayed to a low level upon reaching the sensors. Frames 47 and 48 would appear to fall between the picture presented by Fig. 8.3a and the other frames in Fig. 8.3b. The concentration of the events was not particularly great, but two sweeps exibited a coherence with the upper sensor. The amplitudes of the events were large, being 119 and 158 $cm^2\ s^{-2}$ at the central sensor.

In order to examine whether a particular event was prevalent during periods of sediment motion, the events were summarised as given in Table 8.2. Events exhibiting coherence with the other sensors were also presented in Table 8.2. Of a total of 135 events, 55 were sweeps, 40 bursts, 32 up-accs and 8 d-decs, suggesting events with $u' \geq 0$ were dominant during periods of sediment motion. These $u' \geq 0$ events were biased to some extent by the data from frames 84 - 87, in which there were a high number of low amplitude events, in a relatively quiescent record. As mentioned in Section 8.2.2, events appear to occur in groups of one type. The biasing during frames 84 - 87 can be partially attributed to this and the nature of the record. Even accounting for this, the dominance of the $u' \geq 0$ events was still evident. Of the 18 coherent events, 11 were sweeps, 6 bursts, 1 up-accs and 0 d-decs. The apparent biasing from frames 84 - 87 was not as pronounced in this case, probably because the coherent events are generally of large amplitude in relation to the other events.

Table 8.3 summarises the 541 events contributing to 90% of the stress during trial 186. Of these, 228 where classed as bursts, 175 as sweeps, 102 as up-accs and 36 as d-decs, giving 264 events where $u' < 0$ and 277 where $u' \geq 0$. Similarly, of 105 coherent events, 55 were

bursts, 44 sweeps, 5 up-accs and 1 d-decs, giving 56 events where u' $\angle$ 0 and 49 events where u' $\rangle$ 0. Ratios of the number of u' $\rangle$ 0 to u' $\angle$ 0 events during periods of sediment motion and for the total number of events during trial 186 are 1.81 and 1.05 respectively. For coherent events the respective ratios are 2.0 and 0.88. This further reinforces the view that events in which u' $\rangle$ 0 are dominant during periods of sediment motion.

Soulsby, Davies and Wilkinson (1983) compared sediment concentrations, taken as positive or negative in comparison to a 12 minute mean, with events in the u'w' time series. It was observed from a 48 minute record close to peak velocities that concentrations of sediment were appreciably higher during sweeps and up-accs (u' $\rangle$ 0). Bursts were found to be independent of sediment concentrations, whilst d-decs indicated a slight tendency to occur at lower concentrations. Apparently comparable results were reported by Gillette and Porch (1978), in an examination of wind velocities and dust concentations above a dirt road. Sweeps provided the greatest contribution to transport by carrying dust-laden air. In this case it was stated the dust was settling, rather than being taken into suspension, as considered by the afore mentioned workers and the present study.

It would appear that despite the crudity of the comparisons in this study they are supported by the two studies mentioned. What does emerge is the difficulty in correlating sediment motion and events in the u'w' time series. This was perhaps not surprising, with measurements taken 100.0 cm above the bed.

8.3 SUMMARY AND CONCLUSIONS

In this chapter an attempt was made to correlate periods of

sediment motion, observed by the photographic unit, with events in the u'w' time series, recorded 100 cm above the bed. Within such periods the composition of the events in terms of bursts, sweeps, up-accs and d-decs was examined.

Of the 93 frames examined, enabling 92 comparisons with the u'w' time series, sediment motion was observed in 27 instances. This took the form of pebble displacements or a cloudiness of the entire frame of the film. Events used in the comparisons were those comprising 90% of the stress in a 12 minute interval. In several cases sediment motion was apparent during periods of relatively high intensity in the u'w' records. In other cases sediment motion apparently occurred during quiescent periods. This apparent lack of correlation may have been a result of recording u'w' too far from the bed.

A number of coherent events of larger amplitude were observed between the e.m. heads at 100.0 and 172.5 cm. A greater degree of coherence was evident between adjacent sensors. This apparently contradicts the results presented by McLean and Smith (1979), possibly because, in their case, cross-correlations were given between all readings recorded every 0.2 second for the averaging interval. The results from this study confirm those of Ferguson (1979). Coherent events varied from 9 to 14 per 12 minute record, apparently independent of the 12 minute averaged velocity.

Events during which $u' < 0$ and $u' > 0$ occurred in groups of 5 - 20, supporting the observations of Soulsby (1983). Such groupings may also have occurred in the laboratory work of Praturi and Brodkey (1978).

In addition, events during which $u' > 0$ were dominant during periods of sediment motion. This was also true for the coherent

events. Similar results were reported by Soulsby, Davies and Wilkinson (1983) and Gillette and Porch (1978).

No firm conclusion can be drawn as to whether events in the u'w' time series can be correlated with sediment motion. This may be largely due to the recording of u'w' too far from the bed and the relatively infrequent sampling interval of the photographic unit. Larger amplitude events exhibited coherence throughout the 72.5 cm above a height of 100 cm. Events occurred in groups of $u' < 0$ and $u' > 0$, the latter apparently dominant during sediment motion. The movement of pebbles during trials 186 would suggest that sand may well have been brought into suspension at other stations. However, the apparently linear nature of the log profiles discussed in Chapter 7 suggests that such suspensions would be intermittent.

Fig. 8.1 A 12 minute record of u'w' for trial 186. Data were recorded 100.0 cm above the bed. The 40 events comprising 90% of the stress ($-\overline{u'w'}$ = 7.50 cm^2 s^{-2}) are shaded. B = Burst; S = Sweep; U = up-acc; D = d-dec.

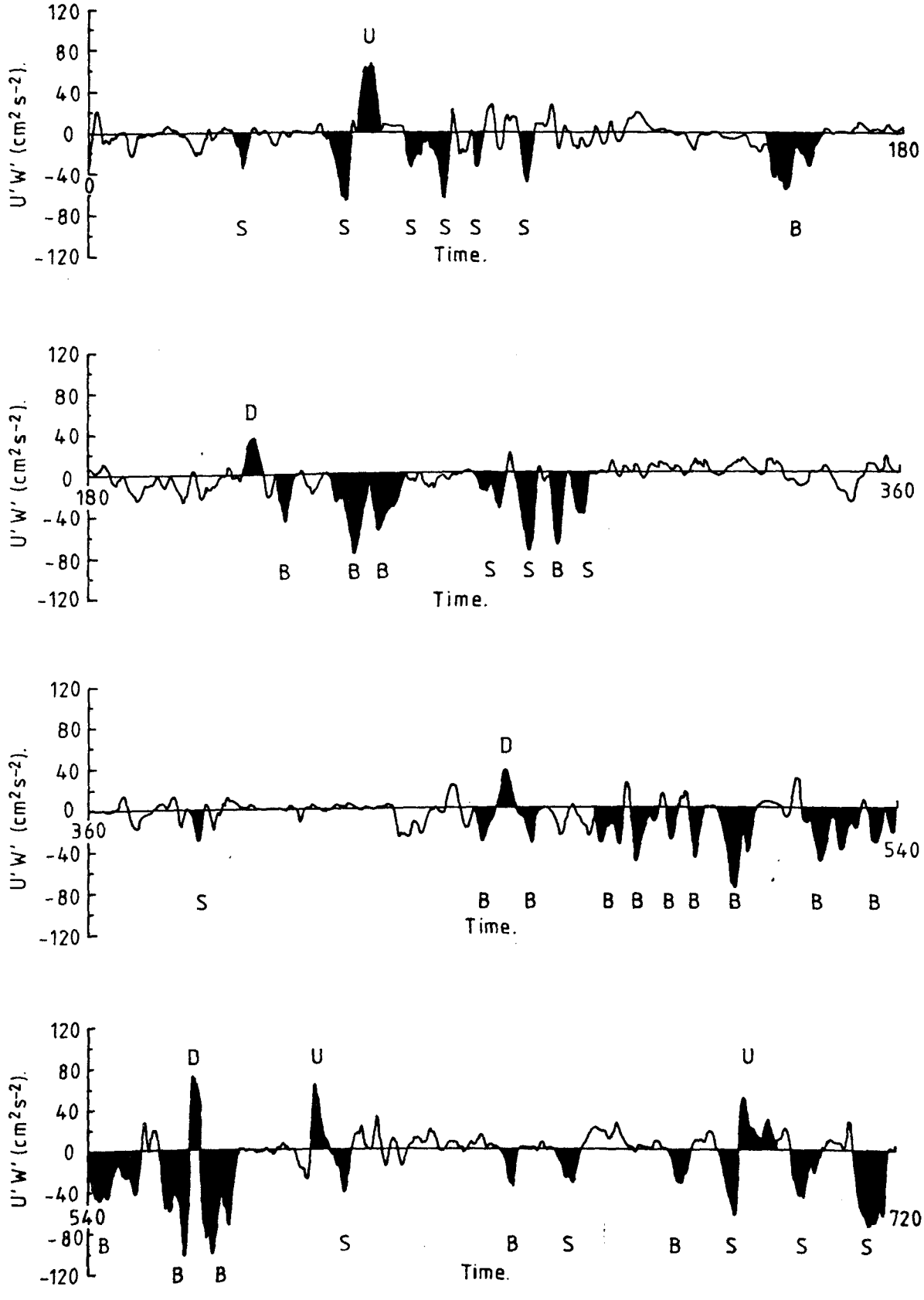
120
80
40
0
-40
-80
-120
U'W' (cm²s⁻²).
U
S S S S S S B
Time.
0
180
D
B B B S S B S
360
540
720

Fig. 8.2 Amplitude plots for events comprising 90% of the stress. Data recorded 100.0 cm above the bed corresponds to that given in Fig. 8.1. Events apparently coherent between all three sensors are marked ↑ on the time axis.
1 = up-acc; 2 = sweep; 3 = d-dec; 4 = burst.

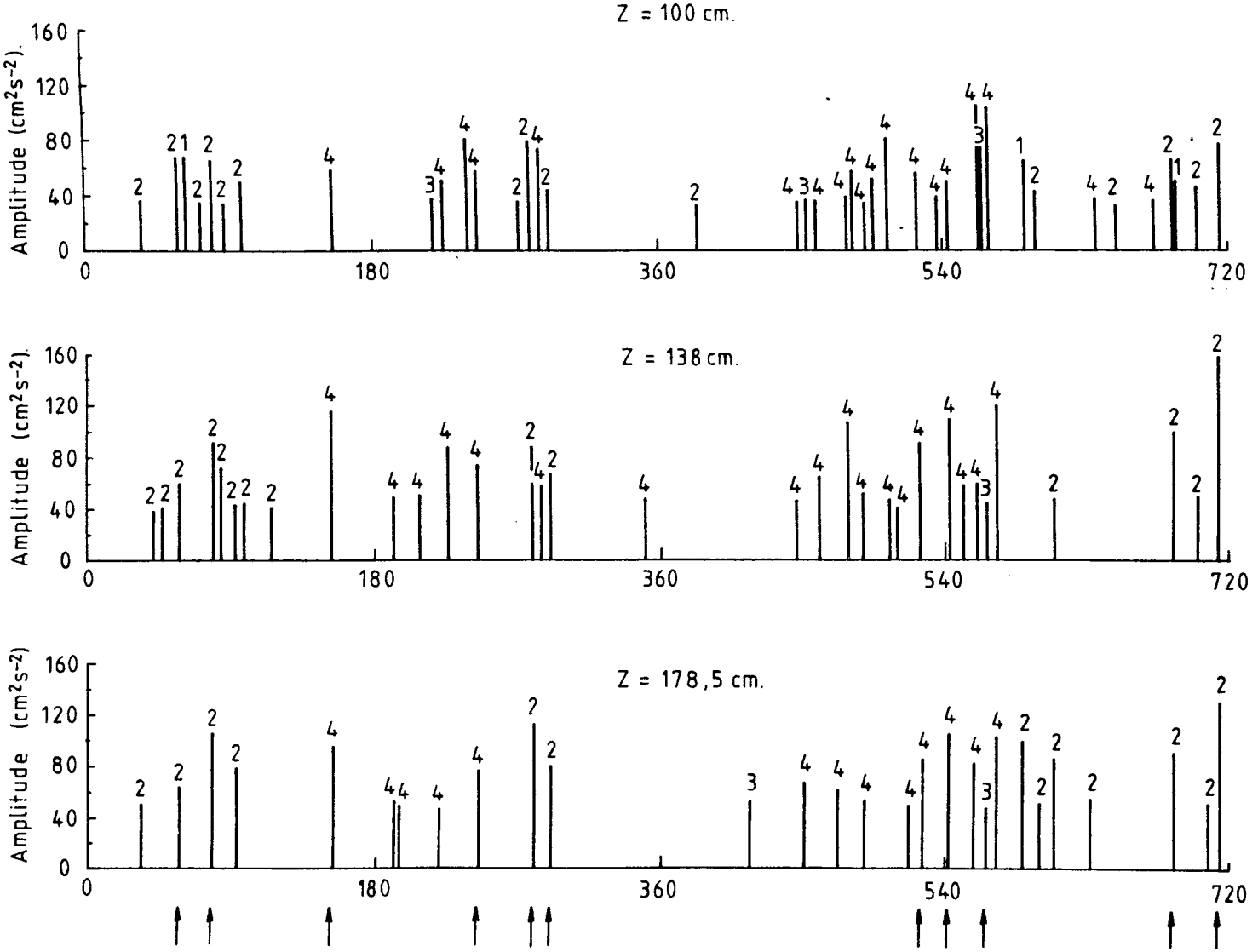
Z = 100 cm.
Z = 138 cm.
Z = 178,5 cm.
Amplitude (cm²s⁻²).
160
120
80
40
0
0
180
360
540
720
Time (s).

Fig. 8.3 a) (TOP) Amplitude plot for frames 1 - 12 during trial 186, 100.0 cm above the bed. Frames in which sediment motion was observed are denoted by | |, with arrows on the abscissa indicating coherence between events at all three sensors. Events numbered as in Fig. 8.2.

b) (BOTTOM) Amplitude plot for frames 37 - 48 during trial 186, 100.0 cm above the bed. The nomenclature is defined above.

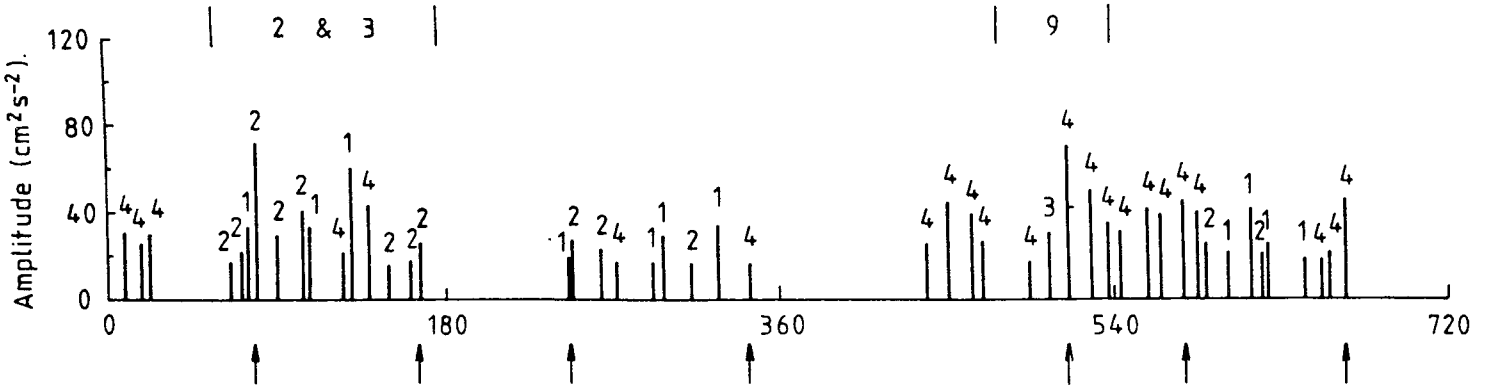
2 & 3
9
120
80
40
0
Amplitude (cm²s⁻²).
0
180
360
540
720
Time (s).

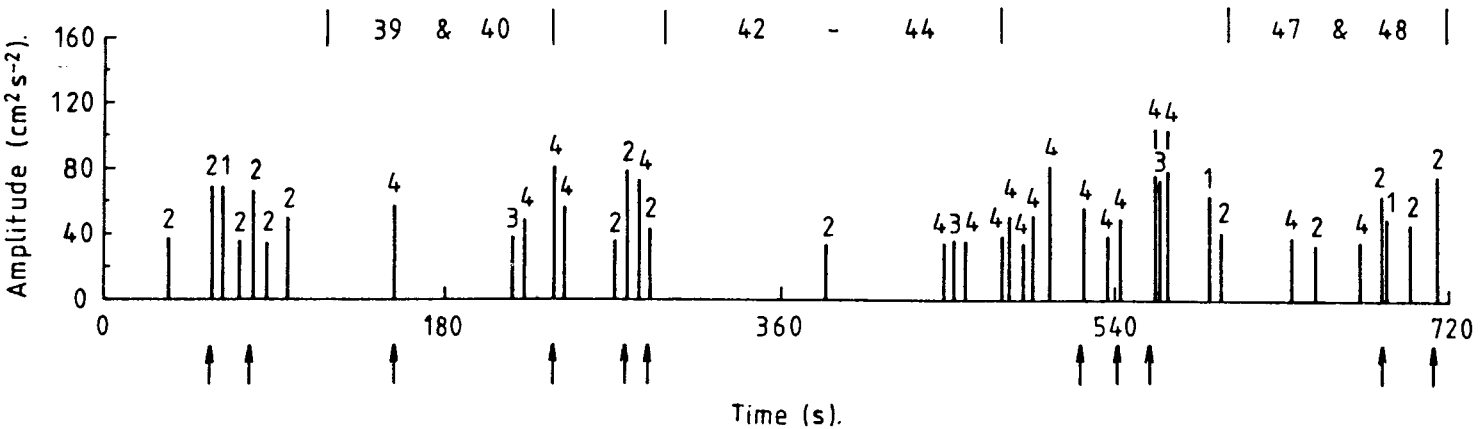
39 & 40
42 - 44
47 & 48
160
120
80
40
0
Amplitude (cm²s⁻²).
0
180
360
540
720
Time (s).

TABLE 8.1 SUMMARY OF PHOTOGRAPHIC UNIT DATA. ONLY FRAMES IN WHICH SEDIMENT WAS OBSERVED TO MOVE IN RELATION TO THE PREVIOUS FRAME ARE GIVEN

FRAME NUMBER (= MINUTE-1 FROM START OF TRIAL)	POSSIBLE NATURE OF PARTICLE	SECTOR OF MOTION	DIRECTION OF MOTION
2	PEBBLE (1)	2C	0°
3	" (1)	ABSENT	
9	?	3C	0°
17	CLOUDY	FRAME	——
20	PEBBLE (2)	1A	——
24	CRUSTACEAN	3B	0°
25	"	3B	40°
26	"	3B	90°
27	"	3C	135°
29	"	3C	90°
30	"	ABSENT	
35	PEBBLE (3)	2C	——
39	" (3)	2C	330°
40	" (3)	2C	340°
42	" (3)	2C	0°
43	CLOUDY	FRAME	——
44	"	FRAME	——
47	PEBBLE (3)	2C	0°
48	"	ABSENT	
49	CLOUDY	FRAME	——
50	CLOUDY	FRAME	——
53	PEBBLE (4) PEBBLE (5)	2B 3C	——
54	PEBBLE (4) PEBBLE (5)	ABSENT 2B	330°
55	PEBBLE (5)	2B	0°
69	PEBBLE (6)	3C	——
76	PEBBLE (7)	2D	——
77	"	2D	330°
78	"	2C	350°

FRAME NUMBER (= MINUTE-1 FROM START OF TRIAL)	POSSIBLE NATURE OF PARTICLE	SECTOR OF MOTION	DIRECTION OF MOTION
79	PEBBLE (7)	2D	0^{o}
84	PEBBLE (8)	2D	——
85	"	2D	310^{o}
86	"	2D	330^{o}
87	"	2D	340^{o}

When a particle first appears in the field of view no angle can be recorded, denoted as —— in right hand column. 'ABSENT' refers to the disappearance of the particle from the field of view. Pebbles are numbered in their order of observed motion.

TABLE 8.2 SUMMARY OF EVENTS OCCURRING DURING PERIODS OF SEDIMENT MOTION

FRAMES	EVENTS CONTRIBUTING TO 90% OF $-\overline{u'w'}$ IN THE FRAMES					COHERENT EVENTS IN THE FRAMES				
	TOTAL	B	S	U	D	TOTAL	B	S	U	D
2 & 3	13	2	8	3	–	2	–	2	–	–
9	5	4	–	–	1	1	1	–	–	–
17	5	3	2	–	–	–	–	–	–	–
20	5	2	2	–	1	–	–	–	–	–
35	7	–	5	2	–	1	–	1	–	–
39 & 40	4	3	–	–	1	1	1	–	–	–
42 – 44	5	3	1	–	1	–	–	–	–	–
47 – 50	20	2	9	9	–	3	–	3	–	–
53 – 55	8	5	3	–	–	–	–	–	–	–
69	3	2	1	–	–	–	–	–	–	–
76 – 79	20	9	7	2	2	3	2	1	–	–
84 – 87	40	5	17	16	2	7	2	4	1	–
TOTAL	135	40	55	32	8	18	6	11	1	–

B ≡ burst; S ≡ sweep; U ≡ up-accs; D ≡ d-dec.

TABLE 8.3 SUMMARY OF EVENTS OCCURING DURING TRIAL 186.

U_{100} ($cm\ s^{-1}$)	EVENTS CONTRIBUTING TO 90% OF $-\overline{u'w'}$					COHERENT EVENTS				
	TOTAL	B	S	U	D	TOTAL	B	S	U	D
46.1	48	23	13	11	1	9	5	3	1	–
47.9	61	32	13	8	8	9	6	3	–	–
47.5	58	30	20	7	1	13	10	3	–	–
44.5	40	19	15	3	3	11	4	6	–	–
48.7	51	17	22	11	1	11	4	7	–	–
42.1	64	20	23	20	1	13	5	6	2	–
40.8	55	31	13	6	5	14	9	5	–	–
40.0	91	26	33	22	10	11	4	6	1	–
37.5	73	30	23	14	6	14	8	5	1	–
TOTAL	541	228	175	102	36	105	55	44	5	1

B ≡ burst; S ≡ sweep; U ≡ up-accs; D ≡ d-decs.

CHAPTER 9 - SUMMARY AND CONCLUSIONS

9.1 INTRODUCTION

A purpose-built measuring and recording system, deployed over the majority of the tidal cycle at a number of stations in the Eastern Irish sea, was used to observe simultaneously the turbulent velocity fluctuations and velocity profile within 2 m of the bed. In the latter stages of the study, a photographic system was deployed to observe possible sediment motion and the nature of the bed. The design, construction and performance of the system, in particular that of the rotors and the photographic unit, have been detailed. The analysis of the data was primarily concerned with: the hydrodynamic nature of the boundary layer and factors influencing the measurements; a comparison of the Reynolds stress, determined by the eddy correlation technique, with u_*^2 from the log-law; possible variations in z_0 and u_*^2 with tidal phase; and a limited examination of the photographs, in conjunction with the structure of the Reynolds stress, to correlate possible sediment motion with events in the turbulence.

9.2 THE AREA AND METHODS OF MEASUREMENTS

A total of 98 trials were made at 21 stations during three cruises in the Eastern Irish Sea. The water depth varied from 7.5 - 50.0 m, and sediment types from thick mud, combinations of sand and shell fragments, to sand and pebbles. A comprehensive survey of the area indicated the sea bed to be featureless along a line west of Blackpool (see Fig. 2.2). In contrast, bed forms of the order of 2 m in height were observed to the north of Great Ormes Head. The water column, although often heavily stratified at the depth of the seasonal thermocline, was neutrally stratified within 2 m of the bed.

Upon anchoring at a chosen station, the support vessel was allowed to swing into a stable position after slack water. The sensors, attached to a rigid frame, were lowered to the bed and the data recorded on board ship. Unfortunately the desired remote deployment of the turbulence rig was not achieved because of problems with the data logger. The rig remained on the bottom for periods of between 30 minutes and 5 hours, dependent on the mean flow direction and variations in the ship's position. The orientation of the rig with respect to the flow was constantly monitored on board ship, by viewing the e.m. head signals on chart recorders. A total of 302 hours 11 minutes of data was recorded, of which approximately 1/3 was judged suitable for detailed analysis.

The turbulence rig carried four 5 cm diameter, two component e.m. heads to record the turbulent velocity fluctuations. At three heights, the horizontal (u) and vertical (w) components were recorded. For the most part, the remaining head was used to record the horizontal u and v components, enabling an estimate of the mean angle of flow with respect to the rig. Four Aanderaa type Savonious rotors were placed on the same support to record the mean velocity profile. In the latter stages of the programme a photographic unit was deployed to observe possible sediment motion and bedforms. The velocity sensors were spaced in the vertical by approximately 45 cm, with the lower sensors positioned at that height above the bed. Useful mean flow velocities, from which the data could be reliably analysed, varied from 20 cm s^{-1} to 60 cm s^{-1}, although velocities as low as 5 cm s^{-1} were recorded close to slack water.

Very few problems were encountered in the deployment of the rig. The major exception to this was the parting of the lifting bridle on one occasion because of a design fault. On several occasions the

rig was dragged along the bed when the wind was variable in strength or direction, but this caused few serious problems.

9.3 THE INSTRUMENTATION

The Aanderaa rotors proved adequate for recording the mean velocity profile within 2 m of the bed, with all the rotors obeying the same calibration curves within the ± 1% accuracy of the calibrations. Rotor performance appeared not to be impaired by wear or ageing of the components. The directional response of the rotors was good in comparison to that of the e.m. heads. Despite this, corrections to the data were necessary for angles of flow not equal to 0^{o}, to reduce systematic errors. Above a mean in situ flow of 30 cm s^{-1}, it was estimated that inertial 'pumping' of the rotors by turbulent flutuations superimposed on the mean flow was negligible. At 20 cm s^{-1}, the minimum mean velocity that was reliably recorded, this effect may have resulted in overreading by ~ 1 cm s^{-1}, becoming insignificant at 30 cm s^{-1}. The rotor threshold (~ 2.0 cm s^{-1}) was well below the previously stated in situ minimum velocity.

The e.m. heads and their associated electronics displayed a linear response over the calibration range of 0 - 150 cm s^{-1}. The resolution of each channel, dictated by the noise level of the electronics, was at least 5.0 mm s^{-1}. Directional response was far from ideal, but was adequate if corrected within an arc of the mean flow direction of -10^{o} to $+30^{o}$. Over a period equivalent to three times the longest in situ trials, the d.c. drift did not exceed 1.0 mm s^{-1}, enabling an e.m. head to be reliably used to estimate the mean flow direction.

The velocity sensors were controlled by electronics positioned on the rear leg of the turbulence rig. Linear electronics were used to

power the e.m. heads and sample the resulting signals. The analogue signals were then digitised and transferred serially, along with the rotor data, via the connecting cable to the research vessel. Data was then recorded on a 9 track Kennedy tape recorder.

The photographic unit, consisting of a commercially available super 8 cine camera and flash unit, failed to achieve the desired sampling rate. Instead of recording a frame a second for five minutes and repeating the sequence every hour, only one frame was taken per minute for the life time of the flash unit batteries, and this amounted to approximately 90 flashes. This arose because of the failure to develop a self contained turbulence rig, incorporating a larger power source to supply the means of illumination. A spherical perspex port, polished by the author, was successfully used to correct for distortion of the image that would have resulted from the refraction of the light by a plane port. Despite the unit's inadequacies, it proved capable of monitoring the nature of the bed and the sediment motion. Throughout its deployment the unit was self contained.

Although the development of the turbulence rig never achieved a state in which it could be deployed remotely, it performed almost without problems for three cruises each of approximately 2 weeks duration.

9.4 PRELIMINARY DATA MANIPULATION

Of the 98 trials, recorded at 21 stations during three cruises, 36 comprising data from 12 stations were analysed in detail. The criteria that determined this selection were firstly the presence of a uv recording head, which enabled angular corrections to be made, and secondly the availability of a lengthy continuous record.

D.C. offsets on the u channels of the e.m. heads were estimated from the peak in time series of 12 minute mean head - rotor velocities, existing at an angle of flow of 0^{o}. Offsets in the w channels were estimated by the shift required to bring the fluctuations about a zero mean at 0^{o}. Stability in the w channel offsets was ± 0.6 cm s^{-1} over a 2 week cruise, but the u channel exhibited a maximum drift of 3.4 cm s^{-1}, attributed to long term instability of the electronics.

A further check on the u offset was provided by equating the mean velocity at the rotor, situated at the same level on the uv sensor, to the square root of the sum of the squares of the u and v components plus their offsets. Minimising the sum of the errors of the resulting equation enabled u and v offset estimates. As a result the angle of flow with respect to the rig could be determined to within ± 4^{o}. Using previous flume calibrations, rotor velocities, those from the u channel and the Reynolds stress could be corrected.

Time series of velocities, u_{*} and Reynolds stress readily exposed poor quality data, resulting from poor rig orientation or redeployments of the rig during a trial.

Finally, parameters were averaged over 12 minutes to gain a balance between the desire for stationarity in the data and the inclusion of the entire energy spectra.

9.5 SUMMARY OF RESULTS AND CONCLUSIONS

To make a valid comparison of the stress as determined by the eddy correlation and log-law techniques, it is important that the prevailing conditions approximate as closely as possible to: non-accelerating and non-rotational flow over a hydrodynamically rough surface; neutral stratification; a constant Reynolds stress

in the layer in which measurements were made.

Since the Ekmann depth was of the order of 80 m and measurements were within 2 m of the bed the flow could be considered non-rotational.

Comparisons between the lower and upper uw recording e.m. heads at the 12 selected stations suggested the existence of a constant stress layer. At 7 of these stations there was a discrepency between the central uw recording e.m. head and the others of about 10 - 15 % in the stress values. This discrepancy was attributed to a misalignment of the central e.m. head by less than 2^{o} relative to the others. Bedforms were not thought to be the cause, since in all but one instance the stress at the central head was least in value. In the other case the bed was featureless.

An absence of an increase in dispersion of the values of C_D at lower Reynolds number, suggested by Sternberg (1968) to characterize the boundary from transitional to rough flows, indicated the flow to be hydrodynamically rough.

From C.T.D. measurements the water column was found to be neutrally stable within 5 m of the bed. A diagramatic prediction of the degree of gravitional stratification, presented by Soulsby (1983), combined with the linear nature of the log profiles, indicated there to be little suspended sediment. Sediment transport was most likely by bedload only.

The existence of tidally non-accelerated flow was the one condition which could not be satisfied. By applying a criterion suggested by Soulsby and Dyer (1981), flow was defined as accelerating during 75% of the recorded data. Corrections presented by the above workers were used to determine u_* and z_0. For this a value for the constant γ was estimated to be 0.066 ± 0.177, which is

comparable to that determined by Soulsby and Dyer (1981) of 0.04.

It was thought inadvisable to use values of $|d\bar{U}/dt|$ as a measure of accelerating flow, except for rough estimates. The Soulsby and Dyer (1981) criterion was preferable since it gave a measure of the departure of the velocity gradient from a steady value.

Several factors combined to provide a large uncertainty in the ratio $u_*^2/-\overline{u'w'}$. The most pronounced were the inherent variability of the stress, which was of the order of ± 30 - 50%, and a possible tilt of the turbulence rig by up to ± 2.5°. The latter could introduce a systemmatic error in $-\overline{u'w'}$ of the order of ± 30%, conceivably varying the ratio between 1.58 and 0.73, whereas the two methods could in fact be recording the same value of stress. Pumping of the rotors was negligible when determining u_*^2 for mean flows above 30 cm s^{-1}. Below this, data was neglected when determining the ratios.

A least squares technique was applied to the log profiles enabling a statistical significance to be placed on u_* and z_0. As data sets were relatively small in a number of trials, the technique was applied with the constraint that the line passed through the origin when comparing stress by the two methods.

Ratios were considered for values of u_*^2 uncorrected and corrected for accelerating effects. Stress measured using the e.m. heads was corrected for losses resulting from cut off in the cospectral content. Approximately a quarter of the trials indicated the techniques were comparable within the 95% confidence limits, with little overall difference between comparisons when corrected or uncorrected for acceleration. Ratios for the majority of trials fell within the extremes due to sensor misalignment previously quoted.

Evidently there was no variation in ratio with tidal phase and κ_0 was independent of bedform and sediment type. Ratios for the entire data set gave values of 1.287 ± 0.043 (uncorrected u_*^2) and 1.268 ± 0.048 (corrected u_*^2), equivalent to κ_0 of 0.353 and 0.355 respectively. Such a large discrepancy between these values and the assumed (0.4) is unlikely to be entirely attributable to inadequate correction for cospectral loss in the e.m. heads. These values were comparable to that of 0.379 obtained using the method of Soulsby and Dyer (1981) while neglecting accelerating flow. The results therefore suggest a value of κ_0 which is increasingly used in atmospheric work (0.35), rather than the commonly accepted laboratory and marine value (0.40 - 0.42).

It is difficult to find support for the above results from previous work in marine turbulence, since, to the author's knowledge, there have been no similar experiments. The work of McPhee and Smith (1976), discussed in Section 6.2, suggested values of $-\overline{u'w'}$ derived from the momentum equation to be comparable with those of u_*^2, derived using $\kappa_0 \doteq 0.35$ in the log - law. This has to be regarded with some suspicion, since there was some uncertainty to as whether a constant stress layer existed when u_*^2 was determined. Despite this, the extensive data set considered in the present work, indicating a discrepency between the two methods, strongly suggests the need for further investigation. Perhaps, as suggested in Section 9.6, the comparison of the two methods in the idealised conditions of a flume would resolve some uncertainties.

Only in one instance did the ratio appear to exhibit a dependence on z_0, this during trials 125 and 127, where high ratios corresponded with high values of z_0. Possibly the dependence was relatively weak and bed roughness variations between stations were

insufficient to highlight differences. Variations would suggest a mechanism effecting the velocity profile, but which cannot be explained by suspended sediment or shielding of the bottom rotor by bedforms.

A tidal hysteresis in stress was only apparent at one station where $z/\delta > 0.1$. This supported the work of Bowden and Ferguson (1980), who suggested that tidal hysteresis would become evident when the range $z/\delta = 0.1 - 0.2$ was exceeded and adverse pressure gradients enhanced Reynolds stress.

An apparent z_0 minima at peak velocities at a number of stations, a situation previously reported by a number of workers, could be attributed for the most part to a failure to account for accelerating effects when considering the log-law. Only during trials 125 and 127 was there evidence of a variation in z_0 with tidal phase after removing accelerating effects. An initial z_0 maxima, rapidly falling to a constant value, was thought attributable to streamlining of sand ripples as the tidal cycle progressed. Such a streamlining had been previously reported by Dyer (1980). Corrected and uncorrected values of z_0 and C_{100} agreed well with the wide range of values reported by other workers for a variety of bedforms and sediment types. C_{100} was evidently related to sediment size and bed roughness. Lower values ($\sim 2.2 \times 10^{-3}$) for finer unrippled sediments and higher values (up to $\sim 8.0 \times 10^{-3}$) for coarser sediments and heavily rippled beds. The values of C_{100} were derived assuming a κ_0 of 0.4. Doubt about the appropriate value may reduce the above range to $(1.65 - 6.0) \times 10^{-3}$.

Despite the sparsity of the data from the photographic unit a number of positive results emerged. A comparison of events comprising 90% of the Reynolds stress with periods of sediment motion

failed to correlate periods of high or low stress with sediment motion. Events for which u' > 0 were dominant during periods of sediment motion.

Larger amplitude events were generally those that exhibited coherence between 100.0 and 172.5 cm above the bed, suggesting the possibility of correlating events observed at 100 cm with sediment motion. Such events varied between 9 and 14 per 12 minutes, apparently independent of velocity. Events for which u'< 0 and u' > 0 occurred in groups of 5 - 20, supporting previous observations by Soulsby, Davies and Wilkinson (1983) and Praturi and Brodkey (1978).

9.6 SUGGESTED IMPROVEMENTS AND POSSIBLE FURTHER WORK

Obviously the inherent variability of the Reynolds stress cannot be removed, but some of the more serious systematic errors could be reduced by instrumental improvements. The inclusion of an inclinometer, developed, but not deployed due to the failure to develop the remote recording system, would reduce considerably the uncertainties in the misalignment of the e.m. heads. Orientation of the sensors into the flow at all times would have considerably improved deployment durations. This could have been achieved to some degree by the inclusion of some form of vane and a joint permitting the central sensor support to swivel. Use of annular e.m. heads (Griffiths et al, 1978), the response being less sensitive to misalignment, would improve confidence in values of stress by eddy correlation. An interesting addition may have been to include propeller type rotors (e.g. Braystoke), less prone to 'pumping', to ascertain whether pumping was indeed negligible at λ 30 cm s^{-1}.

Perhaps a comparison of the two techniques in the idealised conditions of a flume, but with varying roughness length and flow

conditions, might help to resolve the apparent uncertainty in κ_0.

The attempt to correlate sediment motion with events in the u'w' spectrum was obviously inadequate. Deployment of a T.V. camera, e.m. head close to the bed and the investigation of a wide range of bed types, especially finer sediment, would give a considerable improvement.

APPENDIX 1 DATA SUMMARY

TABLE A1.1 STATION DATA

STATION	POSITION		DEPTH	BOTTOM SEDIMENT
	LATITUDE (N)	LONGITUDE (W)	(M)	CHARACTERISTICS
1	53° 22.8'	4° 7.9'	22.5-28.5	FCS
2	53° 21.2'	4° 8.8'	9.5-16.0	FCS
3	53° 22.8'	3° 47.2'	7.5-14.0	FCS
4	53° 24.2'	3° 46.8'	20.5-27.0	MCS
5	53° 23.8'	3° 37.5'	28.0-34.0	MSS
6	53° 46.5'	3° 17.0'	15.5-21.0	SM
7	53° 23.1'	3° 52.7'	15.5-21.0	FCS
8	53° 22.1'	3° 52.5'	17.5-22.5	MSSP
9	53° 27.4'	3° 52.0'	33.0-38.5	FCS
10	53° 25.0'	3° 52.6'	22.5-29.0	FCS
11	53° 46.1'	3° 8.0'	7.5-16.0	SM
12	53° 46.1'	3° 17.7'	15.5-22.5	SM
13	53° 46.0'	3° 29.9'	24.0-30.5	TMS
14	53° 45.9'	3° 42.2'	36.5-42.5	MSS
15	53° 46.0'	4° 4.3'	43.0-46.5	MSSP
16	53° 45.8'	3° 52.8'	38.5-42.5	MSSP
17	53° 45.8'	3° 41.9'	38.0-43.0	MSS
18	53° 22.0'	3° 52.5'	17.0-23.0	MSSP
19	53° 33.2'	3° 53.2'	43.5-50.0	SG
20	53° 39.5'	3° 53.0'	40.0-46.5	SG
21	53° 26.8'	3° 26.8'	32.5-39.0	FCS

FCS ≡ Fine Clean Sand
MCS ≡ Medium Clean Sand
MSS ≡ Medium Sand and Shells
SM ≡ Sand and Mud
MSSP ≡ Medium Sand, Shells and Pebbles
TMS ≡ Thick Muddy Sand
SG ≡ Sand and Gravel

TABLE A1.2 TURBULENCE RIG DEPLOYMENTS

TRIAL	DATE	DEPLOYMENT TIME (G.M.T.)	STATION (1)	USEFUL RECORD LENGTH (HRS. MINS.) (2)	TIDAL STATE
		JOHN MURRAY CRUISE 4/81			
90	15-16/4/81	22.42-02.37	1	—	EBB
91	16/4/81	10.43-15.35	1	—	FLOOD
		TRIALS 92 TO 94 WERE ACCIDENTLY OVER WRITTEN			
95	18/4/81	18.22-20.57	2	—	EBB
97	19/4/81	06.38-07.57	2	—	FLOOD
98	"	19.10-21.03	3	—	FLOOD
99	20/4/81	01.14-04.36	4	—	EBB
100	"	07.47-10.38	4	—	FLOOD
101	"	12.11-17.05	4	—	EBB
102	"	19.15-22.53	4	—	FLOOD
103	21/4/81	01.53-04.58	3	—	EBB
104	"	07.29-10.57	3	—	FLOOD
105	"	13.56-16.40	3	—	EBB
106	"	19.31-23.20	3	—	FLOOD
107	22/4/81	02.05-05.22	3	—	EBB
108	"	07.46-12.00	5	—	FLOOD
109	"	14.04-18.20	5	—	EBB
110	"	20.36-23.32	5	—	FLOOD
111	23/4/81	02.36-05.43	5	—	EBB
112	"	16.56-19.27	6	—	EBB
113	"	21.37-23.47	6	—	FLOOD

NOTES (1) AND (2) ARE EXPLAINED AT THE END OF THIS TABLE

TRIAL	DATE	DEPLOYMENT TIME (G.M.T.)	STATION (1)	USEFUL RECORD LENGTH (HRS. MINS.) (2)	TIDAL STATE
		JOHN MURRAY CRUISE 9/81			
120	25/7/81	21.52–22.55	7	—	EBB
121	26/7/81	00.32–04.32	7	—	FLOOD
122	〃	08.04–08.42	7	—	EBB
123	〃	13.11–17.38	7	1.36 (2)	FLOOD
124	〃	20.04–23.41	7	1.24 (2)	EBB
125	27/7/81	02.10–06.18	8	3.36 (2)	FLOOD
126	〃	08.12–12.00	8	3.36 (2)	EBB
127	〃	14.33–19.05	8	3.48 (2)	FLOOD
128	27–28/7/81	22.22–01.13	9	NONE (2)	EBB
129	28/7/81	04.04–07.27	9	3.12 (2)	FLOOD
130	〃	10.06–14.54	9	NONE (2)	EBB
131	〃	16.35–19.37	9	1.36 (2)	FLOOD
132	28–29/7/81	22.47–02.50	10	4.00 (2)	EBB
133	29/7/81	04.45–08.49	10	NONE (2)	FLOOD
134	〃	10.18–15.22	10	4.24 (2)	EBB
135	〃	16.50–21.13	10	NONE (2)	FLOOD
136	29–30/7/81	22.58–03.45	10	NONE (2)	EBB
137	31/7/81	00.50–03.47	11	2.48 (2)	EBB
138	〃	08.00–11.47	11	3.47 (2)	FLOOD
139	〃	12.44–14.11	11	NONE (2,3)	EBB
140	〃	19.54–21.42	11	1.24 (2)	FLOOD
141	1/8/81	10.13–12.30	12	1.48 (2)	FLOOD
142	〃	13.36–18.13	12	4.00 (2,3)	EBB
143	1–2/8/81	20.20–00.12	12	2.36 (2)	FLOOD
144	2/8/81	01.40–06.50	12	4.36 (2)	EBB
145	〃	08.18–12.37	12	2.48 (2)	FLOOD
146	〃	13.49–18.25	12	2.00 (2)	EBB
147	2–3/8/81	21.43–00.36	13	2.00 (2)	FLOOD
148	3/8/81	02.48–07.17	13	3.24 (2)	EBB

TRIAL	DATE	DEPLOYMENT TIME (G.M.T.)	STATION (1)	USEFUL RECORD LENGTH (HRS. MINS.) (2)	TIDAL STATE
149	3/8/81	08.48–12.12	13	2.00 (2)	FLOOD
150	4/8/81	07.26–07.51	13	NONE (2)	EBB
151	〃	09.38–12.49	13	NONE (2)	FLOOD
152	〃	16.18–19.32	13	1.36 (2)	EBB
153	4–5/8/81	22.01–01.22	14	2.12 (2)	FLOOD
154	5/8/81	04.06–07.04	14	1.48 (2)	EBB
155	〃	10.14–14.12	14	2.12 (2)	FLOOD
156	〃	15.48–18.28	14	0.48 (2)	EBB
157	5–6/8/81	22.39–01.33	14	1.36 (2)	FLOOD
		SHACKLETON CRUISE 7/82			
160	29/7/82	14.39–17.00	15	—	FLOOD
161	〃	20.20–23.55	15	—	EBB
162	30/7/82	02.42–05.51	15	—	FLOOD
163	〃	12.27–12.57	15	—	EBB
164	〃	15.14–17.58	15	—	FLOOD
165	30–31/7/82	20.48–01.39	15	—	EBB
166	31/7/82	04.54–16.52	15	—	FLOOD
167	31/7/82	11.32–13.40	16	NONE (3)	EBB
168	〃	17.12–19.44	16	NONE (3)	FLOOD
169	31/7–1/8/82	22.20–02.08	16	2.48 (3)	EBB
170	1/8/82	05.18–08.38	16	2.36 (3)	FLOOD
171	〃	11.15–15.18	16	2.24 (3)	EBB
172	〃	18.38–20.00	17	1.12 (3)	FLOOD
173	1–2/8/82	23.30–03.36	17	3.24 (3)	EBB
174	2/8/82	05.17–09.29	17	4.00 (3)	FLOOD
175	〃	11.35–15.08	17	3.00 (3)	EBB
176	〃	18.34–21.24	17	2.36 (3)	FLOOD
177	3/8/82	00.10–03.59	17	3.36 (3)	EBB
178	〃	18.35–21.51	18	3.16 (1)	FLOOD

TRIAL	DATE	DEPLOYMENT TIME (G.M.T.)	STATION (1)	USEFUL RECORD LENGTH (HRS. MINS.) (2)	TIDAL STATE
179	3-4/8/82	23.21-03.36	18	4.12 (1)	EBB
180	4/8/82	06.19-10.10	18	3.48 (1)	FLOOD
181	"	15.47-17.31	19	NONE (1)	EBB
182	"	18.57-22.51	19	1.48 (1,3,4)	FLOOD
183	5/8/82	01.17-05.08	19	NONE (1,3,4)	EBB
184	"	08.08-10.54	19	NONE (1)	FLOOD
185	"	13.00-17.11	19	4.00 (1)	EBB
186	"	20.00-22.31	20	1.48 (1,C)	FLOOD
187	6/8/82	08.56-10.48	20	1.48 (1,C)	FLOOD
188	"	14.10-16.11	20	NONE (1,C)	EBB
189	7/8/82	02.04-05.36	20	3.24 (1)	EBB
190	"	08.44-11.31	20	2.14 (1)	FLOOD
191	"	15.02-18.30	20	3.24 (1)	EBB
192	7-8/8/82	21.25-00.45	20	NONE (1,C)	FLOOD
193	8/8/82	03.13-06.16	20	2.36 (1,C)	EBB
194	"	09.35-11.49	20	1.36 (1,4)	FLOOD
195	"	21.05-23.00	21	1.48 (1,4)	FLOOD

The height in cm of the sensor pairs above the sea bed, numbered from 1 to 4 upwards, is given for each cruise below.

	1	2	3	4
J.M. 4/81	52.0	93.0	133.0	175.0
J.M. 9/81	56.0	96.5	138.0	178.5
SH. 7/82	47.5	100.0	138.0	172.5

NOTES: (1) The station number refers to the stations given in table A1.1 and shown in Fig. 2.2.

(2) Numbers not underlined,but bracketed refer to the number

of the sensor measuring the uv component of flow as indicated on the previous page. Underlined numbers refer to inoperative rotors, whilst a bracketed C denotes that the camera was deployed. Only trials with uv measuring sensors were analysed fully, as explained in chapter 4. The column headed USEFUL RECORD LENGTH, in the above tables, has been left blank when a uv sensor was not deployed.

APPENDIX 2

LINEAR REGRESSION ANALYSIS

In the study of turbulent flow the estimates of the uncertainties in the turbulence parameters (e.g. z_0 and u_*), when using the log-law, have often been based on the estimates of uncertainty in the calibrations of the profiling meters (see Sternberg, 1968 and Channon and Hamilton, 1971). Alternatively, Heathershaw and Simpson (1978) have suggested that uncertainties in z_0 and τ_0 can be estimated by considering the variability of the stress. Both methods can be considered valid, in particular the latter, which appears to account for the Reynolds stress variability present in benthic boundary layer flows.

The disadvantage in the above is that the variability of the data is not quantified in terms of statistical significance. The approach adopted in this work enables a degree of confidence to be placed on the parameters. The method is by no means new, using a least squares technique to minimise the sum of the squares of the deviations in the ordinate terms. A fuller explanation can be found in Zar (1974).

Consider the general form of a straight line:

$$y = mx + c \quad , \qquad \text{A2.1}$$

It can be shown that the confidence limits on the gradient (m) and intercept (c) can be given by:

$$\partial m = \frac{t}{(n-2)^{1/2}} \frac{\sigma_y}{\sigma_x} (1-r^2)^{1/2} \quad , \qquad \text{A2.2}$$

$$\partial c = \frac{t}{(n-2)^{1/2}} \frac{\sigma_y}{\sigma_x} X (1-r^2)^{1/2} \quad , \qquad \text{A2.3}$$

where t = Student's t parameter.

n = number of data points.

σ_x = standard deviation of the x values.

σ_y = " " " " y " .

r = correlation coefficient between x and y.

X = root mean square of the x data values.

The confidence limits derived from this method depend on the value of t, available from the majority of text books containing statistical tables. A parameter given with a confidence limit of 95% indicates that the parameter is 95% certain to exist between the limits given.

When applied to this work, for the logarithmic profiles n = 4 (the number of rotors used). Equation 1.11 of chapter 1 can be rearanged as:

$$\bar{U} = \frac{u_*}{\kappa_0} \ln z - \frac{u_*}{\kappa_0} \ln z_0 \quad , \qquad \text{A2.4}$$

where $d \ll z$.

Comparing equation A2.4 with equation A2.1

$$\frac{u_*}{\kappa_0} \equiv m \text{ (gradient)} \quad \text{and} \quad \frac{u_*}{\kappa_0} \ln z_0 \equiv c \text{ (intercept)}$$

given that the error in the product of x and y is:

$$\partial(xy) = (xy) \left[\left[\frac{\partial x}{x} \right]^2 + \left[\frac{\partial y}{y} \right]^2 \right]^{1/2}$$

then $$\partial u_* = \frac{\partial m}{m} \kappa_0 m = \kappa_0 \partial m \quad , \qquad \text{A2.5}$$

also $$\ln z_0 = -c/m$$

$$\partial \ln z_0 = c/m \left[\left[\frac{\partial c}{c} \right]^2 + \left[\frac{\partial m}{m} \right]^2 \right]^{1/2}$$

and from A2.2 and A2.3 $$\partial c = \partial m X$$

also $$\partial \ln z_0 = \frac{1}{z} \partial z_0$$

then $$\partial z_0 = z_0 \frac{\partial m}{m} \left[X^2 + (\ln z_0)^2 \right]^{1/2} \quad , \qquad \text{A2.6}$$

Since adopting this technique, it has come to the author's notice that Wilkinson (1984) has also used it during work at I.O.S. Taunton.

APPENDIX 3

LIST OF SYMBOLS USED IN CHAPTERS 6 - 8

A_q, B_q	Fourier coefficients.
C_D, C_{100}	drag coefficient: C_{100} applies to U_{100}.
d	displacement height: elevation at which mean drag may appear to act on flow above roughness elements.
M_2	semi-diurnal tidal coefficient.
N	number of data points (Fourier analysis).
q	coefficient number (Fourier analysis).
u', v', w'	turbulent velocity fluctuations in x, y, z respectively
U_{100}	mean velocity at z = 100.0 cm.
$-\overline{u'w'}$	Mean u'w' product over averaging interval.
u_*	friction velocity.
$\dot{u}_*$	rate of change of friction velocity [= du_*/dt].
$\tilde{u}_*$	apparent value of friction velocity after correction for acceleration.
x, y, z	coordinate axis.
x(t)	series in time (t) (Fourier analysis).
$\bar{x}$	mean of x(t) (Fourier analysis).
z_0	roughness length.
$\tilde{z}_0$	apparent value of z_0 after correction for acceleration
γ	dimensionless constant.
δ	boundary layer thickness.
Λ	length scale associated with acceleration [= $u_*\|u_*\|/\dot{u}_*$].
κ_0	von Karmann's constant.
ρ	density of sea water.
$-\rho\overline{u'w'}$	u'w' component of Reynolds stress over averaging interval.
τ_0	bed shear stress.

REFERENCES

Aanderaa, 1981. Operating manual for the R.C.M. 4/5 current meter. Technical description No. 119. Supplied by Aanderaa Instruments.

Adams, C.E. and Weatherly, G.L., 1981. Some effects of suspended sediment stratification on an oceanic bottom boundary layer. J. Geophys. Res., 86, 4161 - 4172.

Anwar, H.O., 1981. A study of turbulence structure in a tidal flow. Est. Coast. Shelf Sc., 13, 373 - 387.

Beer, T., 1983. Enviromental oceanography : An introduction to the behaviour of coastal waters. Pergamon Press, 262pp.

Bendat, J.S. and Piersol, A.G., 1971. Random data: analysis and measurement procedures. Wiley - Interscience, New York, 407pp.

Bowden, K.F., 1955. Some observations of turbulence near the sea bed in a tidal current. Quat. J. Roy. Met. Soc., 81, 640 - 642.

Bowden, K.F., 1962. Turbulence. In Hill, M.N. (ed.), The Sea, Vol. 1, Wiley - Interscience, New York, 802 - 825.

Bowden, K.F., 1962a. Measurements of turbulence near the sea bed in a tidal current. J. Geophys. Res., 67, 3181 - 3186.

Bowden, K.F., 1978. Physical problems of the benthic boundary layer. Geophysical Surveys, 3, 255 - 296.

Bowden, K.F., 1983. Physical oceanography of coastal waters. Ellis Horwood Ltd., 302pp.

Bowden, K.F. and Fairbairn, L.A., 1956. Measurements of turbulent fluctuations and Reynolds stresses in a tidal current. Proc. Roy. Soc., London, A 237, 422 - 438.

Bowden, K.F., Fairbairn, L.A. and Hughes, P., 1959. The distribution of shearing stresses in a tidal current. Geophys. J. R. Astron. Soc., 2, 288 - 305.

Bowden, K.F. and Ferguson, S.R., 1980. Variations with height of the turbulence in a tidally - induced bottom boundary layer. In Marine Turbulence. Edited by J.C.J. Nihoul. Elsevier Scientific Publishing Company, Amsterdam. 259 - 286.

Boxall, S. R., 1985. Thermohaline fine structure of the Tyrrhenian Sea Unpublished Ph. D. thesis, University of Liverpool (In prep.).

Bradshaw, P., 1975. An Introduction to Turbulence and its Measurement. Pergamon Press, Oxford, 218pp.

Bradshaw, P., 1978. Introduction. In Bradshaw, P. (ed), Turbulence, Springer - Verlag, Berlin, 1 - 44.

Businger, J.A., Wyngaard, J.C., Izumi, Y. and Bradley, E.F., 1971. Flux-profile relationships in the atmospheric surface layer. J. Atmos. Sci., 28, 181 - 189.

Caldwell, D.R. and Chriss, T.M., 1979. The viscous sublayer at the sea floor. Science, 205, 1131 - 1132.

Cannon, G.A., 1971. Statistical characteristics of velocity fluctuations at intermediate scales in a coastal plain estuary. J. Geophys. Res., 76, 5852 - 5858.

Carter, D.J.T., 1982. Prediction of wave height and period for a constant wind velocity using the JONSWAP results. Ocean Engin., 9, 17 - 33.

Channon, R.D. and Hamilton, D., 1971. Sea bottom velocity profiles on the continental shelf south-west of England. Nature, Lond., 231, 383 - 385.

Charnock, H., 1959. Tidal friction from currents near the sea bed. Geophys. J. R. Astron. Soc., 2, 215 - 221.

Corino, E.R. and Brodkey, R.S., 1969. A visual investigation of the wall region in turbulent flow. J. Fluid Mech., 37, 1 - 30.

Dronkers, J.J., 1964. Tidal Computations in Rivers and Coastal Waters. North - Holland Publishing Company - Amsterdam, 518pp.

Dyer, K.R., 1971. Current velocity profiles in a tidal channel. Geophys. J. Roy. Astron. Soc., 22, 153 - 161.

Dyer, K.R., 1980. Velocity profiles over a rippled bed and the threshold of movement of sand. Estaur. Coast. Mar. Sci., 10, 181 - 199.

Ferguson, S.R., 1979. Measurement and analysis of bottom turbulence in the Eastern Irish Sea. Unpublished Ph. D. thesis, University of Liverpool.

Fernholz, H.-H., 1978. External Flows. In Bradshaw, P. (ed.), Turbulence, Springer - Verlag, Berlin, 45 - 107.

Gaul, R.D., 1963. Influence of vertical motion on the Savonius rotor current meter. A. & M. College of Texas, Dept. Oceanogr. Meterol., Project 329, Ref. 63 - 4T, 29pp.

Gillette, D.A. and Porch, W.M., 1978. The role of fluctuations of vertical and horizontal wind and particle concentration in the deposition of dust suspended by wind. J. Geophys. Res., 83, 409 - 414.

Glover, T., Harwood, G.E. and Lythgoe, J.N., 1977. A Manual of Underwater Photography. Academic Press, 219pp.

Gordon, C.M., 1974. Intermittent momentum transport in a geophysical boundary layer. Nature, Lond., 248, 392 - 394.

Gordon, C.M., 1975. Period between bursts at high Reynolds number. Physics Fluids, 18, 141 - 143.

Gordon, C.M., 1975a. Sediment entrainment and suspension in a turbulent tidal flow. Marine Geol., 18, M57 - M64.

Gordon, C.M. and Dohne, C.F., 1973. Some observations of turbulent flow in a tidal estuary. J. Geophys. Res., 78, 1971 - 1978.

Gordon, C.M. and Witting, J., 1977. Turbulent structure in a benthic boundary layer. In Nihoul, J.C.J. (ed.), Bottom Turbulence, Elsevier, Amsterdam, 59 - 81.

Grant, H.L., Stewart, R.W. and Moilliet, A., 1962. Turbulence spectra from a tidal channel. J. Fluid Mech., 12, 241 - 268.

Griffiths, G., Collar, P.G. and Braithwaite, A.C., 1978. Some characteristics of electromagnetic current sensors in laminar flow conditions. I.O.S. internal report No. 56 (Unpublished Manuscript).

Hamilton, D., Sommerville, J.H. and Stanford, P.N., 1980. Bottom currents and shelf sediments, southwest of Britain. Sediment. Geol., 26, 115 - 138.

Hammond, T.M. and Collins, M.B., 1979. Flume studies of the response of various current meter rotor/propellers to combinations of unidirectional and oscillatory flow. Dt. Hydrogr. Z., 32, 39 - 58.

Harvey, J.G. and Vincent, C.E., 1977. Observations of shear in near-bed currents in the southern North Sea. Est. Coast. Mar. Science, 5, 715 - 731.

Heathershaw, A.D., 1974. "Bursting" phenomena in the sea. Nature, Lond., (A) 248, 394 - 395.

Heathershaw, A.D., 1976. Measurements of turbulence in the Irish Sea benthic boundary layer. In McCave, I.N. (ed.), The Benthic Boundary Layer, Plenum Press, New York, 11 - 31.

Heathershaw, A.D., 1979. The turbulent structure of the bottom boundary layer in a tidal current. Geophys. J. Roy. Astr. Soc., 58, 395 - 430.

Heathershaw, A.D. and Simpson, J.H., 1978. The sampling variability of Reynolds stress and its relation to boundary shear stress and drag coefficient measurements. Estuar. Coast. Mar. Sci., 6, 263 - 274.

Jackson, P.S., 1981. On the displacement height in the logarithmic velocity profile. J. Fluid Mech., 111, 15 - 25.

Jenkins, A.J. and White, H.E., 1976. Fundementals of Optics. McGraw - Hill. 746pp.

Lesser, R.M., 1951. Some observations of the velocity profile near the sea floor. Trans. Amer. Geophys. Un., 32, 207 - 211.

Ludwick, J.C., 1975. Variations in the boundary-drag coefficient in the tidal entrance to Chesapeake Bay, Virginia. Marine Geol., 19, 19 - 28.

McCave, I.N., 1973. Some boundary-layer characteristics of tidal currents bearing sand in suspension. Mem. Soc. Roy. Sci. Liege, 6 ser., 6, 187 - 206.

McLean, S.R., 1983. Turbulence and sediment transport measurements in a North Sea tidal inlet (The Jade). In Sundermann/Lenz (ed.), North Sea Dynamics, Springer - Verlag, Berlin Heidelberg, 436 - 452.

McLean, S.R. and Smith, J.D., 1979. Turbulence measurements in the boundary layer over a sand wave field. J. Geophys. Res., 84, 7791 - 7807.

McPhee, M.G. and Smith, J.D., 1976. Measurements of the turbulent boundary layer under pack ice. J. Phys. Oceanogr., 6, 696 - 711.

Mertens, L.E., 1970. In - Water Photography. Wiley - Interscience , 391pp.

Millward, A., 1973. The high speed water channel. University of Liverpool Report No. FM/A3/1973.

Miyake, M., Donelan, M., McBean, G., Paulson, C., Badgley, F. and Leavitt, E., 1970. Comparison of turbulent fluxes over water determined by profile and eddy correlation techniques. Quart. J. Met. R. Soc., 96, 132 - 137.

Monin, A.S. and Yaglom, A.M., 1971. Statistical Fluid Mechanics. The M.I.T. Press, Cambridge, Mass., 769pp.

Nece, R.E. and Smith, J.D., 1970. Boundary shear stress in rivers and estuaries. Proc. Am. Soc. Civ. Eng., 96, (WW2), 335 - 358.

Nikuradse, J., 1933. Laws of flow in rough pipes. National Advisory Committee on Aeronautics, Tech. Mem. 1292, 60pp. (translation from German, 1950).

Pantin, H.M., 1977. Quaternary sediments of the northern Irish Sea. In Kidson, C. and Tooley, M.J. (Eds.), The Quaternary History of the Irish Sea, Steel House Press, Liverpool, 27 - 54.

Praturi, A.K. and Brodkey, R.S., 1978. A stereoscopic visual study of coherent structures in turbulent shear flow. J. Fluid Mech., 89, 251 - 272.

Schlichting, H., 1968. Boundary-Layer Theory. McGraw Hill, New York, 748pp.

Scholtz, S. and Panofsky, H.A., 1980. Wind characteristics at the Boulder Atmospheric Observatory. Boundary-Layer Met., 19, 155 - 164.

Seitz, R.C., 1971. Results of a field study using the 3-axis Doppler shift current meter. Chesapeake Bay Inst., Tech. Rep. No. 72, Johns Hopkins Univ., Baltimore.

Seitz, R.C., 1973. Observations of intermediate and small scale turbulent water motion in a stratified estuary (Parts 1 and 2). Chesapeake Bay Inst., Tech. Rep. No. 79, Johns Hopkins Univ., Baltimore.

Serkin, H.C. and Kronengold, M., 1974. The effects of tilt on a Savonious Rotor exposed to a turbulent flow regime. I.E.E.E. Transactions on Geoscience Electronics, GE-12, 55 - 69.

Simpson, J.H., 1975. Observations of small scale vertical shear in the ocean. Deep-Sea Res., 22, 619 - 627.

Simpson, J.H., Hughes, D.G. and Morris, N.C.G., 1977, The relation of seasonal stratification to tidal mixing on the continental shelf. Deep-Sea Res., Deacon Birthday Volume, A Voyage of Discovery, edited by M. Angel, 327 - 340.

Smith, J.D., 1974. Turbulent structure of the surface boundary layer in an ice - covered ocean. Rapp. P. -v. Reun. Cons. Int. Explor. Mer., 167, 53 - 65.

Smith, J.D., 1977. Modeling of sediment transport on continental shelves. In Goldberg, I.D., McCave, I.N., O'Brien, J.J. and Steele, J.H. (eds.) The Sea, Vol. 6, Wiley - Interscience, New York, 539 - 577.

Smith, J.D. and McLean, S.R., 1977. Spatially averaged flow over a wavy surface. J. Geophys. Res., 82, 1735 - 1746.

Soulsby, R.L., 1977. Similarity scaling of turbulence spectra in marine and atmospheric boundary layers. J. Phys. Oceanogr., 7, 934 - 937.

Soulsby, R.L., 1980. Selecting record length and digitization rate for near - bed turbulence measurements. J. Phys. Oceanogr., 10, 208 - 219.

Soulsby, R.L., 1981. Measurements of the Reynolds stress components close to a marine sand bank. Marine Geol., 42, 35 - 47.

Soulsby, R.L., 1983. The bottom boundary layer of shelf seas. In Johns, B. (ed.), Physical Oceanography of Coastal and Shelf Seas, Elsevier, Amsterdam, 189 - 266.

Soulsby, R.L., Davies, A.G. and Wilkinson, R.H., 1983. The detailed processes of sediment transport by tidal currents and by surface waves. I.O.S., Report, No. 152, 80pp.

Soulsby, R.L. and Dyer, K.R., 1981. The form of the near-bed velocity profile in a tidally accelerating flow. J. Geophys. Res., 86, 8067 - 8074.

Sternberg, R.W., 1966. Boundary layer observations in a tidal current. J. Geophys. Res., 71, 2175 - 2178.

Sternberg, R.W., 1968. Friction factors in tidal channels with differing bed roughness. Marine Geol., 6, 243 - 260.

Sternberg, R.W., 1969. Camera and dye-pulser system to measure bottom boundary-layer flow in the deep sea. Deep-Sea Res., 16(1), 549 - 554.

Sternberg, R.W., 1970. Field measurements of the hydrodynamic roughness of the deep-sea boundary. Deep-Sea Res., 17, 413 - 420.

Sternberg, R.W. and Creager, J.S., 1965. An instrument system to measure boundary layer conditions at the sea floor. Marine Geol., 3, 475 - 482.

Tann, H.M., 1976. The estimation of wave parameters for the design of offshore structures. I.O.S. Report No. 23 (Unpublished manuscript).

Taylor, P.A. and Dyer, K.R., 1977. Theoretical models of flow near the bed and their implications for sediment transport. In Goldberg, E.D., McCave, I.N., O'Brien, J.J. and Steele, J.H. (Eds.), The Sea, Vol. 6, Wiley-Interscience, New York, 579 - 602.

Tennekes, H. and Lumley, J.L., 1974. A First Course in Turbulence. The M.I.T. Press, Cambridge, Mass., 300pp.

Thorpe, S.A., Collins, E.P. and Gaunt, D.I., 1973. An electromagnetic current meter to measure turbulent fluctuations near the ocean floor. Deep-Sea Res., 20, 933 - 938.

Townsend, A.A., 1956. The Structure of Turbulent Shear Flow. Cambridge University Press, 315pp.

Tucker, M.J., 1972. Electromagnetic current meters: an assessment of their problems and potentialities. Proc. Soc. Underwater Technology, 2, 53 - 58.

Tucker, M.J., Smith, N.D., Pierce, F.E. and Collins, E.P., 1970. A two-component electromagnetic ships log. J. Inst. Navig., 23, 302 - 316.

U.N.E.S.C.O., 1981. Background Papers and Supporting Data on The Practical Salinity Scale 1978. UNESCO Technical Papers in Marine Science, No. 37.

U.N.E.S.C.O., 1981a. Background Papers and Supporting Data on the International Equation of State of Seawater 1980. UNESCO Technical Papers in Marine Science, No. 38.

Vincent, C.E. and Harvey, J.G., 1976. Roughness length in the turbulent Eckmann layer above the sea bed. Mar. Geol., 22, M75 - M81

Weatherly, G.L., 1972. A study of the bottom boundary layer of the Florida current. J. Phys. Oceanogr., 2, 54 - 72.

Weatherly, G.L., 1975. A numerical study of time - dependent turbulent Eckmann layers over horizontal and sloping bottoms. J. Phys. Oceanogr., 5, 288 - 299.

Weatherly, G.L., 1977. Bottom boundary layer observations in the Florida current. In Nihoul, J.C.J. (ed.), Bottom Turbulence, Elsevier, Amsterdam, 237 - 254.

Wilkinson, R.H., 1983/1984. A method for evaluating statistical errors associated with logarithmic velocity profiles. Geo - Marine Letters, 3, 49 - 52.

Willmarth, W.W. and Lu, S.S., 1972. Structure of the Reynolds stress near the wall. J. Fluid Mech., 55, 65 - 92.

Wimbush, M. and Munk, W., 1970. The benthic boundary layer. In Maxwell, A.E. (ed.), The Sea, Vol. 4, Pt. 1, Wiley - Interscience, New York, 731 - 758.

Wiseman, W.J., Crosby, R.M. and Pritchard, D.W., 1972. A three dimensional current meter for estuarine applications. J. Mar. Res., 30, 153 - 158.

Zar, J.H., 1974. Biostatistical analysis. Prentice Hall, New Jersey, 620pp.